Quantum Solids of Two Dimensional Electrons in Magnetic Fields

Yong P. Chen

A Dissertation
Presented to the Faculty
of Princeton University
in Candidacy for the Degree
of Doctor of Philosophy

Recommended for Acceptance
by the Department of
Electrical Engineering

November 2005

Report Documentation Page

Form Approved
OMB No. 0704-0188

1. REPORT DATE	2. REPORT TYPE	3. DATES COVERED
NOV 2005		**00-00-2005 to 00-00-2005**

4. TITLE AND SUBTITLE	5a. CONTRACT NUMBER
Quantum Solids of Two Dimensional Electrons in Magnetic Fields	5b. GRANT NUMBER
	5c. PROGRAM ELEMENT NUMBER
6. AUTHOR(S)	5d. PROJECT NUMBER
	5e. TASK NUMBER
	5f. WORK UNIT NUMBER
7. PERFORMING ORGANIZATION NAME(S) AND ADDRESS(ES) **Princeton University,Department of Electrical Engineering,Princeton,NJ,08544**	8. PERFORMING ORGANIZATION REPORT NUMBER
9. SPONSORING/MONITORING AGENCY NAME(S) AND ADDRESS(ES)	10. SPONSOR/MONITOR'S ACRONYM(S)
	11. SPONSOR/MONITOR'S REPORT NUMBER(S)

12. DISTRIBUTION/AVAILABILITY STATEMENT
Approved for public release; distribution unlimited

13. SUPPLEMENTARY NOTES

14. ABSTRACT

This thesis studies the solid phases of two-dimensional electrons subject to a perpendicular magnetic field (i.e., the ?quantum Hall system?). Traditionally, such a solid known as ?Wigner cystal? (WC), is believed to be the ground state of a two dimensional electron system (2DES) when the Landau level (LL) filling factor =nh/eB (n being the electron density and B the magnetic field) is sufficiently small (thus following the termination of quantum Hall states). Due to disorder in realistic samples, the solid is pinned, therefore insulating. Collective oscillation of crystalline domains of the solid around disorder gives rise to a ?pinning mode? resonance in the frequency dependent conductivity, which we measure with rf/microwave spectroscopy. The resonance has interesting behaviors in its dependence on samples, n, B and temperature (T) and contains valuable information about disorder. For example we are able to show that the most relevant disorder that pins the solid comes from the interface that vertically confines the 2DES, with a (sample dependent) disorder correlation length that can become shorter than 10 nm. Most importantly, the resonance is a characteristic signature of pinned electron solids, as well as a tool to study their physical properties. We show that many such solid phases can exist, in different regimes of ; and their properties also depend largely on , which captures the quantum correlation between electrons. Among the new solid phases that we have discovered in the state-of-the-art 2DES samples are the Wigner crystal phases formed in the partially filled top LL around integer Landau fillings. In high LLs, these ?integer quantum Hall Wigner crystals? (IQHWC) join with other phases, such as the bubble and stripe phases, to form a rich array of charge density wave phases. In the lowest Landau level (LLL), we have observed two distinct solid phases which we name as solid ?A? and ?B? phases respectively. The ?A? phase is observable for <2/9 (but reentrant around the =1/5 fractional quantum Hall liquid (FQHL)) and transitions to the ?B? phase which dominates at sufficiently low . The two phases coexist in intermediate (0.18 > > 0.12). Moreover, the resonance of ?A? phase is found to show dispersion with respect to the size of transmission line indicating that ?A? phase has a large correlation length. Many-body quantum correlations appear to play an important role in giving rise to the different solids. In particular, ?A? phase appears to be a solid intimately related to FQHE. Possible interpretations involving a composite fermion crystal and/or a FQHL-WC mixed phase are discussed. We have also studied the T-dependence of the pinning mode resonance of a Wigner cystal (in high magnetic fields) and in particular its melting behavior. In a given

15. SUBJECT TERMS

16. SECURITY CLASSIFICATION OF:			17. LIMITATION OF ABSTRACT	18. NUMBER OF PAGES	19a. NAME OF RESPONSIBLE PERSON
a. REPORT	b. ABSTRACT	c. THIS PAGE			
unclassified	**unclassified**	**unclassified**	**Same as Report (SAR)**	**229**	

I certify that I have read this thesis and that
in my opinion it is fully adequate, in scope and in quality,
as a dissertation for the degree of Doctor of Philosophy.

Daniel C. Tsui (Principal Adviser)

I certify that I have read this thesis and that
in my opinion it is fully adequate, in scope and in quality,
as a dissertation for the degree of Doctor of Philosophy.

Lloyd W. Engel (National High Magnetic Field Lab.)

I certify that I have read this thesis and that
in my opinion it is fully adequate, in scope and in quality,
as a dissertation for the degree of Doctor of Philosophy.

Herbert A. Fertig (Indiana University)

Approved for the Princeton University Graduate School:

Dean of the Graduate School

Abstract

This thesis studies the solid phases of two-dimensional electrons subject to a perpendicular magnetic field (i.e., the "quantum Hall system"). Traditionally, such a solid, known as "Wigner cystal" (WC), is believed to be the ground state of a two dimensional electron system (2DES) when the Landau level (LL) filling factor $\nu=nh/eB$ (n being the electron density and B the magnetic field) is sufficiently small (thus following the termination of quantum Hall states). Due to disorder in realistic samples, the solid is pinned, therefore insulating. Collective oscillation of crystalline domains of the solid around disorder gives rise to a "pinning mode" resonance in the frequency dependent conductivity, which we measure with rf/microwave spectroscopy.

The resonance has interesting behaviors in its dependence on samples, n, B and temperature (T) and contains valuable information about disorder. For example, we are able to show that the most relevant disorder that pins the solid comes from the interface that vertically confines the 2DES, with a (sample dependent) disorder correlation length that can become shorter than 10 nm.

Most importantly, the resonance is a characteristic signature of pinned electron solids, as well as a tool to study their physical properties. We show that many such solid phases can exist, in different regimes of ν; and their properties also depend largely on ν, which captures the quantum correlation between electrons.

Among the new solid phases that we have discovered in the state-of-the-art 2DES samples are the Wigner crystal phases formed in the partially filled top LL around integer Landau fillings. In high LLs, these "integer quantum Hall Wigner crystals" (IQHWC) join with other phases, such as the bubble and stripe phases, to form a rich array of charge density wave phases.

In the lowest Landau level (LLL), we have observed *two* distinct solid phases, which we name as solid "A" and "B" phases respectively. The "A" phase is observable for $\nu<2/9$ (but *reentrant* around the $\nu=1/5$ fractional quantum Hall liquid

(FQHL)) and transitions to the "B" phase which dominates at sufficiently low ν. The two phases coexist in intermediate ν ($0.18 \gtrsim \nu \gtrsim 0.12$). Moreover, the resonance of "A" phase is found to show dispersion with respect to the size of transmission line, indicating that "A" phase has a large correlation length. Many-body quantum correlations appear to play an important role in giving rise to the different solids. In particular, "A" phase appears to be a solid intimately related to FQHE. Possible interpretations involving a composite fermion crystal and/or a FQHL-WC mixed phase are discussed.

We have also studied the T-dependence of the pinning mode resonance of a Wigner cystal (in high magnetic fields) and in particular its melting behavior. In a given sample, the melting temperature (T_m) is found to be mainly determined by ν, in contrast to the case for any other known solids (including, particularly, a classical 2D electron solid) whose T_m is determined by the solid density n. This not only attests to the quantum solid nature of the Wigner cystal in our samples; but also constitutes, to our best knowledge, the only example of a solid whose T_m has been shown to mainly depend on inter-particle quantum correlation (here through ν).

The appendices of the thesis contain more background/supporting material, as well as some theoretical results. In one appendix we develop a model for pinned *bilayer* Wigner crystals, helped by the knowledge of pinning and disorder that we have earlier learned from our experiments on single layer 2DES. We propose that pinning mode resonance can distinguish a (pesudospin) antiferromagnetic WC (AFMWC) from a ferromagnetic WC (FMWC), the latter of which can be viewed as a supersolid-like phase. Our model shows that pinning is *enhanced* in a FMWC, which possesses interlayer coherence (IC), compared to an AFMWC without IC and predicts a decreasing pinning mode frequency ($f_{\rm pk}$) with the effective layer separation in a FMWC, opposite to the behavior in an AFMWC, and an abrupt drop of $f_{\rm pk}$ at a FMWC to AFMWC transition.

Acknowledgements

A large number of people have kindly helped me in one way or another in relation to this thesis, the bulk work of which was conducted in two places (Princeton and Tallahassee) and between 2002 and 2005.

First, I thank my thesis advisor Daniel Tsui, who has been largely responsible for my transition from a pure mathematician to an experimenting physicist since I started this PhD in 1999. I am particularly grateful to him for introducing me the opportunity to work on the problem of electron solid (the subject of this thesis) and work in National High Magnetic Field Laboratory (NHMFL) in Tallahassee, both of which turn out to be extremely scientifically fulfilling. His encouragement , trust as well as critics, his scientific insights, taste and judgment, and his style of inspirational education have all been blessings for my entire PhD and will continue influencing me profoundly. Thank you, Dan, for teaching me the "dao" of science.

I am also very fortunate to have worked with another superior teacher, Lloyd Engel, who is my co-advisor and host in NHMFL. Without the cutting edge microwave technology that Lloyd had developed in the earlier years, all experimental discoveries described in this thesis would remain as theorists' fantasies at best. Lloyd made his seemingly infinite supply of knowledge in experimental physics accessible to me even in the most weird hours, and burnt many late nights' oil helping edit my papers. Thank you, Lloyd, for also making a life in science so entertaining.

Two of my co-workers, Rupert Lewis and Sambandamurthy ("Murthy") Ganapathy, both postdocs based in Tallahassee, were directly involved with the research in this thesis. Rupert not only started me up in the microwave measurements, he is my major collaborator in a large part of my thesis research (especially on integer Landau level Wigner crystals and "A and "B" solid phases in lowest Landau level). I also thank Rupert for sending me many of his data on bubble and stripe phases. Murthy has been my major collaborator on Wigner crystal melting as well as offering

great philosophical influence on data analysis. Their participation and help in the measurements during many of my "magnet times" lead to maximum utilization of the magnet resources and many data that I would not have been able to measure if running alone. Their contributions and roles will be more specifically acknowledged later in the individual chapters. Above all, thank you Rupert, and Murthy, for making our lab such a fun fraternity.

I also thank fellow graduate students in the microwave lab Zhi-hai Wang and Brenden Magill for assistance in some of the data acquisition and Zhi-hai for discussion and communication about his bilayer Wigner crystal experiments (which motivated the pinned bilayer Wigner crystal model in Appendix K).

Over the years, I have greatly benefited from many other former or current postdocs in the group. I thank Peide Ye, who taught me the fabrication of microwave samples and provided many valuable comments on my research; Gabor Csathy, who taught me a great deal on low temperature experiments, provided me many his DC measurement data and was always ready to help in many other ways; Guillaume Gervais, for a source of scientific excitement; Michael Hilke, who mentored my first low temperature research project in Princeton; Wei Pan and Zhi-gang Jiang, for many interesting discussions; Jin-jin Li for help on thin-film measurements as well as Leonid Rokhinson and Hwa-yong Noh for general lab help earlier-on in my PhD.

I have also received kind help and learned a great deal from many of the fellow graduate students in Prof.Tsui's group, especially Keji Lai and Ravi Pillarisetty on clean room processing, Wanli Li for providing valuable sample information and I also thank Amlan Majumdar and Jie Yao for earlier help in the lab.

The high quality GaAs/AlGaAs samples for studying electron solids were all provided by Loren Pfeiffer and Ken West from Bell Labs. They were processed in the fabrication facilities at Princeton EE department. I am particularly grateful for generous help from Eric Shaner and Guillaume Sabouret in Lyon's group as well as Nathan

Bishop and Oki Gunawan in Shayegan's group.

All microwave measurements were performed at NHMFL (supported by NSF Cooperative Agreement No. DMR-0084173 and by the State of Florida). Most high field experiments were conducted in the user magnets with technical assistance from many scientists and engineers in the NHMFL operations department. I particularly thank Eric Palm, Tim Murphy, Glover Jones (and earlier April Teske) for their assistance and patience with my experiments, as well as Scott Hannahs (especially for his help on Labview) and Bruce Brandt for help on magnet times. I also thank Bob Smith and John Pucci for assistance in operating the 45T hybrid magnet and for honoring many of my urgent helium request, Mike Davidson for assistance in sample microscopy, Andy Powell and Lee Bonninghausen in electronics shop and numerous staff in the magnet control room.

Many support and secretarial staff have helped made easy the administrational stuff related to my research. I particularly thank Alice Hobbs in the condensed matter group of NHMFL, Jamie Kubian in Princeton EE department, as well as many others that have worked over the years as program assistants for Tsui/Chou groups in Princeton.

Financial supports for our research were provided by Air Force Office of Scientific Research, Department of Energy, National Science Foundation and NHMFL in-house research program. I also acknowledge a Gordon Wu fellowship during the earlier part of my PhD.

I thank also a number of faculty members in Princeton or NHMFL for inspirational interactions: Ravin Bhatt, Steve Lyon and Mansour Shayegan; Nick Bonesteel, Jan Jaroszynsky and Kun Yang. I particularly thank Prof. Bhatt for lending me a panoramic office in his group during my last year in Princeton. I have also benefited greatly from numerous discussions with Cheng-gang Zhou and Dima Novikov in Bhatt group, Emanuel Tutuc in Shayegan group and Xin Wan and Akakii Melikidze in Kun

Yang's group. Of course I also thank Professors Shayegan and Lyon for being in my final public oral examination committee (in addition to my advisor).

I also acknowledge discussions that have influenced my work or writing of this thesis with Alan Bishop, Moses Chan, Tat Chui, Rene Cote, Herb Fertig, Misha Fogler, Bert Halperin, Ganpathy Murthy, Woowon Kang, Michael Lilly, Leonid Levitov, Nick Read, Boris Spivak, Philip Stiles, Xiao-Gang Wen, Bob Willett, Clare Yu and many others in the academic community who have kindly shared with me their knowledge and enthusiasm about relevant physics subjects. I am particularly grateful to Prof. Herb Fertig who read my thesis and gave me feedbacks at a short notice.

I thank all my friends in Princeton, as well as many Seminoles and even gators, who, with all the help, inspiration and pleasant distractions, have made my PhD and the three years of residence in Florida particularly memorable time. I also thank my old friend Bo in Institute of Advanced Studies, who kindly provided accommodation during some of my sample processing trips to Princeton, and interesting comments to my work from a string theorist's perspective.

Now at the end of my PhD, I want to thank the people who kindly recommended me to enter Princeton: Wanda Andreoni in IBM Zurich Lab, Paul Schechter in MIT physics department, and my late MIT mathematics advisor Gian-Carlo Rota, who unfortunately passed away shortly after writing his recommendation for me, and has been a unique source of inspirations in all the years.

A large part of my thesis, believe it or not, was actually written after I started working as a postdoc in Randy Hulet's group in Rice University. I thank all my colleagues there for their understanding of this apparent violation of Lorentz invariance.

Finally I thank my parents Chen Xing-hua and Li Xiang-yuan, for everything. Although knowing little about my research, they have always educated me since my childhood to look for truths and beauties underneath the surface, which is particularly fitting in the case of studying 2D electrons! To them I dedicate this thesis.

Contents

道可道，非常道。（老子：《道德经》）

The Tao ("dao") that can be told of
Is not the Absolute Tao.
------Lao Tsu: "Tao Te Ching" (6th century BC)

Chapter 1

Introduction

The stories that we are going to tell in this thesis are about the solid phases formed by two dimensional electrons whose 2D motion is quantized by a perpendicular magnetic field. Realized in semiconductor structures, these electron solids embody effects from both electron-electron interaction and disorder, two of the fundamental themes in modern condensed matter physics. Quantum correlations often reveal themselves as the underlying driving force in forming a variety of solid phases as well as enabling many of their fascinating yet intriguing properties.

1.1 Electron Solids: A Resume

1.1.1 Electron solid at zero magnetic field

The solid phase of electrons, also known as "Wigner cystal" (WC), was originally proposed by Eugene Wigner (Wigner, 1934), who found that at zero temperature (T=0), an electron gas[1] of sufficiently low density n (that the Coulomb interaction sufficiently dominates the kinetic energy)[2] would crystalize into a solid, in order to minimize the Coulomb interaction.

[1] in a background of neutralizing positive charges
[2] Detailed energetic analysis can be found in the review article by Fertig (1997).

Such an electron solid had been sought after for years since its prediction. In three dimensions, such a low[3] n, strongly interacting electron system is quite difficult to realize in real materials without having disorder effects overwhelm the interaction, and a 3D WC (supposed to be a BCC lattice) of electrons[4] has not been experimentally observed (Ceperley, 1999; Young *et al.*, 1999).

In two dimensions (2D), ultra low density and nearly defect-free 2D electron system (2DES) can be realized by holding electrons with an electric field on liquid helium surface, and an electron crystal was observed (Grimes and Adams, 1979) which had the predicted triangular lattice structure (Bonsall and Maradudin, 1977). However, the realized density n was so low in this system that the electron crystal is "classical", in the sense that the thermal energy corresponding to the experimental temperature (k_BT) far exceeds the quantum kinetic (Fermi) energy[5] ($E_f \propto n$).

In the late 70s, it was suggested (Lozovik and Yudson, 1975; Fukuyama *et al.*, 1979) that Wigner crystallization can be greatly facilitated by applying a strong magnetic field (B) perpendicular to a 2DES, even if the n is too high for the zero-B WC (Tanatar and Ceperley, 1989) to form. This result, due to the magnetic field suppressing the kinetic energy of electrons, opened up a road to observe "quantum" WC in the high quality 2DES realized in semiconductor structures (see reviews in Ando *et al.* (1982); Davies (1998)) which typically has relatively high n. Such a magnetic field induced Wigner cystal (MIWC)[6] and as we will see, many other related solid phases in the "quantum Hall system" (QHS, a 2DES or 2D hole system (2DHS)

[3]More accurately, the relevant number is the dimensionless r_s, defined as the mean separation between electrons normalized by the Bohr radius in the system.

[4]"Classical" 3D WC formed with other, larger Coulomb particles have been realized (Murray *et al.*, 1990; Thomas *et al.*, 1994; Tan *et al.*, 1995).

[5]Such a classical WC differs qualitatively from a "quantum" WC. For example, a classical WC melts at a higher T at higher n, whereas a quantum WC melts at a lower T at higher n (Fukuyama *et al.*, 1979). See alse Chapter 6.

[6]In recent years, zero-B 2D WC in semiconductor structures has also been discussed (for example Yoon *et al.* (1999); Spivak and Kivelson (2004), particularly relating to the apparent metal-insulator transition (MIT, see review in Abrahams *et al.* (2004)).

subjected to a perpendicular B), will be the main subject of this thesis[7].

1.1.2 Quantum Hall Effects

A particularly interesting aspect of MIWC is its intimate connection to the quantum Hall effects (QHE), which were discovered in 2D systems before the MIWC. Excellent reviews of the QHE are given in Prange and Girvin (1990); Das Sarma and Pinczuk (1997); Girvin (1999) and Stormer (1999). Here we merely recollect a few aspects in relation to the Wigner crystal.

Placed under a perpendicular B, 2D electrons are quantized into Landau energy levels with occupancy given by the Landau filling factor $\nu = nh/eB$. The integer quantum Hall (IQH) effect (v. Klitzing *et al.*, 1980), observed around ν=K (where K is an integer), is commonly explained in terms of single particle localization. The localization is due to disorder, which always exists in semiconductor samples. Later in Chapter 4 we will see that in very low disorder samples, collective localization of a many-body ground state such as a crystal, can give rise to the IQHE as well.

The fractional quantum Hall (FQH) effect (Tsui *et al.*, 1982), observed for many fractions ν=p/q, on the other hand, is strictly a many-body phenomenon due to electron-electron interaction (Laughlin, 1983). It is established that, at certain fractional values of ν , electrons can collectively condense into an incompressible quantum liquid with fractionally charged quasi-particles. Much of the fractional quantum Hall effects (FQHE) have been accounted for by the highly successful composite fermion (CF)/composite boson (CB) model (Jain, 1989; Read, 1989; Zhang *et al.*, 1989; Kivelson *et al.*, 1992). CF/CB are electrons bound with even/odd number of magnetic flux quanta and the FQHE correspond to the IQHE of CFs or to a Bose-condensate of CBs (Girvin and MacDonald, 1987; Jain, 2000)[8]. Although the quantized Hall plateau in

[7] we will use the terms such as "(2D) electron solid", "(2D) Wigner crystal/solid" and "MIWC" rather interchangeably.

[8] Even in the lowest Landau level (LLL, ν <1) such that electron's single particle kinetic energy is

FQHE is given by quasi-particle localization by disorder, observation of the FQHE generally requires much cleaner samples (compared to IQHE) so that the effect of electron-electron interaction is manifested.

1.1.3 Magnetic Field Induced Wigner Crystal in the Lowest Landau Level

Although it had long been believed that the ground state of a 2DES under sufficiently high B (low ν) should be a Wigner crytal (MIWC), it was not until around 1990 that experimental evidence for the MIWC started to accumulate. This was partly because the WC, an interaction driven state, also requires sufficiently clean samples, otherwise single particle localization (magnetic freeze-out) occurs at high B instead of Wigner crystallization. More importantly, WC is always *pinned* by disorder in the sample (even for weak disorder), and is an insulator. Therefore, although DC transport found that FQH states terminate into an insulating phase at sufficiently high B (Willett *et al.* (1988)), it was not easy to distinguish a pinned WC from an insulator due to, for example, single-particle localization, not mentioning the fact that ohmic DC transport measurements become prohibitively difficult when the resistance of the insulator becomes too large at high B. However, a combination of many experiments (for example Willett *et al.* (1988); Jiang *et al.* (1990); Goldman *et al.* (1990); Glattli *et al.* (1990); Li *et al.* (1991); Buhman *et al.* (1991); Williams *et al.* (1991); Goldys *et al.* (1992); Paalanen *et al.* (1992a)) ranging from DC, nonlinear IV, RF, noise to optical measurements jointly made a case for a MIWC (more complete accounts of earlier works on Wigner cystal can be found in reviews of Shayegan (1997), Fertig (1997), Chui (1994) and the theses of Y.P.Li (1993) and C.C.Li (1999)). It has been generally believed that the high-B insulating phase (HBIP, by which we

quenched, CFs can acquire effective kinetic energy from many body and quantum correlation effects. For example, at ν=1/2, Fermi surface of CFs have been observed (Willett *et al.*, 1993)

mean the insulator terminating the series of QH states at high B) observed in good quality 2DES is a pinned electron solid with substantial WC order, although direct measurements, such as imaging, of the WC periodicity are not yet available. As we will show later, however, multiple solid phases, in the LLL (high B), are found in the very low disorder samples available today (Chen *et al.*, 2004c) and the microscopic nature of those electron solids (which we still refer to as MIWC) is far from clear.

Experimentally, the transition to the HBIP has been determined to be near ν=1/5 (Willett *et al.*, 1988; Jiang *et al.*, 1990; Goldman *et al.*, 1990) in high mobility 2DES samples, following the termination of the FQH series (1/5 being the lowest ν FQH state observable at low T in 2DES). This is in reasonably good agreement with theoretical calculations[9] for a FQHE to MIWC transition (Lam and Girvin, 1984; Levesque *et al.*, 1984; Zhu and Louie, 1995). It is worth mentioning that the Landau level filling factor ν, which controls much of the quantum Hall physics, is a "quantum" parameter and is a measure of inter-electron quantum correlation. Indeed, $\nu = nh/eB = 2(l_B/r)^2$, where the magnetic length $l_B = \sqrt{\hbar/eB}$ measures the size of single-electron wavefunction in the LLL and $r = 1/\sqrt{\pi n}$ is the mean separation between electrons. Therefore, the transition from WC to FQH liquid can be viewed as a quantum melting driven by quantum correlations between electrons. We will see later that such quantum correlation (controlled by ν) is still important in the solid phase.

1.1.4 Charge Density Waves in High Landau Levels

Rather recently, two types of states were discovered in DC transport (Lilly *et al.*, 1999a; Du *et al.*, 1999) in the second excited LLs and above (ν >4): state with highly anisotropic longitudinal magnetoresistance near the half filling (for example, ν=9/2), and "reentrant integer quantum Hall" (RIQH) state near quarter fillings

[9]Considering the difficulties that theories have in accurately determining the ν boundary.

(for example, 4+1/4 and 4+3/4) which is similar to IQHE with Hall quantization occurring at the value of the adjacent IQHE. These states have been identified as the "stripe" and "bubble" phases predicted earlier for the high LLs (Koulakov *et al.*, 1996; Fogler *et al.*, 1996; Moessner and Chalker, 1996). The predicted "stripe" phase is a uni-directional charge density wave (CDW) and the "bubble" phase is an isotropic crystal with multiple electrons (or Landau holes) per crystal site. Later RIQH states were also discovered (Eisenstein *et al.*, 2002) in the 1st excited LL ($2 < \nu < 4$), which may be due to similar "bubble" crystals. Together with the Wigner crystal phase[10] predicted (MacDonald and Girvin, 1986) and discovered (Chen *et al.*, 2003) around integer ν (=1,2,3,4...), they constitute a rich array of CDW phases formed *in the partially filled top LL*, where the filled LLs is often treated as an inert background in approximation[11]. The "bubble" crystals, as well as the Wigner cystals around integer ν, are pinned electron solids. The "stripe" phase, has been discussed as an electron liquid crystal (Fradkin and Kivelson, 1999).

One strong support for the pinned solids (both in the LLL and high LL) comes from the observation of the so called "pinning mode" resonance, which is the main tool used in this thesis and will be briefly introduced in the next section (and discussed in more details later). Except for the "stripe" phase, we have observed pinning mode resonances for all the above-mentioned isotropic, pinned 2DES solid phases in quantum Hall systems.

1.2 Microwave Response of Electron Solids

AC electromagnetic response, from a general point of view, is a powerful probe of the electronic state and dynamics of 2DES. This is particularly the case for the pinned

[10] WC with 1 electron per crystal site can be viewed as an 1-electron bubble and is a special case of CDW.

[11] A pinned crystal in the top LL does not participate in the conduction and therefore manifests as an RIQHE (in contrast to an insulator in the LLL), with the quantized Hall conductance determined by the filled LLs.

electron solid phases.

1.2.1 Disorder Pinned Wigner Crystal

As mentioned earlier, a WC is always pinned by disorder in real samples and is therefore an insulator. Disorder[12] has two other effects on a WC that are important to us:

1. Disorder destroys the long range order of the 2D WC (Imry and Ma, 1975; Chitra *et al.*, 2002) and makes the WC break into multiple domains, i.e., to develop a finite correlation length.

2. Disorder opens up a pinning gap in the otherwise gapless magnetophonon excitation of a 2D WC in perpendicular B (Bonsall and Maradudin, 1977; Fukuyama and Lee, 1978). This gapped excitation is also known as the "pinning mode" and it gives rise to a resonance in AC absorption, or frequency (f) dependent real diagonal conductivity (Re$[\sigma_{xx}(f)]$).

One can define various correlation lengths for a pinned WC (Fertig, 1999; Fogler and Huse, 2000; Chitra *et al.*, 2002) which turn out to be closely related to the properties of pinning mode, as we will discuss in more detail in Chapter 3. The pinning mode resonance corresponds to the collective oscillation of crystalline domains of the elastic solid in the disorder potential and is experimentally excitable by microwaves[13]. This resonance is a characteristic feature of a pinned electron solid, and as we will later see, both properties of the crystal itself and of the disorder are important in determining its behavior.

[12] provided it is not so strong as to destroy the WC order altogether

[13] In this thesis we use microwave in the broad sense to also include RF.

1.2.2 Microwave Spectroscopy and Pinning Mode Resonance

The ability to meaningfully measure the microwave response of the electron solid is a nontrivial task and took years of technological developments. Not only does it need to deal with low temperatures and high magnetic fields, the real signal can also be easily overwhelmed by instrumental response (for example that from the coaxial cables used in the measurements, or due to poor impedance match). Some of the earliest attempts (Andrei *et al.*, 1988) to probe the magneto-phonon excitations of MIWC suffered from instrumental problems and did not convincingly reveal WC resonances (Stormer and Willett, 1989; Andrei *et al.*, 1989; Glattli *et al.*, 1990; Williams *et al.*, 1991; Stormer and Willett, 1992; Williams *et al.*, 1992). Later experiments employing surface acoustic waves (SAW, Paalanen *et al.* (1992a); Willett (1994)), lower frequency (rf) measurements (Li *et al.*, 1995a,b, 1996), or microwave strip-lines (with more careful data extraction) (Glattli *et al.*, 1990; Hennigan *et al.*, 1998) found features that can be attributed to a pinned WC.

The first cleanly-resolved, single-peak microwave resonance of MIWC (Engel *et al.*, 1997a; Li *et al.*, 1997), was obtained from microwave transmission measurements using coplanar wave-guide (CPW, Wen (1969); Engel *et al.* (1993)). In these experiments the microwave signal was generated at room temperature, sent one-way into the cryostat to the sample and detected in the cold space (Engel *et al.*, 1993; Li, 1999). Further developments combining high quality (low loss, low heat load) coaxial cable and careful cold-sinking have enabled round-trip transmission of microwave signal (in and out of the cryostat, with the signal both generated and detected at room T). This has greatly simplified the measurements of the full complex conductivity of the 2DES, allowing convenient microwave vector network analysis over a broad range of frequency reaching from as low as $\sim$20MHz to as high as $\sim$20GHz.

Fig. 1.1 demonstrates an example of $\mathrm{Re}[\sigma_{xx}(f)]$ measured with such a technique on one of the samples studied in this thesis (Sample P, a GaAs/AlGaAs heterojunction,

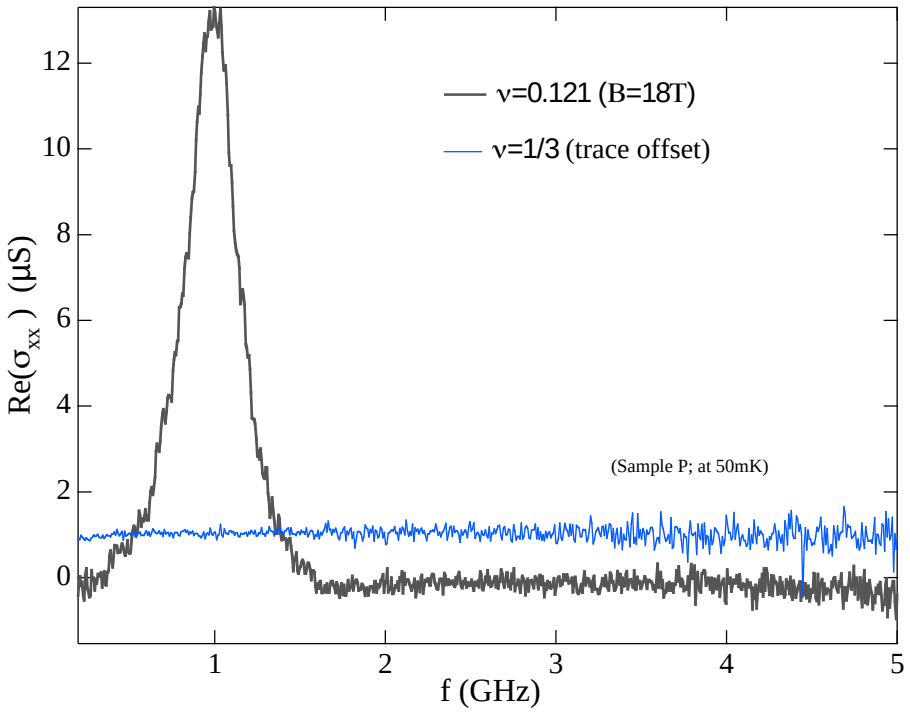

Figure 1.1: Example of a WC pinning mode resonance measured on sample P (n=5.3×10^{10}cm^{-2}) at ν=0.121 and T=50 mK (Ye *et al.*, 2002b). The flat spectrum (offset for clarity) measured at $\nu = 1/3$ FQH liquid is shown for comparison.

see Chapter 2 for more details). The pinning mode resonance (near 1 GHz) is clearly seen in the spectrum at 18T, in the Wigner crystal regime (Ye *et al.*, 2002b). The flat spectrum in a liquid state (at ν=1/3) is also shown as a comparison.

The basic experimental approach of this thesis is to utilize our broad-band microwave technique, especially its function of measuring Re$[\sigma_{xx}(f)]$ (deduced from the microwave power absorption due to 2DES), as a spectroscopy tool to study 2DES solids. The pinning mode resonance is used in particular as a handle to reveal new solid phases, to study physical properties of electron solids, and to learn valuable information about disorder.

1.3 Outline of the Thesis

The organization of the rest of the thesis are as follows:

Chapter 2 describes the 2DES samples used and the experimental methods, particularly the microwave measurements technique.

Chapter 3 discusses current understanding (or lack of it) of pinned WC's and the pinning mode and addresses the question "what pins the Wigner crystal?". We demonstrate the major properties of the pinning mode with our experimental data. In light of recent theories, we discuss what our data may tell us about disorder.

Chapter 4 reports the discovery of "integer quantum Hall Wigner crystal" (IQHWC) in partially filled top LL (around ν=1,2,3,4 etc.). We also briefly discuss other charge density wave phases measured with microwave spectroscopy in high LLs and their connection with IQHWC.

Chapter 5 reports the discovery of two distinct solid phases in the lowest LL (high B) in very low disorder samples. We present data about the transition between the two phases ("A" and "B" phases), the solid ("A") to FQHE liquid (at $\nu = 1/5$) transition and the dispersive behavior of the pinning mode of "A" phase. We discuss physical insights our data give regarding the nature of these different solids, particularly emphasizing the role of many-body quantum correlations.

Chapter 6 reports our studies of the T-dependence of the pinning mode of the MIWC and focuses on the question "how does a WC melt?". Our data, again reveal the importance of quantum correlations in determining the WC melting temperature and show that the MIWC is, in this sense, a unique quantum solid.

Chapter 7 is the concluding chapter and in particular, attempts to construct an experimental "global phase diagram" of 2DES solid phases in the quantum Hall system, from our microwave spectroscopy measurements on low disorder samples.

Further topics and directions related to each chapter (2-6) are discussed at the section "Notes and Further Directions" at the end of the respective chapter, whereas

only the more "global" future research prospectives are included in the concluding chapter (7).

Some supplementary materials (additional sample information and data) are relegated to the Appendices. Also included are a few theoretical notes. In particular in Appendix. K, we present a model of pinned bilayer WC and propose that studying its pinning mode may reveal the signatures of interlayer quantum coherence or different quantum magnetism in bilayer systems.

Chapter 2

Samples and Experimental Methods

2.1 Samples

We have used in this thesis high quality GaAs/AlGaAs-based 2DES samples fabricated from the modulation doped wafers grown with molecular beam epitaxy (MBE, see reviews in Ploog (1981); Einspruch and Frensley (1994); Pfeiffer and West (2003)) by Dr. Loren Pfeiffer in Bell Labs. Sample processing[1] (most importantly, lithographically fabricating the CPW transmission line) procedures can be found in Appendix B. Brief accounts on each sample/wafer and a preview of the specific physics (solid phases) studied are given below in Table 2.1. Information about the individual pieces of the samples are also described in later chapters when discussing the measurements. More supplementary information (such as growth parameters and cool-down procedures) are relegated to Appendix C.

In particular, the 2DES density n of Sample P can be tuned, by cool-down variations and backgating, in a large range (from $\sim 1\times 10^{11}\mathrm{cm}^{-2}$ to full depletion). Sample

[1] Done in the clean room facilities in Princeton

wafer name	structure	nominal n	nominal μ	phases/phenomena observed with microwave spectroscopy
P (2-12 -97-1)	hetero-junction	6×10^{10}cm^{-2}	6×10^{6}cm^2/Vs	Chap. 3 & Appen. H: **High-B WC** [$\nu \lesssim 1/5$];
				Chap. 4 & Appen. I: **IQHWC** [around ν=1]
R (7-21 -00-1)	30nm QW	3×10^{11}cm^{-2}	24×10^{6}cm^2/Vs	Chap. 4: **IQHWC** [around ν=1,2,3,4]; **"bubble" crystal** and **"stripe" phase** [ν >4]; **N=1 LL RIQHE** [2<ν<3]
WP (7-20 -99-1)	50nm QW	1×10^{11}cm^{-2}	10×10^{6}cm^2/Vs	Chap. 5: **"A" and "B" Phases** of high-B WC [$\nu \lesssim 1/5$];
				Chap. 4 & Appen. I: **IQHWC** [around ν=1,2,3]
QW65 (8-30 -99-1)	65nm QW	5×10^{10}cm^{-2}	8×10^{6}cm^2/Vs	Chap. 5: **"A" and "B" Phases** of high-B WC [$\nu \lesssim 1/5$];
QW15 (10-09 -01-1)	15nm QW	5×10^{10}cm^{-2}	1×10^{6}cm^2/Vs	Chap. 3: **High-B WC** [$\nu \lesssim 1/3$]

Table 2.1: Summary of 2DES samples studied. Under the name of each wafer, we also give the corresponding Pfeiffer's wafer number in the bracket. Each density (n) and mobility (μ) are nominal as-cooled values. Also listed are the phases/phenomena (highlighted with bold-face) studied on each sample, along with the relevant chapter where the phenomena/data are discussed. Except for the "stripe" phase, all other phases are pinned isotropic electron solids and show pinning mode resonances in the microwave conductivity spectra. See text for more details and Appendix C for supplementary information.

QW65 and QW15 also have a moderate range of tunable n ($\sim$2.5-6$\times10^{10}$cm^{-2} for QW65 and $\sim$ 2-5$\times10^{10}$cm^{-2} for QW15). Samples P, QW15 and QW65 have been used in the studying of melting of MIWC in Chapter 6.

For the purpose of studying the anisotropic stripe phase (Chap. 4.2), several pieces of sample R were fabricated from the same wafer with CPW's of different orientations (and of various sizes).

Both samples WP and QW65 show two solid phases ("A" and "B" phases) in the high-B WC regime. Several pieces of QW65 were fabricated from the same wafer with CPW of various sizes to study the dispersion of "A" phase (Chap. 5).

QW15 only differs from QW65 in the width of the QW, thus together they give an excellent opportunity to study the effect of vertical confinement (Chap. 3).

2.2 Microwave Measurements

2.2.1 Coplanar Wave Guide (CPW) and Microwave Transmission

Essential in our microwave measurements is the coplanar waveguide (CPW) (Wen, 1969). CPW is widely used in the monolithic millimeter-wave integrated circuit (MMIC) technology (Russer and Bieble, 1994). It has also been successfully employed to measure the microwave conductivity of 2DES (Engel *et al.*, 1993; Li *et al.*, 1997; Ye *et al.*, 2002b). To make the CPW, we lithographically deposited metal films on the sample surface (see Appendix B for the fabrication process). A typical measurement circuit is shown schematically in Fig. 2.1(A) and a local cross section shown in Fig. 2.1(B). A network analyzer serves both as the generator and detector of the microwave signal. The microwave propagates along the CPW, couples capacitively to the 2DES, and drives the 2DES (mainly under the slot) with the AC electric field ($\vec{E}$, perpendicular to the propagation direction of CPW), at the microwave frequency

f=$\omega/2\pi$. In our experiments, we measure the relative power absorption[2] (P) by the 2DES. If the microwave frequency f matches that of some excitation mode in the 2DES (for example the pinning mode), a resonant absorption will be detected.

The CPW can be modeled as a transmission line and the 2DES as a "shunt" that loads the transmission line (see Fig. 2.2). This allows one to relate the microwave transmission of the 2DES to its diagonal[3] conductivity σ_{xx} (more specifically, to first order for small $|\sigma_{xx}|$, the transmitted power is related to Re(σ_{xx}) and the phase shift related to Im(σ_{xx}). We mainly measures the power absorption for the work in this thesis.). Here we make a few points most relevant to our experiments and understanding of the data. More background information and technical details can be found in Appendix D, and also in (Liao, 1990; Engel *et al.*, 1993; Li, 1999).

We use below w to denote the slot width of the CPW (Fig. 2.1(B)), l its total length and Z_0 its characteristic impedance (Liao, 1990). The CPW was designed such that in the absence of 2DES, Z_0=$\sqrt{L'/C'}$=50 Ω, (where L' and C' are the center conductor inductance and the center conductor to ground capacitance per unit length respectively, see Fig. 2.2). This matches Z_0 to the standard 50 Ω characteristic impedance of other parts of the microwave measurement circuits and reduces the signal reflections (enhances the transmission and more importantly reduces the influence of standing waves).

Under the following conditions (Engel *et al.*, 1993):

1) at sufficiently high f and low 2DES conductivity (most importantly, this requires $\xi \ll w$, where the microwave "penetration depth"[4] $\xi = \sqrt{|\sigma_{xx}|/(C_g\omega)}$, with C_g=$\epsilon_0\epsilon_r/d$ being the geometric capacitance per area between the center conductor and the 2DES (located at depth d in a material with dielectric constant $\epsilon_0\epsilon_r$. For GaAs, ϵ_r=13.)

2) no reflections at the ends of the CPW and

[2]defined as P_{in}/P_{out}.

[3]It can be shown that the measurements are not sensitive to the Hall conductivity σ_{xy} (Li, 1993).

[4]This is the characteristic depth of the microwave electric field leaking under the CPW side plane.

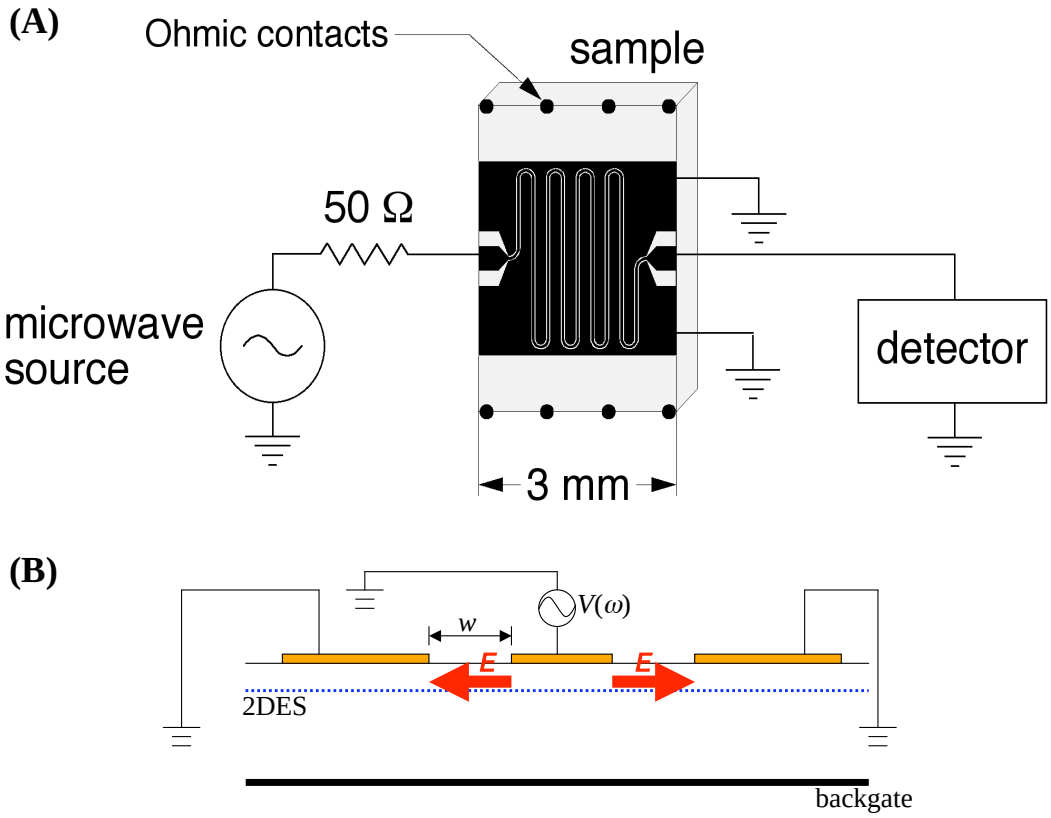

Figure 2.1: **(A)** Scheme of microwave circuit used in our experiments. Sample size is typically ∼3×5 mm. Dark regions on sample surface represent metal films deposited to make the CPW (the one shown here has a meander shape). The geometry of the CPW may vary from sample to sample, but have been carefully designed to match the 50Ω characteristic impedance. **(B)** Schematic local cross section (not to scale) of the sample with CPW. w is the width of each slot region, separating the center conductor (driver by microwave source $V(\omega)$) and the side planes (grounded). $\vec{E}$ represents the AC electric field in the slot region driving the 2DES, which is typically $d\sim$ 0.2-0.5 μm below the surface. Sample substrate is GaAs, typically sitting on a backgate.

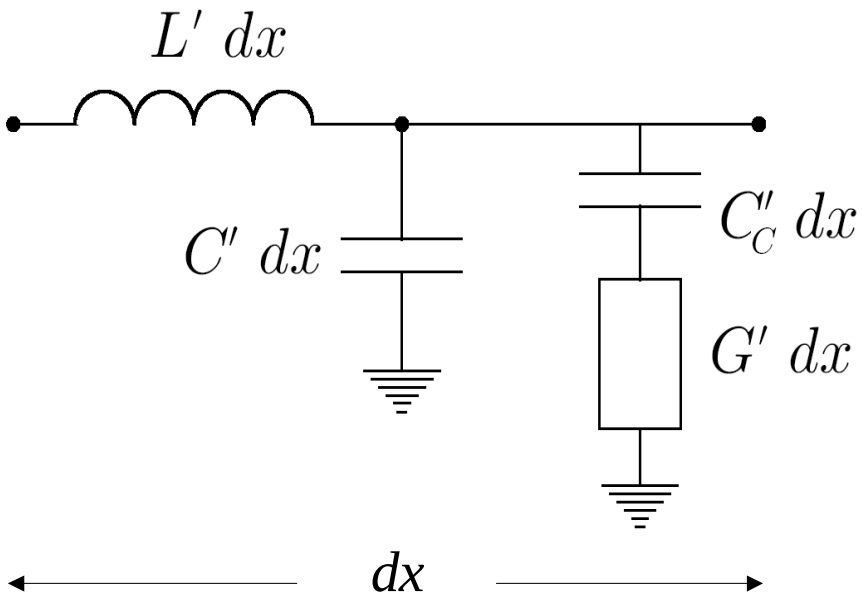

Figure 2.2: A simple transmission line model of using CPW to measure 2DES conductivity. L' is the inductance of the center conductor per unit length and C' the capacitance between the center conductor to the ground (side plane) per unit length. The 2DES constitutes a shunt admittance from the CPW center conductor to the ground. $C_c^{'}$=sC_g is the capacitance from the center conductor (of width s) to the 2DES (of depth d below the surface) per unit length, where C_g=$\epsilon_0\epsilon_r/d$ is the capacitance per unit area. If ξ=$\sqrt{|\sigma_{xx}|/(C_g\omega)}$=$\sqrt{|\sigma_{xx}|d/\epsilon_0\epsilon_r}$$\ll w$, the microwave electric field is mainly confined in the slots, and the shunt capacitance ($C_c^{'}$ term) has negligible contribution compared to that of the shunt conductance (G' term, where G'=$2\sigma_{xx}/w$ is conductivity per unit length of the 2DES under both slots (thus the factor of 2)). In this case the CPW simply acts as contacts to 2DES.

3) the 2DES is in its long wave length limit;

one has the following simple relation between the relative power absorption (P) of the 2DES and its real part of diagonal conductivity (Re[σ_{xx}]):

$$P = \exp((2lZ_0/w)\mathrm{Re}[\sigma_{xx}]) \tag{2.1}$$

In most of situations, the above conditions are satisfied and this allows Re[σ_{xx}] to be readily extracted[5]. An exception is in Chapter 5, where as will be seen, the 2DES (in the "A" phase) is not in its long wavelength limit. However, even in such situations we still cast our measured P, into a real diagonal conductivity which we define Re[σ^c_{xx}]=$(w/2lZ_0)\ln(P)$. In this thesis we always present our data in the form of Re[σ_{xx}] (or Re[σ^c_{xx}]), with the understanding that it is the absorption P that we have measured in our experiments.

In Fig. 2.3 we demonstrate representative CPW electric field profiles (see the figure caption for more details). Under the condition $\xi \ll w$, the CPW confines the electric field (E) mainly in each slot region, giving E a step function profile (neglecting edge effects related to the 2DES, as seen in Fig. 2.3. See also Fogler and Huse (2000)). This introduces a finite wavevector in the measurement through the dominant Fourier component $q \sim \pi/w$. However, if the correlation length[6] of the WC is much smaller than w, (which is often the case, except for the "A" phase introduced in Chap. 5) the 2DES solid is effectively subjected to a uniform electric field, meaning it is in the $q \sim 0$ limit.

The meander shaped CPW is commonly used to obtain larger geometric factors ($2l/w$) therefore increasing the strength of absorption signal (P), as seen from Eq. 2.1. Straight line CPWs have also been often used in our experiments, mainly to examine the effect of orientation of microwave field $\vec{E}$, or to investigate dispersion (w depen-

[5]The accuracy is typically within 10-15%, by comparing with more elaborate numerical analysis (Engel *et al.*, 1993) or with known sum-rules of the pinning mode resonance (see Chapter 3).

[6]More specific meanings of the "correlation length" will be discussed in later chapters.

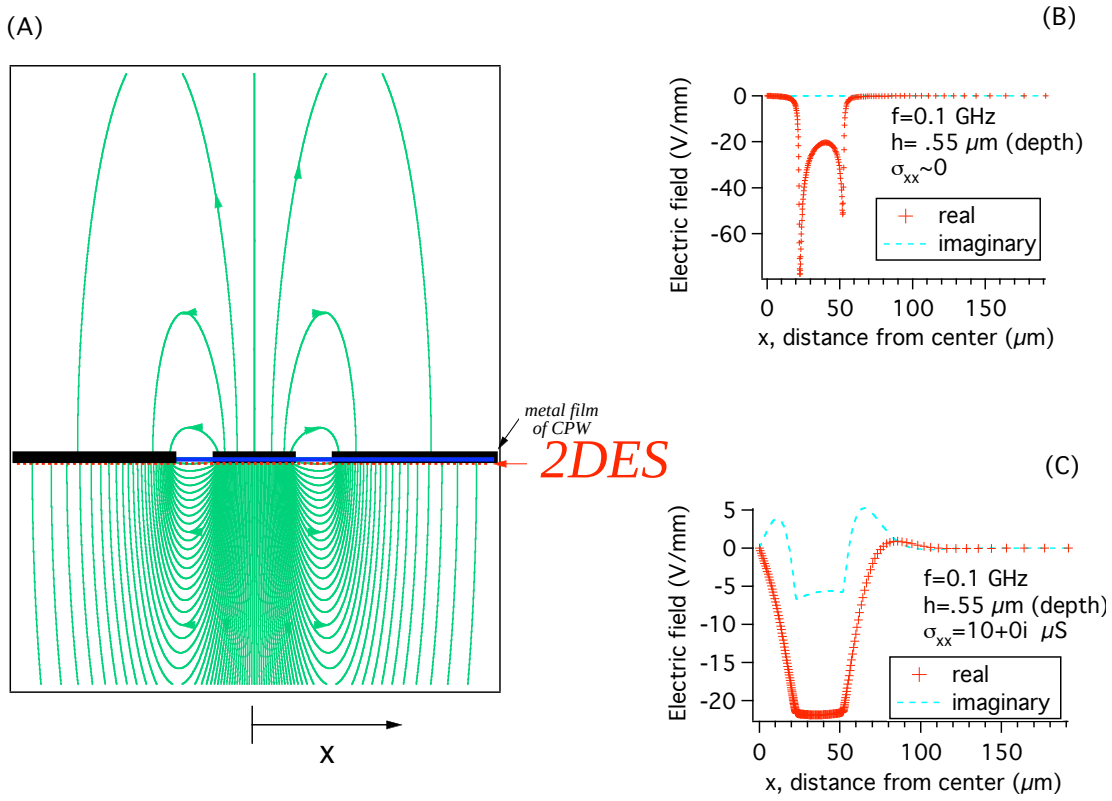

Figure 2.3: Calculated CPW electric field profiles (data from L. W. Engel). **(A)**: Scheme of the electric field lines near the CPW. **(B)**: An example of the spatial profile of the electric field in the plane of the 2DES, when the CPW is unloaded (i.e., with negligible 2DES conducvitity). The field is calculated for a meander CPW ("M30") and for the typical parameters of sample QW65 (see Appendix C). x is the distance (along the direction transverse to the local CPW center conductor) away from the center, as illustrated in (A). **(C)**: An example of the spatial profile of the electric field in the plane of the 2DES, calculated similarly as in (B) except that the CPW is loaded by the 2DES (with 10μS of conductivity).

dence)[7] effects when the 2DES is not in the long wavelength limit. Various CPW's used for all the samples are summarized in Table D.1 in Appendix D.2 (specific CPW information for each sample is also given when discussing the data later).

Since in our experiments, the analyzer measures the relative power transmission P_t through the entire circuit (Fig. 2.1), proper normalization is required to extract the contribution due to the 2DES. This is especially necessary when measuring the f-dependence, because there is usually a significant f-dependence in the microwave attenuation not associated with the 2DES, mainly that due to the coaxial cable. Thus a "reference" transmission P_0, is normally measured, in the limit of vanishing 2DES conductivity (i.e., vanishing absorption due to the 2DES). Such a reference can be obtained, for example, when the 2DES is depleted (other examples will be given in Sec. 2.2.3 and later chapters). With the normalization, we simply have[8] $P{=}P_0/P_t$, or if related to $\mathrm{Re}[\sigma_{xx}]$, $\mathrm{Re}[\sigma_{xx}] = -\frac{w}{2lZ_0}\ln|P_t/P_0|$.

A picture of the sample mounted on a metal block is shown in Fig. 2.4. The block is either immersed in the ^{3}He-^{4}He mixture in a dilution refrigerator (DF) or kept in good thermal contact with the DF mixing chamber. Custom-made semirigid SiO_2 dielectric coax cables with low microwave loss and low thermal conductivity were used to transmit microwaves between the top of the cryostat (300K) and the sample (block). In typical measurements the microwave input is kept in the low power limit, by reducing the power till the measured signal (P) no longer changes. More information can be found in Appendix E about the setup in the NHMFL, where we have used three different cryostat/magnet systems: "C120", a vacuum-loading DF with sample base $T{\sim}$ 35 mK and a 14 Tesla superconducting magnet (16T if pumping a λ plate); "SCM1", a top-loading DF with sample base $T{\sim}$50 mK and a 18 Tesla superconducting magnet (20T if pumping a λ plate); and "PDF", a top-loading "portable dilution fridge" with sample base $T \sim 60$ mK, placed in either a 33 Tesla

[7]For larger w, it is easier to fabricate straight CPW than the meander one.

[8]Note we have defined earlier P as relative *absorption*, which is the reciprocal of *transmission*.

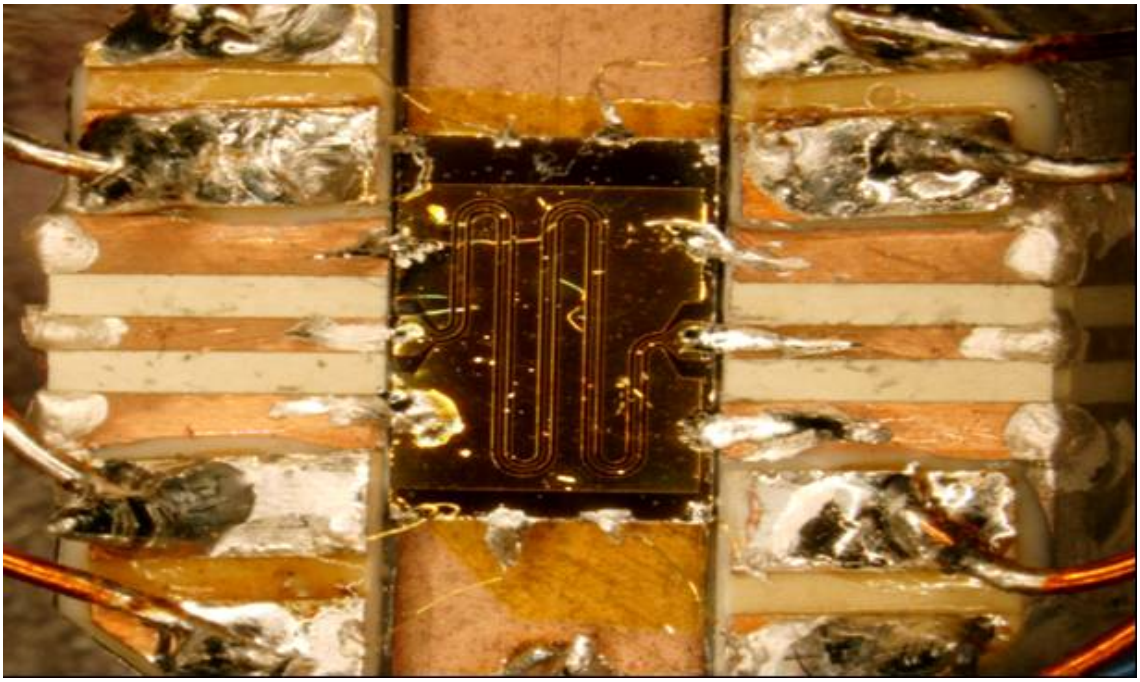

Figure 2.4: Picture of a sample mounted on a block. The sample is $\sim 3\times5$ mm in size and is equipped with a CPW ("M60") of l=15.5 mm and slot w= 60 μm. The CPW on the sample is joined by "indium bridges" to the circuit-board CPW on the block. The circuit board CPW further mates (mechanically via pressed pins) to the semirigid coax at the side of the block (not shown). Also seen are (gold) DC wires making connection to the (indium) ohmic contacts on the sample.

resistive magnet or a 45 Tesla hybrid magnet.

We typically perform two types of measurements:

1) Fix frequency f, sweep magnetic field B. This basically measures the AC magneto conductivity and gives what we call a "B-trace" that is often analogous to the usual quantum Hall trace.

2) Fix B, sweep f. This is the spectroscopy mode of the measurements and the resulted spectra are also called "f-trace".

Although both mode of measurements were routine and will be discussed briefly in the next two subsections, the spectroscopy is our main tool, with which the majority of the data presented in this thesis were measured.

2.2.2 AC Magneto-conductivity

AC magneto-conductivity (B-traces) are mainly measured to provide "orientation" for the broad-band spectroscopy studies on a sample. In particular, we extract the 2DES density n from the SdH oscillations or QHE minima in the measured B-trace[9].

Fig. 2.5 shows an example of such AC magneto-conductivity measured on sample R (30nm QW). Despite the relatively challenging environment of the hybrid magnet cell in which the measurement was done, the trace clearly shows many FQH states. A feature is even seen at ν=4/11, one of the high order FQH states[10] so far only identified in the best quality DC transport data (Pan *et al.*, 2003).

Because the AC response of the coaxial cable has negligible B dependence, we usually do not need to normalize the measured B-dependent "raw" absorption data. This simply introduces a constant offset in the B-trace but does not affect the identification of physically significant features (such as QHE states) in it. Also, if we are mainly interested in locating the quantum Hall states, B-traces are often measured at slightly elevated microwave power, which gives better signal to noise ratio.

More examples of B-traces, measured on other samples, can be found in Appendix F.

2.2.3 Spectroscopy

The work in this thesis are mainly based on measurements of spectra, and we have seen in Chapter 1 (Fig. 1.1) some examples of $\mathrm{Re}[\sigma_{xx}(f)]$.

As mentioned earlier, appropriate normalization of the "raw" transmission data by a certain "reference" transmission ($P_0(f)$) is usually needed in measuring the f-traces ($\mathrm{Re}[\sigma_{xx}(f)]$). The most obvious choice of the reference spectrum is measured when the 2DES is completely depleted. If total depletion is not attainable, $P_0(f)$

[9]We normally fit the QHE minima positions (B) against the expected $1/\nu$ and extract n from the slope.

[10]thought to be due to FQHE of composite fermions (CF)

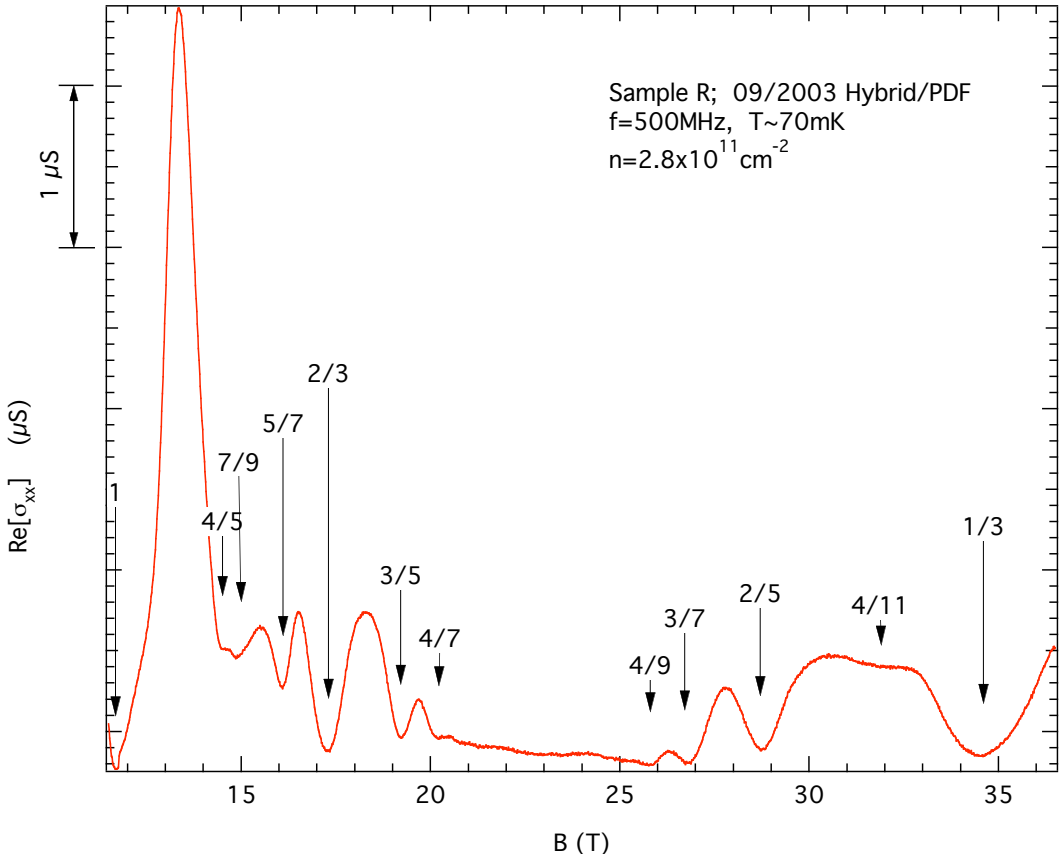

Figure 2.5: Representative B-trace measured from a piece of Sample R (30 nm QW). The CPW used was a meander "M30" (Appendix. D). Selected filling factors are labeled.

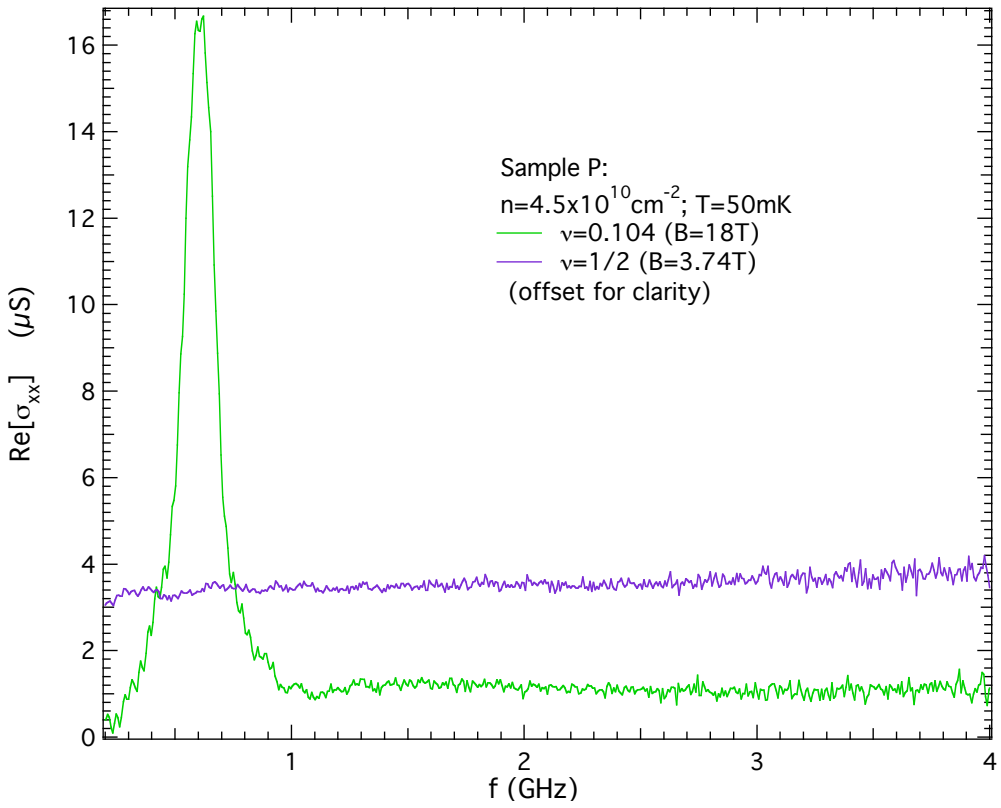

Figure 2.6: Spectra measured in Sample P. Normalized by the reference transmission obtained at full depletion of 2DES, the spectrum at ν=1/2 is nearly flat, and that at ν=0.104 (WC regime) shows a clear resonance.

can be estimated from the transmission measured under condition under which the transmission is expected to have a weak f dependence. One of the most commonly used "reference" conditions is at ν=1/2, which typically has a nearly flat spectrum relative to the depletion reference, as demonstrated below in Fig. 2.6 for Sample P.

Other possible reference conditions include that at IQHE minima, at other half fillings such as $\nu = 3/2$, at high power, or at high enough temperature (at which electron solids have melted). Examples of references as such will be encountered in later chapters. Obviously, what constitutes a good reference may very much depend on the specific situation at hand. For example, $\nu\sim1/3$ may be a good reference for the pinning mode resonance in WC (see Fig. 1.1). However, if one were to study the

weak f dependence around ν=1/3 itself, other references at conditions sufficiently different from ν=1/3 should be used (preferably a depletion reference). It is not uncommon, especially for relatively weak resonances or f-dependent features, to use several different references to check the consistency of the experimental findings.

2.3 Additional Notes and Further Directions

Many further developments in our CPW-based measurement technology can be imagined (some are currently being implemented), such as extending the frequency range (so far we have from $\sim$ 20 MHz to 20 GHz), extending the finite-q measurement capability (so far we have successfully used slot width w ranging from $\sim$20 μm to 80 μm, where w defines a $q\sim \pi/w$), compatibility and more versatility with gates[11], improvement in the electron cooling and cold-sinking of coax center conductor, ability of rotating the sample/block etc. Some of these issues are breifly discussed in Appendix D as well. Such technical developments may enable probing additional new physics than presented in this thesis and we will make some "glimpses" in later chapters on such opportunities.

In terms of measurements and data extraction, further improving the measurement sensitivity and accuracy can have particular benefits for quantities such as the resonance amplitude and integrated intensity (S). It can also be potentially interesting to look at the imaginary part of σ_{xx} (also briefly discussed in Appendix D, see also Li *et al.* (1995a)) jointly with Re[σ_{xx}] (on which we have so far focused).

[11]It is also interesting to perform the microwave measurements with CPW (used itself as front gate) biased at a nonzero DC voltage relative to the 2DES (particularly when depleting the 2DES under the CPW).

Chapter 3

Properties of the Pinning Mode

The kind of resonance (in $\mathrm{Re}[\sigma_{xx}(f)]$) of which we gave examples earlier (Sec. 1.2.2,and Sec. 2.2.3) is identified as the pinning mode of the WC (Li *et al.*, 1997; Ye *et al.*, 2002b)[1] and is our main tool in this thesis to study the electron solids. We give in this chapter a brief account of current physical understanding of the pinning mode and illustrate some of its properties with data in high-B WC. As will be seen, the pinning mode, as a signature of a disordered WC, reflects both the electron-electron interaction (which drives Wigner crystallization) and electron-disorder interaction (which pins the WC). Studying the pinning mode may enable us to learn important information about disorder, such as what actually pins the WC, and the characteristics of such disorder. In the next three chapters (4-6) we will also employ the pinning mode to study some more "intrinsic" physical properties of the electron solids[2].

[1] See also Sec. 7.1 for a recollection of key features of the resonance supporting its identification as the pinning mode.

[2] The "0th order" physics highlighted in these three chapters, in fact, mostly relies just on the appearance and disappearance of the pinning mode resonance.

3.1 Pinning Mode and Disordered Wigner Crystal

In this section we review some important physical concepts drawn from the major theoretical developments over the past 20 years (Bonsall and Maradudin, 1977; Fukuyama and Lee, 1978; Normand *et al.*, 1992; Fertig, 1999; Fogler and Huse, 2000; Chitra *et al.*, 2002) relevant to the pinning mode. They will be discussed in the context of our current experimental knowledge[3], aiming for a coherent physical picture, to understand the nature and behavior of the pinning mode, in terms of the static and dynamic properties of a WC subject to disorder.

A more succinct summary of the major results relevant to the current understanding of the pinned WC can also be found in Appendix K.2.

Of the properties of the pinning mode resonance, the peak frequency ($f_{\rm pk}$) is particularly interesting to us. It is the quantity that can be extracted most accurately in experiments and has been calculated explicitly by theories. As we will soon see, the behavior of $f_{\rm pk}$ can directly yield information about disorder. Other quantities, such as the line width and oscillator strength (integrated intensity), also contain important information about the pinned WC.

3.1.1 Magneto-phonon of WC

A pinning mode, in essence, is the *collective* oscillation of the pinned WC around disorder. It can also be viewed as the disorder-gapped magneto-phonon excitation of the WC, and the gap is simply the experimentally measured pinning mode peak frequency in the long wavelength limit.

The following block diagram (Fig. 3.1) schematically illustrates the origin of the magneto-phonon[4]. A clean 2D WC (Bonsall and Maradudin, 1977) has two phonon

[3]We will, however, refrain from a full-blown discussion of all related experimental details, since the focus of this thesis is on the phases and physical properties of quantum electron solids (Chap. 4-6)

[4]Realistic, calculated curves can be found in Bonsall and Maradudin (1977); Fukuyama and Lee (1978); Normand *et al.* (1992).

branches, the longitudinal mode $\omega_L(q)$, (basically the plasmon mode, which exists in 2DES in general), and the transverse (shear) mode $\omega_T(q)$ (one of the main characteristics of a solid). For the typical experimentally accessed q, $\omega_T \ll \omega_L$ (see Appendix A for representative values).

In the presence of a perpendicular B, the Lorentz force mixes the longitudinal and transverse motion and gives rise to two hybridized branches: $\omega_+(q)$ and $\omega_-(q)$, given by the following expression (Normand *et al.*, 1992; Klironomos and Dorsey, 2005)

$$\omega_\pm^2 = \frac{1}{2}(\omega_c^2 + \omega_L^2 + \omega_T^2) \pm \frac{1}{2}\sqrt{(\omega_c^2 + \omega_L^2 + \omega_T^2)^2 - 4\omega_T^2\omega_L^2} \tag{3.1}$$

The high-lying[5] $\omega_+(q)$ is gapped at the cyclotron frequency ω_c, typically above the microwave frequency range (see Appendix. A) and does not concern us in this thesis. The low lying $\omega_-(q)$, or the "magneto-phonon" mode, is gapless and at high fields ($\omega_c \gg \omega_L, \omega_T$, which is easily satisfied in realistic situations), it has the simple expansion

$$\omega_-(q) = \omega_L(q)\omega_T(q)/\omega_c \tag{3.2}$$

which gives a $q^{3/2}$ dispersion and clearly reflects the mixing of longitudinal and transverse modes.

In the presence of disorder, this low lying magneto-phonon mode is gapped and becomes the pinning mode[6]. The dispersion of magneto-phonon is now (Normand *et al.*, 1992)

$$\omega_-(q) = \frac{\sqrt{(\omega_0^2 + \omega_L^2(q))(\omega_0^2 + \omega_T^2(q))}}{\omega_c} \tag{3.3}$$

where ω_0 is a phenomenological "pinning frequency" that reflects the strength of the pinning disorder.

In the long wavelength limit ($q \sim 0$, the case most studied in theoretical calculations

[5] basically the magneto-plasmon mode

[6] Disorder also slightly modifies the gap of the ω_+ (Chitra *et al.*, 2002).

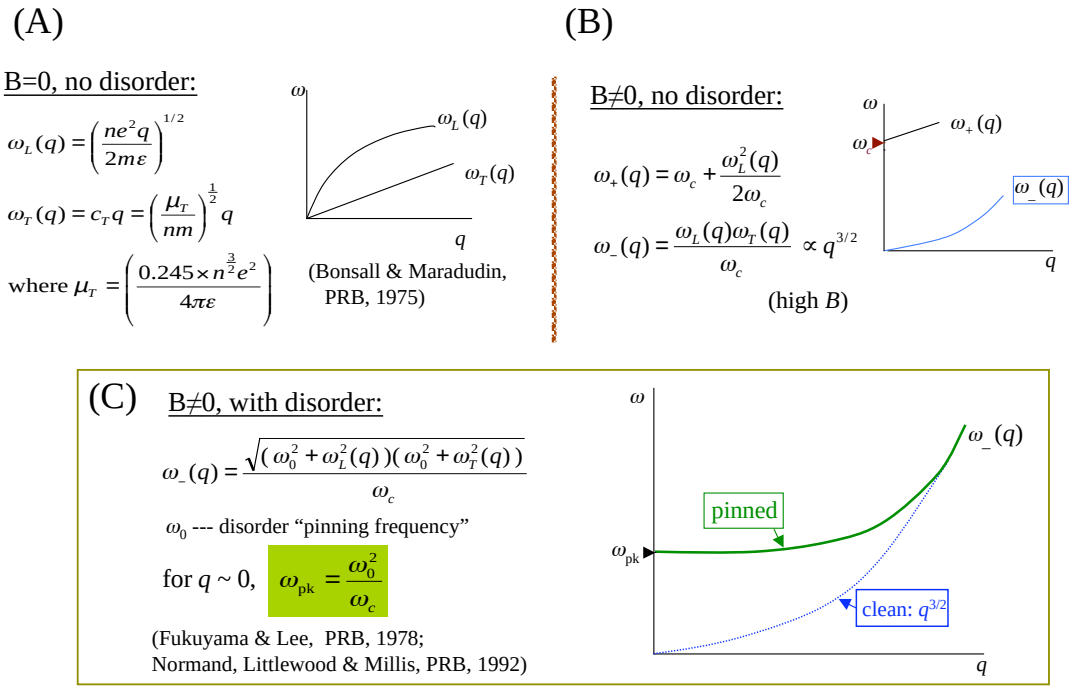

Figure 3.1: Schematics (not real calculations) of phonon modes in 2D WC. (A) Zero-B Clean 2D WC: Longitudinal phonon (plasmon) and transverse (shear) phonon modes. The formula shown for the shear modulus (μ_T) is based on calculations for classical WC (Bonsall and Maradudin, 1977). (B) Clean 2D WC in perpendicular B: magneto-plasmon ($\omega_+(q)$) and magneto-phonon ($\omega_-(q)$) modes. (C) Disordered 2D WC in perpendicular B: gapped magneto-phonon mode (pinning mode). Magneto-plasmon mode is not drawn.

(Fukuyama and Lee, 1978; Fertig, 1999; Fogler and Huse, 2000; Chitra *et al.*, 2002) as well as experimental measurements[7]), the mode is at the gap frequency:

$$\omega_{pk} = \omega_0^2/\omega_c \tag{3.4}$$

and manifests itself as a resonant power absorption (equivalently, a resonance in $\mathrm{Re}[\sigma_{xx}(f)]$) when the WC is subject to a *spatially uniform* AC electric field at the mode frequency. In the "classical" theories of the pinning mode (Fukuyama and Lee, 1978; Normand *et al.*, 1992), ω_0 is a constant that models an effective[8], *harmonic* disorder potential[9,10]. This results in a $\omega_{\mathrm{pk}} \propto 1/B$. Experiments on pinning mode resonance have observed an f_{pk} ($=\omega_{\mathrm{pk}}/2\pi$) that increases with increasing B (Li *et al.*, 1997), in contradiction with the predicted "classical" WC behavior. To resolve this issue (at least partially), one needs to consider the interplay (Fertig, 1999; Fogler and Huse, 2000; Chitra *et al.*, 2002) between the electron wave function in the WC with disorder, as we discuss in the next subsection.

3.1.2 Interplay of WC and Disorder; B-dependence of f_{pk}

The interplay of WC and disorder underlies the entire physics of the pinned WC. From a "philosophical" point of view, when considering a quantum[11] WC of density n subject to a disorder $V(r)$, and (as the default case for us) placed in a high B, we have at hand three "intrinsic" and "microscopic" length scales[12]:

[7] The full dispersion of magneto-phonon (particularly at large wave vectors) is so far not accessible in our experiments.

[8] Note this is an "collective" *effective*(a highly abused word!) potential that the WC feels, and is *not* the same concept as the more "microscopic" effective disorder potential to be discussed in the the next Subsection 3.1.2.

[9] As a matter of fact, one can show rather generally, using a simple classical mechanics model, that 2D electrons in any harmonic potential ($\frac{1}{2}m_e\omega_0^2 r^2$ per electron) placed in high B would have a low lying collective mode at $\omega = \omega_0^2/\omega_c$ (Li, 1999).

[10] Another physical meaning of ω_0 is that it corresponds to the pinning mode frequency at B=0 (note the high-B expansion 3.4 no longer applies there)

[11] by this we mean the constituent electrons have wavefunctions rather than being point charges

[12] not to be confused with the correlation lengths of WC, to be discussed in Sec. 3.1.5.

1) the lattice constant (related to the separation between electrons) $a \sim 1/\sqrt{n}$;

2) the magnetic length (which is a measure of the single electron wavefunction size) $l_B = \sqrt{\hbar/eB}$;

3) the disorder correlation length ξ_0 (exact definition of ξ_0 will be given shortly).

In principle, the interplay of WC and disorder involves all three quantities. We note here that a (or n) reflects the electron-electron interaction, and l_B is a single electron *quantum* parameter. The ratio of l_B and a, which is basically the Landau filling ν ($\nu \propto (l_B/a)^2$), reflects many-body quantum correlation between electrons (Maki and Zotos, 1983). We start here with the interplay between l_B and ξ_0, which is the interplay of WC and disorder on a quantum single-particle level, as considered in recent theories on pinned WC (Fertig, 1999; Fogler and Huse, 2000; Chitra *et al.*, 2002). In sec. 3.1.3 we will discuss interplay of n and disorder, an interplay which can be understood classically, as due to effects of elasticity within a "weak pinning picture" (Fukuyama and Lee, 1978; Chitra *et al.*, 2002)). Later in the thesis we will also see that *many-body* quantum correlation is still important in the high-B WC (despite $\nu \ll 1$) from our experimental findings. However, quantum many-body effects in pinned WC have so far remained largely un-addressed by theories.

The interplay between single electron wave functions and disorder, or between l_B and ξ_0, can be understood qualitatively from Fig. 3.2, where locally, the disorder (of correlation length ξ_0) is illustrated a "bump" of characteristic size ξ_0. The physical essence is that, the effect of disorder on the electron is sensitive to l_B (electron wavefunction size) if $l_B > \xi_0$, in which case the overlap between the "bump" and the electron wavefunction evidently increases if l_B shrinks; however, in the opposite regime ($l_B > \xi_0$), further compressing l_B (increasing B) brings little change to the effect of the disorder on the electron. The above idea can be made more precise using the important concept of "effective disorder" for electrons.

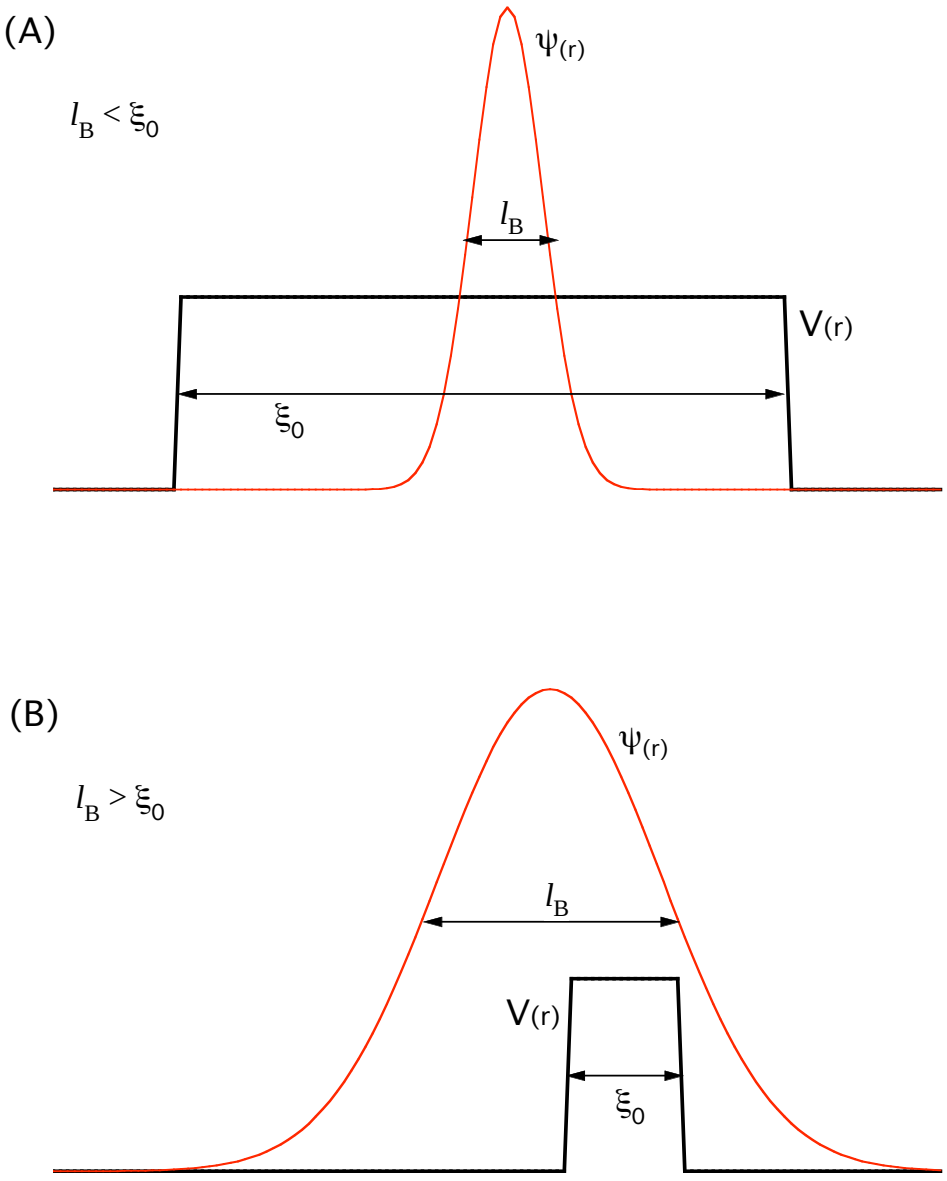

Figure 3.2: Illustration of interplay of electron wavefunction (of size l_B) and disorder (with characteristic correlation length ξ_0). Here the disorder is simply modeled as a "pit" (bump) with length scale ξ_0. (A) $l_B<\xi_0$: compressing l_B does not change the overlap between the electron wavefunction (ψ) and disorder, thus does not change the *effective disorder* that electron feels. (B) $l_B>\xi_0$: compressing l_B increases the overlap between electron wavefunction and disorder, thus the *effective disorder* is stronger.

Concept of Effective Disorder

Here we use $V_0(r)$ to denote the "physical disorder" that is independent of any electronic state ($V_0(r)$ is present in the sample even without electrons). It has been shown that what determines the pinning of WC, is an "effective disorder" $V_{\text{eff}}(r)$ which depends on the electronic state. More specifically (Fertig, 1999; Fogler and Huse, 2000; Chitra *et al.*, 2002), $V_{\text{eff}}(r)$ is defined as the physical disorder $V_0(r)$ convoluted with the appropriate electron form factor (which is basically $|\psi(r)|^2$, where $\psi(r)$ is the single electron wavefunction. In the LLL, this is simply a Gaussian with size l_B). Such convolution is essentially averaging the physical disorder $V_0(r)$ using the electron form factor ($|\psi(r)|^2$) as a "kernel" (Fogler and Huse, 2000). If $l_B<\xi_0$, the averaging results in a $V_{\text{eff}}(r)$ that is essentially still the same[13] as $V_0(r)$. However, if $l_B>\xi_0$, convoluting $V_0(r)$ with $\psi(r)$ tends to "smooth out" any short length scale (shorter than l_B) variation in $V_0(r)$, and the resulted[14] $V_{\text{eff}}(r)$ has its correlation length given by l_B instead of by ξ_0.

The interplay of l_B and disorder profoundly affects the B-dependence of the pinning mode peak frequency (f_{pk}). An analytic formula for f_{pk} is derived in (Chitra *et al.*, 2002), assuming a *Gaussian-correlated white noise*[15] disorder ($V_0(r)$):

$$f_{\text{pk}} = C\frac{W}{\xi^6}\frac{1}{\mu_T}\frac{1}{B} \tag{3.5}$$

In the above equation, C is some constant involving only charge e, μ_T is the shear modulus of the WC (at sufficiently small ν, it is thought to be close to the classical value (given in Fig. 3.1, as calculated by Bonsall and Maradudin (1977)) and only depends on n). W and ξ are disorder strength and disorder correlation length, defined

[13] This can be best understood in the limit of $l_B \ll \xi_0$, where $\psi(r)$ acts like a delta-function to $V_0(r)$, and recall that convolution with a delta function leaves any function unchanged ($V * \delta = V$).

[14] Again, this is best understood in the limit $l_B \gg \xi_0$, where $V_0(r)$ now acts like a delta-function, and $\delta * \psi = \psi$.

[15] We will come back to this point later in Sec. 3.1.4 and 3.2.2. The Gaussian white noise assumption will be shown, in fact, likely to be incorrect in realistic samples.

via the two-point correlator

$$\langle V(\vec{r})V(\vec{r}')\rangle = W D_\xi(|\vec{r}-\vec{r}'|) \tag{3.6}$$

where $D_\xi(r)$ is the correlation function with characteristic decay length ξ. In our case, the Gaussian white noise simply means $D_\xi(r)$ is a Gaussian ($\sim e^{-r^2/\xi^2}$). Most importantly, the V above should be understood as the effective disorder $V_{\rm eff}$. Therefore[16]: ξ=max(l_B,ξ_0).

In the so called "quantum regime" (l_B>ξ_0, Chitra *et al.* (2002)), $f_{\rm pk}$ is expected to *increase* (the above formula 3.6 predicts $f_{\rm pk}\propto B^2$) with increasing B , which is also qualitatively consistent with the picture we had in Fig. 3.2. In the "classical regime" (l_B<ξ_0), the above formula predicts $f_{\rm pk}\propto 1/B$, which is consistent with earlier "classical" theories on pinning mode of the WC (Fukuyama and Lee, 1978; Normand *et al.*, 1992).

As will be seen later, the actual B-dependence of $f_{\rm pk}$ found in experiments can be quite complicated[17] and it is possible that more than one type of disorder (with more than one characteristics lengths) can be present in real samples (Appendix. H). However, the idea of an interplay between l_B and ξ_0 gives a useful framework to understand the data, and very importantly, allows probing the disorder from the behavior of $f_{\rm pk}$ vs B (see also Sec. 3.1.4). An example, for the case of a narrow quantum well (QW15), will be presented in Sec. 3.2.2.

Comparing Eq. 3.5 and Eq. 3.4 shows that ω_0 (the effective harmonic pinning frequency of the *deformed* WC (Sec. 3.1.1)) is $\propto\frac{W/\xi^6}{\mu_T}$. The numerator represents the effect of disorder and the denominator represents the WC stiffness (μ_T, the shear modulus, which is larger for higher n, i.e, stronger Coulomb-interaction) and they

[16]One can show mathematically, that a Gaussian white noise disorder (with strength W and correlation length ξ_0) convoluted with ψ (also a Gaussian) is still a Gaussian white noise with basically the same W. However the resulted $\xi\sim$max(l_B,ξ_0)

[17]Especially for the heterojunction sample P (Appendix. H). The cases for narrow (Sec. 3.2.2) and wide quantum wells (Chap. 5, Appen. J) will be seen later in the thesis.

compete with each other in determining $f_{\rm pk}$. This leads to the concept of *weak pinning*, discussed in the next subsection.

3.1.3 Weak pinning and n-dependence of $f_{\rm pk}$

At fixed B, if one lowers n, this reduces electron-electron interaction and makes WC softer (i.e, reducing shear modulus μ_T); thus electron-disorder interaction is *relatively* promoted (electrons "fall deeper into the disorder") and the WC becomes more pinned, resulting in a increase in $f_{\rm pk}$. This phenomenon that softer crystal is pinned more (and stiffer crystal is pinned less) is known as "weak pinning"[18] (Fukuyama and Lee, 1978) and is directly reflected by $f_{\rm pk}\propto 1/\mu_T$ seen in Eq. 3.5. For a classical WC made of point charges (thought to be also a good approximation for MIWC at sufficiently high B), its μ_T is calculated to be $\propto n^{3/2}$ (Fig. 3.1, and Bonsall and Maradudin (1977)) thus $f_{\rm pk}\propto n^{-3/2}$ is predicted (Chitra *et al.*, 2002).

Experimentally, the n-dependence of $f_{\rm pk}$ was studied earlier by Li *et al.* (2000a). The $f_{\rm pk}$ was found to increase with decreasing n (n is lowered by a backgate), which we also found on our samples[19]. This is qualitatively consistent with the weak pinning picture. However, so far various powers γ ($f_{\rm pk}\propto n^{-\gamma}$) have been observed and γ is often seen to decrease with decreasing n (from closer to 3/2 at higher n to close to 1/2 at lower n, see for example Li *et al.* (2000a) or our data for Sample P in Appen. H). No definite explanations have been found for this. Possibilities include some n-induced loss of pinning (at low n), crossover to strong-pinning[20] at low n, or complications related to μ_T.

[18] Meaning that the disorder is sufficiently weak so that it does not localize any individual electron, but rather *deforms* the WC against its rigidity and localize electrons collectively.

[19] Preliminary data by G. Sambandamurthy *et al.* for sample P found $f_{\rm pk}$ to decrease with decreasing n at extremely low n ($\lesssim 0.9\times10^{10}{\rm cm}^{-2}$). Further investigation is clearly needed.

[20] meaning part of the WC is pinned by disorder at certain spatial location (like being nailed) and oscillate around it, in which case the WC elasticity acts like spring constant and $f_{\rm pk}$ is expected to decrease with decreasing n

3.1.4 Effect of Disorder Statistics

There is no a-priori reason to believe, that the disorder in real samples would necessarily obey the Gaussian-correlated white noise statistics (Sec. 3.1.2), which was assumed in Chitra *et al.* (2002) to facilitate analytical derivations. In fact, Fertig (1999) proposed that relevant disorder to pin the WC to be some *dilute* "pits"[21] (roughness) at the interface with typical size (ξ_0) on the similar order with l_B. With such disorder, Fertig investigated (mainly through numerical simulation) the expected dependence of $f_{\rm pk}$ on B. For $l_B<\xi_0$ (the "classical regime"), one still expects $f_{\rm pk}\propto 1/B$ on fairly general grounds (when $l_B<\xi_0$, the microscopic effective disorder is the same as the physical disorder, regardless of its statistics, and the only B-dependence in $f_{\rm pk}$ comes from the classical effect of Lorentz force, see also footnote 9) and is the same behavior as in (Eq. 3.5); for $l_B>\xi_0$ (quantum regime), however, he found[22] $f_{\rm pk}$ to increase nearly linearly with increasing B, different from the B^2 dependence found in the white-noise case (Eq. 3.5). Physically, the linear-B-dependence of $f_{\rm pk}$ in the quantum regime can be understood as follows (see also Fig. 3.2(B)): when the "pits" (bumps) are *dilute*, the decrease of l_B increasing the effective disorder (due to increasing overlap between the electron wavefunction ψ and the disorder potential) would only occur if there is an overlap between ψ and the pit to start with; so that the effective disorder strength in Eq. 3.5 needs to be scaled with a factor that is proportional to l_B^2 (the area under the electron wavefunction) to account for the finite probability for the electron to encounter a "pit" overlapping with its wavefunction. In constrast, for white noise disorder, ψ is always subject to the disorder and the probability factor would be 1 (see also footnote 16). Therefore Eq 3.5 should be modified, such that now

$$f_{\rm pk} \propto \frac{W l_B^2}{l_B^6}\frac{1}{\mu_T}\frac{1}{B} \propto B$$

[21] More about this in Sec. 3.2.2

[22] See Sec. 3.2.2 for more details.

in the quantum regime ($l_B > \xi_0$) for "dilute pits" disorder[23].

Thus, although the qualitative features of the interplay of single electron wavefunction with disorder as illustrated in Fig. 3.2 are likely to hold quite generally, specific disorder statistics can affect the B-dependence of $f_{\rm pk}$ in the quantum regime ($l_B > \xi_0$), due to the difference in how the physical disorder is averaged by the electron wavefunction. This offers an opportunity to experimentally probe the disorder statistics by carefully studying the pinning mode behavior. As we will see later (Sec. 3.2.2), dilute disorder, mainly near or at the interface (like the "pits" proposed by Fertig (1999)), is likely to be a picture closer (than the Gaussian correlated white noise) to the actually disorder responsible for the pinning of the WC in a real sample (QW15).

3.1.5 Correlation lengths in WC

In the presence of any disorder[24], a 2D WC will be deformed (from the ideal triangular lattice) and lose the long range positional order (Imry and Ma, 1975; Chitra *et al.*, 2002). Thus the WC breaks into domains with finite correlation length (domain size). One obvious correlation length is the "Fukuyama-Lee" length (Fukuyama and Lee, 1978; Normand *et al.*, 1992), denoted as L_a, which is defined as the length scale at which the average deviation[25] of electrons in WC from their ideal positions (clean WC) becomes comparable to the lattice constant a. Although L_a corresponds to the intuitive WC "crystallite" size in the polycrystalline picture of a pinned WC, it is in fact not the relevant correlation length for the pinning mode properties. Instead, the Larkin length (Fertig, 1999; Fogler and Huse, 2000; Chitra *et al.*, 2002) and magnetophonon localization length (Fertig, 1999; Fogler and Huse, 2000), discussed in the following, are now thought to determine $f_{\rm pk}$ and linewidth (Δf) of the pinning

[23]The more precise formula Fertig (1999) derived is given in Sec. 3.2.2.

[24]We suppose it is not so strong that it destroy the WC order completely

[25]Here we imagine undeformed lattice points as $\vec{R}_i$ and the deformed lattice as $\vec{R}'_i$. Fix one lattice point (say $\vec{R}_0$) as the origin, as one moves outward, the average deviation $<|\delta\vec{R}_i|>=<|\vec{R}'_i\text{-}\vec{R}_i|>$ generally grows with increasing distance $R=|\vec{R}_i|$.

mode respectively.

Larkin length (L_c)

The Larkin length (L_c) is a *static* correlation length of the WC, and is defined as the length scale at which the average deviation of electrons in the WC from their ideal positions (clean WC) becomes comparable to the *effective* disorder correlation length ξ. It is a concept that had been well developed in the context of pinned vortices in superconductors (Blatter *et al.*, 1994) and physically, L_c represents the length scale that the WC " fully feels the effect of the disorder", and reflects the balance between pinning and elasticity (static deformation). One can show (Fogler and Huse, 2000; Chitra *et al.*, 2002) that L_c is directly related to $f_{\rm pk}$ of the pinning mode as[26]

$$L_c = \sqrt{\frac{2\pi\mu_T}{neBf_{\rm pk}}} \tag{3.7}$$

where μ_T is the shear modulus (Sec. 3.1.1).

In our samples, the typical L_c is on the order of 1 μm (see Appendix A). The afore-mentioned Fukuyama-Lee length (WC domain size) L_a can be related to L_c as $L_a{\sim}L_c(a/\xi)^3$ (Chitra *et al.*, 2002). Since in WC, typically[27] $\xi{\ll}a$ so we have[28] $L_a{\gg}L_c$.

[26]This can be obtained by simply equating $\omega_T(q_c)$ and pinning frequency ω_0, where $q_c{=}2\pi/L_c$ is the effective wave vector set by L_c and ω_T comes from the fact that the main static deformation comes from the shear deformation, because the appropriate longitudinal (compressional) modulus of WC is typically much larger than the shear modulus as a result of long range Coulomb interaction (Fogler and Huse, 2000; Chitra *et al.*, 2002).

[27]$\xi{=}\max[l_B,\xi_0]$. We have $l_B{\ll}a$ and also, as it turns out (Fertig (1999), and see Sec. 3.2.2), $\xi_0{\ll}a$.

[28]This is in contrast to a conventional 2D charge density wave (Fukuyama and Lee, 1978; Grüner, 1994), where the charge modulation occurs sinusoidally on the length scale of the "lattice constant" a (whereas for a WC, $l_B{\ll}a$), so the effective disorder correlation length [recall that the convolution of physical disorder ($V(r)$) with the sinusoidal form factor ($e^{2\pi ir/a}$) in CDW is the same sinusoidal factor ($e^{2\pi ir/a}$) multiplied by the Fourier component of the physical disorder at $2\pi/a$]. Hence $\xi{=}a$ and $L_c{=}L_a$.

Magnetophonon localization length (L_B)

The observed pinning mode resonance of MIWC can have quality factor Q ($=f_{\rm pk}/\Delta f$, where Δf is the full width at half maximum) as high as 10 (Li *et al.*, 1997). One prominent question is: why is the resonance so sharp? Naively, one expects the mode to be broadened by random disorder and to have $Q\sim1$ (Fukuyama and Lee, 1978). The reason for the observed sharp linewidth is now thought as a combined effect of high magnetic field and strong Coulomb interaction (Fertig, 1999; Fogler and Huse, 2000; Fogler, 2004). The physical picture is the following: when the pinning mode (magnetophonon) is excited, domains of WC all move in a circular fashion due to the Lorentz force (the mechanism that mixes the longitudinal and transverse motions); because the effective bulk modulus of the WC is very large (compared to the shear modulus) due to strong Coulomb interaction (Fertig, 1999; Fogler and Huse, 2000), all parts (domains) of the WC would prefer to move *together* coherently (in phase), otherwise at times different parts would come closer to each other and cause a high Coulomb energy cost. Thus the *motional correlation length* (the length scale at which the magnetophonon propagates) can in principle become very large and far exceeding the *static* correlation length L_c (or even L_a). The mechanism that actually makes this length (denoted as L_B) finite is magnetophonon localization, which consequently broadens the pinning mode resonance. An estimate[29] for L_B, linking it to Δf is given in Fogler and Huse (2000) as $L_B\sim\nu(e^2/h)(4\epsilon\Delta f)^{-1}$. However, currently, theoretically estimated Δf is often significantly smaller than the observed Δf (Fertig, 1999; Fogler and Huse, 2000). Additonally, the observed Δf also has a rather complicated B-dependence that is not explained (Ye *et al.*, 2002b). We still need a more complete understanding of many aspects of the line width.

[29]One can obtain this by setting $\omega_L^2(q_B)/(2\omega_c)=2\pi\Delta f$, where $q_B=2\pi/L_B$.

3.1.6 Oscillator Strength of Pinning Mode

Another important quantity for the pinning mode resonance is its integrated intensity (S, also called the oscillator strength). A sum rule has been derived[30] by Fukuyama and Lee (1978) as

$$S = \frac{ne\pi f_{\rm pk}}{2B} = \frac{\nu e^2 \pi f_{\rm pk}}{2h} \tag{3.8}$$

thus directly relating $S/f_{\rm pk}$ to the participating density (or filling factor) of the WC.

Fig. 3.3 demonstrates the $S/f_{\rm pk}$ measured from sample P (heterojunction. Sec. 2.1), which enters the high-B WC phase with well defined resonance at $\nu \lesssim 1/5$. We see that at sufficiently high B ($\nu \lesssim$ 0.15 for this sample), the Fukuyama-Lee rule is well satisfied[31], within the experimental uncertainties[32] (typically 20-30%) of S extracted from the Re$[\sigma_{xx}(f)]$ sectra.

The significant deviation from the Fukuyama-Lee result near ν=1/5 seen in the figure is evidently an effect due to the 1/5 FQH liquid (while the WC is supposed to "quantum" melt into the FQH liquid as $\nu \rightarrow 1/5$), which we will discuss more later, in Sec. 5.3.3.

We want to emphasize here that the n from the Fukuyama-Lee sum rule (3.8) refers to the *total density participating in the WC*, *not* the total 2DES density (measured, say from the SdH oscillation). This is important when only part of the 2DES forms the solid[33]. For example, this is used, in the next Chapter, as one of the evidence for top LL crystallization (the IQHWC).

[30] We have re-derived this sum rule in Appendix G to correct a factor-of-2 error in the result of Fukuyama and Lee (1978).

[31] Although the Fukuyma-Lee sum rule was derived within the "classical" WC picture (Fukuyama and Lee, 1978), it is found experimentally to be satisfied more generally, even when the measured $f_{\rm pk}$ itself (see Appen. H) does not actually follow the "classical" behavior ($1/B$ dependence) predicted in Fukuyama and Lee (1978).

[32] mainly due to the uncertainties/fluctuations in the background (reference) level in the microwave transmission.

[33] In this case n should be understood as the (total number of electrons in the sample participating in the solid)/(total area of the *sample*), i.e, it is proportional to the solid fraction in the system.

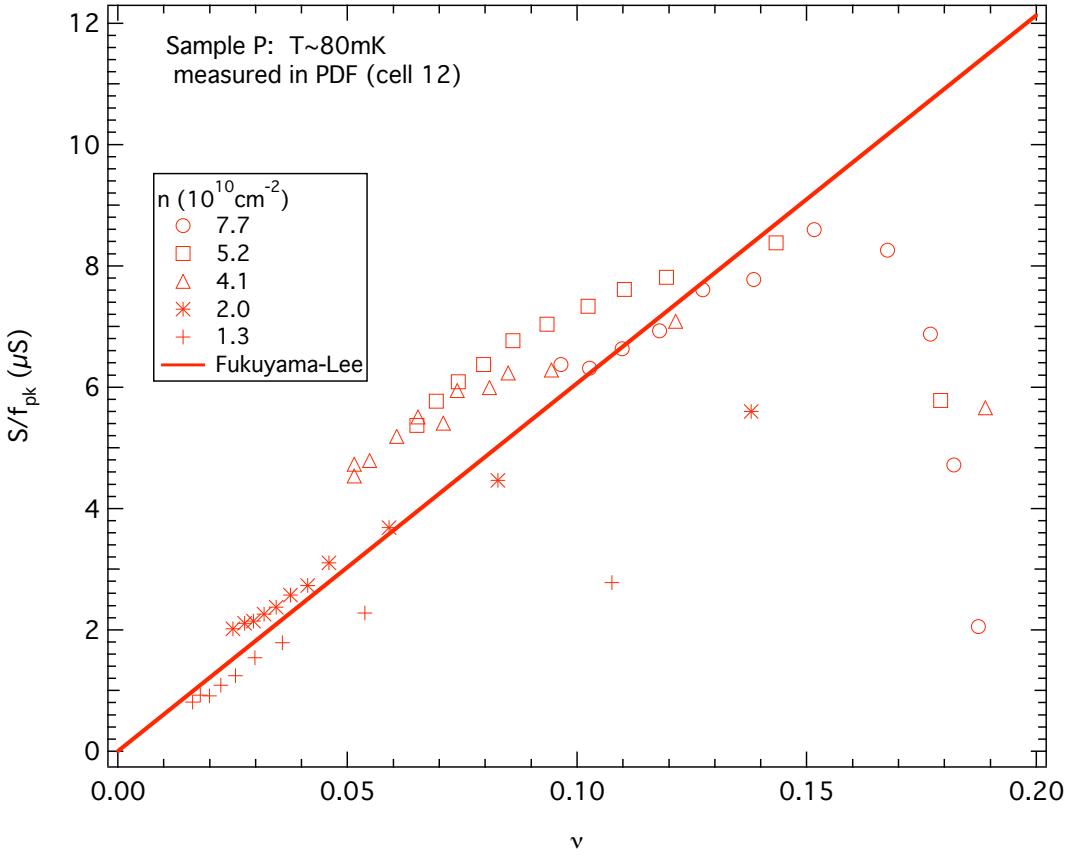

Figure 3.3: $S/f_{\rm pk}$ measured in the high-B WC phase in Sample P (heterojunction) and its comparison to Fukuyama-Lee's theoretical result.

3.2 What Pins the Wigner Crystal?

What (physical) disorder is actually responsible for the WC pinning has been a long standing question, not mentioning that accurate knowledge about the disorder in real samples is often very limited. Theoretical studies (Ruzin *et al.*, 1992; Fertig, 1999) suggest that remote charged impurities, which could strongly affect the electron mobility at B=0 and FQHE physics, are generally not effective in pinning the (weakly-pinned) WC. Fertig (1999), as mention earlier, proposed some dilute, short-range (comparable to l_B) interface "pits" as a more possible source of disorder that pins the WC. Particularly, Fertig's *interface* pinning model predicted $f_{\rm pk}$ that were on the similar order of magnitude to experimentally observed values, and was able to at least qualitatively account for the behavior of increasing $f_{\rm pk}$ with increasing B observed in the earlier experiments (Li *et al.*, 1997), which was difficult to explain with long range disorder and in the "classical" theories (Fukuyama and Lee, 1978). Theories by Chitra *et al.* (2002), on the other hand, assumed the disorder to be a Gaussian-correlated white noise, but without specification for the physical source for such white noise disorder. The WC pinning mode resonance spectra data presented in this section (particularly those measured from a narrow QW, which highlights the effect of vertical confinement), as we will see, give valuable insight to the nature and characteristic of the pinning disorder.

3.2.1 Effect of Vertical Confinement

Fig. 3.5 shows representative spectra measured from samples QW65 and QW15. They were grown in the same way by MBE, with the only difference being the width of the quantum well (65 and 15 nm respectively), thus allowing us to focus on the effect of vertical confinement. As we see, the $f_{\rm pk}$ of the resonance in QW65 is typically ∼100-200 MHz, whereas in QW15, $f_{\rm pk}$ becomes ∼ 6-8 GHz, almost two orders of

magnitude higher.

In QW15 (compared to QW65), electrons are subjected to a much narrower vertical confinement and the electron wavefunction penetrates more into the barrier, thus electrons are to a greater extent subject to any disorder at or near the interface[34]. The significantly increased $f_{\rm pk}$ in QW15, is therefore a strong indication that such disorder is likely to be the important source of pinning, at least in the case of the narrow QW. In other words, the proposed source of pinning of WC, by Fertig (1999), as coming from the roughness and fluctuation ("pits") in the interface, is not inconsistent with our experimental findings.

3.2.2 Learning about Disorder

More information about disorder can be learned from in particular, looking at how $f_{\rm pk}$ changes as a function of B. From Fig. 3.4 we can already see that in QW65, $f_{\rm pk}$ at 18T is lower than $f_{\rm pk}$ at a lower field (11T), whereas the opposite order occurs in QW15. Later we will see (Chap. 5) that QW65 actually shows a more complicated phenomenon with two resonances in its spectra (especially at higher n), interpreted as coming from two LLL solid phases ("A" and "B"). Here we focus on the spectra measured in QW15 and discuss characteristics of the disorder that may be inferred from its B dependence of $f_{\rm pk}$.

Fig. 3.5 shows a so-called "carpet" or "waterfall" plot of a series of $\mathrm{Re}[\sigma_{xx}(f)]$ spectra, measured at many B fields ranging from 5.3T to 18T (offset vertically from the bottom to top). Likely because of the tight vertical confinement[35] (which resulted in a relatively low electron mobility $\sim 1\times10^6 \mathrm{cm}^2/\mathrm{Vs}$, see Sec. 2.1 and Appen. C), ν=1/3 is the last (meaning the highest B) FQH state seen[36] (whereas for high mobility 2DES samples the last FQHE typically occurs at ν=1/5) and for $\nu \lesssim 0.3$, the resonance

[34]Note, for example, that the sub-band energy is much more affected for a given depth "pit" for a narrower QW

[35]See also Yang *et al.* (2003).

[36]For a B-trace in Sample QW15, see Appenix F

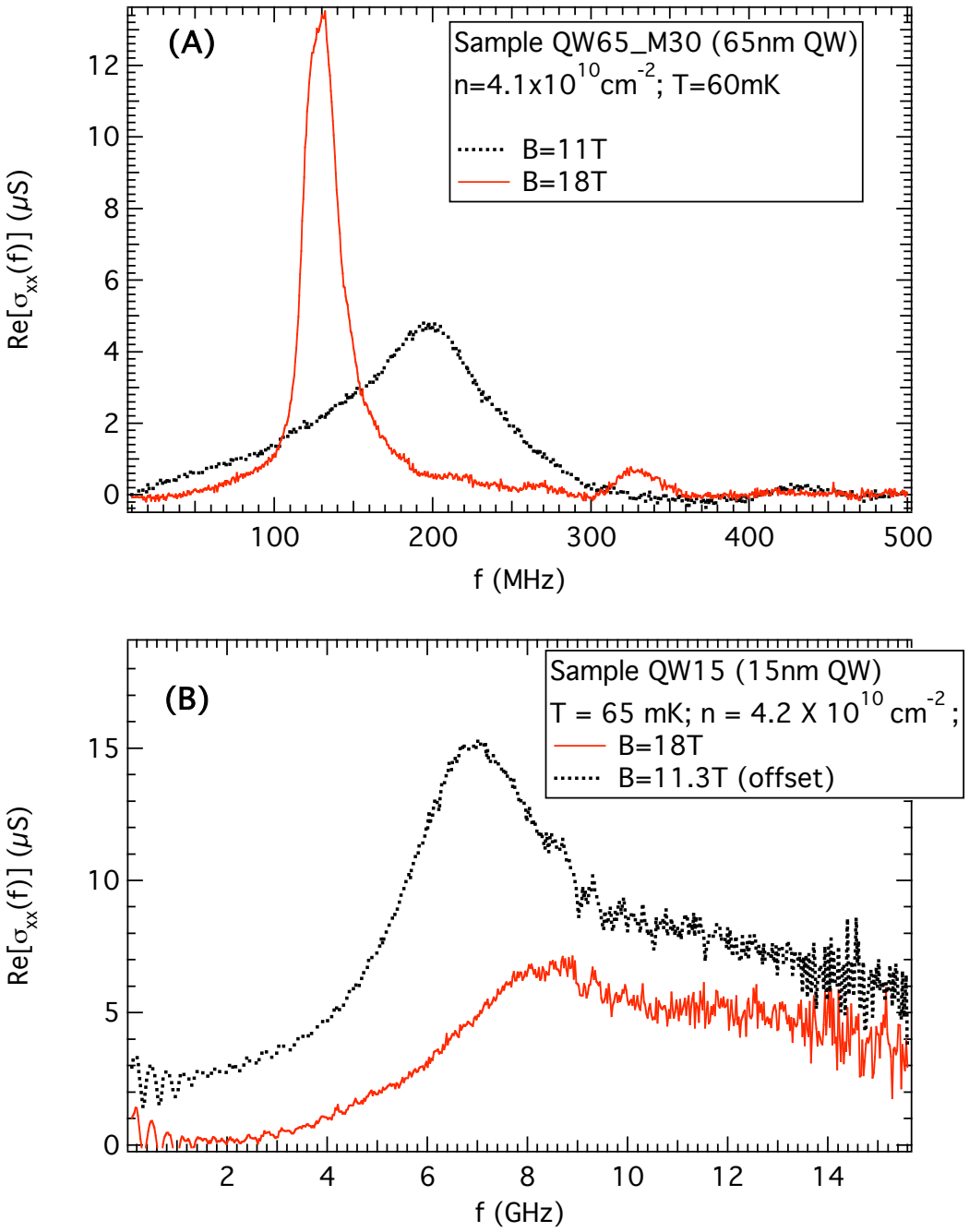

Figure 3.4: Pinning mode resonance spectra measured from two quantum wells of (A) 65nm and (B) 15nm width, under otherwise similar conditions. The limited variation of $f_{\rm pk}$ at different B's on each sample is much smaller than going from one sample to the other.

from pinned WC can be observed[37].

Two important things that we can learn from the above data are:

1) The monotonic increase of $f_{\rm pk}$ with increasing B, over the significant B range observed, is consistent with the "quantum regime" ($l_B > \xi_0$) in the qualitative picture of interplay of l_B and disorder as discussed in Sec. 3.1.2. Since l_B at 18T (the highest B we measured; and $f_{\rm pk}$ is still increasing with B at 18T) is 6nm, we infer that the correlation length of the physical disorder in our sample $\xi_0 \lesssim$ 6nm. This is in fact, not inconsistent with the typical lateral size of roughness that can occur in the GaAs-on-AlAs interface in MBE grown 2DES samples (Sakaki *et al.*, 1987), nor is it inconsistent with the "pit" size (∼3 nm) of interface disorder that Fertig (1999) proposed in the analysis of the 2DHS data from earlier measurements (Li *et al.*, 1997), which also show similar increasing[38] $f_{\rm pk}$ with increasing B.

2) The increase of $f_{\rm pk}$ with B, from ∼9T to 18T, is almost linear (the more dramatic drop of $f_{\rm pk}$ as $B \to 5$T is most likely an effect due to approaching FQHE (1/3 in this case), which we will discuss more in Chap. 5). This is clearly inconsistent with the Gaussian-correlated white noise model for disorder used by Chitra *et al.* (2002), who predicted a much faster B^2 increase of $f_{\rm pk}$, as discussed in Sec. 3.1.4. On the other hand, with the dilute interface "pit" model, Fertig (1999) derived the following formula for $f_{\rm pk}$ in the "perturbative regime"

$$f_{\rm pk} \sim \frac{\Lambda}{4\mu_T l_B^2} \tag{3.9}$$

where the quantity $\Lambda = V_0^2 \xi_0^4 n_i^2$ characterize the disorder, and V_0, ξ_0, n_i are the potential depth, size scale, and density of the pits respectively. This predicts that $f_{\rm pk}$ increases linearly instead of quadratically with B, and is a direct consequence of the

[37] This is consistent with earlier work on low mobility 2DES samples, which show resonance for $\nu \lesssim 1/3$ (Engel *et al.*, 1997a; Ye *et al.*, 2002a). It is also an empirical knowledge from experimental observations, that the appearance of 1/3 FQHE is the minimum requirement on the quality of a sample to show the high-B WC resonance.

[38] Also observed by Engel *et al.* (1997a) in earlier 2DES samples.

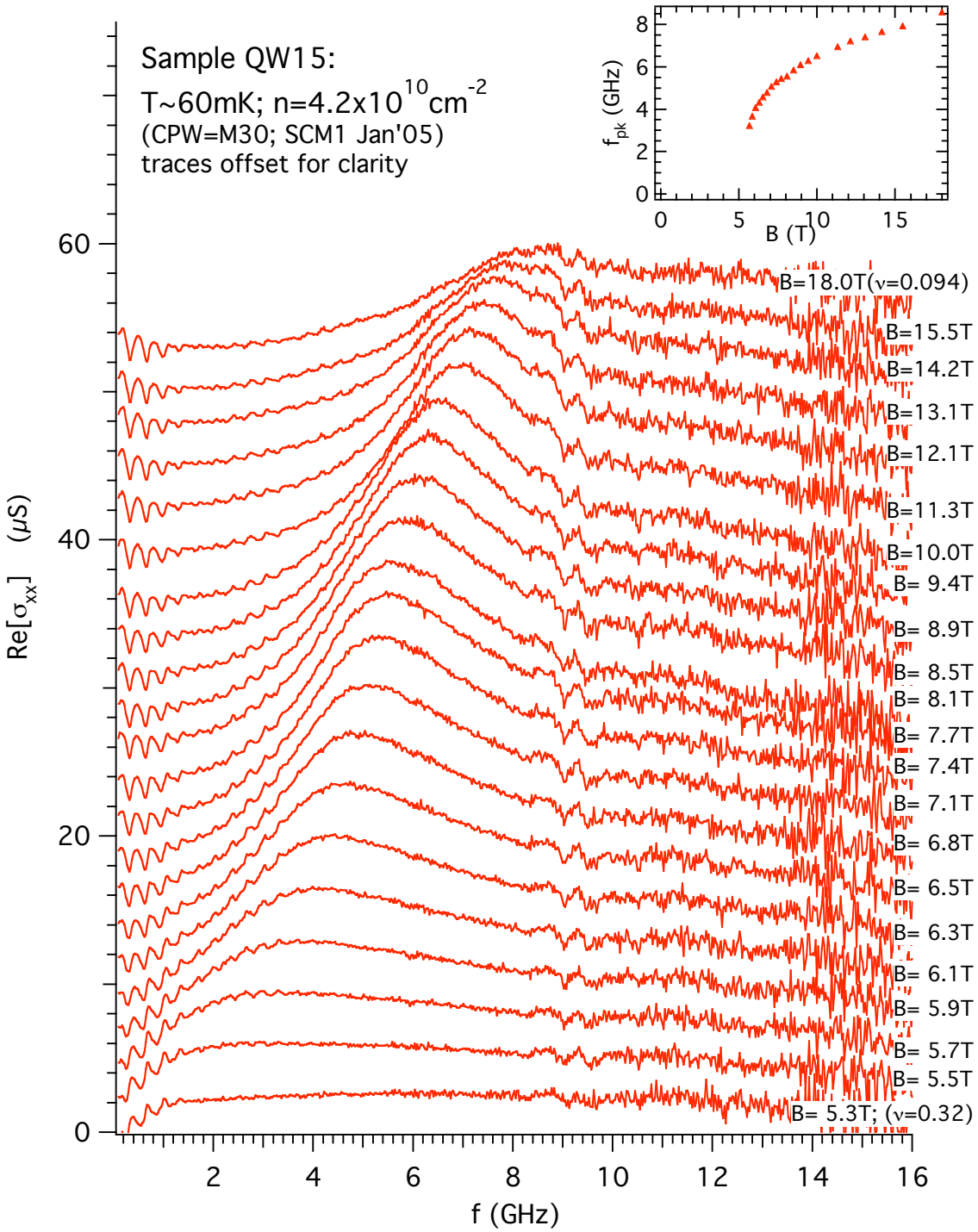

Figure 3.5: Spectra measured from sample QW15. Traces are offset for clarity. Magnetic Field (B) of each trace is labeled at right. Inset shows the peak frequency of the resonance ($f_{\rm pk}$) as a function of B.

disorder statistics having changed to dilute distribution of short range ($\xi_0 < l_B$), localized disorder (such as "pits"), as we discussed in Sec. 3.1.4. Further analysis by Fertig (1999), mainly through numerical simulation[39], introduced additional corrections to $f_{\rm pk}$ that predict it to grow with B *sublinearly*. This is in fact consistent with the sublinear[40] behavior[41] of $f_{\rm pk}$ vs B observed in Fig. 3.5. Another mechanism that can also give rise to a sublinear $f_{\rm pk}$ vs B, which we propose and discuss in more detail in Appendix H, is the presence of at least two types of disorder of different correlation lengths (one with a shorter $\xi_1 < l_B$, which dominates the pinning and causes $f_{\rm pk}$ to grow with B; and another with relatively longer $\xi_2 > l_B$ (which on its own would cause $f_{\rm pk} \propto 1/B$) that slows down the growth of $f_{\rm pk}$ vs B and makes it sublinear).

In conclusion, we have demonstrated from our measured data, that the disorder that dominates the pinning in QW15 is most likely some dilute disorder near the interface with length scale below 6nm.

3.3 Additional Notes and Further Directions

In this chapter we have reviewed our present understanding of the disorder pinned Wigner crystal and the pinning mode (resonance). Current theories have provided a fairly appealing framework to connect properties of the pinning mode to those about disorder. For $f_{\rm pk}$ and oscillator strength S especially, even some more quantitative understanding have been achieved. This framework also enables us to obtain important insights about pinning disorder, as we have demonstrated particularly for Sample QW15.

The important concept of electronic state-dependent, "effective" disorder discussed in Sec. 3.1.2 is based on single particle quantum effects (l_B). Such a concept

[39] using "quantum harmonic approximation" and taking more careful account of the actual fraction of electrons that are pinned.

[40] Also seen and evident in Li *et al.* (1997).

[41] In Fig. 3.5, between ∼9 to 18 T, we notice the slope decreases at higher B, and the line does not actually pass the origin.

can be quite useful in other regimes of the QH system (not only restricted to WC) as well, for example, in the studies of effects of disorder on scaling and "QH phase transitions" (Li, 2005). In Appendix K, we will also exploit the idea of "effective disorder" with *many body* quantum effects, in the context of a model for pinned bilayer Wigner crystals.

We have mentioned in this chapter (and presented some data) about one of our wide QW samples (QW65). In its case, not only is its $f_{\rm pk}$ significantly lower than that in QW15, its $f_{\rm pk}$ (if sufficiently far away from the 1/5 FQHE as well as the "A"-"B" phase-coexistence regime), as we will later see (Chap. 5 and Appen. J), typically decreases with increasing B, suggesting that the dominant pinning disorder there must have relatively longer ξ ($\gtrsim$ 10nm). Although the much reduced pinning (low $f_{\rm pk}$) in QW65 corroborates the importance of interface disorder that we have stressed, it remains an interesting question whether in such a wide QW, the main source of disorder may still come from the interface (such as the "pits") as in QW15[42]. More accurate and quantitative analysis will likely require going beyond the infinitely-thin 2DES approximation in current theories, and considering the z-extent of the electron wavefunction (form-factor)[43]. Studying effects of in-plane magnetic field ($B_{||}$) could be relevant to this question as well.

The disorder model discussed in this chapter is based on current theories, and gives a good start for understanding the pinning mode. However, the disorder in an actual samples could be more complicated. Appendix H contains data from sample P (heterojunction), which are *qualitatively* difficult to explain with current theories. A phenomenological model involving disorder of two different length scales is proposed there.

[42]particularly in view of the fact that the only difference in QW65 and QW15 is the width of the GaAs QW channel, see Appen. C

[43]It is also interesting to ponder the effect of convoluting such a form factor with a physical disorder, which may also have some z-dependence (near the interface, for example), to construct an effective disorder with (x, y, z) correlation

The discussion of disorder statistics we give in this chapter are mainly based on physical pictures. More rigorous treatment could be made using random field theory (two dimensional random processes). Obviously, further theoretical development as well as experimental work are needed to take full advantage of the exciting possibility of performing "disorder spectroscopy" using the pinning mode resonance as a tool.

The pinning mode resonance is not expected to occur if disorder is too strong (Wulf, 1999; Efros, 1985; Polyakov and Shklovskii, 1993). Experimentally, it was found that for the high-B WC resonance to be observed, a 2DES sample must be of sufficient quality to display 1/3 FQHE (Engel *et al.*, 1997a; Ye *et al.*, 2002a).

In this chapter we have not addressed the finite temperature (T) effect on the pinning mode. This will be discussed in Sec. 6.2, which as we will see, offers important insight on the nature of the resonance as a collective pinning mode. T-dependence of $f_{\rm pk}$ and Δf can also contain valuable information about disorder (Yi and Fertig, 2000).

Two general issues about the pinning mode, for which there are particularly serious gaps between observation and understanding, are: the effect of FQHE and the behavior of the linewidth.

Effects of FQHE concern the behavior of the pinning mode near a FQHE, or special fractional fillings, and the influence of many body quantum correlations (dependent on ν) on the pinning mode in general. Such effects have received very little treatment in the theories on pinned WC (Fertig, 1999; Fogler and Huse, 2000; Chitra *et al.*, 2002), though it is likely to be important in understanding, for example, exactly why experimentally observed resonance generally grows (increasing amplitude) with increasing B, *down to fairly small* ν, whereas theories neglecting the FQHE (for example, Chitra *et al.* (2002)) expect the amplitude to decrease with increasing B. Also of great interest is the behavior of $f_{\rm pk}$ when (the WC) approaching the FQHE (the drop of $f_{\rm pk}$ is very generally observed). In Chap. 5 we will discuss more about

the influence of FQHE on WC from data measured on very low disorder (low pinning) samples.

For Δf, we have mentioned that although current theories (Fertig, 1999; Fogler and Huse, 2000) have given important insights on the sharpness of the resonance and developed a framework relating Δf to magnetophonon localization, much remains to be understood, particularly about the complicated behavior of Δf found in experiments (Ye *et al.*, 2002b). More general questions include: how does many body correlation affect magnetophonons (such as near rational fractional ν) ? What kind of disorder are mainly responsible for the localization of magnetophonons (are they the same kind of disorder that determine $f_{\rm pk}$)?

In the following we list some further experimental ideas, especially involving samples of "controlled difference" (like QW65 and QW15), to gain more insights about disorder and the pinning mode include:

1) To study samples with different dopant layer parameters, or different (Al) alloy concentration in the AlGaAs barrier, or even with a thin "buffer" layer (with different Al concentration) near the interface. Of particular interest also, are samples with a *small* amount of Al alloy introduced in the GaAs QW channel. Comparing the effects of such alloy disorder on FQHE (magnetotransport, Li (2005)) and WC (pinning resonance) can be potentially illuminating.

2) To study samples with QW widths between 65nm (QW65) and 15nm (QW15) but otherwise grown in the same way by MBE as QW65/QW15, potentially mapping out disorder correlation length as a function of vertical confinement. It could also be illuminating to compare with photoluminescence or mobility measurements in similar structures that probe the interface roughness (Noda *et al.*, 1990; Sakaki *et al.*, 1987).

3) To connect measurements of the pinning mode with Poisson-Shrödinger-Hartree simulations of the wavefunction to learn more about effects of vertical confinement and wavefunction penetration into the barrier.

4) To exploit alternative ways to change density n other than backgating, for example through illumination[44] or other effects of light (Appendix C). Also interesting would be to have both a front gate[45] and a backgate, giving more ability to tune the wavefunction shape.

[44]Sample WP, whose as-cooled n can be significantly affected by LED illumination, would be a good candidate.

[45]Such a front gate (compatible with CPW and acting on the area of 2DES being measured (i.e., under the slots)) have been tried by Z.H.Wang with some success.

Chapter 4

Solid Phases in the Top Landau Level

4.1 Integer Quantum Hall Wigner Crystal (IQHWC)

4.1.1 Introduction

In this section, we report observation of a resonance in $\mathrm{Re}[\sigma_{xx}(f)]$ using our microwave absorption measurements in a high quality 2D electron system near *integer fillings*. The resonance is qualitatively similar to previously observed resonance of weakly pinned Wigner crystal in high B and very small filling factor regime (Chaps. 1, 3). Data measured in Sample R and around ν = 1,2,3 will be presented. We interpret the resonance as the signature of a Wigner crystal state around integer Landau level.

We emphasize that each ν range where we see this resonance, indicating a WC state, belongs to IQHE plateau regime seen in dc transport. Thus our finding indicates that pinning of a *many-particle* ground state, such as Wigner crystal, can be relevant even for IQHE, which has traditionally been explained by a disorder induced *one-particle* localization mechanism (Prange and Girvin, 1990; Das Sarma and Pinczuk, 1997).

The main references for this section are: Chen *et al.* (2003) and Lewis *et al.* (2004a).

4.1.2 Sample Description and Overview

All data presented in this section were measured using Sample[1] R, a very high quality 2DES in a GaAs/AlGaAs quantum well(QW) structure grown by molecular beam epitaxy. The QW is 30 nm wide and located $\sim$ 200 nm beneath the surface. The 2DES has as-cooled density $n = 3.0 \times 10^{11}\text{cm}^{-2}$ and 0.3 K mobility about $2.4 \times 10^7\text{cm}^2\ V^{-1}s^{-1}$. The microwave measurements (Chap. 2) were done using a straight line shaped CPW[2], schematically shown in the inset of Fig. 4.1(A).

To orient ourselves, we display in Fig. 4.1(A) a "B-trace" (B-dependent conductivity) measured at a fixed frequency (200 MHz) and $\sim$80 mK. We can readily resolve such FQHE states at 6/5, 4/3, 7/5, 8/5, 5/3, 7/3 and 5/2, attesting to the high quality of the sample. Panel B shows the B-dependent conductivity measured at three different frequencies, in field range of 8 to 14 T, through $\nu = 1$. We see the peak-like "wing" (for example the one near 11T in the middle trace) on the side of $\nu = 1$ has a small amplitude in the 300 MHz trace (bottom), but is greatly enhanced in the 1.2 GHz trace (middle), and reduces to small amplitude again in the 2 GHz trace (top), thus displaying a resonating behavior. Such behavior is most clearly seen through the f-dependent conductivity spectrum $\text{Re}[\sigma_{xx}(f)]$. Panel C shows four spectra measured at ν=1, 3/2, 1.1 and 1.85 (from bottom to top) respectively, all acquired at about 50 mK and in the low microwave power limit. The reference spectrum (Sec. 2.2.3) is taken at a much higher power at $\nu = 1$. Both spectra at $\nu = 1$ and $\nu = 3/2$ are flat within experimental error and can actually be used as alternative references (P_0, see Sec. 2.2.1), giving at most a constant offset in the conductivity obtained but otherwise

[1]More information on sample R can be found in Sec. 2.1 and Appen. C. We have measured two (adjacent) pieces cut from the same wafer.

[2]The orientation is not important for IQHWC, which is isotropic. Dimensions for this CPW (S20) can be found in Appendices C and D.

having little influence in the results. In contrast, the spectrum at $\nu = 1.1(B{=}11.3\text{T})$ shows a strong resonance (near 1.3 GHz) of height more than 10 μS and quality factor Q (f_{pk} divided by FWHM [full width at half maximum] Δf) almost 3. Similarly, the spectrum at $\nu = 1.85(B{=}6.7\text{T})$ also displays a strong resonance, near 1.7 GHz.

This resonance in f-dependent conductivity happens for ν near integers and has been observed around ν = 1, 2, 3 and 4. In this section we focus mostly on the resonances around ν = 1, 2 and 3. The resonance around ν = 4 is much weaker and on one side (ν>4 side) it joins with the "bubble" crystal resonance, as will be discussed briefly in Sec. 4.2. All data shown below in this section were measured at ∼50 mK, and in the low power limit.

4.1.3 Spectra around ν=1

Fig. 4.2(A) shows Re[$\sigma_{xx}(f)$] spectra measured at 45 filling factors ranging from 0.78 to 1.22, in equal increments of 0.01. When ν is sufficiently far from 1 (∼0.8 and 1.2) the spectrum is flat with no resonance. A resonance starts to develop when ν is around 0.84-0.85 (for ν below 1) and 1.15-1.16 (for ν above 1) at frequencies below 1 GHz. The resonance sharpens with increasing peak frequency as ν approaches 1 (from both sides) till becoming sharpest around $\nu = 0.9$ (resonating around 1.2 GHz) and $\nu = 1.1$ (resonating around 1.4 GHz). As ν further approaches 1 the resonance weakens but its peak frequency continues to increase; the last visible resonance is around ν =0.95-0.96 and 1.04-1.05 with frequency reaching nearly 2 GHz. In the immediate vicinity of $\nu = 1$ ($0.96 < \nu < 1.04$) the spectra are again flat. In panel B and C of Fig. 4.2 we plot the peak frequency, f_{pk}, and the full width at half maximum, Δf, of the resonance as functions of ν. Here f_{pk} and Δf are extracted by fitting the resonance to a Lorentzian: $A_0 + A_1/(A_2 + (f - f_{\text{pk}})^2)$, with $\Delta f = 2\sqrt{A_2}$. While f_{pk} monotonically increases as ν moves closer to 1, Δf reaches minima when ν is about 0.1 away from 1, where the resonance has quality factor $Q = f_{\text{pk}}/\Delta f$ of more than 3.

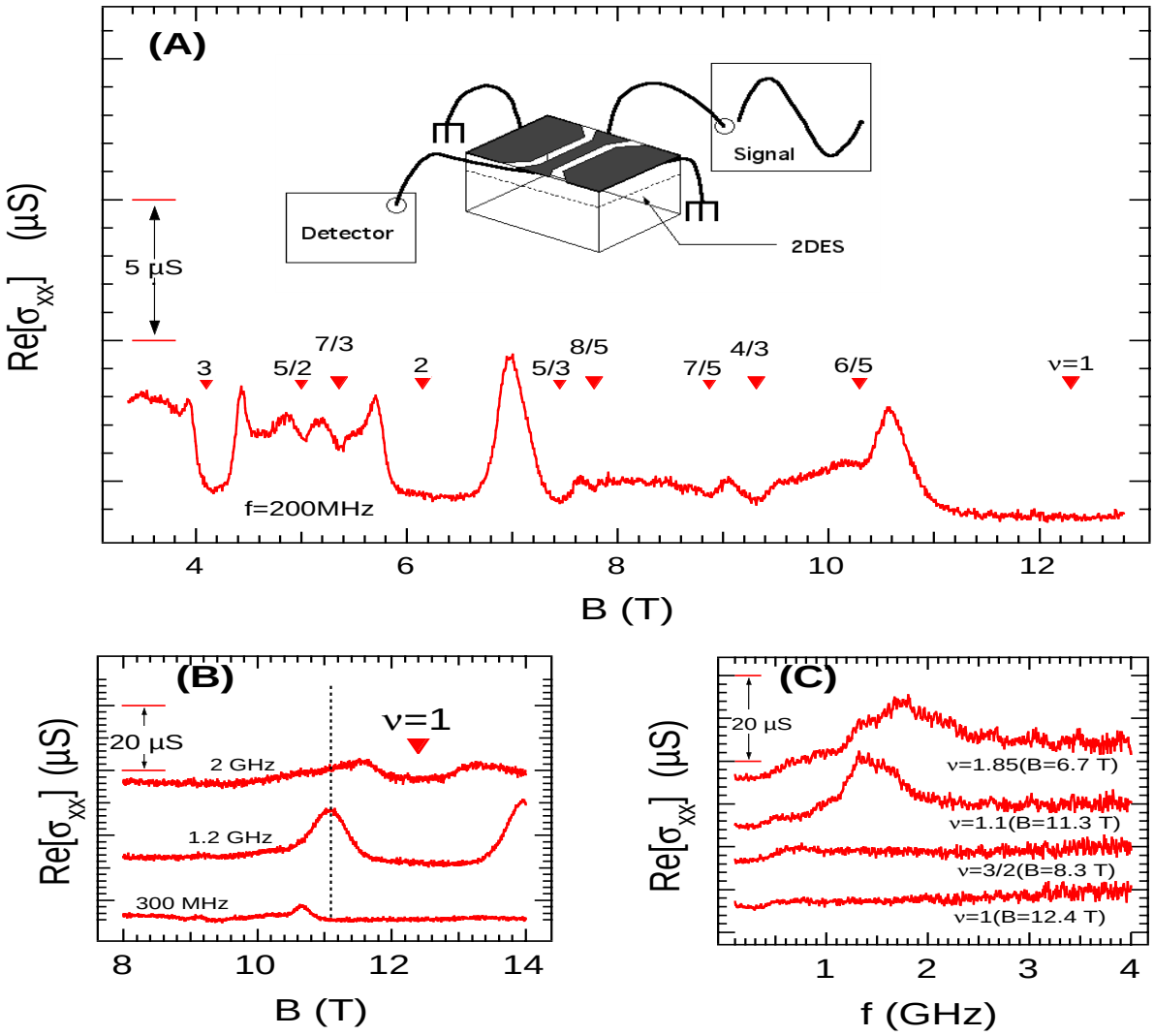

Figure 4.1: Sample R, overview near integer fillings. **(A)** The B-dependent conductivity at 200 MHz and ∼80 mK with a slightly elevated microwave power. Several filling factors are marked. Inset shows the schematic measurement circuit. Dark regions represent the metallic films deposited on the sample to make the CPW. **(B)** B-dependent conductivity around $\nu = 1$ measured at three different frequencies as labeled. Traces appropriately offset vertically for clarity. The temperature during B-sweep is about 80 mK. Dotted line is a guide to the eye for the resonating behavior. **(C)** A few f-dependent conductivity spectra (offset for clarity) measured at ∼50 mK and at various B fields labeled underneath each trace. Data in both panel B and panel C are measured with a low microwave power.

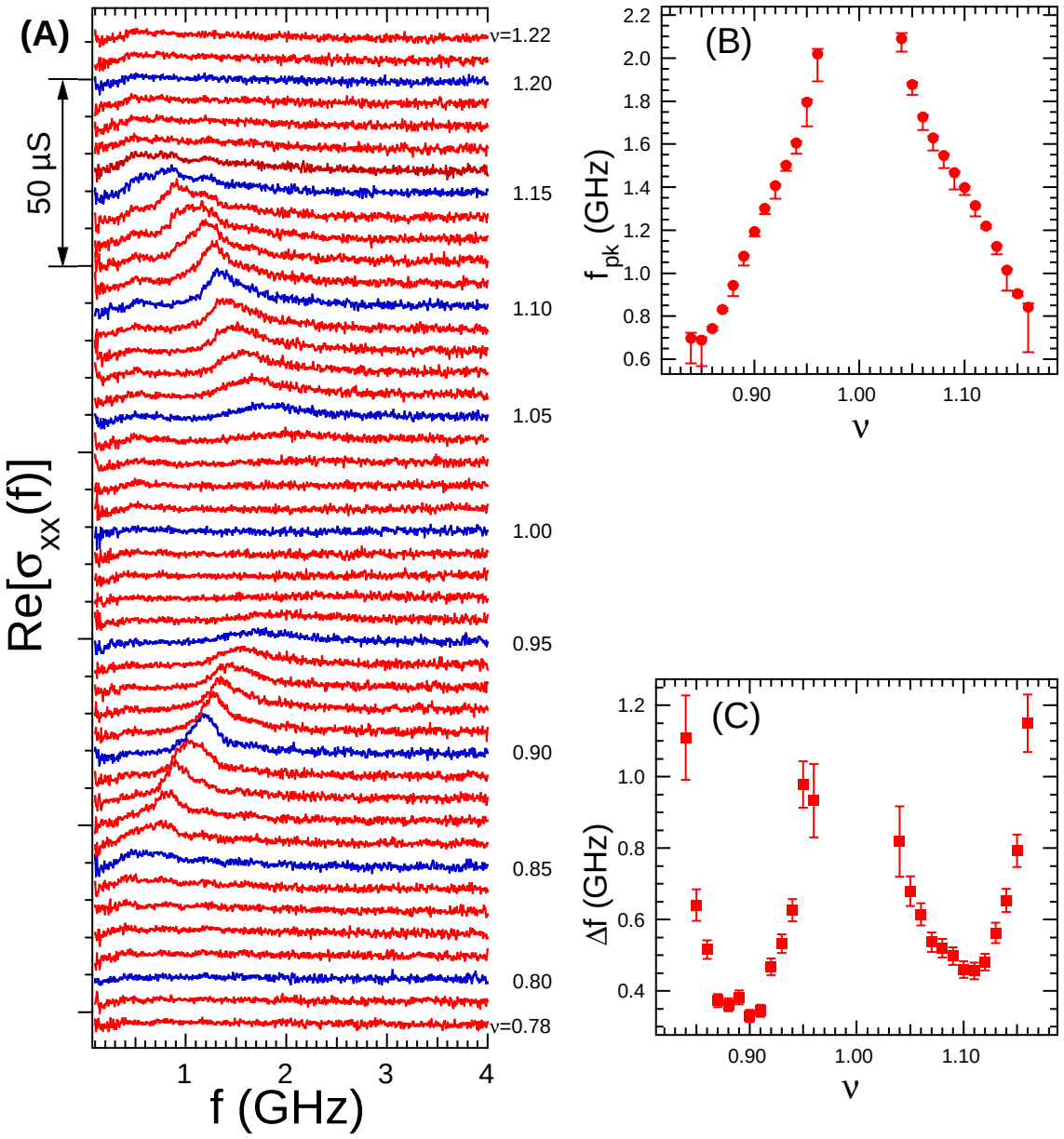

Figure 4.2: **(A)** Frequency dependent conductivity spectra (Sample R) around $\nu = 1$: from $\nu = 0.78$ (bottom trace) to $\nu = 1.22$ (top trace). Adjacent traces differ 0.01 in ν and are offset 6 μS from each other for clarity. Filling factors for selected traces are labeled at right. Measurements are performed at ~ 50 mK. **(B)** $f_{\rm pk}$ versus filling. **(C)** Δf versus filling factor.

4.1.4 Spectra around ν=2

In Fig. 4.3(A) we display Re[$\sigma_{xx}(f)$] spectra measured at 51 filling factors between 1.75 to 2.25, again in 0.01 increments of ν. The strongest resonance on each side of $\nu = 2$ occur at $\nu \sim 1.85$ (with peak frequency about 1.8 GHz) and $\nu \sim 2.12$ (resonating at below 1 GHz); the peak frequency of the resonance always increases as $\nu \to 2$. The qualitative features of the resonance are similar to those around $\nu = 1$; however we notice an evident asymmetry between the two sides of $\nu = 2$ (see also Fig. 4.6 in Sec. 4.1.6) possibly related to the different wave functions in different orbital Landau levels (whereas both sides of $\nu = 1$ belong to the same orbital Landau level). The $f_{\rm pk}$ and Δf of the resonance are extracted as in Fig. 4.2 and plotted in 4.3(B) and 4.3(C) as functions of ν, respectively.

4.1.5 Spectra around ν=3

Fig. 4.4 displays the spectra around ν=3, again showing a qualitatively similar resonance (but generally weaker in strength) to those seen around ν=1 and 2. We will show the $f_{\rm pk}$ in a different form (as a function of n^*) later in Fig. 4.6.

4.1.6 Discussion

The most natural interpretation of our data is that the resonance we observe is due to a Wigner crystal phase formed around integer Landau fillings. For clean enough 2DES, WC has been theoretically assumed to be the ground state of the system for filling factor $\nu = K + \nu^*$ with sufficiently small $|\nu^*|$, where K is some positive integer (MacDonald and Girvin, 1986; Fogler *et al.*, 1996; Haldane *et al.*, 2000; Shibata and Yoshioka, 2003). Such considerations are often based on the simple physical picture that electrons (or holes, for negative ν^*) in filled Landau levels can be assumed to be "inert" and the remaining electrons/holes of "effective filling factor" ν^* and density

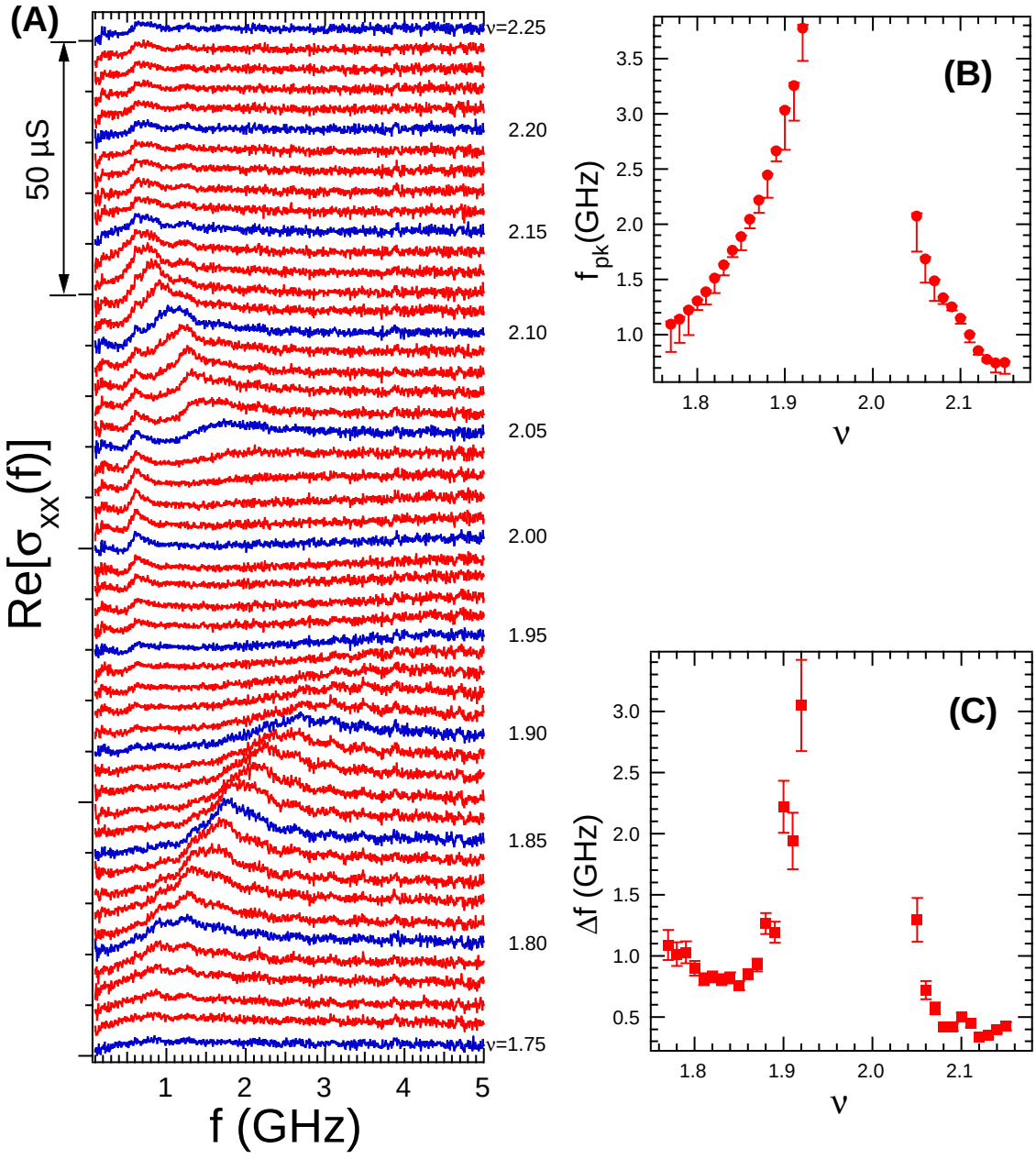

Figure 4.3: **(A)** Frequency dependent conductivity spectra (Sample R) around $\nu = 2$: from $\nu = 1.75$ (bottom trace) to $\nu = 2.25$ (top trace). Adjacent traces differ 0.01 in ν and are offset 4 μS from each other for clarity. Filling factors for selected traces are labeled at right. Measurements are performed at ∼50 mK. (The small spike near 600 MHz in some traces, not moving with B, is likely due to an experimental artifact). **(B)** $f_{\rm pk}$ versus ν. **(C)** Δf versus ν.

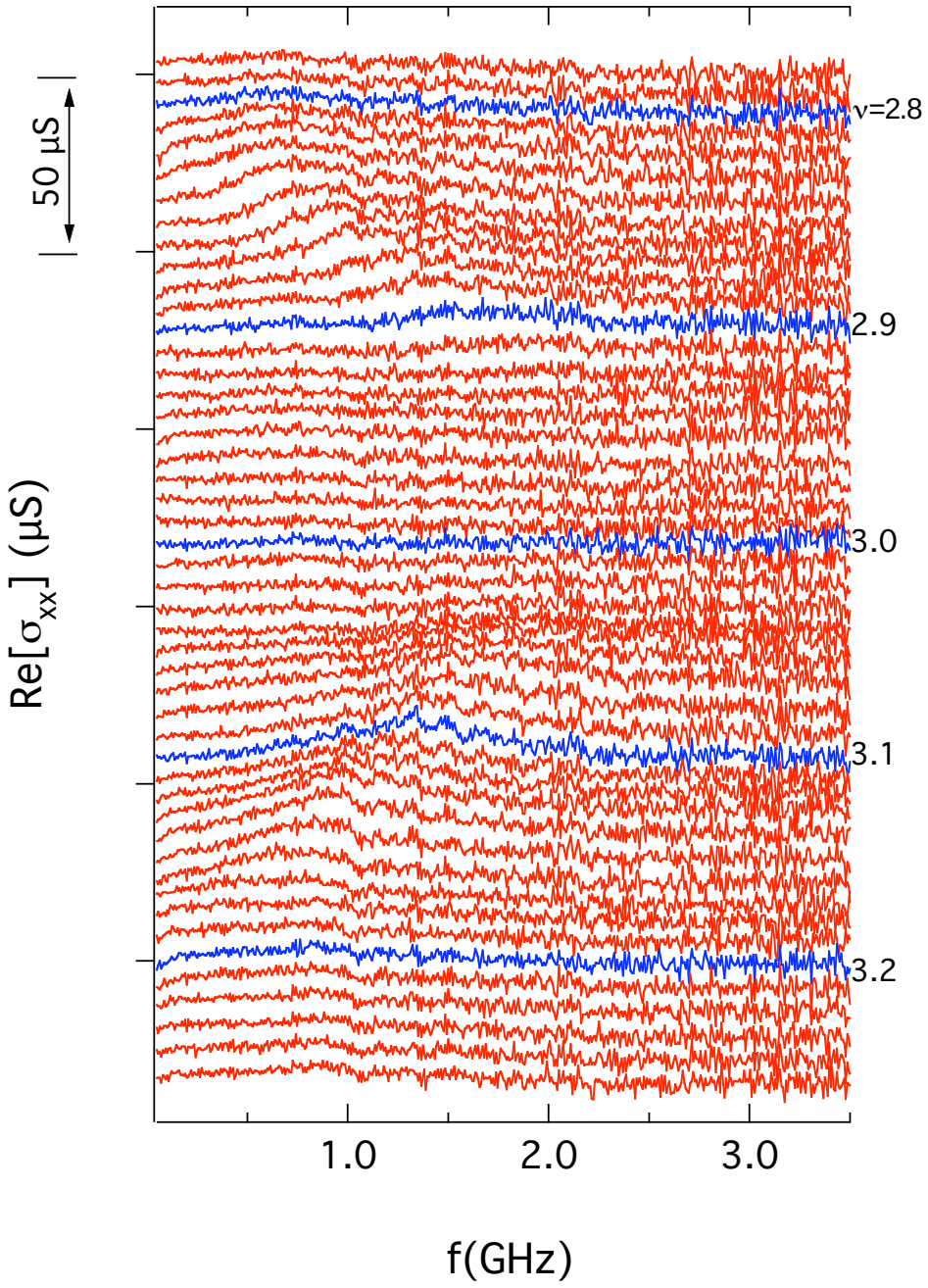

Figure 4.4: Frequency dependent conductivity spectra (Sample R) around $\nu = 3$: from $\nu = 3.25$ (bottom trace) to $\nu = 2.78$ (top trace). Adjacent traces differ 0.01 in ν and are offset for clarity. Filling factors for selected traces are labeled at right. Measurements are performed at ~ 50 mK.

$n^* = (n/\nu)\nu^* = n\nu^*/(K+\nu^*)$ should Wigner-crystallize when the size of their single particle wave function (on the order of the magnetic length $l_B = \sqrt{\hbar/eB}$) becomes small compared to their average spatial separation. Due to interaction with (weak) disorder such a crystalline phase is pinned, rendering the top Landau level insulating, and supports a pinning mode, as we discussed in Chap. 3, that gives rise to the observed resonance[3].

Our resonance is qualitatively similar to the resonance previously observed at small filling factors in the LLL Wigner crystal regime of both electrons and holes (Li *et al.*, 1997; Engel *et al.*, 1997b,a; Ye *et al.*, 2002b; Li *et al.*, 2000a), as well as the recently discovered resonance from the "bubble" crystal phase in high ($\nu > 4$) Landau levels (Lewis *et al.*, 2002), all thought to be caused by the pinning mode of domains of 2DES crystal phases (Chap. 3). The many-particle nature of such a pinning mode is in fact reflected in several features of our observed resonance. For example, the resonance at 14 T, $\nu = 0.89$ is observed up to nearly 200 mK[4], much higher than $hf_{\rm pk}/k_{\rm B} \sim 50$ mK where $f_{\rm pk} \sim 1$ GHz is the resonating frequency. This rules out the pictures of individual particles trapped by disorder or individual (quasi)particle localization-delocalization transition giving rise to the resonance[5] (Kivelson *et al.*, 1992). Furthermore, the resonance (at the lowest temperature) can have quality factor Q more than 3. As discussed in Chap. 3, the collective motion of a large region of particles can average disorder and allow such a high Q (Fertig, 1999; Fogler and Huse, 2000).

Additional insights about our observed resonance, in support of the pinned Wigner

[3]In fact the existence of resonance for $\nu = 1 - \nu^*$ as well as (previously known) for $\nu = \nu^*$ (with ν^* a positive number in certain range) can be considered as a manifestation of the particle-hole symmetry in the LLL. Such a symmetry is difficult to exhibit in dc transport, because at ν=1$-\nu^*$ (IQHWC), the DC R_{xx}=0 (dissipationless) due to filled LL (contributing to the edge conducting channel (Prange and Girvin, 1990)); whereas at small ν (high-B WC), the entire 2DES goes insulating and has diverging R_{xx} (at low T).

[4]A set of T-dependent spectra can be found in Appendix I.

[5]In this kind of single particle picture, the resonant frequency is generally associated with the energy (Δ_σ) needed to promote a particle to delocalized states and this would predict a temperature scale $T_C \sim \Delta_\sigma/k_B$, above which the resonance would not be seen.

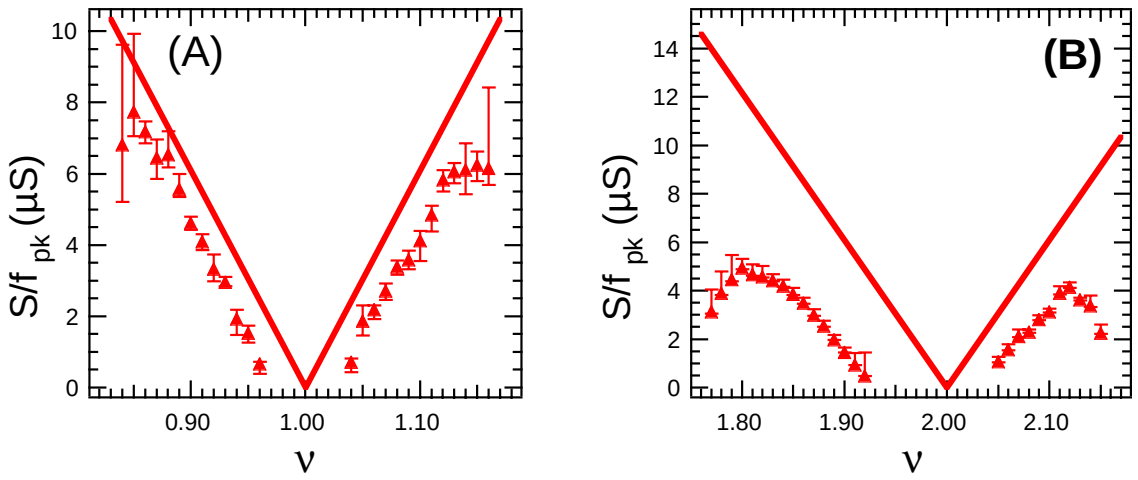

Figure 4.5: **(A):** Oscillator strength divided by peak frequency($S/f_{\rm pk}$) as a function of filling factor, for resonance around $\nu = 1$. Thick solid line is the Fukuyama-Lee result for WC of effective filling factor $\nu^* = \nu - 1$. **(B):**$S/f_{\rm pk}$ as a function of filling factor, for resonance around $\nu = 2$. Thick solid line is the Fukuyama-Lee result for WC of effective filling factor $\nu^* = \nu - 2$. All data from Sample R and at ∼50 mK.

crystal picture, can be gained by integrating the spectrum to extract the oscillator strength[6] S. As we discussed in Sec. 3.1.6, theory by Fukuyama and Lee (Fukuyama and Lee, 1978) has calculated conductivity Re$[\sigma_{xx}(f)]$ that predicts (see also Appendix G) $S/f_{\rm pk} = |n^* e\pi/2B| = |(e^2\pi/2h)\nu^*|$ for pinned 2D WC with density n^* and effective filling factor ν^* under perpendicular B. Fig. 4.5 (A) and (B) display $S/f_{\rm pk}$ calculated for the resonance in Fig. 4.2 (around $\nu = 1$) and Fig. 4.3 (around $\nu = 2$) respectively. We see indeed the data follow a straight line over most of its range. We remark here that the magnitudes of the resonance and S are found to have some significant variations (up to factor of 2) for different cool-downs and samples (from the same wafer), but such linear-like behavior in $S/f_{\rm pk}$ versus ν^* is always observed.

An important feature of our resonance, already evident from the spectra plot, is that the peak frequency of the resonance always monotonically increases with decreas-

[6]The integrated intensity of the pinning mode. For experimental spectrum Re$[\sigma_{xx}(f)]$ measured on a *finite* frequency range $[f_0, f_1]$ and often containing a constant background level, we here extract S by first computing the indefinite integral $S(f) = \int_{f_0}^{f} \mathrm{Re}[\sigma_{xx}(f)]df$ for $f_0 < f < f_1$, then fitting its high frequency part(near f_e) to a straight line and subtracting the slope from the original Re$[\sigma_{xx}(f)]$, then recalculating $S(f)$ and taking the difference of its maximum and minimum values as S.

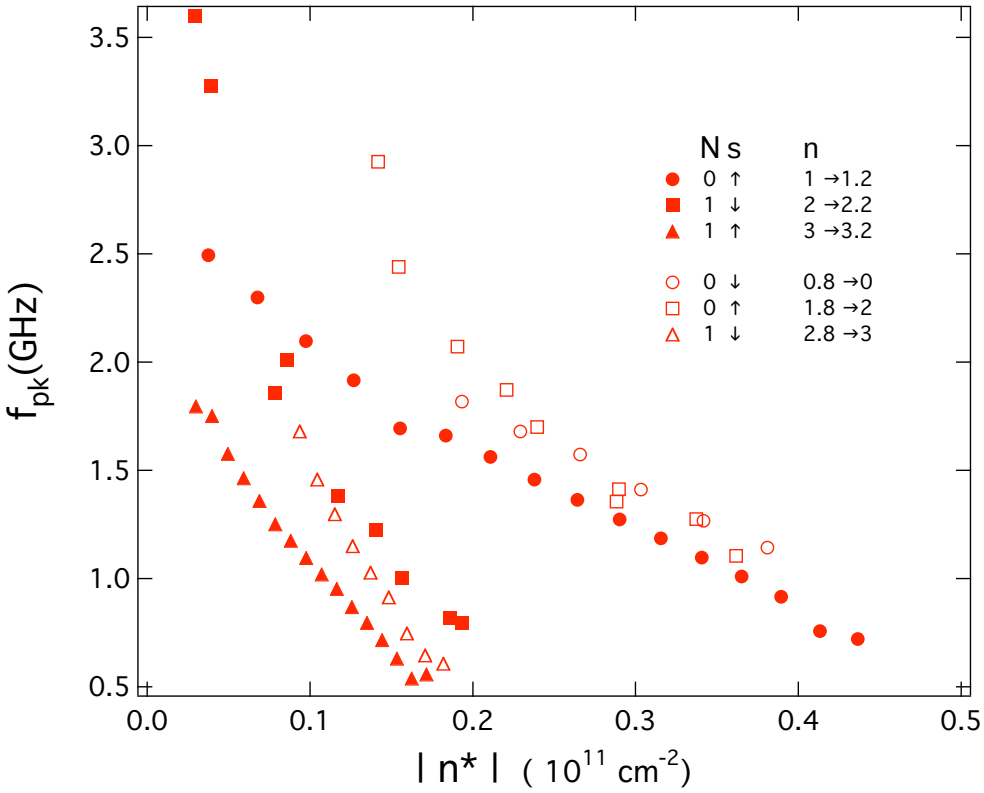

Figure 4.6: Summary of $f_{\rm pk}$ (of the resonance shown in Figs. 4.2,4.3,4.4) vs n^* (of partially filled top LL). N is the orbital LL index and σ the spin index. The solid symbols indicate IQHWC of Landau-electron, and empty symbols for IQHWC of Landau-holes. All data measured in Sample R at $\sim$ 50mK.

ing effective density n^* (in our case the B field has a slight variation, less than 20%, around each integer filling), as shown below in Fig. 4.6 summarizing $f_{\rm pk}$ as functions of n^* around ν=1,2, and 3. This is a key character of the "weak-pinning" picture (Li *et al.*, 2000a; Ye *et al.*, 2002b).

The data in Fig. 4.6 nearly fall into two branches, according to the orbital Landau level index (the asymmetry around ν=2 is especially clearly demonstrated). This may be interpreted as an effect of the different single-particle wavefunction in different orbital LL giving rise to different *effective* disorder (Sec. 3.2.2), which determines $f_{\rm pk}$ of a pinned WC (Sec. 3.1.2).

From the data presented in this section, we notice that the observed resonance is

IQHWC	of Landau (quasi-) elestrons	of Landau (quasi-) holes
around ν=1	1.04< ν <1.16	0.84< ν <0.96
around ν=2	2.04< ν <2.15	1.77< ν <1.92
around ν=3	3.04< ν <3.17	2.81< ν <2.92
around* ν=4	4.05< ν <4.28	3.81< ν <3.96

Table 4.1: Summary of the ν range where IQHWC resonance is observed on Sample R at 50 mK. The typical uncertainty in ν is 0.01.
*Note: For $4.15 \lesssim \nu \lesssim 4.28$, IQHWC resonance coexists with the "bubble" crystal (BC) resonance (Lewis *et al.*, 2004b) in the 2nd excited orbital LL.

mostly visible in a ν^* range of $\nu_l^* < |\nu^*| < \nu_u^*$ (as summarized in Table 4.1. The range[7] can depend on the specific integer filling and even the sign of ν^*). The existence of an "upper limit", ν_u^* , analogous to the case in LLL Wigner crystal, is probably because WC is not the ground state of our 2DES at large enough ν^*. For example, away from $\nu = 1$, as $\nu \to 4/5$ or $\nu \to 6/5$, the system would enter the FQHE state, which is an incompressible liquid. This kind of "quantum melting" of the WC state would account for the observed weakening of the resonance and the drop of $S/f_{\rm pk}$ at large $|\nu^*|$ seen in Fig. 4.5. The existence of a "lower limit", ν_l^*, also corresponding to a "lower limit" for density $n_l^* = (n/\nu)\nu_l^*$, possibly indicates the "carriers" (electrons/holes) are individually localized by disorder for densities n^* below n_l^*. This lower limit of n^* would also imply that higher density, higher quality (low disorder) samples can allow such resonances to be observable around higher integer fillings. We have found resonances around ν=1, 2, and 3, but not around ν=4, in sample WP (with n=1×10^{10}cm^{-2}). Measurements performed on sample P, an even lower density and lower mobility sample ($n\sim 7 \times 10^{10}$cm^{-2} and $\mu\sim 5 \times 10^6$ cm^2 V^{-1}s^{-1}) have only found relatively weak resonance around $\nu = 1$ and none around higher integer fillings. Resonance data from these two samples are presented in Appendix I.

For more disordered 2DES, theories of frequency-driven variable range hopping conduction in IQHE (Efros, 1985; Polyakov and Shklovskii, 1993) predict a linear

[7]It is possible that the range could further expand at even lower T than presented here.

dependence of Re[σ_{xx}] on frequency, which has been confirmed in recent experiments (Hohls *et al.*, 2001; Lewis and Carini, 2001) on samples of mobilities up to 5×10^5 cm^2 V^{-1}s^{-1}. No resonances were seen in these experiments.

In summary, we have observed a microwave resonance around integer fillings in high quality 2DES. On either side of these integer fillings ($\nu = K$), the resonance $f_{\rm pk}$ monotonically increases with decreasing $|\nu^*|$, whereas the resonance is strongest at certain ν away from K. We interpret the resonance as caused by the pinning mode of a Wigner crystal phase of density $n^* = (n/\nu)\nu^*$ formed by electrons/holes in the top Landau level, around the corresponding integer fillings.

4.2 Higher Landau Levels: Bubbles, Stripes and all That

The IQHWC discussed in the last section can be considered as a special case of a charge density wave (CDW) phase. A rich array of other CDW phases can exist in higher LLs (Sec. 1.1.4, see also the review articles by Eisenstein (2001) and Fogler (2003)). For completeness, we give in this section a very brief overview of microwave spectra of these CDW phases, especially in the second excited (N=2 orbital) LL. More details can be found in Lewis *et al.* (2002, 2004b, 2005a). Data presented here were measured with multiple pieces of Sample R (30nm QW, with $n\sim3\times10^{11}$cm^{-2} and $\mu\sim2.4\times10^6$cm^2/Vs) using a variety of CPWs.

Fig. 4.7 displays a set of Re[$\sigma_{xx}(f)$] spectra measured around ν=4 (from ν=3.73 at the bottom to ν=4.29 at the top). For the $\nu<4$ side, we see the broad, relatively weak IQHWC resonance, qualitatively similar to the one observed around ν=1,2 and 3. If we increase ν from 4 to enter the $\nu>4$ side, quite a different picture occurs: initially we also see the IQHWC resonance, but when ν approaches $\sim$4.25 (quarter-filled top LL), another lower frequency, and much sharper resonance clearly develops

and eventually dominates the spectrum. This resonance was in fact found earlier (than the IQHWC resonance) and identified as the pinning resonance of the "bubble crystal" (Lewis *et al.*, 2002), thought to be a WC with a pair of electrons ("M=2 electron bubble") per lattice site (Koulakov *et al.*, 1996; Haldane *et al.*, 2000; Taut, 2001; Shibata and Yoshioka, 2003). Furthermore, there is a finite range of ν in which both the BC resonance and the IQHWC resonance appear in the spectrum (Lewis *et al.*, 2004b), indicating coexistence of the two crystal phases during the apparent IQHWC to BC transition (Lewis *et al.*, 2004b; Gervais *et al.*, 2005a).

The BC resonance seen in Fig. 4.7 (the "electron bubbles") can be observed up to $\nu\sim4.38$ and reappears on the other side of ν=9/2, for $4.64 \lesssim \nu \lesssim 4.80$ (the "hole bubbles"). Details can be found in Lewis *et al.* (2002). The BC resonance is strongest around ν=4+1/4 or 4+3/4, near which DC transport studies found a reentrant IQH state (Lilly *et al.*, 1999a; Du *et al.*, 1999; Cooper *et al.*, 1999) and theoretical calculations predicted a M=2 electron bubble crystal phase.

At half-filled higher LLs (such as near ν=9/2), DC transport (Lilly *et al.*, 1999a; Du *et al.*, 1999) have found highly anisotropic diagonal resistances[8]. Such an anisotropic state has been thought to be consistent with the "stripe" phase[9] earlier theories predicted to occur near the center of higher LLs (Koulakov *et al.*, 1996; Fogler *et al.*, 1996; Moessner and Chalker, 1996). The stripe phase has been suggested to be some electronic liquid-crystal phase with many interesting properties (Fradkin and Kivelson, 1999; MacDonald and Fisher, 2000; Fogler, 2001). Microwave measurements using straight-line CPWs with different electric field ($\vec{E}$) orientations[10] are currently underway to investigate the stripe phase and its transition (when changing ν) to the BC phase (Lewis *et al.*, 2005b). Some features of our preliminary data have been ad-

[8]The low resistance direction (which turns out to be <110>) is typically referred to as the "easy" direction and the high resistance direction (<1$\bar{1}$0>) as the "hard" direction.

[9]We also note a recent theory (Ettouhami *et al.*, 2005) suggesting an anisotropic Wigner crystal phase in higher LLs.

[10]Note for a straight line CPW, the microwave electric field $\vec{E}$ is perpendicular to the longitudinal CPW direction.

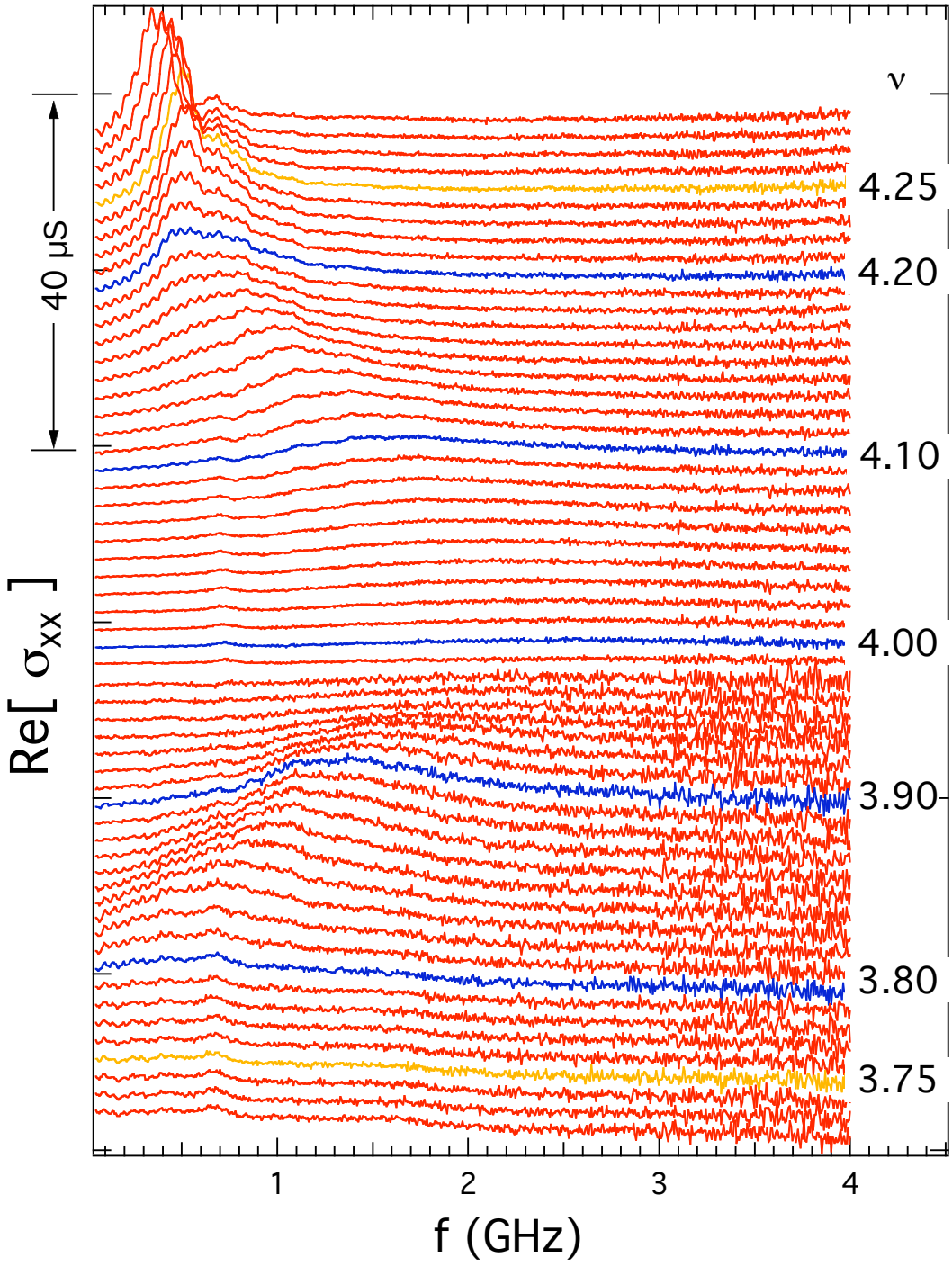

Figure 4.7: Sample R: Spectra around ν=4. At ν>4 side (second excited LL), the IQHWC resonance can coexist with the lower f, much sharper bubble crystal (BC) resonance. Data measured at T∼35mK and using a meander CPW (M30). Traces are all offset for clarity.

dressed by a "quantum depinning transition" theory (Li *et al.*, 2000b) whereas many other aspects (for example an apparent saturation (Lewis *et al.*, 2005b) of BC $f_{\rm pk}$ upon ν approaching 9/2 in the "hard" direction data) remain to be explained.

BC resonance (near quarter filled top LL) similar to the one shown above have also been observed in even higher (N=3, 4) LLs (Lewis *et al.*, 2005b). Measurements also found a resonance, possibly due to a similar bubble phase (particularly near ν=2.58) in the 1st excited (N=1) LL (Lewis *et al.*, 2005a).

4.3 Notes and Further Directions

Preliminary measurements[11] by Sambandamurthy *et al.* (2005a) have found that adding an in plane field ($B_{||}$) can shift the IQHWC and BC[12] pinning resonances to higher frequency, and the effect appears to be larger for higher LL index. The mechanism that gives rise to the phenomenon is currently unclear. Possibilities may include a tilt-induced change of effective vertical confinement (from changing electron orbital wavefunction in the QW), or change in the electron crystal shear modulus μ_t [13]. DC transport have previously shown that $B_{||}$ can affect the high LL CDW phases dramatically (Lilly *et al.*, 1999b; Pan *et al.*, 1999). More recently, a "tilt-induced delocalization"[14] was found Csathy *et al.* (2005b) in the 1st excited LL[15]. It is interesting for example, in view of (Csathy *et al.*, 2005b), to examine whether the ν range of the IQHWC resonance above ν=2 (Table. 4.1) changes under $B_{||}$.

Away from ν=1, instead of simple Landau quasi-particles with single spin-flip,

[11] employing an *in-situ* sample rotator with flexible coax connection.

[12] IQHWC around ν=2 (both sides) and BC near ν=4+1/4 (all in Sample R) have been measured by Sambandamurthy *et al.* (2005a).

[13] note μ_t can be highly nonclassical in high LLs (Ettouhami, 2005)

[14] It was found there, that upon tilting, the "re-entrant IQH" states (Eisenstein *et al.*, 2002) disappear into rather featureless states (classical R_{xy}) and the 1/5th FQHE states (in N=1 LL) merge into nearby (now widened) IQHE plateaus (Csathy *et al.*, 2005b).

[15] We also note here the theoretical work (Yu and Yang, 2002) that predicted a shifted WC-FQHE boundary in LLL under $B_{||}$

the elementary excitations have been proposed to be skyrmions[16] (Sondhi *et al.*, 1993; Fertig *et al.*, 1994), which have received support from subsequent experiments (for example, Barrett *et al.* (1995); Schmeller *et al.* (1995)). Correspondingly, around ν=1, a "Skyrme" crystal has been proposed (Brey *et al.*, 1995; Green *et al.*, 1996; Côté *et al.*, 1997; Green, 2000) and there are some recent experiments hinting at its existence (Bayot *et al.*, 1996; Desrat *et al.*, 2002; Gervais *et al.*, 2005b). These experiments showed a response (in their quantities related to nuclear spin relaxation) that has an orders-of-magnitude difference between near $\nu = 1$ and near other integers. However, our experiments have not found a qualitative difference in the resonance we observed around $\nu = 1$, 2, and 3; and it remains unclear whether the pinning resonance would be sensitive to any exotic underlying spin structure, such as skyrmions, in the electron crystal. Investigating tilting ($B_{||}$) effect on the resonance around ν=1 would be potentially illuminating[17].

So far we have never observed any resonance around fractional fillings such as 1/3, in our samples down to $T\sim$ 50mK, although the possibility of crystallization of fractionally-charged quasi-particles around FQHE was proposed theoretically long ago (Halperin, 1984). Alternatively, such a "fractionally charged WC" (FWC) may also be viewed as the "IQHWC" in composite fermion (CF) integer LLs (Goerbig *et al.*, 2004b). In relation to future efforts to search for such a "FWC", we make the following remarks for the case around 1/3 FQHE[18] :

1) The formula for $f_{\rm pk}$ in Chitra *et al.* (2002) gives $f_{\rm pk}\propto 1/e^3$. Simple substitution of e by $e/3$ implies the $f_{\rm pk}$ for FWC may be much higher than $f_{\rm pk}$ for electron WC

[16] A skyrmion can effective reverses several spins by modulating the spin in a more continuous (and spatially-extended) way and saves exchange energy against Zeeman energy. Skyrmions are thought to be generally less favorable around other odd integer fillings (skyrmions are irrelevant around even integer fillings) than 1 (Wu and Sondhi, 1995).

[17] Particularly interesting are to measure samples WP and/or P, which have their ν=1 at relatively low B due to the lower n of these samples—this not only enables a large tilting range; it also makes (at zero-tilt) the "effective (dimensionless) Zeeman energy" $g\mu_B B/(e^2/4\pi\epsilon l_B)$ to be smaller, a condition believed to favor skyrmions (Schmeller *et al.*, 1995).

[18] since 1/3 FQHE is the strongest FQHE in general, and corresponding to ν=1 in CF LL, we expect here the best chance for observing FWC

(assuming they are otherwise pinned similarly).

2) If we define $\nu^* = \nu - 1/3$, then this correspond to a $\nu^*_{\rm CF}$ (partial filling in top CF LL, here defined as $\nu_{\rm CF}$-1, where $\nu = \nu_{\rm CF}/(2\nu_{\rm CF}+1)$ in our case[19]) to be $\nu^*_{\rm CF} = 9\nu^*/(1-6\nu^*)$. Therefore an IQHWC in the 1st CFLL, for example with $\nu^*_{\rm CF} \sim 0.1$ corresponds to a much smaller $\nu^* \sim 0.01$ around 1/3.

3) FWC will likely require very clean samples and/or very low T, such that interaction between CFs (or fractionally charged quasipaticles) are sufficiently prominent, indicated by, for example, well developed CF-FQH states[20] (Pan *et al.*, 2003).

Obviously, a lot of further experimental[21] as well as theoretical work are needed to look for and understand such a remarkable phase.

Also interesting for further investigation is the issue of IQHWC-FQHE transition/competition. For example, the fact that we observe an resonance at ν=1.8 (Fig. 4.2 and Table. 4.1) is consistent with the absence of a 9/5 FQHE state in DC transport (Pan, 2003). A natural question is, which state (WC or FQHE) is the real ground state at ν=9/5? Would a 9/5 FQHE state show up at elevated T (Pan *et al.*, 2002; Gervais *et al.*, 2005a)?

Another issue is to further clarify the nature of the reentrant IQHE state in the 1st excited LL (Eisenstein *et al.*, 2002; Xia *et al.*, 2004). For example, at least four such states were found between ν=2 and 3 (Eisenstein *et al.*, 2002), near 2.28, 2.42, 2.57, 2.70 respectively. Although these states could be a similar bubble crystal (Fogler, 2003; Lewis *et al.*, 2005a) like those near the 1/4 filled 2nd excited LL (Lewis *et al.*, 2002) , the two states ($\nu \sim$ 2.28 an 2.70) nearer to IQHE could also possibly be reentrant IQHWC (Shibata and Yoshioka, 2003) competing with 1/5 FQHE states in the 1st excited LL. More precise measurements (perhaps at lower T) of $f_{\rm pk}$ at these states, and comparing them to $f_{\rm pk}$ of the nearby IQHWC, may be helpful in resolving

[19] with 1/3 belonging to the "CF-2" series (Jain, 2000)

[20] such as 4/11, whose $\nu_{\rm CF}$=4/3, or even states with 1/5-fillings of CF LL.

[21] Among our samples, it will be particularly interesting to measure Sample WP (which is known to show a 4/11 state) in C120, under the low T ($\lesssim$ 35 mK) now available.

the difference (Lewis *et al.*, 2004b; Goerbig *et al.*, 2004a).

The resonance we observe near quarter filled 2nd excited LL (Fig. 4.7) is identified to be from the predicted BC of M=2 (two electron per site) bubbles (Lewis *et al.*, 2004b). Higher order-M bubbles are also predicted in high LLs (Fogler *et al.*, 1996; Shibata and Yoshioka, 2003). Pushing our measurements to lower T may reveal these rich phases and elucidate the transitions among them.

So far we have conceptually always treated the filled LL's as "inert" background. They can be shown to modify the effective interaction in top LL (Fogler *et al.*, 1996). More quantitative investigation of the n^* dependence of IQHWC pinning mode (both $f_{\rm pk}$ and Δf) may bring further insights for subtle effects such Coulombic, liquid background might have on pinned IQHWC.

Finally we would like to point out, that although the microwave resonance we observed near integer ν constituted the first experimental evidence for IQHWC, signatures of IQHWC can also, at least in principle, be obtained from thermopower measurements (Faniel *et al.*, 2005) or careful T-dependence measurements of DC magneto-resistance tensors (Kivelson *et al.*, 1992). Correlating microwave measurements with these other types of experiment could potentially yield additional insights about IQHWC.

Chapter 5

Solid Phases in the Lowest Landau Level: "A" and "B"

5.1 Introduction

The fundamental question about a two dimensional electron system (2DES) in a perpendicular magnetic field (B) is the nature of the ground state (GS) and the transition/competition between different possible GS. It is generally expected (Lozovik and Yudson, 1975; Fukuyama *et al.*, 1979) that a Wigner solid (WS) (Wigner, 1934) should form at sufficiently high B. On the other hand, a 2DES with areal density n can condense into quantum Hall effect (QHE) states (Prange and Girvin, 1990) with dissipation-free[1] transport at a series of integer or fractional Landau filling factors $\nu=(h/e)(n/B)$, where h/e is the Dirac flux quantum. Calculations (Lam and Girvin, 1984; Levesque *et al.*, 1984; Zhu and Louie, 1995) predicted the transition from the fractional QHE series (which are incompressible quantum liquids) to WS to occur around $\nu=1/5$. DC transport studies (Willett *et al.*, 1988; Jiang *et al.*, 1990) on high quality (low disorder) samples at the lowest temperatures have found $\nu=1/5$ to be

[1] In local dc ρ_{xx} and σ_{xx}.

the lowest ν fractional QHE (FQHE) state. At higher B the 2DES enters an insulating phase. Early experiments (see reviews in Chui (1994); Fertig (1997); Shayegan (1997)) on this high B insulating phase (HBIP) were interpreted as consistent with an electron solid pinned by disorder. In this chapter, we report our radio frequency (rf) spectroscopy experiments on extremely low disorder 2DES and present evidence that the HBIP may consist of not just one, but *two* different solid phases.

Using rf and microwave spectroscopy (Chap. 2), previous experiments (Ye *et al.*, 2002b) have measured a high quality 2DES[2] down to ν as small as $\sim$1/25, and observed a single sharp resonance in the frequency (f) dependent real diagonal conductivity (Re[$\sigma_{xx}(f)$]) of 2DES in the HBIP. Such a resonance, as we have discussed (Chaps. 1, 3), has been taken as signature of an electron solid and interpreted as due to the "pinning mode" (the disorder-gapped magnetophonon) (Fukuyama and Lee, 1978; Normand *et al.*, 1992; Fertig, 1999; Fogler and Huse, 2000; Chitra *et al.*, 2002) of WS crystalline domains oscillating collectively within the disorder potential.

In the experiments described in this chapter, we measured even lower disorder 2DES and observed *two* different resonances in different regimes of HBIP. One resonance ("A") is observable for $\nu<2/9$ (and *reentrant* around ν=1/5 FQHE); it then *crosses over* (as ν is reduced below $\sim$0.18, by increasing B) to the different "B" resonance which dominates at sufficiently low ν ($\lesssim 0.125$). We interpret the two resonances as coming from *two* different solid phases (referred as "A" and "B" phases) which are pinned by disorder. Studying samples with different n has shown that the transition from "A" to "B" is controlled by ν. Moreover, the "A" resonance is found to show dispersion with respect to the size of the transmission line, indicating that the "A" phase has a large correlation length. We suggest that many-body correlations, such as those responsible for the FQHE, are important in giving rise to such different solids. The "A" phase, which occurs at relatively lower B, is most likely

[2]Sample P was measured in Ye *et al.* (2002b).

to be closely related to FQHE and may be an electron solid possessing substantial FQHE-type correlation.

Part of the results in this chapter have been published in Chen *et al.* (2004c).

5.2 Samples and Measurements

The 2DES samples we used were fabricated from WP and QW65, two very high quality AlGaAs/GaAs/AlGaAs quantum well (QW) wafers grown by molecular beam epitaxy. Data from 4 pieces of samples will be presented, and for brevity, will be labeled as Sample 1, 2a, 2b, 2c in this chapter. Sample 1, cut from wafer WP (Appen. C), contains a 50nm-wide QW with n=1.0×10^{11}cm^{-2} and mobility $\mu\sim$1×10^{7}cm^{2}/Vs. Samples 2a-2c are from wafer QW65 (Appen. C), each containing a 65nm-wide QW with n ranging from 5-6×10^{10}cm^{-2} and $\mu\sim$8×10^{6}cm^{2}/Vs. A standard meander (M30) CPW was fabricated on Sample 1, and various types of CPW, to be specified below, were used for Samples 2a-2c.

The rf/microwave measurement methods have been described in Sec. 2.2. For data presented in this chapter, even though the 2DES here is not always in its long wavelength limit as will be seen (therefore Eq. 2.1 does not hold accurately), we have casted our measured P (relative power absorption of 2DES) into a real diagonal conductivity which we define $\mathrm{Re}[\sigma_{xx}^{c}]=(w/2lZ_0)\ln(P)$, where (Sec. 2.2.1) w and l are the slot width and length of the CPW respectively and Z_0=50 Ω.

5.3 Observation of Two Different Resonances: "A" and "B"

5.3.1 "A" and "B" resonances and a ν-induced crossover

Fig. 5.1 shows Re$[\sigma^c_{xx}(f)]$ spectra measured at various B from sample 1, at the temperature (T) ∼60 mK. The traces are displayed in increasing order of B from the bottom (taken at 18.6 T) to the top (at 33 T) and are offset by 3 μS from each other for clarity. The spectrum is flat at B=18.6T, corresponding to the ν=2/9 FQHE liquid state. Upon increasing B, a clear resonance (with peak frequency ($f_{\rm pk}$) ∼150 MHz) can be observed; the resonance is interrupted briefly (with flat spectra) near ν=1/5 FQHE liquid then reappears at higher B. This resonance, reentrant around ν=1/5 (more details about this resonance near ν=1/5 will be presented in section 5.3.3), will be referred to as peak "A" hereafter. At 22.9 T, ν∼0.18, another resonance, labeled as "B", starts to appear ($f_{\rm pk}$ ∼80 MHz). On further increasing magnetic field, resonance "B" grows while "A" continues to shift but eventually weakens. By 33 T (ν=0.125), resonance "B" dominates the spectrum and "A" nearly disappears. From 22.9 T to 33 T (ν from 0.18 to 0.125) the spectra display a clear crossover from "A" to "B"; moreover, in this crossover region they can show complicated structures, for example an intermediate peak like the one labeled "C" appearing between "A" and "B".

We have also observed higher lying but relatively weak resonances such as the one labeled as peak "2" in the figure. Although they appear to have some qualitative similarities with "A" (for example, the qualitative dependence on magnetic field), their origin is not very clear at present. One possibility is that they may be related to the higher harmonics[3] of "A". More details of them will be discussed elsewhere

[3]Although they do not appear to fit *simple* (integer multiples in frequency or wave vector q) harmonic series of "A".

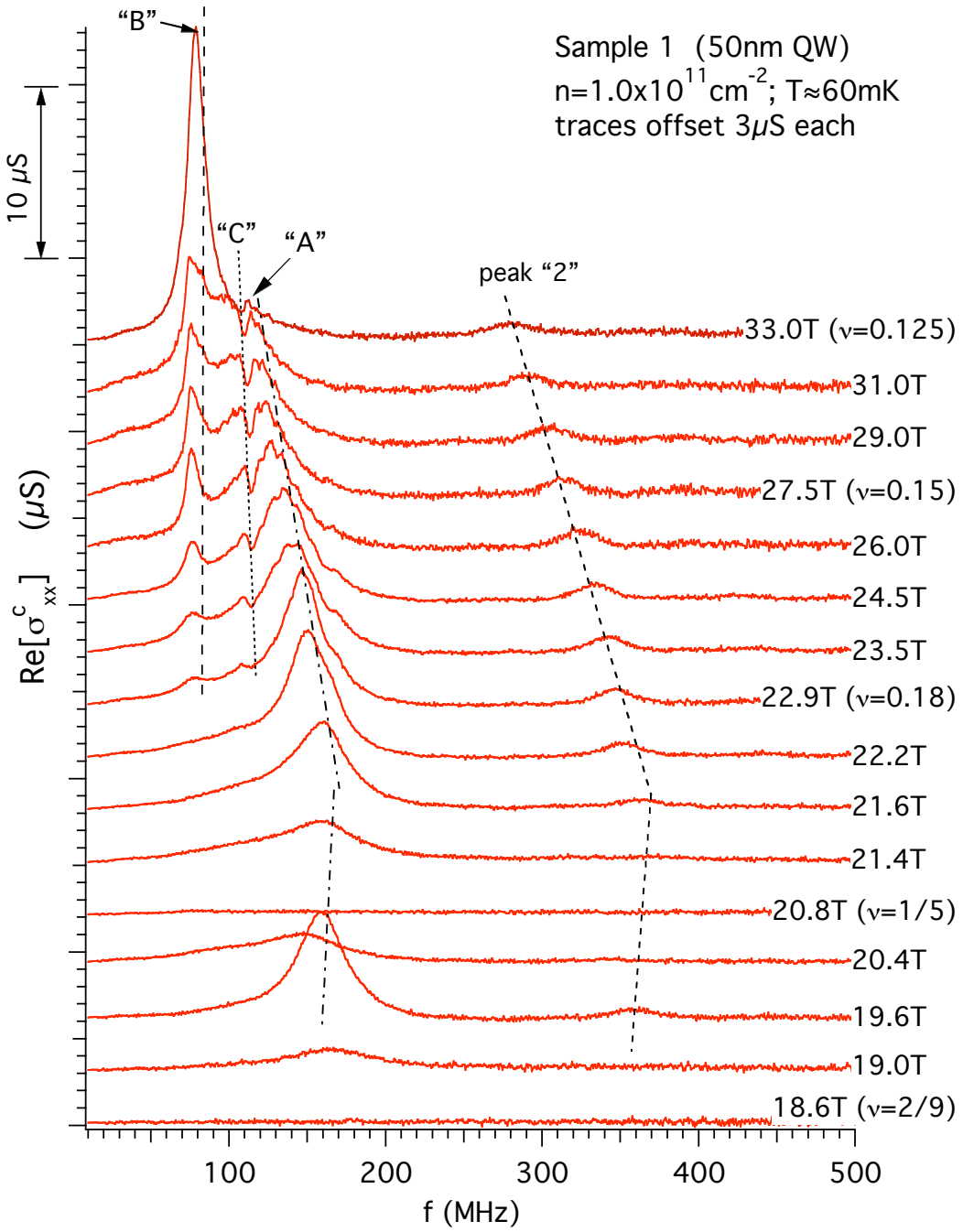

Figure 5.1: Sample 1 (WP_M30): Re$[\sigma^c_{xx}(f)]$ spectra at various B, in increasing order from B=18.6T (bottom) to 33T (top). Adjacent traces are offset for 3μS from each other for clarity. Magnetic fields (and selected ν's) are labeled at right. Measurements were performed at $T \sim$60 mK. From left to right, the long dashed, dotted, dot-dashed, and short dashed lines are guides to the eye, corresponding to peaks "B", "C", "A" and "2" respectively, as explained in the text.

(Lewis *et al.*, 2005b).

Fig. 5.2 summarizes the B-dependence (plotted in (A)) and ν-dependence (plotted in (B)) of the peak frequencies ($f_{\rm pk}$) of the various resonance peaks ("A", "B", "C" and "2") that we see in Fig. 5.1. We notice (as is already evident from the spectra plotted in Fig. 5.1) that during the cross-over (from "A" to "B") regime, $f_{\rm pk}$ of peak "B" has very weak B-dependence. On the other hand, $f_{\rm pk}$ of peak "A" decreases[4] with increasing B.

From now on in this chapter, we will focus on the data from QW65, which typically gives lower n than WP, allowing a larger ν range to be measured.

Fig. 5.3 shows $\mathrm{Re}[\sigma^c_{xx}(f)]$ spectra measured from sample 2a (QW65 with CPW M30), in which we observe behavior similar to that of sample 1, with one resonance ("A") reentrant around ν=1/5 crossing over to a different resonance ("B") dominating at sufficiently small ν (the lowest ν measured here is 0.075). We emphasize that, compared to sample 1, the crossover here occurs at much lower B, but in essentially the same ν (from $\sim$0.18 to $\sim$0.125) range. We plot $f_{\rm pk}$ of the various resonances as functions of B and ν in Fig. 5.4(A) and (B) respectively, showing qualitatively similar behavior as seen in Fig. 5.2. For peak "B", which is now measured down to a smaller ν than in Fig. 5.2, we clearly see (as already evident in the spectra plot Fig. 5.3) that after it dominates the spectrum at sufficiently high B (small ν), its $f_{\rm pk}$ decreases with further increasing B.

The similar ν range of crossover has also been found in other cooldowns of the same sample with yet different as-cooled n. An example is shown in Fig. 5.5 (A), with similar "A" and "B" resonances, and the crossover from "A" to "B" again occurring at $\sim 0.18 \gtrsim \nu \gtrsim 0.125$.

[4]The B (ν) dependence of $f_{\rm pk}$ of "A" peak, interestingly, for ν slightly below 1/5 (while "B" has not yet become significant), is not very far from $1/B$ (or equivalently, linear in ν); at smaller ν the dependence weakens. See also Sec. 5.3.3 and later discussions.

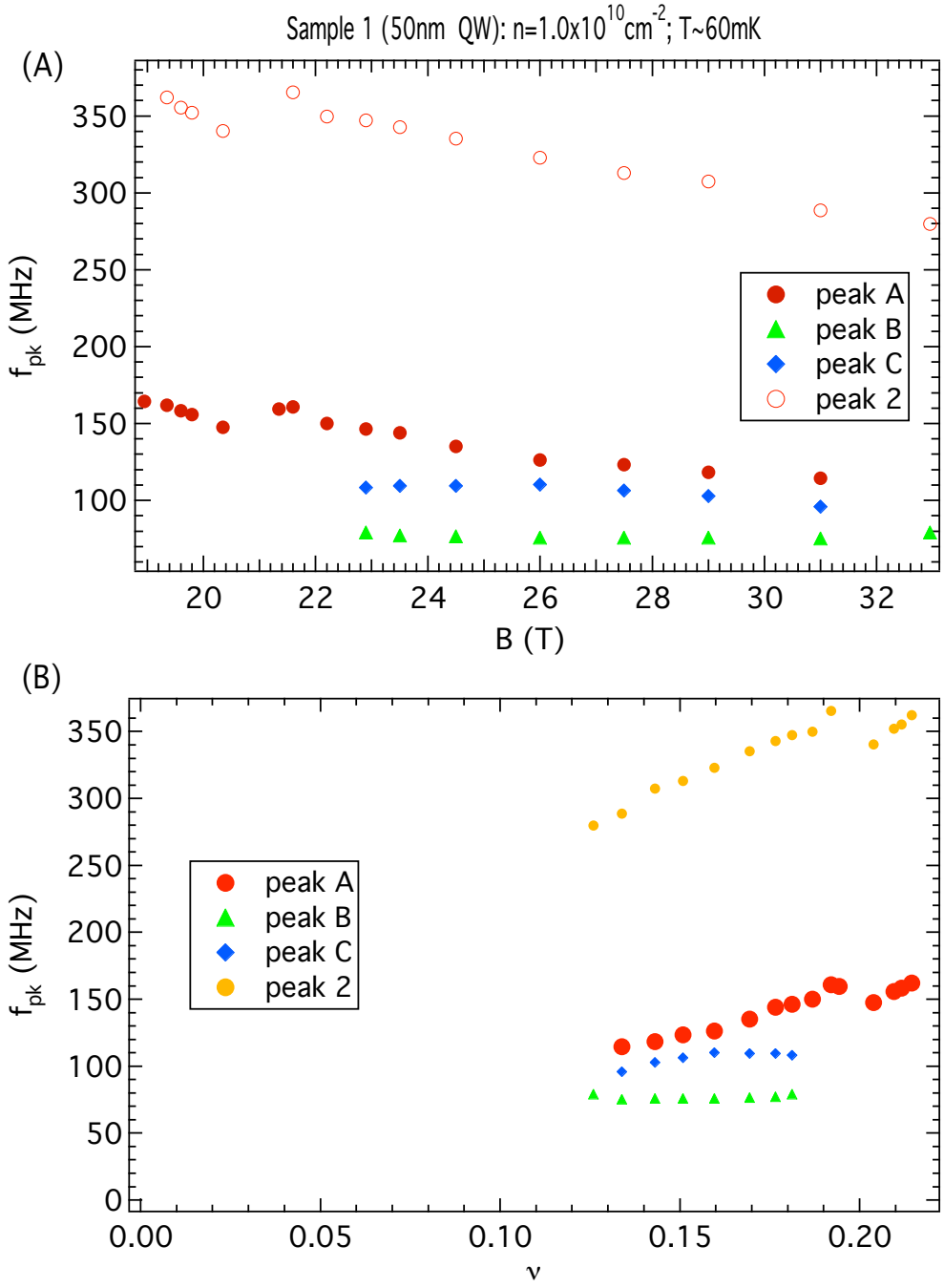

Figure 5.2: Sample 1 (WP_M30), $f_{\rm pk}$ of resonances "A", "B", "C", and "2" plotted in (A): as functions of B; and in (B): as functions of ν. Data measured at $T\sim$ 60 mK.

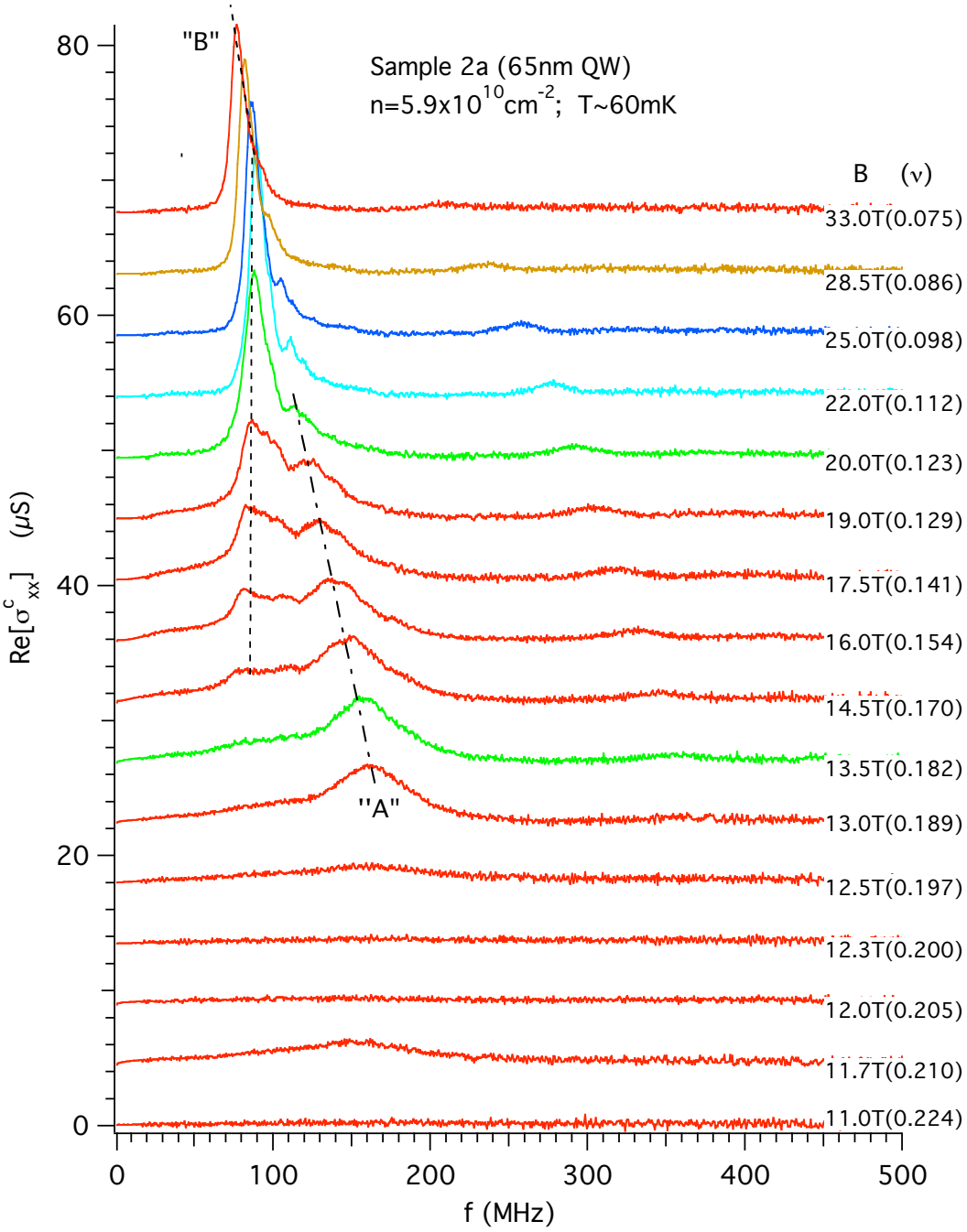

Figure 5.3: Sample 2a (QW65_M30): Re$[\sigma^c_{xx}(f)]$ spectra at various B, in increasing order from 11 T (bottom) to 33 T (top). Adjacent traces are appropriately offset for clarity. Values of B and ν for each trace are labeled at right. Measurements were performed at $T\sim$60 mK. The crossover from "A" to "B" occurs in essentially the same ν range as observed in sample 1 (WP) shown in Fig. 5.1.

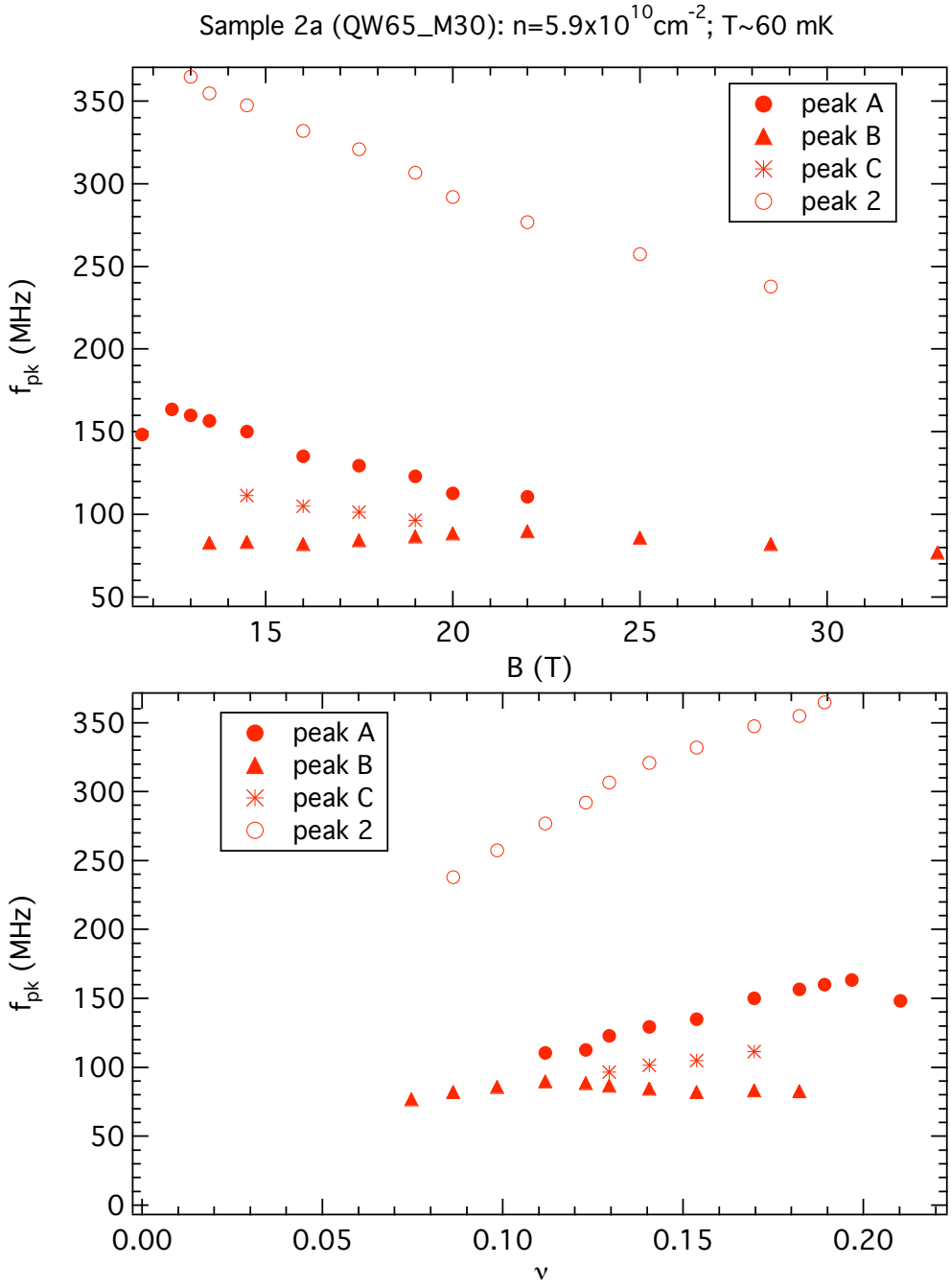

Figure 5.4: Sample 2a (QW65_M30), $f_{\rm pk}$ of resonances "A", "B", "C", and "2" plotted in (A): as functions of B; and in (B): as functions of ν. Data measured at $T\sim$ 60 mK.

5.3.2 Dispersive Behavior of Resonance "A"

A striking difference between resonances "A" and "B" is seen by comparing Fig. 5.5(A), to 5.5(B), which shows the spectra measured at five representative magnetic fields using sample 2b. Sample 2b was cut from the same wafer with sample 2a and only differs in the slot width (w) of the CPW. Both samples show similar resonances "A" and "B", with similar ν range of crossover. However, going from w=30 μm (sample 2a) to 60 μm (sample 2b), we notice that $f_{\rm pk}$ of resonance "A" shifts to lower value while $f_{\rm pk}$ of resonance "B" is not affected; this is true even when resonances "A" and "B" coexist (for example, in the spectrum at 14T). The higher-lying resonance (peak "2") also shifts to lower f by going from w=30μm to 60μm, and in the latter case (Fig. 5.5(B)) we can also resolve at least another even higher-lying weak resonance.

We note that in our measurement, CPW confines the electric field (E) mainly in each slot region of width w (see Fig. 2.3), giving E a step function profile (neglecting edge effects related to the 2DES (Fogler and Huse, 2000), see also Fig. 2.3), and introducing a finite wavevector through the dominant Fourier component $q{\sim}\pi/w$. Therefore we are apparently sensing the dispersion ($f_A(q)$) of resonance "A" using samples with varying w.

5.3.3 Resonance "A" near FQHE

We have seen above that resonance "A" dominates at relatively high ν, from $\sim$0.18 up to 2/9, except for a narrow ν range around 1/5 where there is no resonance. We now examine in more detail the behavior of resonance "A" near FQHE states (ν=1/5 and 2/9). This line of inquiry will yield important insights regarding the electron solid-FQH Liquid transition.

Fig. 5.6 shows a set of spectra in the vicinity of the 1/5 and 2/9 FQHE[5]. The data were measured in sample 2c, a piece cut from QW65 and with a straight CPW

[5]Spectra for ν>2/9 side, where resonance "A" disappears, are not shown

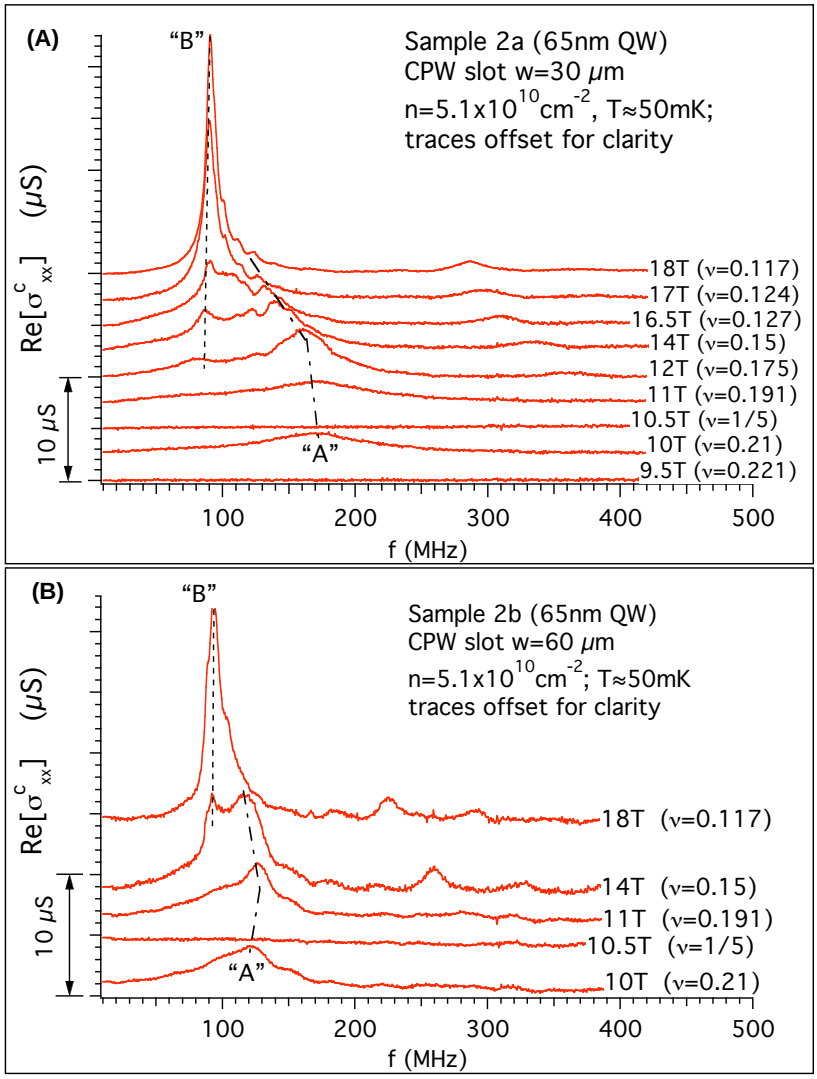

Figure 5.5: **(A)** Sample 2a (QW65_M30): Re$[\sigma^c_{xx}(f)]$ spectra at various B, in increasing order from 9.5T (bottom) to 18T (top). Adjacent traces are appropriately offset for clarity. Values of B and ν for each trace are labeled at right. Measurements were performed at $T\sim$50 mK. Dash and dot-dashed lines are guides to the eye and correspond to resonances "A" and "B", similarly defined as in Fig. 5.1. Compared to sample 1, sample 2a here has about half the density, and the crossover from resonance "A" to "B" also occurs at about half the B, resulting in the similar ν range of crossover. **(B)** Spectra at five representative magnetic fields measured from sample 2b (QW65_M60). Sample 2b, which has a CPW with w=60 μm, is from the same wafer as sample 2a (which has a CPW with w=30 μm) and measured at $\sim$50 mK in a separate cooldown which gave the same density. Traces are appropriately offset for clarity. Compared to corresponding traces in (A), peaks labeled as resonance "B" are seen to occur at the same frequencies but those labeled as "A" shift to lower frequencies. The flat spectrum at ν=1/5 (B=10.5T) is also shown.

(slot w=80μm). The as cooled n here is 6.1×10^{10}cm^{-2}. The traces are displayed (and offset for clarity) from the bottom to the top, in increasing order of ν (ranging from 0.192 to $\sim$2/9, labeled at right). The spectra clearly show that resonance "A" weakens and disappears, *with decreasing* $f_{\rm pk}$, when ν approaches either 1/5 or 2/9.

Fig. 5.7 plots $f_{\rm pk}$ of observed resonance "A" in sample 2c as a function of ν, down to $\nu\sim$0.18 (corresponding to $B\sim$14T, the highest B measured in this experiment. Spectra for ν between $\sim$0.18 to $\sim$0.19 are not shown in Fig. 5.6.). The precipitous drop of $f_{\rm pk}$ near 1/5 and 2/9 FQHE is clearly seen. Another interesting feature we notice is that, when ν is just decreased below $\sim$ 0.192, $f_{\rm pk}$ decreases almost *linearly* with ν. The solid line in Fig. 5.7 shows a linear fit through the $f_{\rm pk}$ data for ν between $\sim$0.18-0.19. The line has a small intercept ($\sim$20MHz) on the $f_{\rm pk}$ axis. We also show, for comparison, a dotted line with a strict $f_{\rm pk}\propto1/B$ (proportional to ν) behavior (Fukuyama and Lee, 1978).

5.4 Discussion

Our data thus reveal two distinct regimes in the HBIP characterized by two different resonances ("A" and "B"): one at 2/9<ν<0.18 (except for a narrow range around[6] ν=1/5) where resonance "A" dominates; and another at ν<0.125 (down to the smallest ν we have accessed) where the rather different resonance "B" dominates [7]. We interpret the two regimes as corresponding to two different (pinned) solid phases, hereafter referred to as "WS-A" and "WS-B" respectively, each being the preferred ground state in the respective ν range. Because of interaction with disorder, either solid is pinned (thus insulating), and can support a pinning mode (Fukuyama and

[6]This reentrant behavior around ν=1/5 is consistent with the earlier observed "reentrant insulating phase" (RIP) around 1/5 (Jiang *et al.*, 1990), and has been thought to result from the competition between the WC energy (monotonic in ν) and FQHE energy (having a "cusp" behavior) (Halperin, 1983, 1984; Jiang *et al.*, 1990).

[7]Data from sample 2a with a relatively low as-cooled density (4.6×10^{10}cm^{-2}) and up to 33T shows resonance "B" to evolve continuously down to $\nu\sim$0.06. No other resonances are observed in the spectrum at such small ν.

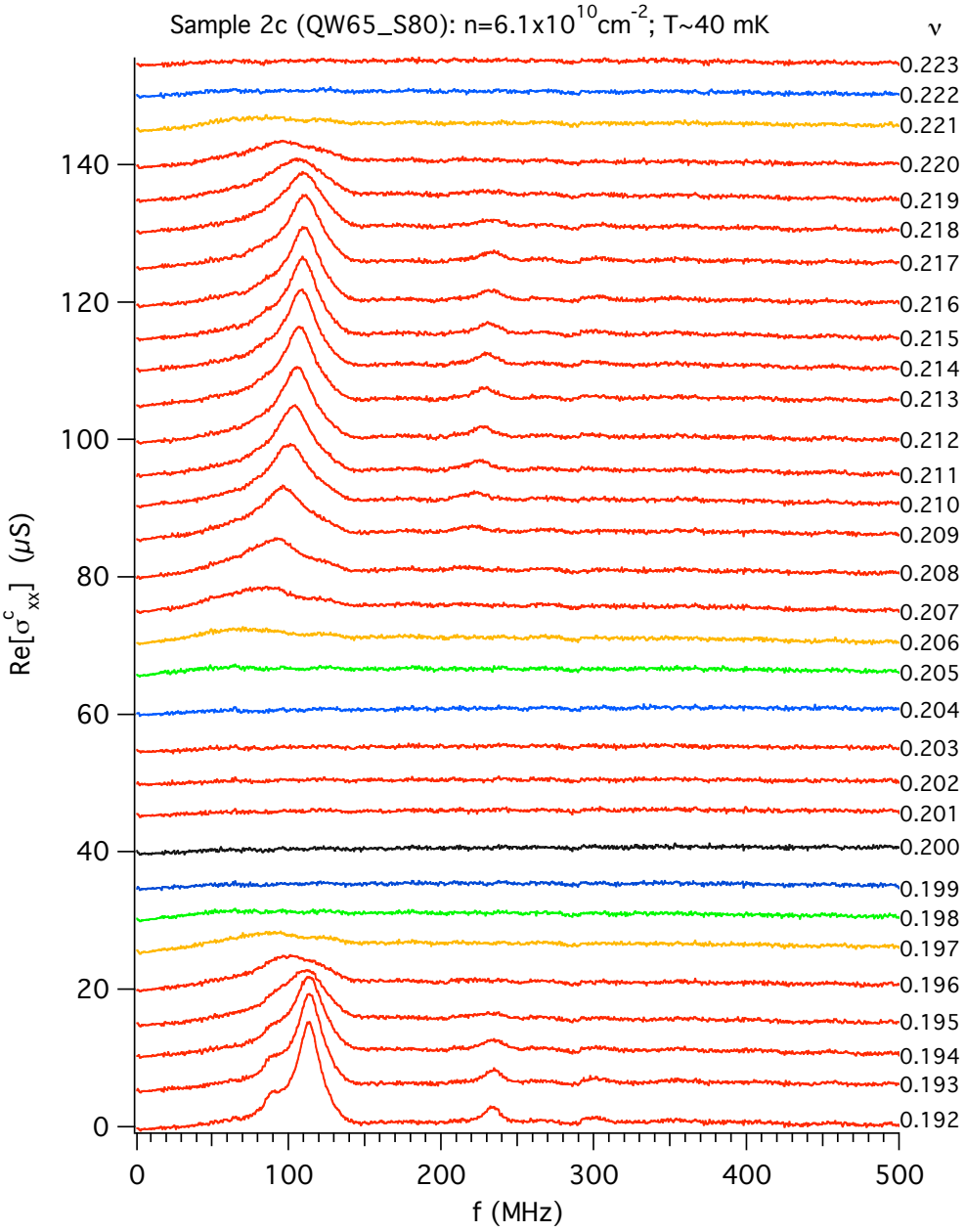

Figure 5.6: Sample 2c (65nm QW): Details of "A" resonance near 1/5 and 2/9 FQHE. Data measured at T$\sim$ 40mK, using a straight CPW (of 80μm wide slots). Filling factor for each trace is labeled at right. Traces offset for clarity.

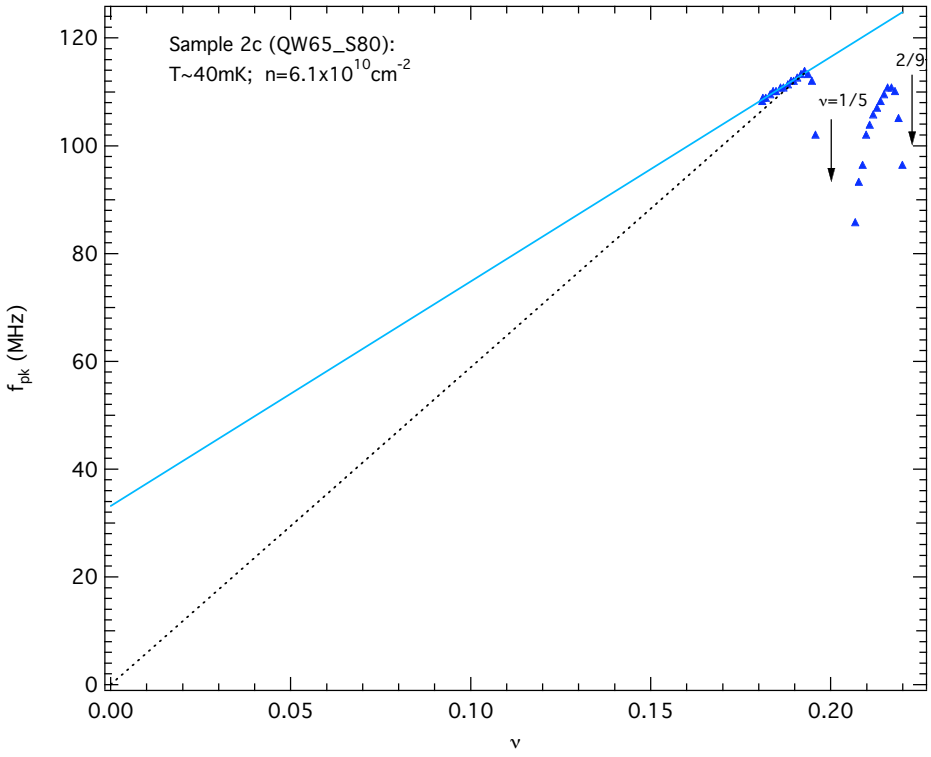

Figure 5.7: $f_{\rm pk}$ of resonance "A" (plotted as a function of ν) measured in Sample 2c (QW65-S80). Data taken at T$\sim$ 40mK down to $\nu\sim$0.18 (B=14T), where "A" resonance still dominates the spectrum. The solid line is a linear fit between $\nu\sim$ 0.18 and 0.191. A comparison is also made with the strictly $1/B$ behavior (proportional to ν), indicated by the dotted line (intercept-free). See text for more details. The special filling factors of 1/5 and 2/9 FQHE are indicated with arrows.

Lee, 1978; Normand *et al.*, 1992; Fertig, 1999; Fogler and Huse, 2000; Chitra *et al.*, 2002) that gives rise to the observed resonance. The $f_{\rm pk}$ in these samples exhibiting two resonances and their crossover are nearly an order of magnitude lower than those seen in previous experiments (Ye *et al.*, 2002b)[8], probably due to significantly reduced pinning disorder.

The striking crossover behavior, which we do not observe for T above[9] $\sim$130 mK , is consistent with a magnetic field induced phase transition from WS-A to WS-B and with coexistence of the two phases (at low T) in the transition regime ($0.18>\nu>0.125$). The intermediate peak[10] "C" disappears at $\sim$100 mK, leaving only peaks "A" and "B" present in the spectra. Though peak "C", like "A" and "B", is reproducible in different cooldowns of the same sample; we have sometimes noticed other delicate features that appear to depend on the way the sample is cooled (for example, peak "B" sometimes briefly splits near ν=0.125 before dominating the spectra at lower ν's). Such complicated behavior may reflect some delicate competition between multiple or intermediate phases in the transition regime.

The apparent crossover from WS-A to WS-B is mainly controlled by the Landau level filling $\nu=nh/eB=2(l_B/r)^2$, where the magnetic length $l_B = \sqrt{\hbar/eB}$ (which measures the size of electron wavefunction) and the mean separation between electrons $r = 1/\sqrt{\pi n}$. This rules out the crossover being caused by interplay of l_B with, for example, some disorder length scale (Chitra *et al.* (2002), see also Chap. 3) or as some n-induced transition, but rather points out the important role played by many-electron quantum correlations, dependent on l_B/r.

The dispersion behavior of resonance "A" as seen in Fig. 5.5 requires WS-A must have a correlation length larger than w of the CPW; otherwise the pinned solid is

[8]Previous experiments (Ye *et al.*, 2002b) found only one resonance with $f_{\rm pk}\sim$1 GHz or higher. Our samples show nearly flat spectrum at such high f.

[9]Typically, the spectrum in the crossover regime displays only a single bump at such high T and becomes flat for $T \gtrsim 160$ mK. For a set of T-dependent traces, see Appendix. J, Fig. J.5.

[10]There has been interesting suggestions by many people, that the peak "C" may be an inter-component mode between "A" and "B", or a "interface mode" of the "A"-"B" domain boundaries.

effectively subjected to a uniform electric field, therefore can not couple to the finite q introduced by w. Measurements on sample 2c with w=80 μm have shown that resonance "A" continues to shift to lower f at the larger w, implying a correlation length (L_{WSA}) in WS-A at least on the order of $\sim$100 μm, which is almost two orders of magnitude larger than what the simple estimate used in Ye *et al.* (2002b) for the Larkin length (L_c, see Sec. 3.1.5) assuming a classical WS would give. On the other hand, the magnetophonon localization length (L_B) in both "A" and "B" phases are estimated (Sec. 3.1.5) to be far exceeding 100μm (see Appendix A), and can not explain why we have only observed dispersive behavior in "A" but not in "B". Our observations suggest that WS-A possesses some long range quantum correlation that is absent in WS-B.

The *decreasing* $f_{\rm pk}$ of WS-A upon transition to FQHE, as seen clearly in Figs. 5.6 and 5.7, is inconsistent with the picture of a second-order phase transition from a WC to FQH liquid (Millis and Littlewood, 1994). In such a picture, the WC is expected to "soften" (with decreasing shear modulus μ_T) upon transition to a FQH state, which is an incompressible liquid that has no shear. This would, for a weakly pinned solid (Fogler and Huse, 2000; Chitra *et al.*, 2002), give rise to an *increasing* $f_{\rm pk}$ ($\propto 1/\mu_T$, see Sec. 3.1.3) upon such a transition, which is exactly opposite to what we have observed.

It was recently proposed, based on rather general arguments, that the solid-liquid transition in a 2DES should occur[11] via a series of intermediate phases (Spivak and Kivelson, 2004). These intermediate phases are suggested to be some electronic "micro-emulsion" (Spivak and Kivelson, 2004), which consists of short length scale mixture between solid and liquid. Such a picture has been applied (Spivak and Kivelson, 2004) to low n 2DES at B=0 to address the observed apparent metal-insulator transition (Abrahams *et al.*, 2004). Some recent experiments (Csathy *et al.*, 2004)

[11]It is suggested that a direct first-order phase transition is generally forbidden in a 2D Coulomb system (Spivak and Kivelson, 2004).

in QH regime were also interpreted with such a picture, involving a mixed phase of WC and FQH liquid. Within this framework, one may interpret our WS-B as an "ordinary" WC, the expected GS of 2DES at sufficiently high B (Lozovik and Yudson, 1975)[12]; and interpret WS-A as such a mixed phase of WC and FQH liquid at relatively high ν when the transition from WC to FQHE occurs. Although a detailed theory for the collective excitation(s) in such a "micro-emulsion" phase is not yet available, one can generally expect that its liquid fraction should grow[13] upon approaching FQHE; and such FQH liquid fraction, which is not pinned, can effectively act as a "lubricant" and reduce the total pinning[14] experienced by WS-A, consistent with the observed drop of $f_{\rm pk}$ near FQHE. It is also suggested (Normand *et al.*, 1992; Millis and Littlewood, 1994) that the FQHE fraction can damp the WC resonance and reduces the $f_{\rm pk}$. The significant drop of $S/f_{\rm pk}$ near ν=1/5 that we have generally observed (see for example, Fig. 3.3 in Sec. 3.1.6. See also further discussions in Sec. 5.5.) is also consistent with the picture that only part of the 2DES actually participates in the solid phase near ν=1/5. On the other hand, it remains to be understood that exactly how WS-A, if indeed it is such a mixed phase, acquires the apparent long range crystal correlation that gives rise to the observed dispersive behavior.

It has been thought that correlations responsible for FQHE can still be relevant (Pan *et al.*, 2002; Yi and Fertig, 1998; Narevich *et al.*, 2001; Chang *et al.*, 2005) even in the HBIP. More specifically, some theories (Yi and Fertig, 1998; Narevich *et al.*, 2001; Chang *et al.*, 2005) have considered different types of "correlated" WS (^{m}CWS) made of "composite fermions" (CF) or "composite bosons" (CB), the quasiparticles (electrons bound with even or odd number (m) of flux quanta respectively) proposed

[12]This consistent with the observation that WS-B appears to dominate at the low ν limit, see footnote 7.

[13]In this process, the *local* (microscopic) solid density remains unchanged but the macroscopic fraction of solid in the system shrinks.

[14]Especially when the relevant pinning disorder is dilute (Fertig, 1999), see Sec. 3.2.

to largely capture the FQHE correlations (Jain, 1989, 2000), and offering another possible interpretation for the different solid phases we have observed. The theories have predicted a series of phase transitions[15] among these different types of CWS as preferred GS in different regimes of HBIP. Note that in this notation, ^{0}CWS would be a WS made of "bare" electrons, corresponding to the original case proposed in (Lozovik and Yudson, 1975) and is the preferred phase at sufficiently small ν. At relatively higher ν, for example near ν=1/5 (corresponding to our WS-A), so far different theories (Yi and Fertig, 1998; Narevich *et al.*, 2001; Chang *et al.*, 2005) have favored different types of CWS's; and a detailed calculation of the dynamical responses of different CWS's pinned by disorder is not yet available to allow for a direct comparison with our observed resonances. On the other hand, for any ^{m}CWS with $m>0$, one can expect that it may possess long range quantum coherence as in the FQHE (Chang *et al.*, 2005). Although caution should be taken in comparing these theories (for disorder-free 2DES) to experiments on realistic samples, some predictions seem to be consistent with the experiments. For example, ν=0.125, predicted to be a critical filling separating two different CWS phases (Yi and Fertig, 1998; Chang *et al.*, 2005), is in good agreement with our phenomenological value below which WS-B resonance dominates. Generally, it is expected that even modest disorder may have significant influences on the various CWS phases (Narevich *et al.*, 2001) and may stabilize one CWS against another[16], consistent with the fact that in previous microwave experiments (Ye *et al.*, 2002b) on Sample P, with lower mobility ($\sim 5\times10^{6}$cm^2/Vs) than our QW samples, only one resonance in HBIP were observed. Some other predictions, however, seem to be at odds with our observations. For example, the shear modulus of ^{4}CWS (favored in Narevich *et al.* (2001)) is predicted to significantly decrease as ν approaches 1/5; this would result in an increasing $f_{\rm pk}$ of the resonance, which is not

[15] thought to be first order in these theories. See, however, footnote 11.

[16] For example, it is possible that disorder may make ^{0}CWS the preferred phase for $\nu< 0.125$, rather than only at much smaller ν as predicted.

the case we have observed. It is possible, that a mixed phase (Spivak and Kivelson (2004), as discussed in the preceding paragraph) of CWS and FQH liquid also occurs near a CWS to FQHE transition.

In summary, although it is not inconsistent with experimental observations to interpret WS-B as a MIWC of electrons, the microscopic nature of WS-A is much less clear. However, hinted by our data, we may interpret WS-A as some WS with substantial "FQHE character", for example, an intermediate/mixed phase between WS and FQH liquid, and/or a WS made by CF/CBs. It is likely an electron solid phase with also macroscopic quantum coherence[17], and probably, only a tip of the iceberg of its novel physics has been revealed thus far.

5.5 Additional Notes and Further Directions

It is of great interest to directly probe the participating density (n^*) of the solid in the WS-A, particularly in relation to the "mixed phase" picture. One way to do this is through the oscillator strength S of the pinning mode (more specifically, $S/f_{\rm pk}$, as discussed in Sec. 3.1.6). For example, Fig. J.6 in Appendix J shows $S/f_{\rm pk}$ measured from Sample 2c (Fig. 5.6). It is found that $S/f_{\rm pk}$ drops upon approaching 1/5 or 2/9 FQHE. However, one needs to be careful when comparing the value of $S/f_{\rm pk}$ in WS-A to the Fukuyama-Lee sum rule, because the 2DES here is *not* in its long wavelength limit, whereas Fukuyama-Lee sum rule is derived only for q=0. Measurements using CPW with even wider w (for example 120μm) than those we have used so far would be very valuable. Going to wider w may also directly yield the correlation length in WS-A, as the w above which $f_{\rm pk}$ no longer changes.

It is also interesting to extract the density from the dispersion observed in WS-A, by fitting $f_{\rm pk}$ vs q=π/w to the predicted (Normand *et al.*, 1992) WC dispersion

[17] thus can be considered as an electronic supersolid, in the similar sense that a FQH liquid can be considered as a superfluid (after a Chern-Simons gauge transformation, Kivelson *et al.* (1992)).

(Eq. 3.3). Measurements with a few more w (for example, 120μm and 40μm) in addition to those presented in this chapter (30, 60 and 80 μm) would be desirable for an accurate extraction of density from the dispersion.

An interesting feature we have noticed about WS-A, when it is well developed (with resonance "A" dominating the spectrum) at ν sufficiently below 1/5 (away from the immediate transition regime to FQHE) but not too low (to have WS-B becoming significant), is that its $f_{\rm pk}$ decreases with increasing B (decreasing ν), in fact often with a dependence that is not very far from a $1/B$ behavior (Fig. 5.7 and Figs. 5.2, 5.4). This suggests that the relevant disorder that pins WS-A must have a correlation length larger than l_B (Chap. 3). On the other hand, the $f_{\rm pk}$ of WS-B, when it coexists with WS-A, generally shows much weaker B-dependence and sometimes even increases with increasing B (Figs. 5.2, 5.4). One very interesting possibility is that WS-A is less subject to short-range disorder, which apparently still exists in the system and is relevant for the pinning of WS-B. Recent experiments[18] by Li (2005) have suggested that FQHE can be relatively insensitive to a moderate amount of short range disorder. Thus our speculation that WS-A is a solid with "substantial FQHE character" appears to be not inconsistent with the experimental findings so far. It will be illuminating, to measure a wide QW, similar to WP or QW65 but with a *small* amount of Al alloy disorder introduced, and see how this may affect WS-A and WS-B resonances respectively.

We have found (on sample QW65_M30) that when the 2DES n is lowered by a backgate to below $\sim 4\times10^{10}$cm^{-2}, the two phases WS-A and WS-B become not well-resolved[19] (see Figs. J.1, J.2, J.3 in Appendix J). Interestingly, we found $f_{\rm pk}$ to also deviate more from the $1/B$-like behavior at lower n, as shown below in Fig. 5.8.

[18]In the experiments, it was found that adding a *small* amount of Al alloy disorder (which is short range) in the 2DES channel appear to have little effect on the FQHE characteristics, despite having significantly lowered the electron mobility at B=0.

[19]It will be illuminating to measure the dependence on w (CPW) at such low n, and check if one can still observe dispersive behavior in the spectrum at ν where WS-A is well resolved at high n.

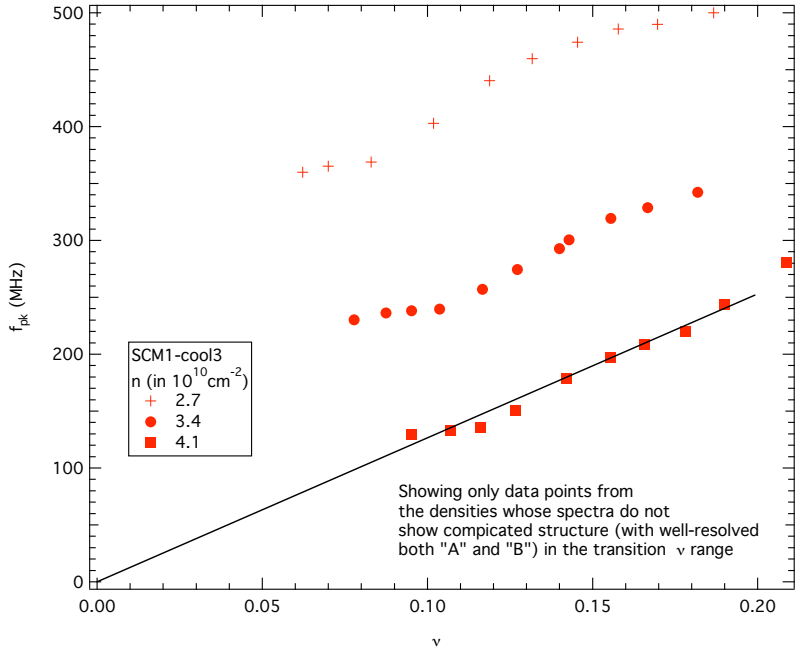

Figure 5.8: As n is lowered (by backgating) in QW65, into the regime where "A" and "B" are not well resolved, $f_{\rm pk}$ of the observed resonance deviate more from a $1/B$ dependence.

This suggests an increased significance of short range disorder (possibly due to the wave function being pushed closer to one interface by the back gate voltage) at such low n, and also suggests that the $1/B$ like behavior in $f_{\rm pk}$ is associated with a better developed "A" phase. Further measurements using both a total front gate and a total back gate (so one can change the wavefunction symmetry without changing n) can be illuminating.

Preliminary measurements (on QW65_M30) by Sambandamurthy *et al.* (2005a) have found that, applying a small negative DC bias on the CPW metal films (used as a front gate to deplete electrons underneath) does not affect $f_{\rm pk}$ in WS-A but shift $f_{\rm pk}$ in WS-B to higher f (see Fig. J.4 in Appendix J). We do not yet understand such observations [20]. It will be illuminating to perform measurements (and consis-

[20]However, if the insensitivity of $f_{\rm pk}$ in WS-A to electron depletion under the CPW is somehow related to the macroscopic quantum coherence in WS-A, it will be interesting to look for, for example, Josephson-like phenomena using the gated CPW center conductor as an effective junction between WS-A under neighboring slots.

tency check) with DC-biased CPW on samples with straight line CPW and on more disordered samples (such as sample P) where only one resonance is found in HBIP.

In the following we briefly list some more directions for future experiments:

1) Combining T-dependence and w-dependence (dispersion) measurements. This may give insights, for example, on how the correlation length (L_{WSA}) of WS-A evolve with T.

2) Using CPW with much narrower[21] w than those have been used, to probe, for example, the dispersion of WS-B, and WS-A dispersion in high-q regime, as well as possibly the WC dispersion in more disordered sample (with only one resonance in HBIP, such as sample P).

3) The origin of the high lying peaks such as peak "2" (and even higher f peaks such as those seen in Figs. 5.5 and 5.6) remains to be clarified. They may be some higher harmonics of "A" resonance, but other possibilities, such as some multi-(magneto)phonon mode (Murthy, 2004), have been suggested. More systematic studies on n and w dependence of these peaks can be helpful.

4) Although we have been focused on spectroscopy (Re$[\sigma^c_{xx}(f)]$) measurements. AC magneto-conductivity (see Appendix F) measured at various f can also be interesting. For example, it remains to be seen, whether features associated with low rational fraction filling such as 1/7 and 1/9 (Pan *et al.*, 2002) may appear in high-f magnetoconductivity (Lee *et al.*, 1991).

The data presented in this chapter suggest that multiple quantum phases can exist and compete in the LLL. We expect that pushing all our measurements to even lower T can generally be very profitable. Not only can we gain more insights about the transition between the various phases discussed so far, lower T may potentially reveal many more new phases[22] and a plethora of rich physics in the HBIP.

[21] some modification or improvement in microwave technique are likely to be needed for going to CPW with very narrow w.

[22] For an example of multiple phases only revealed at very low T in the 1st excited LL, see Xia *et al.* (2004).

Chapter 6

Melting of a 2D Quantum Electron Solid

6.1 Introduction

The melting temperature (T_m) of a solid is generally determined by the ambient pressure, or indirectly by its density (n) through the equation of state. This remains true even for helium solids (Wilks, 1967), where quantum effects often lead to unusual properties (Kim and Chan, 2004b). It is also true for a classical two dimensional (2D) solid formed by electrons (Grimes and Adams, 1979), which melts at $T_{cm} = e^2\sqrt{n}/(4\pi\epsilon k_B\Gamma)$ (where ϵ is the dielectric constant, k_B the Boltzman constant and $\Gamma\sim130$). In this chapter, we present experimental evidence which shows that for a 2D *quantum* electron solid formed under a perpendicular magnetic field (MIWC) (Shayegan, 1997), its T_m (in a given sample) is not determined by n, but by quantum correlation between the electrons through the Landau level filling factor ν=nh/eB. At a fixed ν, which is a measure of the quantum mechanical wave function overlap between the electrons, T_m is found to be insensitive to n. To our best knowledge, this constitutes the only example of a solid whose T_m has been shown to mainly depend on

inter-particle quantum correlation, which can be readily tuned (here by a magnetic field) independently of the solid density. Moreover, we found that T_m is *increased* for a 2D electron solid subject to stronger vertical confinement or pinning disorder, opposite to the phenomenon of "melting point depression" (Christensen, 2001) of most solids when subject to geometric confinement or stronger pinning.

We know that electrons are expected to crystallize into a solid ("Wigner crystal" (Wigner, 1934)) when the (Coulomb) interaction energy between the electrons sufficiently dominates over the kinetic energy. One example of such an electron solid was found in a very low density (n) two dimensional electron system (2DES) realized on helium surfaces (Grimes and Adams, 1979). Because of the low n, the quantum zero-point motion (given by the Fermi energy $E_f = nh^2/2\pi m$ where m is the electron mass) is negligibly small and at finite temperatures (T) as in the experiment (Grimes and Adams, 1979) the kinetic energy originates mainly from the *classical* thermal motion (k_BT). The melting of such a "classical" 2D electron solid is determined only by the competition between the thermal kinetic energy and Coulomb interaction ($e^2\sqrt{n}/4\pi\epsilon$) and is thought to be describable by the Kosterlitz-Thouless theory of 2D melting (Kosterlitz and Thouless, 1973; Young, 1979; Nelson and Halperin, 1979). Experimentally, the melting was found to occur (Grimes and Adams, 1979) at $T_{cm} = e^2\sqrt{n}/(4\pi\epsilon k_B\Gamma)$ with $\Gamma\sim$130, in excellent agreement with theoretical predictions (Morf, 1979; Chui and Esfarjani, 1991).

The 2DES as realized in high-quality GaAs/AlGaAs structures in our experiments has comparably high n, thus (in the absence of magnetic fields) the quantum zero-point motion (E_f) is significant and the 2DES does not solidify even at T=0. However, it is well known that a sufficiently strong perpendicular magnetic field (B) tends to suppress the kinetic energy of 2D electrons and induce the solidification (Lozovik and Yudson, 1975; Fukuyama *et al.*, 1979). On the other hand, at finite B the motion of electrons is quantized into Landau levels (LL) and delicate many-body quantum

correlations (Laughlin, 1983; Kivelson *et al.*, 1987) among electrons can cause the 2DES to condense into fractional quantum Hall (FQH) (Tsui *et al.*, 1982) liquid states at certain rational fractional values of Landau level filling factor $\nu = nh/eB$. Experimentally, the "magnetic field induced Wigner cystal" (MIWC, reviewed in Shayegan (1997); Fertig (1997)) forms at sufficiently small ν, following the termination of FQH states at low T. It is a DC insulator due to pinning by disorder and, as we have seen, has a characteristic resonance (Chap. 3) in its frequency (f) dependent real part diagonal conductivity (Re[$\sigma_{xx}(f)$]) due to the "pinning mode" of domains of the elastic solid oscillating collectively around the disorder (Fertig, 1999; Fogler and Huse, 2000; Chitra *et al.*, 2002).

Previously, the melting of a MIWC has been studied in various experiments (Glattli *et al.*, 1990; Goldman *et al.*, 1990; Williams *et al.*, 1991; Paalanen *et al.*, 1992b; Goldys *et al.*, 1992; Kukushkin *et al.*, 1993) and it was commonly presumed (Glattli *et al.*, 1990; Williams *et al.*, 1991; Goldys *et al.*, 1992) that at a fixed ν the melting should be similar to that of a classical electron solid (the expected exact ground state for a 2DES at infinite B) and thus T_m would be determined by n, as is in T_{cm}. In this chapter, we show unambiguously that this is not the case, and in fact T_m in mainly determined by ν, not n and is unrelated to T_{cm}.

In our experiments we have studied the T-dependence of the pinning mode resonance of the MIWC in its Re[$\sigma_{xx}(f)$] spectrum measured by microwave spectroscopy (Sec. 2.2). No resonance can be observed when T is raised above some characteristic T_m, taken as the melting T of the electron solid. By systematically measuring T_m while varying *both* n and B, we found that within the experimental resolution (and in a given sample), T_m is only a function of ν (i.e., $T_m(n, B) = T_m(n/B)$) down to ν as small as $\sim$0.05 attained in our experiments. At a fixed ν, T_m is insensitive to n. Since $\nu = nh/eB = 2(l_B/r)^2$, where the magnetic length $l_B = \sqrt{\hbar/eB}$ is a measure of the size of the single electron wavefunction and $r = 1/\sqrt{\pi n}$ is the mean separation

between the electrons, our findings reflect the quantum nature of the 2D electron solid formed at finite B and demonstrate that its melting (T_m) is mainly determined by the inter-electron quantum correlation through ν.

We have performed the melting studies on samples from three different wafers: P (heterojunction), QW15 (15nm wide QW) and QW65 (65nm wide QW). By backgating and/or different cooldowns, the electron densities (n) in these samples can be tuned to various extents, to be specified below. Typically at their respective as-cooled n, sample P has mobility $\mu\sim6\times10^6\mathrm{cm}^2/\mathrm{Vs}$, QW15 has $\mu\sim1\times10^6\mathrm{cm}^2/\mathrm{Vs}$ and QW65 has $\mu\sim8\times10^6\mathrm{cm}^2/\mathrm{Vs}$.

6.2 T-dependence of WC pinning resonance and determination of T_m

Fig. 6.1 shows T-dependence of the microwave resonance of the electron solid and the determination of T_m at two different values of n in sample P with ν fixed at a representative value of 0.128. In Fig. 6.1a, n=5.6×10^{10}cm^{-2}(B=18T) and the Re[$\sigma_{xx}(f)$] spectrum displays a clear resonance near 600MHz at low T(∼50mK). As T is increased, the resonance weakens. The resonance disappears into the noise background at ∼250mK, taken as the melting T_m of the electron solid. The inset of Fig. 6.1a shows that the resonance amplitude (obtained from a Lorentzian fit) extrapolates to zero at a similar T_m. From the spectra, one can see that at elevated T (but below T_m), f_{pk} also decreases slightly from the base T (50 mK) value, but by no more than 20%, indicating that the electron solid remains well pinned[1]. In Fig. 6.1b, n has been reduced to 2.1×10^{10}cm^{-2}(using a backgate voltage of −300V) while B is also reduced to 6.86T to keep ν the same value as in Fig. 6.1a. In this case the resonance of the

[1]We also notice that T_m is much lower than the temperature scale corresponding to the pinning frequency ω_0 (Fukuyama and Lee, 1978; Normand *et al.*, 1992; Chitra *et al.*, 2002), calculated from the resonance frequency (f_{pk}=$\omega_{\mathrm{pk}}/2\pi$) as $(\omega_{\mathrm{pk}}\omega_c)^{1/2}\sim2\pi\times70$ GHz∼3 K.

electron solid occurs near 1.6GHz at low T and disappears at a $T_m\sim$ 270mK, which is similar to that in Fig. 6.1a, within the experimental uncertainty in determining T_m (typically $\sim$10%).

6.3 Melting Temperature of MIWC

We have measured T_m in 4 different cooldowns of sample P at an extensive number of combinations of n and B, at which a resonance from the MIWC can be detected. We plot all these T_m data as a function of ν in Fig. 6.2. Sample P has a particularly large range of tunable n, from $\sim$1.2$-$8.1$\times10^{10}$cm^{-2}, covering a ν range from $\sim$0.21 down to $\sim$0.03. For nearly fixed ν, we have always found T_m to be insensitive to n, within the experimental error in T_m (typically less than 10%). T_m can vary from cooldown to cooldown by up to $\sim$15% (at similar ν) but this does not affect our conclusion. We thus find T_m to be mainly determined by ν and T_m vs ν as plotted in Fig. 6.2 defines a melting curve for the electron solid. A linear fit of T_m vs ν gives a guide to the eye shown as the dashed line, which lies within 20% from all the (T_m, ν) data points and within 10% from a majority (70%) of them. In the inset of Fig. 6.2 we plot the "reduced" $t_m = T_m/T_{cm}$ from two similar cooldowns versus ν, where $T_{cm} = e^2\sqrt{n}/(4\pi\epsilon k_B\Gamma)$ is the melting T of a classical 2D electron solid defined earlier (we have taken the value (Morf, 1979; Chui and Esfarjani, 1991) of Γ=127). In contrast to T_m, t_m can vary significantly (sometimes by a factor of 3) for nearly fixed ν. Thus t_m versus ν does not give a well defined melting curve for the electron solid, confirming that T_m is not determined by n or T_{cm}. At a fixed high B, T_m decreases[2] with increasing n, in contrast to T_{cm}, which always increases with increasing n.

Fig. 6.3 shows the (T_m,ν) melting curve measured on QW15 (15nm wide QW). Sample QW15 has a tunable n=2.7-4$\times10^{10}$cm^{-2}. Likely due to the relatively narrow

[2]We notice that this is also in contrast to the "thermal depinning temperature" of WC domains (T_{dp}), which can be estimated (Fertig, 2005) as $T_{dp}\sim(1/k_B)m\omega_0^2\xi^2(L_c/a)^2\propto n^{3/2}$ (where ξ is the disorder correlation length, a the WC lattice constant and L_c the Larkin domain size (Chap. 3)).

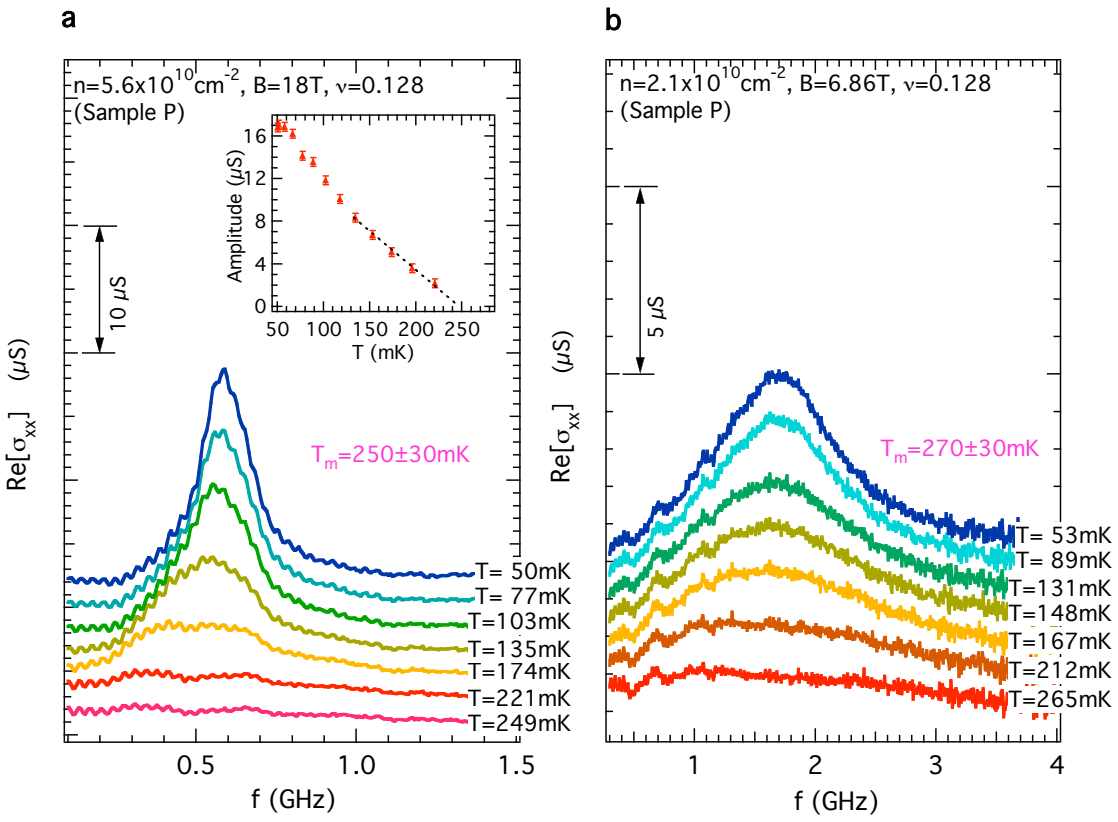

Figure 6.1: Temperature (T) dependence of the microwave spectra of the 2D electron solid measured from sample P at two different densities (n) with the same Landau filling factor (ν). **a**, T-dependence of the spectra at n=5.6×10^{10}cm^{-2}with ν=0.128 (magnetic field B=18 Tesla). Spectra at a series of representative T's are shown and offset for clarity. The pinning resonance of the electron solid observed at T=50mK is seen to weaken with increasing T and disappear at ∼250mK, taken as the melting temperature (T_m) of the electron solid. The ripples seen in the spectra and the weak, broad bumps (near 0.3 GHz and 0.65 GHz) visible in the high-T spectra are due to experimental artifacts. Inset shows the amplitude of the resonance extrapolates to zero at the similar T_m. **b**, T-dependence of the spectra at n=2.1×10^{10}cm^{-2}with ν=0.128 (B=6.86 Tesla). The low T resonance disappears at a T_m similar to that shown in **a** (n=5.6×10^{10}cm^{-2}), despite here that n has been reduced by more than a factor of 2. A negative voltage between the backgate and the 2DES enables *in-situ* reduction of n from the as-cooled values.

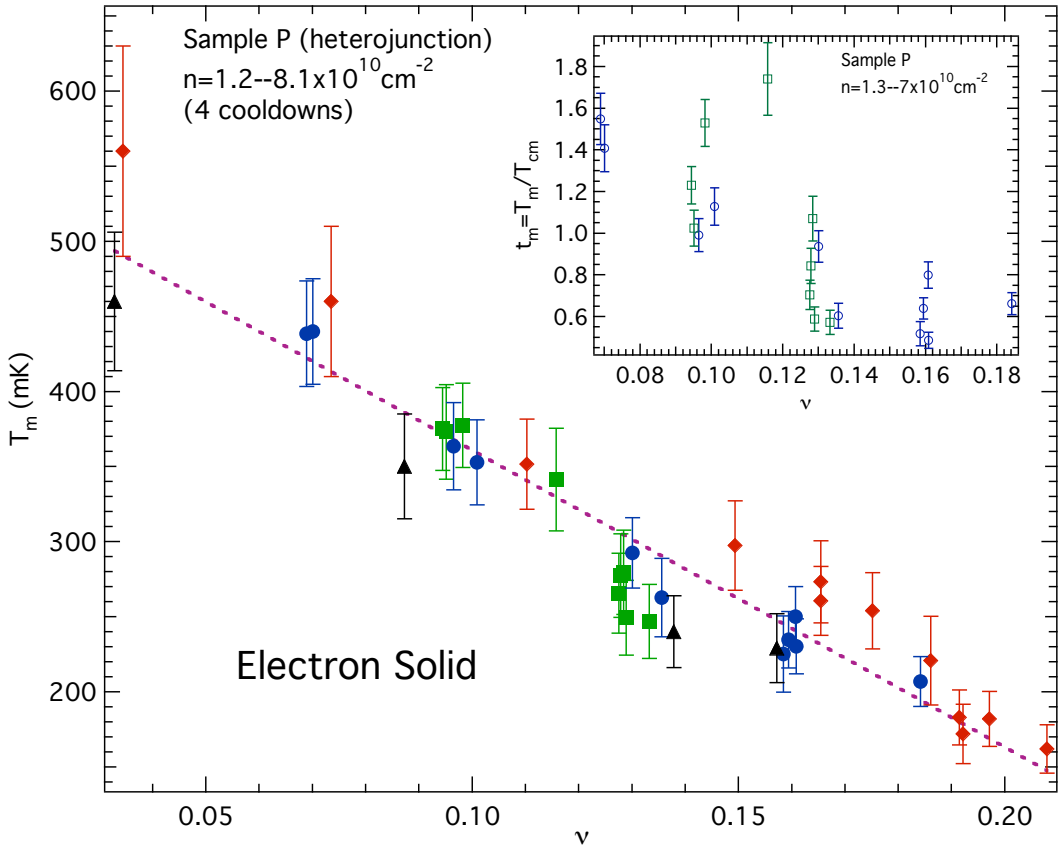

Figure 6.2: (T_m,ν) phase diagram for the electron solid in sample P. The T_m's are measured in a total of 4 cooldowns (shown as diamonds, circles, squares and triangles), over a wide range of densities (n=1.2−8.1×10^{10}cm^{-2}) and magnetic fields. Within the experimental uncertainty, T_m versus ν gives rise to a well-defined melting curve of the electron solid. The dashed line is a guide to the eye, obtained by a linear fit through all the data. Typical error bars in T_m are less than 10%. The inset shows the "reduced" t_m versus ν from two cooldowns. t_m is defined as T_m normalized by the classical 2D electron solid melting temperature $T_{cm} = e^2\sqrt{n}/(4\pi\epsilon k_B\Gamma)$ (where we take Γ=127). t_m versus ν does not result in a well-defined melting curve, indicating that the melting temperature T_m is not determined by n or T_{cm}.

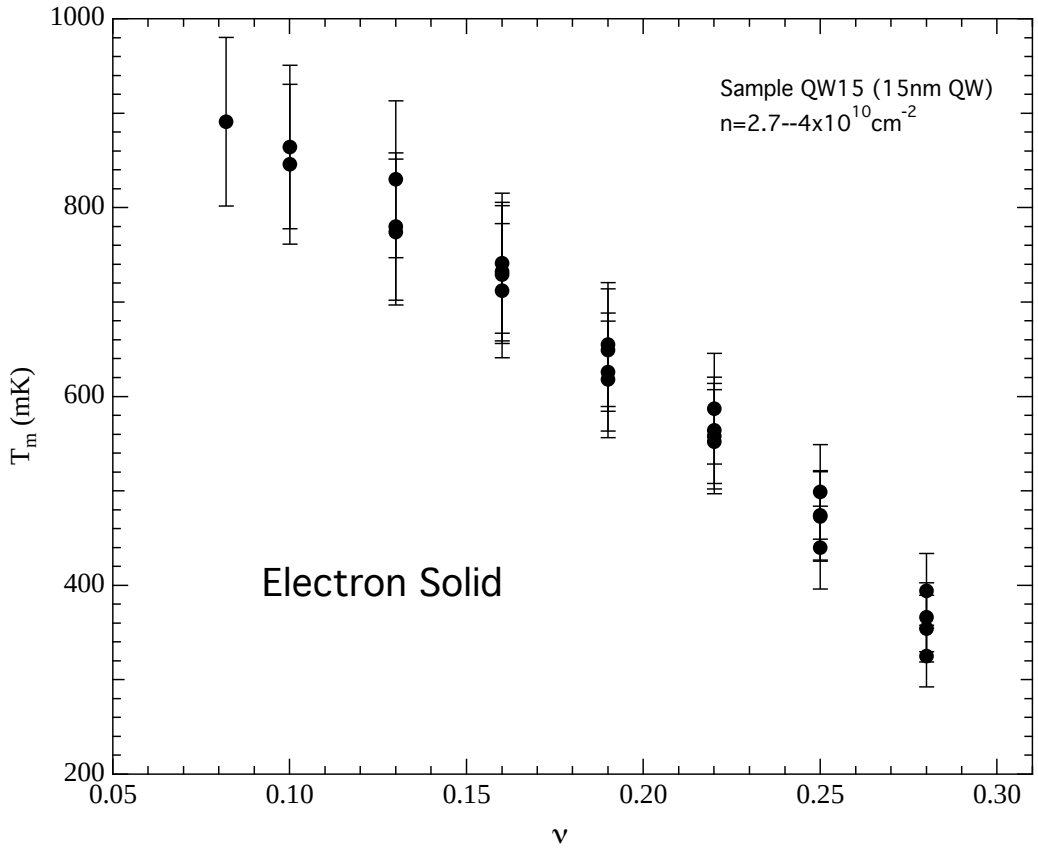

Figure 6.3: (T_m,ν) melting curve of the electron solid measured in QW15, a narrow QW of width 15nm. QW15 has a tunable n=2.7-4$\times10^{10}$cm^{-2} and enters an electron solid phase at $\nu<$ 0.3.

width[3] of the QW, this sample enters the solid phase for ν<0.3 (Sec. 3.2.1) and the typical $f_{\rm pk}$ observed is ∼6-8GHz. We found T_m again to be mainly determined by ν, though the value of T_m is higher than in sample P at similar ν.

We have measured T_m in QW65 (a 65nm QW) and also found a well-defined (T_m,ν) melting curve as presented below in Fig. 6.4. Data shown are measured using multiple pieces from the same wafer (with different CPWs) and from multiple cooldowns. The range of n is from 4.0 to 6.0$\times10^{10}$cm^{-2}. The variation of T_m due to different pieces or cooldowns is less than 10% and does not affect our conclusions. QW65 has been

[3]see also Yang *et al.* (2003).

shown to have two different resonances (Chen *et al.* (2004c), and this thesis, Chap. 5) in its Re[$\sigma_{xx}(f)$] spectrum, dominant in different regimes of ν and interpreted as from *two* different electron solid phases ("A" and "B"). Solid "A" is dominant for $0.18 \lesssim \nu < 2/9$ (but *reentrant* around $\nu = 1/5$) and solid "B" is dominant for $\nu \lesssim 0.1$, with the two solids coexisting in the transition regime[4] ($0.1 \lesssim \nu \lesssim 0.18$). These different ν regimes are separated with dashed vertical lines in Fig. 6.4. T_m is seen to drop as ν approaches 1/5 and 2/9. This is consistent with the ground states of 2DES being FQH *liquids* at $\nu = 1/5$ and 2/9 (both labeled as dashed arrows in the figure). We also notice that T_m tends to depend on ν more weakly at $\nu \lesssim 0.1$ (where "B" phase dominates) than at higher ν. The typical $f_{\rm pk}$ of the resonances are on the order of only ~ 100 MHz (Chen *et al.*, 2004c), attesting to the much reduced pinning disorder in the sample. Compared to sample P (Fig. 6.2), QW65 has lower T_m at similar ν.

6.4 Discussion

Recent theories (Yi and Fertig, 1998; Chang *et al.*, 2005) and experiments (Chen *et al.* (2004c), and this thesis, Chap. 5) have suggested that quantum correlation between electrons are still important in the solid phase terminating the FQH states. Our findings reflect the quantum nature of such an electron solid and indicate its melting is also determined by the inter-electron quantum correlation through ν. The well-defined (T_m,ν) melting curve we obtained thus constitutes the phase boundary between a quantum solid and a correlated quantum liquid (Chitra *et al.*, 2002). At certain special fractional ν such as 1/7 and 1/9, the melted phase of the solid has been suggested to be a FQH liquid (Price *et al.*, 1993; Pan *et al.*, 2002). We have not observed special features (Price *et al.*, 1993; Kukushkin *et al.*, 1993) in the measured

[4]In this regime, T_m (at which the spectrum becomes flat) measured is the characteristic T above which no solids are detected in the system (i.e., *both* solids "A" and "B" have melted).

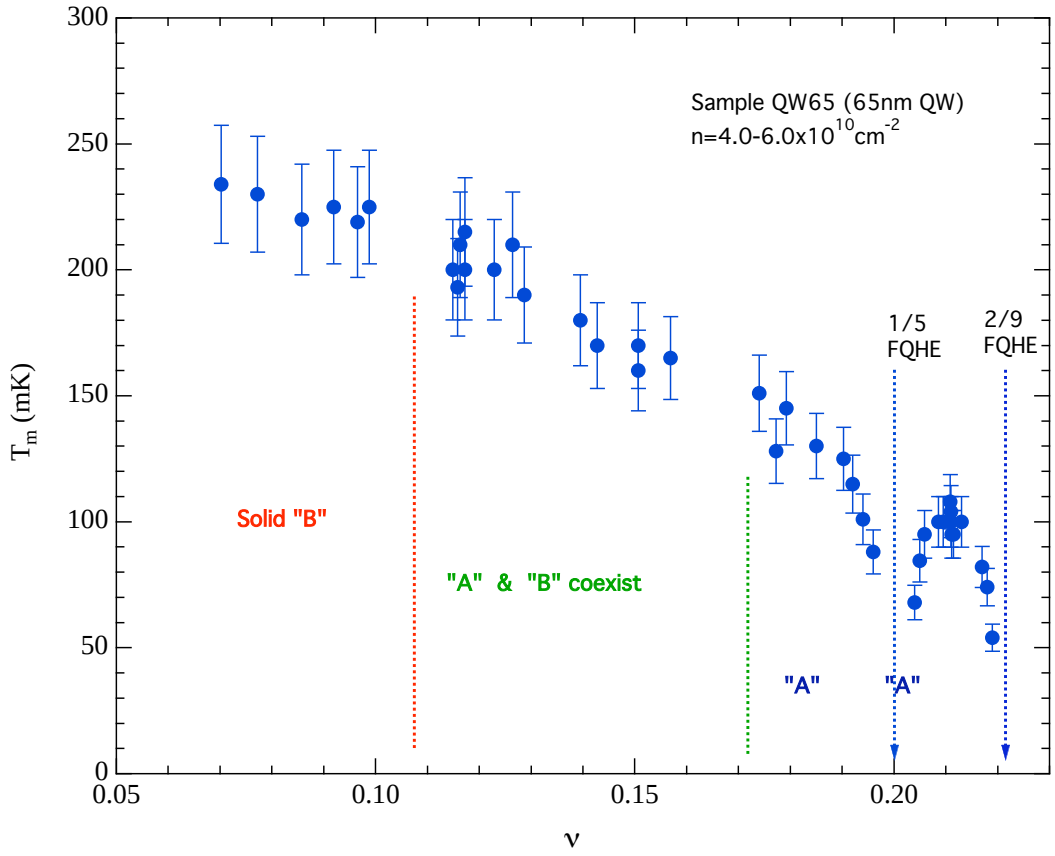

Figure 6.4: (T_m,ν) melting curve of the electron solids measured in QW65 (multiple pieces). QW65 is a 65nm wide QW, with a tunable n=2.6-5.9$\times 10^{10}$cm^{-2}. The data shown are measured in multiple cooldowns and from multiple pieces cut from the same wafer. QW65 can have two different solid phases ("A" and "B", as lableled in the figure), dominant in different regimes of ν and an "A"-"B" coexistence regime at intermediate ν. As solid "A" approaches ν=1/5 or 2/9 FQH liquid state, its T_m drops. At ν<0.1, where solid "B" dominates, T_m has weaker ν-dependence than at low ν.

(T_m,ν) melting curve near ν=1/7 or 1/9. We note at such ν, the 2DES can be a mixture of more than one solid phases, as observed in the low disorder QW65. Our measured T_m is the temperature at which *all* the solids in the system have melted. Theories for T_m involving such mixed phases have been lacking so far.

The T_m we measured in three samples are of the same order of magnitude as the melting temperature of other samples estimated previously using various experimental techniques (Glattli *et al.*, 1990; Goldman *et al.*, 1990; Williams *et al.*, 1991; Paalanen *et al.*, 1992b; Goldys *et al.*, 1992; Kukushkin *et al.*, 1993). At similar ν, samples QW65, P and QW15 have successively lower T_m and the typical $f_{\rm pk}$ in their observed pinning mode resonance is also successively lower. The different $f_{\rm pk}$'s of the three samples reflect the different strengths of pinning disorder, which has been suggested to come mostly from the interfaces (Fertig, 1999) confining the 2DES (see also Sec. 3.2). Thus the stronger pinning disorder tends to stabilize (Tsukada, 1977) the 2D electron solid to higher T_m. Such behavior is opposite to what is usually found in other solids, for example in the vortex solid in a high-temperature superconductor subjected to artificial pinning centers (Paulius *et al.*, 2000) or a helium solid in a porous glass (Beamish *et al.*, 1983), where a reduction (Christensen, 2001) of T_m due to increased disorder is found in both cases.

It is also interesting to compare the quantum nature of our 2D electron solid to the quantum solids of helium (Wilks, 1967; Dobbs, 2001; Adams, 2004). In a helium solid, the size of atoms is fixed by nature and the quantum parameter is the De Boer parameter $\lambda \sim h/(a\sqrt{Mv})$ (where M is the atomic mass, a the inter-atomic distance and v the inter-atomic potential strength) which is fixed at fixed n. The T_m of helium solids is only determined by n. In the case of a 2D electron solid formed in high B, the size of single electron wavefunction (l_B) is readily tunable by B, independently of n. The quantum parameter here is $\nu = nh/eB$ and we have found that T_m of such an electron solid is mainly determined by ν rather than n.

6.5 Additional Notes and Further Directions

In this chapter, we have focused on the melting temperature (T_m) of the MIWC, and shown that T_m is mainly controlled by ν, or the quantum correlation between electrons. Many interesting issues about the melting of a WC remain to be better understood. For example, how exactly does the melting process occur? What is the nature of the melted phase?

We have performed extensive measurements (the details will be presented elsewhere) of the T-dependence of the WC pinning mode resonance, particularly on sample P. One interesting feature we found (in sample P, at relatively low n) is another characteristic temperature $T_1 < T_m$, such that $f_{\rm pk}$ of the resonance does not change appreciably below[5] T_1 but decreases with increasing T above T_1. An example is shown here in Fig. 6.5. Interestingly, we have also noticed that most of the T_1 we have measured appear to be around $2hf^0_{\rm pk}/k_B$, where $f^0_{\rm pk}$ is the $f_{\rm pk}$ at base T ($\sim$50mK). It remain to be understood, whether T_1 may be related to a two-stage WC melting process considered theoretically (Kosterlitz and Thouless, 1973; Nelson and Halperin, 1979; Young, 1979; Fertig, 1997), or is mainly a finite-T property of the pinning mode (Yi and Fertig, 2000), and whether it is related to characteristic temperatures found in some other experiments (Goldys *et al.*, 1992; Kukushkin *et al.*, 1992; Li *et al.*, 1995a, see also Shayegan (1997), Fig. 9.10).

Additional insights on the melting of WC may be obtained from systematically examining the T-dependence of various correlation lengths of WC (L_c, L_B (Chap. 3), and in the case of WS-A phase, L_{WSA} (Chap. 5) from the dispersion measurements). Performing T-sweeps (for example, from above to below T_m) and monitoring the conductivity at fixed B and f may also be illuminating (Sambandamurthy, 2004).

More accurate extraction of quantities (for example S and $S/f_{\rm pk}$) from the spec-

[5]Note that we have checked (using on-block thermometers as well as features in the measured signal, such as the amplitude of the resonance shown in the inset of Fig. 6.1) that the sample did cool below T_1. Also note we can only observe T_1 if it is above the base T (typically 50-60mK).

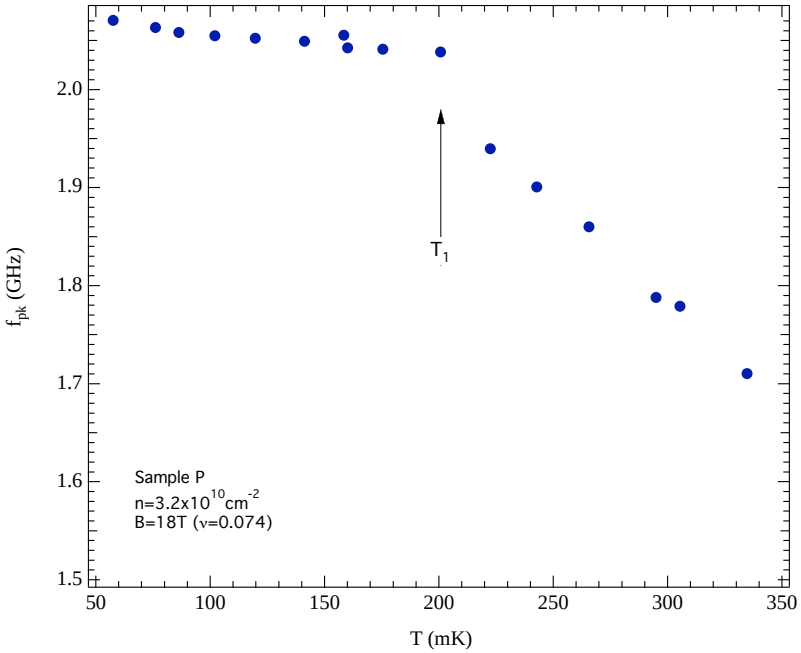

Figure 6.5: Sample P: $f_{\rm pk}$ as a function of T measured at n=3.2×10^{10}cm^{-2} and B=18T.

tra at elevated T (when features in the spectra are often weak)[6] can be generally very valuable. Systematic investigations of the spectrum at $T>T_m$ could also yield information on the melted WC. It may also be interesting to perform (f,T) scaling type of measurements (Engel *et al.*, 1993) either near the thermal melting ($T\sim T_m$) or quantum melting (transition to FQHE) of WC.

For sample WP, DC transport studies (Pan *et al.*, 2002) have found FQHE features at small rational fillings such as 1/7 and 1/9, only at elevated T (above some characteristic T_m, interpreted by Pan *et al.* (2002) as the temperature where the WC melts into a FQH liquid). Careful corroborating the microwave spectroscopy measurements and the DC measurements[7] at elevated T can be illuminating.

In the limit of infinite B ($\nu\rightarrow 0$), a MIWC is expected to behave as a classical

[6] Appropriately choosing the reference spectrum (Sec. 2.2.3) is especially important.

[7] And/or AC magnetoconductivity measurements (Append. F). So far, our preliminary measurements of AC magneto-conductivity in sample WP at elevated T have not found FQHE features at 1/7 or 1/9.

WC (with $T_m \propto \sqrt{n}$, instead of being controlled by ν as we found in this chapter). Extending our measurements to the highest possible B is of obvious interest[8].

[8]It is particularly interesting to measure QW65, whose T_m tends to saturate at the low ν end in Fig. 6.4, to higher B than what we have used (the highest B in Fig. 6.4 is 33T).

Chapter 7

Summary and Perspectives

7.1 Summary

In this thesis, we have studied the solid phases of 2DES subjected to a perpendicular magnetic field (the quantum Hall system) using microwave spectroscopy. For each of the isotropic, pinned electron solid phases studied, we have measured its characteristic pinning mode resonance due to the collective oscillation of the solid around disorder. Some important generic features of such a resonance, supporting its identification as an electron solid pinning mode, are recollected here:

- The resonance is not observed when a solid phase is not expected, for example, in FQH liquids (see, for example, Fig. 5.6), or at sufficiently high T (Chap. 6);
- The resonance frequency ($f_{\rm pk}$) is generally higher for more disordered samples. We have found that the most important source of pinning disorder appears to be from the interface (Chap. 3), consistent with theories by Fertig (1999). On the other hand, the resonance is not observed for samples too disordered to show FQHE, consistent with the expectation that localization of electrons by disorder in these samples occur individually, instead of collectively via Wigner crystallization.

- Behavior of $f_{\rm pk}$ can be largely understood within the framework of collective "weak pinning" theory of WC (Fertig, 1999; Fogler and Huse, 2000; Chitra *et al.*, 2002), especially using the interface pinning model (Fertig, 1999), as we discussed in Chap. 3.

- The resonance can survive up to a temperature that significantly exceeds the T scale corresponding to the $f_{\rm pk}$ ($hf_{\rm pk}/k_B$), ruling out the individual particle excitation as giving rise to the resonance (Kivelson *et al.*, 1992). Such a feature is more evident for samples of lower pinning disorder. For example, in sample QW65 (Sec. 3.2.1, Chap. 5 and Chap. 6), the typical resonance can survive to 100mK or higher, whereas its $f_{\rm pk}$ is on the order of 100 MHz ($hf_{\rm pk}/k_B\sim$ 5mK) only.

- The resonance is relatively narrow (with Q=$f_{\rm pk}/\Delta f$ generally well above unity). This is now understood (Fertig, 1999; Fogler and Huse, 2000) as a combined effect of high magnetic field (B) and long range Coulomb interaction (Chap. 3), where collective motion of large regions of the solid can effectively average disorder and produce a sharp resonance.

- The integrated intensity ("oscillator strength") S of the resonance, when the solid phase is well developed (for example, sufficiently far away from FQHE) agrees with in a factor of 2 (see, for example, Fig. 3.3 and Fig. 4.5) with the pinning mode sum rule derived by Fukuyama and Lee (1978) (provided also, that the 2DES is in its long wavelength limit).

In low disorder samples, there is a plethora of electron solids, or more general charge density wave (CDW) phases we have studied with microwave spectroscopy. They include:

- WC in the LLL, following the termination of FQHE at high B. We have found (in wide QW samples with very low pinning) in fact, two different solid phases

(Chap. 5), WS-A and WS-B, in different regimes of ν: WS-A dominant for $2/9>\nu>0.18$ (but reentrant around 1/5), and WS-B for $\nu \lesssim 0.12$. In the transition regime ($0.18 \gtrsim \nu \gtrsim 0.12$), the two phases coexist.

- WC around IQHE (Sec. 4.1): ν near 1, 2, 3, 4. These are WC formed by electron/holes in the partially filled top LL.

- A series of CDW phases in the higher LLs (Sec. 4.2), including the "bubble" crystal (BC) at ν near $K+1/4$ and $K+3/4$, where K=4, 5, 6, 7; the re-entrant IQHE states in the 1st excited LL, in particular at $\nu\sim 2.58$, probably also a BC phase (Lewis *et al.*, 2005a). Studies of the "stripe" phase[1] at ν near 9/2, 11/2, 13/2, and 15/2 are also underway (Lewis *et al.*, 2005b; Sambandamurthy *et al.*, 2005a).

One highlight in our studies is the finding of the importance of many-body quantum correlations in the 2DES solids, even in the LLL, where the overlap between *single particle* wavefunctions can be quite small (Maki and Zotos, 1983). Such many-body correlations appear to determine the transition between WS-A and WS-B (Chap. 5). In particular, WS-A is found to have a very large correlation length, apparently absent in WS-B, and may be a solid phase with substantial FQH-liquid-like correlation (Chap. 5).

Our systematic studies on the melting of WC in the LLL (Chap. 6) have found that the melting temperature (T_m) is a function of Landau filling ν, therefore determined by the many body correlation between electrons, in contrast to a classical 2DWC where T_m is determined by density n. This again confirms the quantum nature the electron solid we studied.

In addition to revealing many physical properties of the quantum electron solids, studies of the pinning mode resonance have enabled us to learn important information

[1]The stripe phase has been suggested to be a liquid crystal-like phase (Fradkin and Kivelson, 1999), or an anisotropic WC (Ettouhami *et al.*, 2005).

about disorder (Chap. 3), such as its correlation length and even its statistics. We have shown that the vertical confinement of the 2DES can greatly affect the pinning of a WC, and an important source of pinning disorder is likely from the interface. Our data has provided support for the interface pinning model given in Fertig (1999), which suggests that pinning is provided by some dilute "pits", the size of which can reach below ∼10 nm.

7.2 Perspectives

Quantum Hall systems have been extensively investigated for over two decades, revealing an extremely rich array of physical phenomena. Among them, the pinned electron solid phases, the subject of this thesis, represent a regime where both interaction and disorder are equally important (Tsui, 1999). There are ample reasons to believe, that many new and novel physics are yet to be uncovered, and much more remain to be learned about these electron solids. Microwave spectroscopy, as we have seen, is a particularly powerful tool to study such pinned solid phases, which have been difficult to probe with conventional DC transport.

We have listed many open questions and directions for further research, specific for the topics presented, at the end of earlier chapters. Numerous uncharted territories can be explored by extending the experimental parameter space in many ways, for example, going to lower temperature (T), higher magnetic field (B), wider ranges of wave vector (k), frequency (f), density (n) and adding an in plane magnetic field ($B_{||}$). In addition to the resonance, investigating other aspects of the spectrum, for example, its low f tail can be interesting as well (see, for example, Fogler (2002)). One can also readily go beyond $\mathrm{Re}[\sigma_{xx}(f)]$ and look at the full complex $\sigma_{xx}(f)$ (see Appendix D). Other than the continuous wave (CW) mode, one can also perform pulsed microwave measurements, which may be particularly interesting to study the

magnetophonon dynamics[2].

There is also a wide variety of new samples that can be interesting to study with microwave spectroscopy. In addition to samples with controlled disorder (for example, Al alloy) and varying structure parameters (for example, QW width) mentioned in Chaps. 3 and 5, one may also go beyond the single layer 2DES samples, and study the Wigner crystal phase(s) in 2DHS[3] (Santos *et al.*, 1992; Li *et al.*, 1997), bilayer electron (Manoharan *et al.*, 1996) and bilayer hole[4] (Tutuc *et al.*, 2003) systems, and even 1D WC[5] (Schulz, 1993). In addition, novel physics may also arise when one ventures into samples based on other materials (than GaAs), such as AlAs (Shkolnikov *et al.*, 2005), whose 2DES can have anisotropic effective mass (Gunawan *et al.*, 2004), or Si/SiGe system (Lai *et al.*, 2004).

Other than the magnetic field induced WC, the WC (realized at sufficiently low n) at B=0 (Chitra and Giamarchi, 2004) is also interesting in many ways, especially in relation to the apparent 2D metal-insulator transition (Yoon *et al.*, 1999; Abrahams *et al.*, 2004; Spivak, 2002; Spivak and Kivelson, 2004; Kravchenko and Sarachik, 2004). It will be interesting to see if the new generation of samples with very low n *and* high quality[6] have pinning frequency[7] ω_0 (Chap. 3) low enough (to be within the measurable f range) so the (B=0) pinning mode can be studied with the microwave. Microwave spectroscopy can also yield unique information in other regimes

[2]For an example of studying a classical Coulomb crystal using a chopped (optical) source to, see Nunomura *et al.* (2000, 2002).

[3]Although the microwave resonance in the 2DHS WC was measured by Li *et al.* (1997), the new generation of high quality hole samples may yield new physics not seen in earlier samples.

[4]The bilayer WC is a particularly interesting direction (see Appenix K). In a bilayer system, the layer index can play the role of spin and one may realize such novel phases as a anti-ferromagnetic (AFMWC) and ferromagnetic WC (FMWC). The FMWC is an interlayer coherent WC and may also be considered as an electronic supersolid (see Appenix K for details.). Another potentially interesting situation is when two layers have highly unbalanced n, such that one layer is a (pinned) WC and the other in a liquid state. Microwave studies on bilayer hole systems are currently underway by Wang *et al.* (2005).

[5]Perhaps using an array of quantum wires (Demel *et al.*, 1988; Fukui *et al.*, 1990).

[6]see, for example, Csathy *et al.* (2005a)

[7]At B=0, one expects that the pinning mode $\omega_{\rm pk}$=ω_0 (Fukuyama and Lee, 1978; Chitra *et al.*, 2002).

of quantum Hall systems, for example at IQHE or near QH transitions, involving the localization physics (Hohls *et al.*, 2001; Engel *et al.*, 1993), and near ν=1/2, involving the composite fermion physics (Evers *et al.*, 2001).

Placed in the more general context of condensed matter physics, microwave absorption/transmission spectroscopy has been utilized to study various interesting systems, such as charge density waves (Grüner, 1988), spin density waves (Quinlivan *et al.*, 1990), electron glasses (Helgren *et al.*, 2004) and superconductors (SC) (both conventional SC (Biondi *et al.*, 1958; Tinkham, 1974) and high-Tc SC (Turner *et al.*, 2003; Gaiffulin *et al.*, 2000; Basov and Timusk, 2005)). The powerful ability for such a tool (especially broad band microwave spectroscopy) to probe charge ordering, dynamics (including collective excitations) and disorder effects (such as pinning) can make it a particularly promising tool for studying many rich and complex phenomena in strongly correlated electron systems (see for example, Dagotto (2005)). It can be illuminating to apply the microwave tool to study, for example, superconductor-insulator transitions (Sambandamurthy *et al.*, 2005b), the rich vortex physics (Blatter *et al.*, 1994), and the recently observed (in high-Tc superconductors) "checker-board" pattern (Hoffman *et al.*, 2002; Vershinin *et al.*, 2004; Hanaguri *et al.*, 2004) that has been suggested by many to come from some Wigner cystal of cooper pairs (see, for example Franz (2004); Chen *et al.* (2004a); Tešanović (2001); Demler *et al.* (2004)).

One of the fundamental tasks of condensed matter physics is to discover and study various quantum matter, such as quantum gas, quantum liquid and quantum solid, in both atomic and electronic systems. Macroscopic quantum phenomena (such as superfluidity, superconductivity, and FQHE) often occur as one of the most fascinating aspects of these quantum matter. Recently, evidences for a "supersolid" have been found in the quantum solid of helium (Kim and Chan, 2004b,a; Leggett, 2004). One particularly exciting possibility that has emerged from this thesis, is that some anal-

ogous supersolid [8] may also exist in the quantum solids of electrons we studied (see Chapter 5 and Appendix. K). An electronic supersolid has also been also proposed for the cooper-pair Wigner crystal (Anderson, 2004; Franz, 2004), in relation to the afore-mentioned checker-board pattern, and could hold the key to many mysteries of high-Tc superconductivity.

What we have learned is a handful
What we haven't learned is an ocean

——*Thiruvalluvar (1st century BC)*

[8] more broadly defined as a phase with both long range crystal order and phase coherence, or with both diagonal and off-diagonal long range order, see for example Leggett (1970)

Appendices

Appendix A

Physical Quantities

For convenience we list here certain physical quantities used and their representative values under typical situations, along with their parameter dependence. The values given should be assumed to provide a general guidance rather than high precision.

In the following ϵ means $\epsilon_0\epsilon_*$ (ϵ_*=13 for GaAs) and m means $m_0 m_*$ (m_*=0.068 for GaAs electrons) where ϵ_0 and m_0 are vacuum dielectric constant and bare electron mass respectively. The permeability of GaAs is taken to be close to be that of vacuum (i.e. μ_*=1).

All energies are given in Kelvin through E/k_B, and the conversions among temperature, frequency and energy scales are:

1 K = 20.8 GHz = 86 μeV

1 GHz = 48 mK = 4.1 μeV

1 μeV = 11.7 mK = 244 MHz = 1.6×10^{-25} Joule

All angular frequencies ω below are given in Hz (after dividing ω by 2π).

quantity	formula	representa--tive value	evaluated at	material
mean electron separation r	$1/\sqrt{\pi n}$	564 Å	n=1×10^{10}cm^{-2}	
triangular lattice constant a	$(2/\sqrt{3}n)^{1/2}$	1075 Å	n=1×10^{10}cm^{-2}	
Coulomb E_c	$e^2/4\pi\epsilon r$=$e^2\sqrt{\pi n}/4\pi\epsilon$	23 K	n=1×10^{10}cm^{-2}	GaAs
Fermi energy E_f	$\pi n\hbar^2/m$	4.1 K	n=1×10^{10}cm^{-2}	n-GaAs
r_s	r/a_B=$me^2/(4\pi\epsilon\hbar^2\sqrt{\pi n})$	5.6	n=1×10^{10}cm^{-2}	n-GaAs
ν	nh/eB	0.417	n=1×10^{10}cm^{-2} B=1 T	
l_B	$(\hbar/eB)^{1/2}$	257 Å	B=1 T	
E_l	$e^2/(4\pi\epsilon l)$	128 K	l=100 Å	
	if l=l_B: $e^2(eB)^{1/2}/(4\pi\epsilon\hbar^{1/2})$	50 K	B=1 T	GaAs
cyclotron ω_c	eB/m	411 GHz	B=1 T	n-GaAs
$\hbar\omega_c$	$\hbar eB/m$	19.7 K	B=1 T	n-GaAs
Zeeman energy	$g\mu_B B_{\rm tot}$	0.3 K	$B_{\rm tot}$=1T	n-GaAs
plasmon freq. ω_L	$\sqrt{ne^2q/(2m\epsilon)}$	162 GHz	n=1×10^{10}cm^{-2} q=2π/μm	n-GaAs
shear freq. ω_T	$(\frac{0.245n^{1/2}e^2}{4\pi m\epsilon})^{1/2}q$ [assuming classical μ_T]	25.4 GHz	n=1×10^{10}cm^{-2} q=2π/μm	n-GaAs
pinning freq. ω_0	$(\omega_{pk}\omega_c)^{1/2}$ =$(2\pi f_{pk}eB/m)^{1/2}$	161 GHz	f_{pk}=1 GHz B=10 T	n-GaAs
$S/f_{\rm pk}$	$ne\pi/(2B)$=$\nu\pi e^2/(2h)$	6.08 μS	ν=0.1	
Larkin length L_c	$(2\pi\mu_T/(neBf_{\rm pk}))^{1/2}$= $(0.245en^{1/2}/(2\epsilon Bf_{\rm pk}))^{1/2}$ [assuming classical μ_T]	1.32 μm	f_{pk}=1 GHz n=1×10^{10}cm^{-2} B=1 T	GaAs
magnetophonon localization L_B	$\nu(e^2/h)(4\epsilon\Delta f)^{-1}$= $(ne/B)(4\epsilon\Delta f)^{-1}$	8.5 μm	ν=0.1 Δf=1 GHz	GaAs
classical WC melting $T_{\rm cm}$	$e^2\sqrt{n}/(4\pi\epsilon k_B\Gamma)$ with Γ=127	179 mK	n=1×10^{10}cm^{-2}	GaAs
microwave λ	$c/(f\sqrt{\mu_*\epsilon_*})$	8.3 cm	f=1 GHz	GaAs
microwave penetration ξ (Chap. 2)	$\sqrt{\lvert\sigma_{xx}\rvert d/\omega\epsilon}$	0.37 μm	$\lvert\sigma_{xx}\rvert$=1μS f=$\frac{\omega}{2\pi}$=1 GHz d=0.1 μm	GaAs

Table A.1: Selected quantities relevant for 2DES solids. Universal physical constants c,e, h and $\hbar$ have the usual meaning. n is the 2DES density. B is the perpendicular magnetic field. a_B is the Bohr radius of the system and r_s=r/a_B is also equal to E_c/E_f (In D dimensions, r/a_B=$\pi^2 2^{1-2/D}K^{-4/D}(E_c/E_f)$, where $1/(Kr^D)$ = n). Quantities dependent on ϵ are calculated for GaAs and those dependent on m for GaAs electrons (n-GaAs). For Zeeman energy we use the g=0.44, also for n-GaAs. Formula for L_B is according to the estimate in Fogler and Huse (2000).

Appendix B

Sample Processing Procedures

B.1 General Steps

B.1.1 Wafer Cleaving and Thinning

Use scriber and glass slides to cleave a rectangular piece of sample from the wafer. The typical size is ∼3×5 mm and should be checked before cleaving to make sure it fits appropriately with the CPW pattern to be fabricated, as well as any DC contacts to be put on.

We often thin our sample (typically down to ∼150 μm) to facilitate tuning the 2DES density with a backgate in the experiment. The steps are:

1. Glue sample (front side) with black wax on the grinding chuck;
2. Grind the back side of the sample with SiC (power mixed with water) on glass plate;
3. Polish the back side with Al_2O_3 (powder mixed with water) on polishing pad;
4. Dissolve wax with warm TCE then take sample out carefully;
5. Clean the sample (see Section B.1.3 below for cleaning steps).

Now the samples is ready for putting on ohmic contacts. In the case when the wafer is "fresh" to start with (for example recently out of MBE) with no backside thinning done, sample cleaning, with organic solvents, is not needed and not recommended before the ohmic contacts step.

B.1.2 Ohmic Contacts

Most of our samples have ohmic contacts[1]. For them, we use indium (simply put by hand with solder iron on the edge of the sample). The contacts are then "alloyed" in an alloy station (with forming gas flowing) at 440°C for 10mins. Afterwards the residual indium on the surface should be scraped away (for example using a wooden tip) before the lithographical fabrication of CPW (next step).

B.1.3 CPW Fabrication

1. Sample cleaning: in acetone for 30 then 15 then 5 secs (if more substantial cleaning is desired to give an even cleaner surface for patterning, instead of just acetone, clean with TCE, acetone then IPA, 5mins and 80°C (hotplate) heating in each one); blow dry;

2. Glue on a thin cover glass: with any photoresist (PR), bake on 110°C hotplate for 10mins for better adhesion.

3. Spin-on PR: used PR 4210, 4000RPM for 30sec[2].

4. Bake: in over 90°C for 20 mins (or hot plate 110°C for 2 mins).

[1]These contacts are needed in the experiment to ground the 2DES and enable tuning the electron density with a backgate. They also provide a cooling mechanism for the electrons (via DC wires).

[2]Since our CPW typically has relatively large feature sizes ($\gtrsim 10\mu$m), fabrication parameters such as these have a quite decent tolerance window. For example we also used 3500RPM, 60sec and the results were just fine. PR4110 was found to work well too.

5. Expose with mask aligner: 8-10 secs (if using the exposure-filtered mask aligner in Princeton-POEM clean room, 30-50 secs)

6. Develop: in AZ350 (or AZ400):H2O (3.5:1) for 60secs in total (develop till the pattern is clear and continue for 15 secs more); flush in DI; blow dry.

7. Evaporate: with thermo-evaporator, evaporate 200 Å of Cr (to enhance Au adhesion) followed by $\sim$ 3000 Å of Au. The center conductor of CPW should have a sheet resistance on the order of 0.1 Ω or lower. Thicker Au film has the advantage of reducing the CPW center conductor resistance (thus reducing the signal loss) but may make lift-off more difficult.

8. Lift off in acetone: heat in 80°C acetone for 20mins followed (if needed) by careful and gentle ultrasonic agitations (for as short as possibly needed).

The CPW (see Chapter 2.2.1 for consideration in its designing) masks we used were either home made (for the straight CPW patterns) or ordered from Advance Reproduction Co. (ARC, 978-685-2911, North Andover MA).

B.2 Other Issues

B.2.1 Etching

Occasionally it is desirable to etch away the 2DES, for example, near the "taper" regime where the CPW meets the edge of the sample (the etching can thus give a uniform slot width under which the 2DES is measured). The place where the etching is desired should be patterned using the standard lithography steps (Williams, 1990) similar to the ones described in Sec. B.1.3, with the area to be protected from etching covered by a hard-baked (for example 110°C hotplate for 4 min or 90°C oven for 30min) layer of PR.

The etchant used is H_2SO_4:H_2O_2:H_2O (1:8:160), which (in the case of our n-type GaAs samples grown along <100> direction) has an etch rate $\sim 0.26\mu$m per min (Williams, 1990). The growth sheet of the wafer should be consulted to determine the depth to be etched.

B.2.2 Alloyed CPW

Although CPW is usually used to capacitively couple to the 2DES, as in all the measurements presented in this thesis, sometimes we alloy the CPW to contact the 2DES directly and use the CPW itself as the Ohmic contacts. This is beneficial in very low frequency applications (for example to study the "stripe" phase (Chapter 4.2). In this case, we lithographically pattern the CPW as in Sec. B.1.3, then deposit, preferably with an e-beam evaporator, 400Å of Ge, followed by 800Å Au, then 100Å Ni, then 2000Å Au to make the CPW films (instead of the usual Cr-Au ones) and then alloy the CPW in the alloy station (440°C 10min) as we do with usual Ohmic contacts (Sec. B.1.2).

B.2.3 *p*-type GaAs

The procedures described so far were used to process our GaAs 2DES samples (*n*-type). The CPW (capacitively coupled) fabrication (Sec. B.1.3) is generic and can be used on *p*-type samples (for example the wafers grown by Shayegan group) as well. For Ohmic contacts on p-type, InZn instead of indium is used (and if using alloyed CPW as ohmic contact, evaporate Au-Be-Ni-Au or Au-Zn-Ni-Au films), and to etch p-type GaAs grown along <311> direction, H_3PO_4:H_2O_2:H_2O (1:1:40), with an etch rate $\sim$0.1μm per min (refer to Williams (1990) or Shayegan group recipe for details) is used.

Appendix C

Supplementary Sample Information

C.1 General Information

C.1.1 Cool-down Procedures

The general principle here is to try to cool the 2DES in a way that is as reasonably "adiabatic" as possible, so the 2DES can arrive at a good "state" (appropriate density, good homogeneity, etc.) at the end of the cooldown.

Typically, we cool our samples from 300K to 77K in at least one hour ($\lesssim 4$ K/min); then from 77K to 4K in another hour or more ($\lesssim 1$ K/min). The cooling from 4K to base T (~ 50 mK) is determined by dilution fridge (DF) operation and usually takes a few hours.

During the cool-down, we usually ground all DC contacts and also attenuate the coax ports. In the case of cooling into a top-loading DF, direct grounding of the probe-top to the cryostat is also recommended.

C.1.2 Effects of Light

Most samples studied were cooled in dark and LED illumination is generally found to hurt the 2DES state, likely due to the CPW metal films present. The exception is Sample WP (see Sec. C.4), for which LED illumination is necessary to give a good as-cooled 2DES state.

Except for Sample P (see below), extended waiting in darkness at room T before starting the cooling is not necessary and has little effect on the final 2DES state arrived.

C.2 Sample P

Sample P (Pfeiffer wafer # 2-12-97-1) is a GaAs/AlGaAs heterojunction. Its schematic structure is shown in Fig. C.1 (not the actually growth sequence, only layers close to the 2DES and most important for its properties are shown). The wafer was rotated (7 RPM) during the MBE growth.

Sample P has the peculiar property that its as-cooled n can vary significantly by simply varying the length of time (τ_w) the sample is kept in darkness at room T before the starting of cool-down. The longer the τ_w, the *lower* the as-cooled n. For example, when cooled in "SCM1" fridge[1] $\tau_w \sim$ 20 mins typically results in as-cooled $n \sim 1\times10^{11}\text{cm}^{-2}$, whereas $\tau_w \sim$ 120 mins results in as-cooled $n \sim 6\times10^{10}\text{cm}^{-2}$.

Sample P was thinned and a backgate voltage of -100 V can deplete $\sim 1.1\times10^{10}\text{cm}^{-2}$ electrons.

The piece we studied has a meander shape CPW "M30", with length l=28mm and slot width w=30 μm. The CPW information for all samples are also summarized in Appendix D (Table D.1) for convenience.

[1] As-cooled n can also vary somewhat between the cryostats used ("C120", "SCM1" and "PDF" (see Chap. E.1 for a description of the different cryostats).

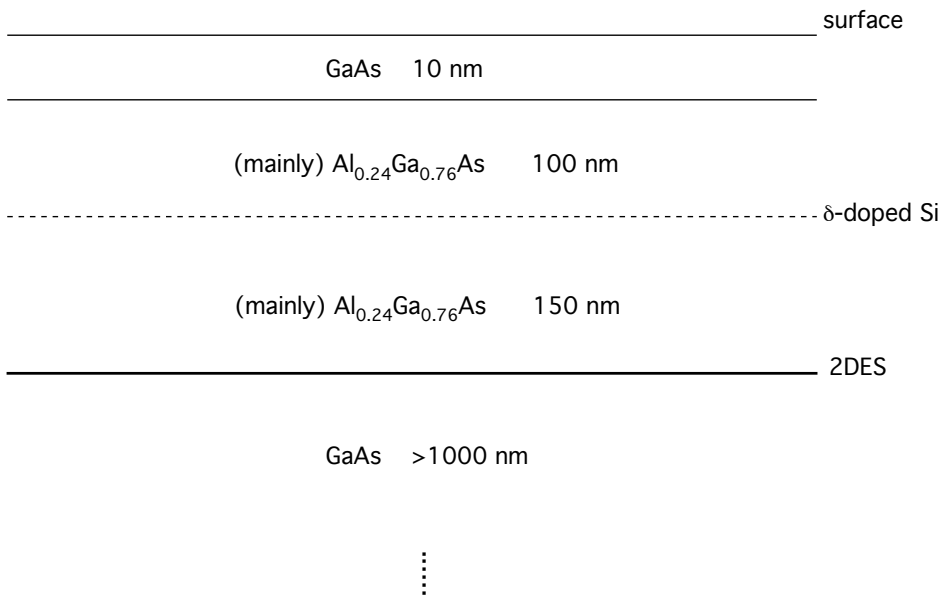

Figure C.1: Structure schematics for Sample P (not the full growth sequence).

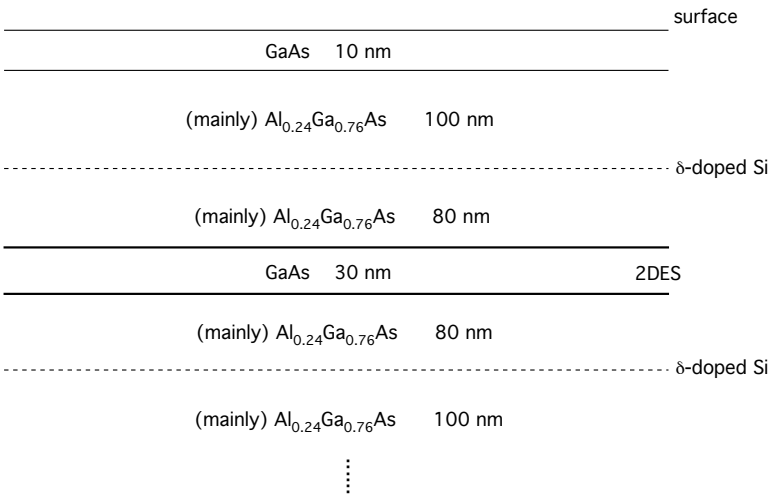

Figure C.2: Structure schematics for Sample R (not the full growth sequence, only layers most important for the 2DES properties are shown).

C.3 Sample R

Sample R (Pfeiffer wafer # 7-21-00-1) is a 30nm wide AlGaAs/GaAs/AlGaAs quantum well (QW), whose schematic structure is shown in Fig. C.2. The wafer was rotated (10 RPM) during the MBE growth.

Totally four pieces of sample R cut from the same wafer were studied. The CPW used are "S20e" (straight CPW with l=2mm and w=20 μm and the electric field along the "easy" direction <110>),"S20h" (straight CPW with l=2mm and w=20 μm and the electric field along the "hard" direction $<1\bar{1}0>$), "S80h" (straight CPW with l=4mm and w=80 μm and the electric field along the "hard" direction $<1\bar{1}0>$) and "M30" (meander l=28mm and w=30 μm) respectively. When distinguish is needed we label the pieces as R_S20e, R_S20h, R_S80h and R_M30 respectively. The different orientation were selected to allow the studying of the anisotropic stripe phase (Chap. 4.2).

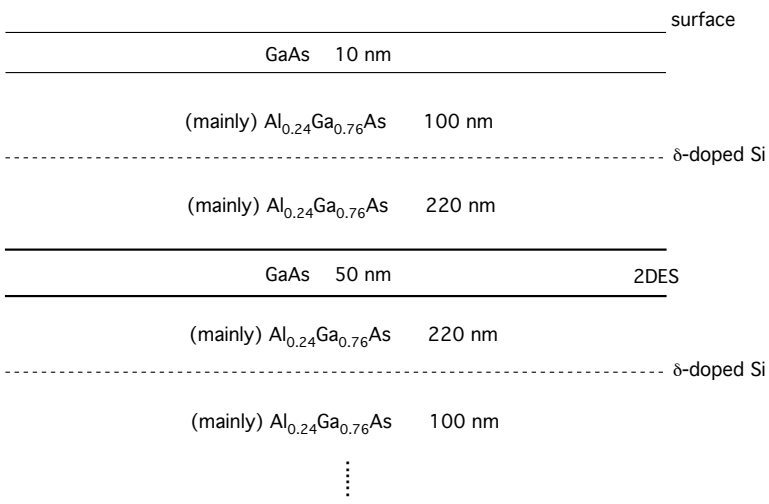

Figure C.3: Structure schematics for Sample WP (not the full growth sequence, only layers most important for the 2DES properties are shown).

C.4 Sample WP

Sample WP (Pfeiffer wafer # 7-20-99-1) is a 50nm wide AlGaAs/GaAs/AlGaAs QW, whose schematic structure is shown in Fig. C.3. The wafer was rotated (10 RPM) during the MBE growth.

LED illumination at $T\sim$10K was needed to induce a good quality 2DES. The dosage used was rather large (compared to the one usually used in DC samples) likely due to the CPW metal films present. The as cooled density n has found to be tunable from $\sim 6\times10^{10}\text{cm}^{-2}$ to $1\times10^{11}\text{cm}^{-2}$, with the amount of current used in the LED (typically $\sim$ 6-11 mA for 1-2 mins)

The piece we studied has a meander shape CPW "M30", with length l=28mm and slot width w=30 μm.

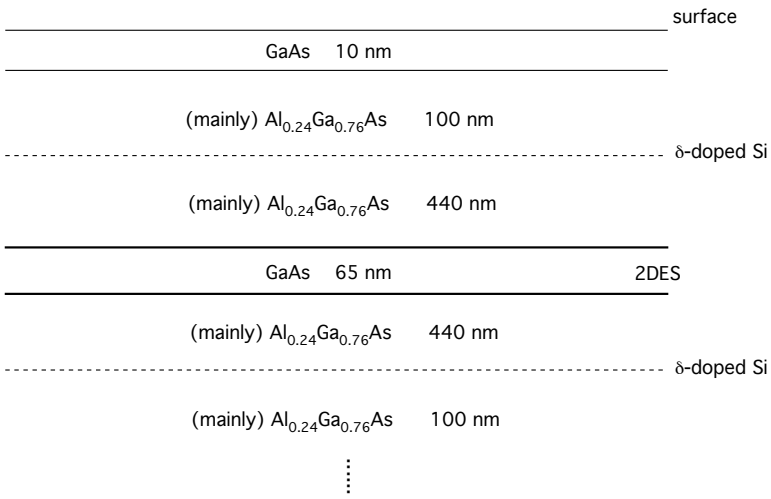

Figure C.4: Structure schematics for Sample QW65 (not the full growth sequence, only layers most important for the 2DES properties are shown).

C.5 Sample QW65

Sample QW65 (Pfeiffer wafer # 8-30-99-1) is a 65nm wide AlGaAs/GaAs/AlGaAs QW, whose schematic structure is shown in Fig. C.4. The wafer was rotated (10 RPM) during the MBE growth.

Five pieces cut from the same wafer were studied, labeled respectively as QW65_M30, QW65_M60, QW65_S80, QW65_S20 according to the CPW used (M30: meander l=28 mm, w=30 μm; M60: meander l=15.5 mm, w=60 μm; S80: straight l=4mm, w= 80 μm; S20: l=4mm, w= 20 μm. The orientation of the straight CPW is not important).

C.6 Sample QW15

Sample QW15 (Pfeiffer wafer # 10-09-01-1) is a 15nm wide AlGaAs/GaAs/AlGaAs QW, whose schematic structure is shown in Fig. C.4 and only differs from that of

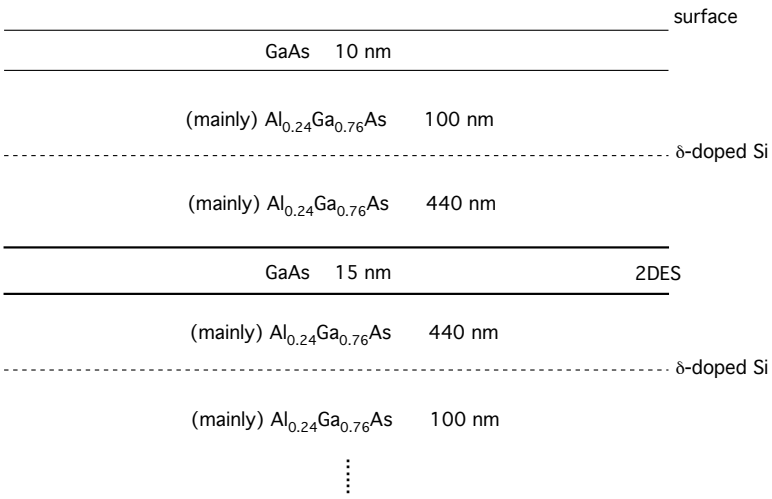

Figure C.5: Structure schematics for Sample QW15 (not the full growth sequence, only layers most important for the 2DES properties are shown).

QW65 in the width of QW. The wafer was rotated (10 RPM) during the MBE growth.

The piece we studied has a meander shape CPW "M30", with length l=28mm and slot width w=30 μm.

Appendix D

Coplanar Wave-Guide

D.1 Characteristic Impedance

This appendix summarizes a few basic facts about Coplanar Wave-guide (CPW) as a transmission line. More complete treatments can be found in (Russer and Bieble, 1994; Wen, 1969) and the general transmission line theory is covered in (Liao, 1990).

Consider a CPW (schematically shown in Fig. D.1 for a local cross section) with s as the center conductor width, w the slot width and fabricated on a substrate of thickness h and relative dielectric constant ϵ_r. The surrounding is assumed to be vacuum or air ($\epsilon_r \sim 1$, which is also a good approximation for helium) .

In our usual applications, s,w,$h \ll \lambda$ (the microwave wavelength). Also the CPW metal films have very small resistance and the side planes can be treated as effectively infinitely extended. In this case, the CPW, when not loaded by 2DES, can be modeled by a standard, loss-less transmission line with two parameters L' and C' (or v_{ph} and Z_0), where L' is the inductance per unit length, C' is the capacitance per unit length (between the center conductor to ground). For the standard transmission line theory (Liao, 1990, chapter 3, section 1), we have $v_{ph}=1/\sqrt{L'C'}$ as the phase velocity and $Z_0=\sqrt{L'/C'}$ the characteristic impedance. L' and C' (or alternatively, v_{ph} and Z_0) are

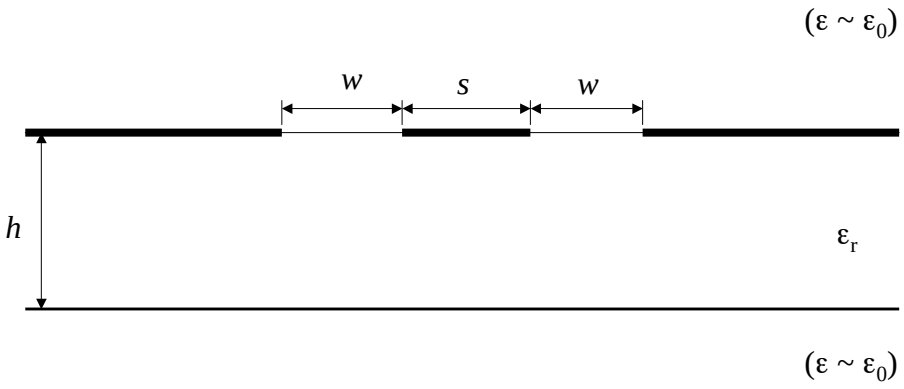

Figure D.1: Schematic CPW (local cross section).

only determined by the CPW geometry and ϵ_r. An excellent approximation can be obtained with conformal mapping (Wen, 1969), giving the following analytic formula (Russer and Bieble, 1994, p.40) for v_{ph} and Z_0 (from which one can solve[1] for L' and C'):

$$v_{ph} = c/\sqrt{\epsilon_{eff}} \tag{D.1}$$

where

$$\epsilon_{eff} = 1 + \frac{\epsilon_r - 1}{2} \frac{K(k')}{K(k)} \frac{K(k_1)}{K(k_1')} \tag{D.2}$$

$$Z_0 = \frac{\eta_0}{4\sqrt{\epsilon_{eff}}} \frac{K(k')}{K(k)} \tag{D.3}$$

where $\eta_0 = \sqrt{\mu_0/\epsilon_0}$.

In the above equations, $K(k)$ is the complete elliptic function of the first kind, with

$$k = \sqrt{1 - k'^2} = s/(s + 2w)$$

and[2]

$$k_1 = \sqrt{1 - k_1'^2} = \frac{\sinh \frac{\pi s}{4h}}{\sinh \frac{\pi(s+2w)}{4h}}$$

In practice, it is often convenient to use an online-available CPW designing calculator, for example

http://www1.sphere.ne.jp/i-lab/ilab/tool/cpw_e.htm

[1]For example, typical values (calculated for the meander "M30" CPW we used) are L'=0.44μH/m and C'=176 pF/m (Li, 1999).

[2]In most situations, h is large compared to s and w, then $k_1 \sim k$ and ϵ_{eff} can be further approximated as simply $(1 + \epsilon_r)/2$.

Wafer	CPW code	CPW length l	CPW slot width w	CPW center conductor width s	remark
P	M30	28 mm	30 μm	45 μm	
R	M30	28 mm	30 μm	45 μm	
	S20e	2 mm	20 μm	30 μm	CPW along <1$\bar{1}$0>
	S20h	2 mm	20 μm	30 μm	CPW along <110>
	S80h	4 mm	80 μm	120 μm	CPW along <110>
WP	M30	28 mm	30 μm	45 μm	
QW65	M30	28 mm	30 μm	45 μm	
	M60	15.5 mm	60 μm	90 μm	
	S20	4 mm	20 μm	30 μm	
	S80	4 mm	80 μm	120 μm	
QW15	M30	28 mm	30 μm	45 μm	

Table D.1: Summary of CPW parameters used in all samples. In the case of R and WQ65, multiple pieces of samples were made from the same respective wafer but with different CPW and each sample is referred to using the joint wafer and CPW name (for example "WQ65_S20") when distinguish is needed.

D.2 List of All CPW's used

For convenience, we list in Table D.1 all the CPW's that have been used in all samples we studied.

D.3 From S parameters to Conductivity

The vector network analyzer can measure any one of the (complex) S-parameters of a two-port network. The meaning of S-parameters[3] is illustrated in Fig. D.2, which shows a two-port network as a part of a transmission line. The a_i (b_i) are the (complex) voltages of the waves propagating through the network, in the directions labeled by the corresponding arrows. In our case when the network is the sample with CPW, the two ports are the center conductor and side plane (ground) respectively.

[3]For more detailed discussion on S-parameters, see Hewlett-Packard Application Note 154 "S-Parameter Design"; HP Application Note 95-1 "S-parameter Techniques for Faster, More Accurate Network Design".

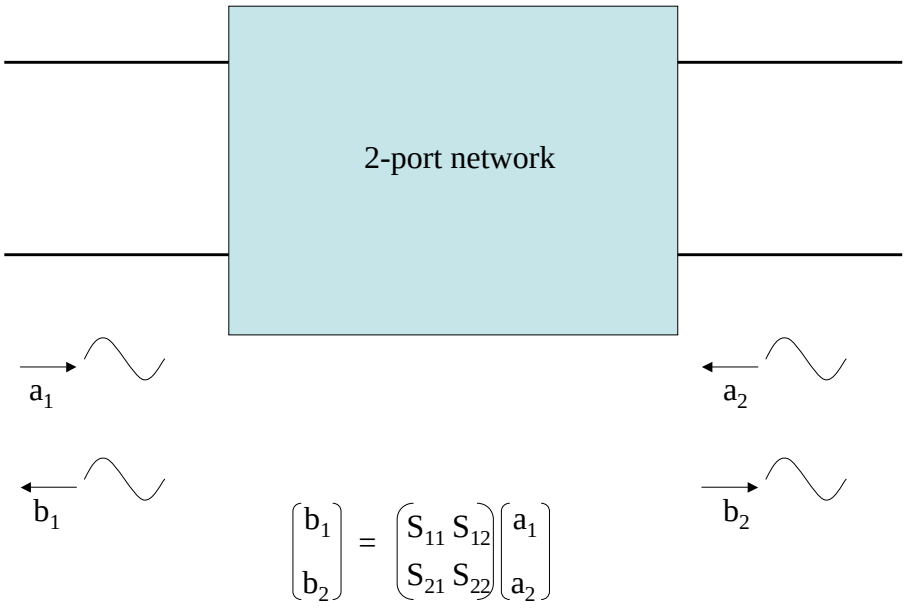

Figure D.2: S parameters of a two-port network.

In our experiments, we always put the analyzer in the mode that measures S_{21}, the (complex) forward transmission coefficient. For a sample with a CPW of length l, S_{21} is related to the "propagation constant" γ as $S_{21}=e^{-\gamma l}$. Applying the standard transmission line theory (Liao, 1990, chapter 3, section 1) to our situation (see also Fig. 2.2 and the discussions in Sec. 2.2.1), $\gamma=\sqrt{(i\omega L')(i\omega C'+G')}$ where $G'=2\sigma_{xx}/W$. It turns out that a binomial expansion gives a fairly good approximation of γ under our experimental conditions and one has:

$$\gamma = i\omega\sqrt{L'C'}(1+\frac{\sigma_{xx}}{i\omega WC'}) = \sigma_{xx}Z_0/W + i\omega/v_{ph} \tag{D.4}$$

Since $|S_{21}|^2$ gives the relative power transmission $P=P_{out}/P_{in}$ (note that S_{21} is a voltage ratio), this leads to Eq.2.1 which we have used to extract $\mathrm{Re}[\sigma_{xx}]$.

D.3.1 Imaginary Part of σ_{xx}

In this thesis we have focused exclusively on $\mathrm{Re}[\sigma_{xx}]$, which is relatively easy to interpret and compare to the theories. We mentioned in the above that the network analyzer measures the complex transmission S_{21} (see Appendix D), which gives both the power absorption P and the phase shift Θ, from which we can extract the real and imaginary part of σ_{xx} respectively (under appropriate conditions, usually satisfied in our experiments, as discussed in Sec. 2.2.1). Our measurement scheme is generally more sensitive to $\mathrm{Re}[\sigma_{xx}]$ than $\mathrm{Im}[\sigma_{xx}]$ (Engel *et al.*, 1993; Li, 1999), nonetheless we obtain them simultaneously[4]. This is demonstrated below in Fig. D.3(A). The pinning mode resonance in the WC manifests in $\mathrm{Re}[\sigma_{xx}(f)]$ as a peak and in $\mathrm{Im}[\sigma_{xx}(f)]$ as a zero-crossing. One can even make a parametric (versus f) 2D plot of the full complex σ_{xx}, as shown in Fig. D.3(B). In this case, a circle[5] is traced counterclockwise as f

[4]For spectroscopy, *in principle* (if the f range is large enough), $\mathrm{Re}[\sigma_{xx}(f)]$ and $\mathrm{Im}[\sigma_{xx}(f)]$, related by KK relation, contain the same information.

[5]One can show, following Fukuyama and Lee (1978), that the area (A) enclosed by this circle is in fact related to the line width (Δf) of the resonance ($A\propto 1/\Delta f^2$)

increases.

Previously, Li *et al.* (1995a) extracted dielectric constant ϵ^0_{xx} from the slope of measured $\mathrm{Im}[\sigma_{xx}(\omega)]$ vs ω. He found a giant ϵ^0_{xx} in the 2DES re-entrant insulating phase (near ν=1/5) and studied its T dependence, and interpreted the findings as consistent with the expected behavior of a pinned WC.

We also mention here, that measurements of the T-dependence of dielectric functions could be used to probe the "electron glass", see, for example[6], Park *et al.* (2005).

D.4 Some Other Practical Issues

We have shown in Fig. 2.4 a picture of an actual sample mounted on a block. The CPW on the sample are connected with indium bridges to the circuit-board CPW on the block. These indium bridges also press the sample against the Cu backgate pad (with a Kepton tape between the sample and the gate). The 90 degree turn of the circuit-board CPW (along the edge of the block), visible at the right hand side, is actually made by electrically joining two such circuit board CPW with silver epoxy (the substrates (appropriately wedged) are joined with a nonconducting glue, such as "hysol").

The substrate (thickness h=25 mils) of the circuit board has a relative dielectric constant 10, and the circuit board CPW currently used typically has the slot width (w) of 22 mils and the center conductor width (s) of 16 mils. To push the microwave measurements to higher[7] f (above $\sim$ 20 GHz, for example), one may need to reduce the dimensions of the circuit board CPW (perhaps fabricated with lithography), such that s,w,$h \ll \lambda$ (Sec. D.1) remains safely satisfied.

[6]They found a temperature, interpreted as the glass-freezing temperature, below which ϵ drops substantially.

[7]The main limit of pushing the measurements to *lower* f (below $\sim$ 10 MHz, for example), on the other hand, comes from the capacitive coupling of the CPW on the sample to the 2DES. A CPW alloyed to directly contact the 2DES (see also Sec. B.2.2) is perhaps more appropriate at such low f.

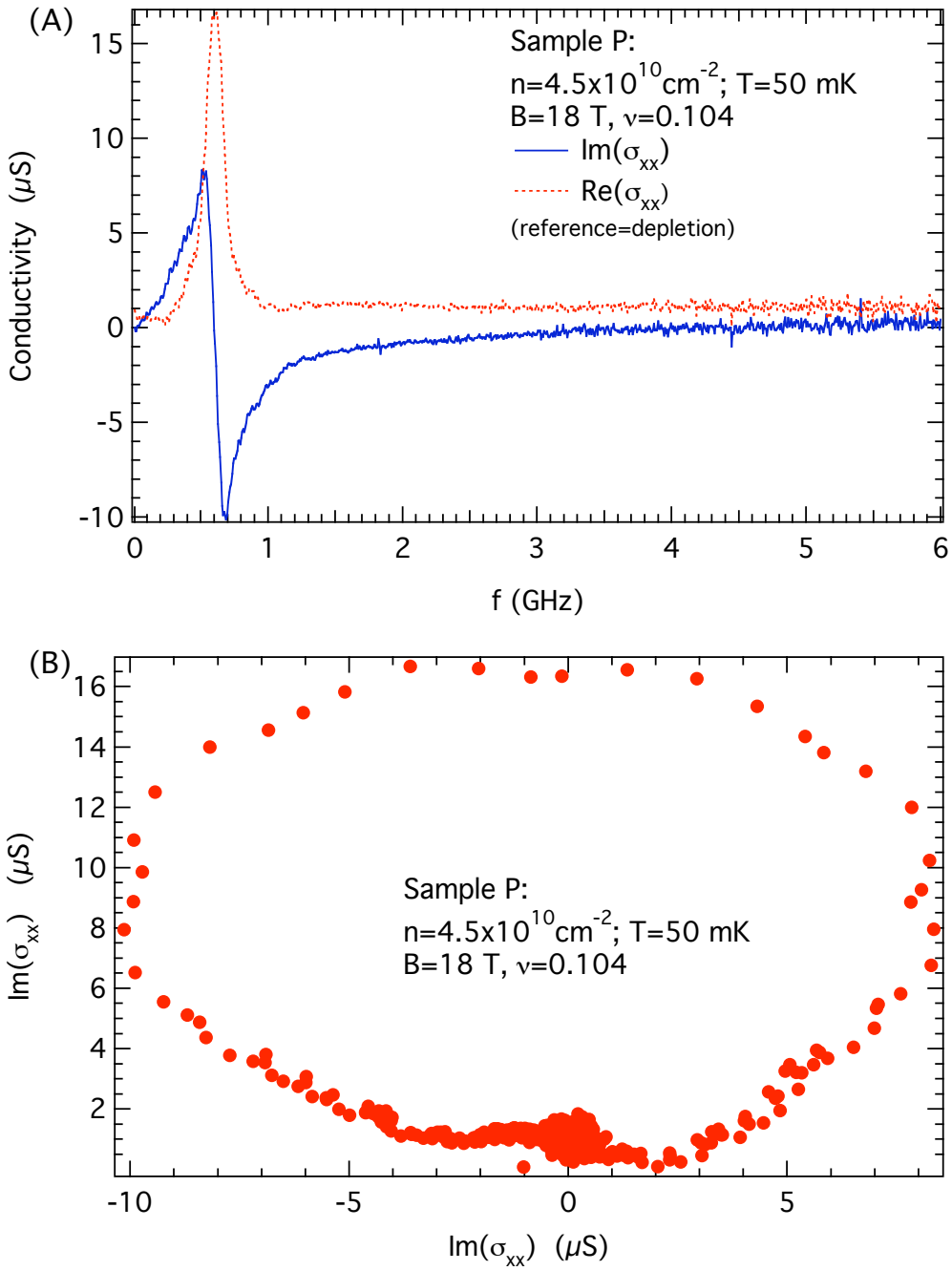

Figure D.3: (A): An example of the real and imaginary parts of conductivity spectrum measured in Sample P in the WC regime. (B): The same data in (A), now plotted in the complex plane, showing the trajectory of the complex conductivity as the frequency (f) is sweeped.

To push the temperature T (more specifically, the electron temperature) to even lower values than currently achieved (below $\sim$ 30mK, for example), one may need to carefully consider the cooling of the CPW, with possibly on-block microwave attenuation (Sambandamurthy *et al.*, 2005a).

Appendix E

Setups in NHMFL

E.1 Cryostats and Magnet Cells

In this section we note some issues specific for the magnet cells/cryostats used in NHMFL.

E.1.1 C120 (14T)

In C120 we have a vacuum-loading dilution fridge (DF), and a superconducting magnet, both made by Oxford Instruments. The mixing chamber (MC) of the fridge can reach a base T of sub 10mK. However, the sample/block (sitting in vacuum and thermally connected to the MC via a copper strip) can only be cooled to $\sim$ 35mK ($\sim$ 60mK if using the sample rotator). The main heat load comes from the coax cables. Over the years, such heat load has been reduced using, for example, superconducting (Nb) coax cables and connectors to block the heat conduction in various places in the DF.

The C120 magnet has a maximum B-field of 14T (16T if pumping the λ plate). The maximum B sweeping rate that will not heat the sample appreciably is $\sim$0.08T/min.

However, in spectroscopy measurements, faster[1] sweep rates (up to 0.3-0.4 T/min) have been often used as long as sufficient stabilization time (∼1min) is given prior to measuring each spectrum.

The temperature is currently read by a ruthenium oxide thermometer on the MC, which is far from the magnetic field region. We have confirmed that the sample/block (using both an on-block thermometer and measured features from the 2DES) temperature can follow the MC temperature down to ∼ 35mK (without the rotator). The temperature can be raised using an externally controlled MC heater. A temperature stabilization time of ∼ 20 minutes is found to be generally sufficient. In addition, a powerful on-block heater enables rapid thermal cycling of the sample without pulling the fridge.

Currently, microwave measurements in C120 can be fully automated with Labview.

E.1.2 SCM1 (18T)

In SCM1 we have a top-loading DF, and a superconducting magnet, both from Oxford. The sample/block is immersed in the ^{3}He-^{4}He mixture and can be in thermal equilibrium with the MC down to ∼ 45-50 mK, as we have checked.

The magnet has a maximum B-field of 18T (20T if pumping the λ plate). We have typically used B sweep rate of 0.2-0.4T/min without noticing significant heating. For accurate B-trace measurements the sweep rate is more limited by the possible hysteresis of the magnet than the heating concern.

In SCM1, the microwave response of the semirigid coax cables (in the probe) has a non-negligible dependence on the helium level (particularly when the level is near 80%) in the dewar (this is in contrast to C120, where the fridge coax is in vacuum and the microwave response has negligible helium level dependence). For accurate spectroscopy measurements, such a dependence needs to be taken into account and can

[1]Note that the *first* sweep (after cool-down) to high B for a superconducting magnet often needs to be significantly slower, $\lesssim$ 0.1T/min.

be corrected by, for example, careful calibration of the reference spectrum (Sec. 2.2.3) at different helium levels.

The ruthenium oxide thermometer in MC (which is subjected to B) has a significant, almost linear positive magnetoresistance for $B \gtrsim$ 3T (below 3T, the magnetoresistance, although can be anomalous, is generally weaker (especially when T is above $\sim$ 100mK)). A reasonably good approximation we have used to correct for the magnetoresistance is given as the following:

$$R_0 = R(B)/(1 + 0.11 \times B/18) \tag{E.1}$$

in which B is in Tesla and $R(B)$ is the resistance reading at B>3T, and R_0 is the estimated resistance reading at 0T and can be converted to a temperature using the B=0 R-T calibration.

The temperature can be raised with an externally controlled MC heater. A temperature stabilization time of $\sim$ 10-15 minutes is found to be generally sufficient for $T \lesssim$ 400mK. Above $\sim$400mK, long term T stabilization is more difficult. However, for the relatively short time to measure each spectrum (typically 2-3 minutes), this usually does not pose a significant problem (which we have checked both from monitoring in real-time the T reading and from measured features in the 2DES). We have also noticed that the efficacy of the heater does have some dependence on the fridge state (for example the still power used).

E.1.3 Resistive (33T) and Hybrid (45T) Cells

The resistive cells have Florida-Bitter resistive magnets with maximum B=33T. The hybrid cell has at present the world's highest DC B-field magnet, using a 11.5 T superconducting magnet outsert and a 33.5T resistive magnet insert to give a combined maximum field of 45T.

When doing experiments in one of these cells, we have used a top loading portable dilution fridge (PDF) inserted in the magnet bore. With our microwave probe, the sample can typically be cooled to $\sim$ 55-70 mK. Although the resistive magnet (and the resistive insert of the hybrid magnet) can be sweeped much faster than a superconducting magnet, we have normally kept the sweep rate below 1T/min to prevent heating. The magneto resistance of the ruthenium oxide thermometers (on the probe) can be corrected for in similar ways as in (E.1).

Setups in the resistive or hybrid cells often need considering the significant fringe B field present in the cells, and the fact that (for safety reasons) the user is prevented from getting near the probe/cryostat when the resistive magnet is energized. Automated data acquisition and remote control are particularly valuable in these environments.

E.2 Automation Programs and Data Deposit

Automatic data acquisition (batch enabled) are enabled by a set of Labview programs which control/communicate with a number of instruments (for example the analyzer, magnet, and the instruments to change the temperature or gate voltage). These programs are under (accessible from the NHMFL intranet)
https://tesla.magnet.fsu.edu/ychen/ExpRes/Magwav
and can be made available upon request (although with no claim of any guarantee for using these programs).

All the raw data and their analysis, including all the Igor programs written for analyzing the data (batch enabled), are deposited at (accessible from the NHMFL intranet)
https://tesla.magnet.fsu.edu/ychen/PeideMac_DataAnabk/DataAna
and are available upon request.

Appendix F

AC Magneto-conductivity

We have focused on "f-traces" data (Re$[\sigma_{xx}(f)]$) in this thesis. In this appendix we give representative B-traces (AC magneto-conductivity) for samples WP, P, QW15 in the following self -explanatory figures; and QW65 in the reprint of a paper[1], also published as Chen *et al.* (2004b) (with discussions on some insights the B-traces can provide). Representative B-traces for Sample R (30nm QW) have been given in Fig. 2.5 in Chap. 2 and Fig. 4.1 in Chap. 4.

[1]QW65 is the sample 1 (QW65_M30) in the paper. The other sample presented in the paper is not discussed in this thesis.

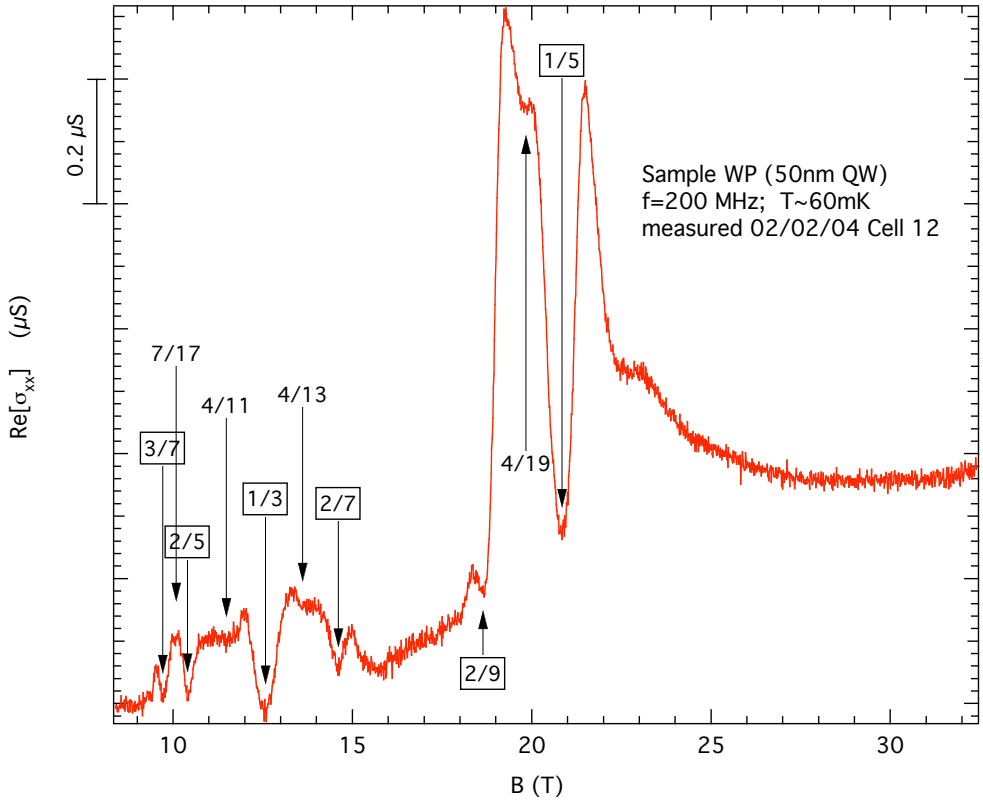

Figure F.1: A representative B-trace measured in Sample WP.

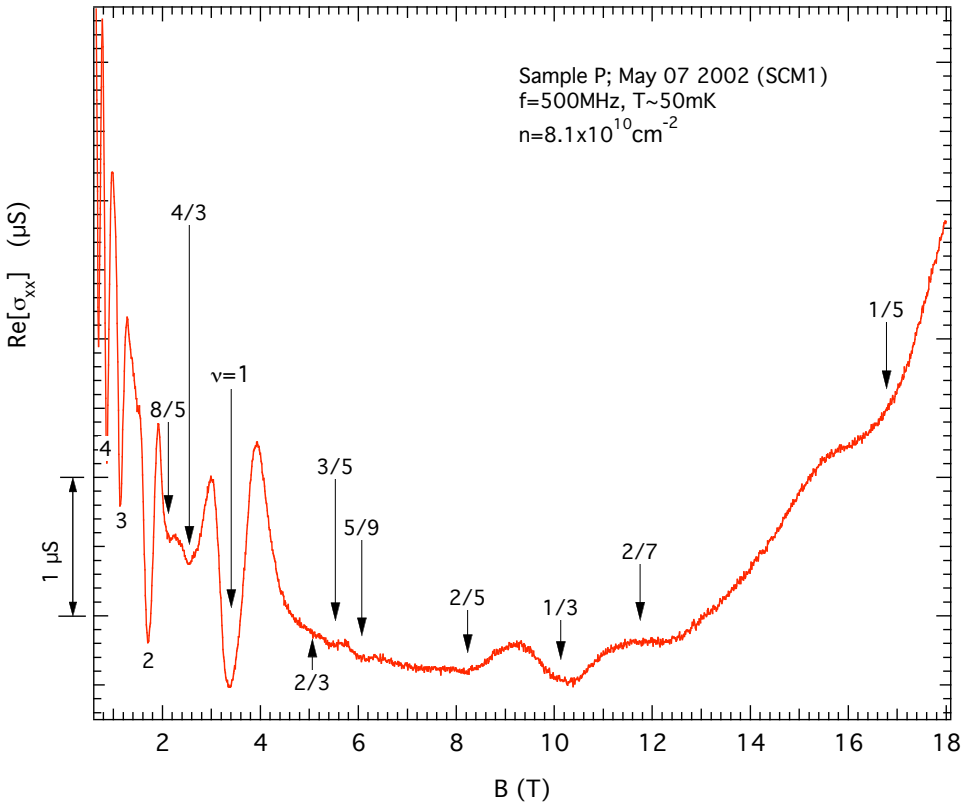

Figure F.2: A representative B-trace measured in Sample P.

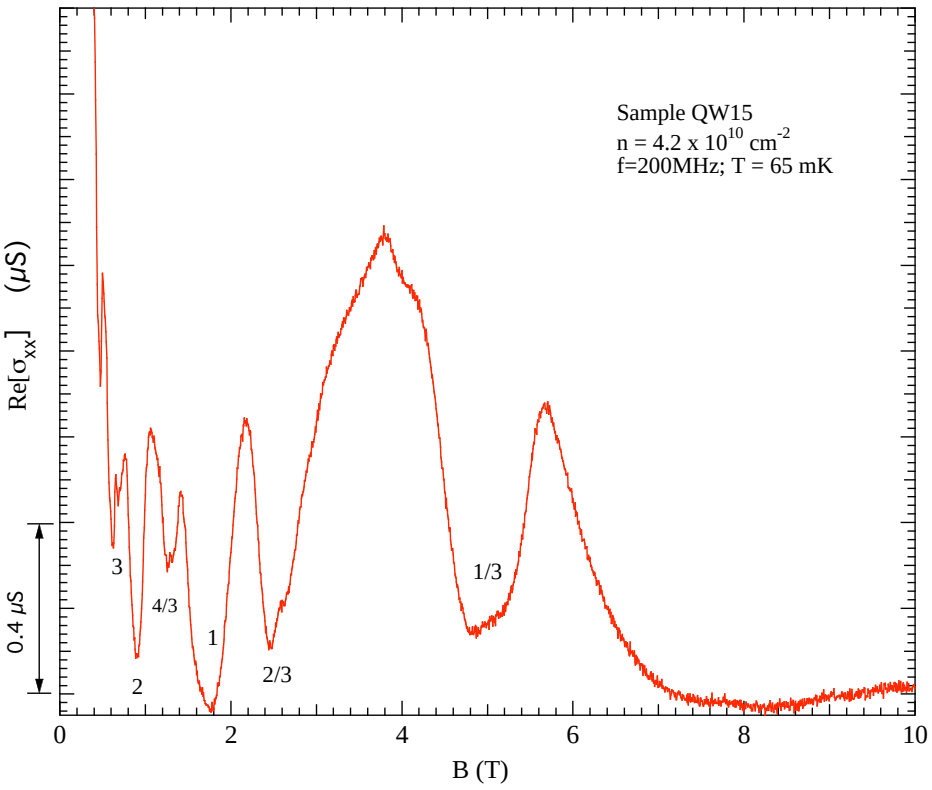

Figure F.3: A representative B-trace measured in Sample QW15 (Sambandamurthy *et al.*, 2005a).

International Journal of Modern Physics B
Vol. 18, Nos. 27, 28 & 29 (2004) 3553–3556

World Scientific
www.worldscientific.com

AC MAGNETOTRANSPORT IN REENTRANT INSULATING PHASES OF TWO-DIMENSIONAL ELECTRONS NEAR 1/5 AND 1/3 LANDAU FILLINGS

YONG P. CHEN[†,‡,*], Z. H. WANG[‡,§], R. M. LEWIS[†,‡], P. D. YE[¶], L. W. ENGEL[‡], D. C. TSUI[†], L. N. PFEIFFER[‖] and K. W. WEST[‖]

[†]*Department of Electrical Engineering, Princeton University, Princeton, NJ 08544, USA*
[‡]*National High Magnetic Field Laboratory, Tallahassee, FL 32310, USA*
[§]*Department of Physics, Princeton University, Princeton, NJ 08544, USA*
[¶]*Agere Systems, Allentown, PA 18109, USA*
[‖]*Bell Laboratories, Murray Hill, NJ 07974, USA*
[*]*yongchen@princeton.edu*

We have measured high frequency magnetotransport of a high quality two-dimensional electron system (2DES) near the reentrant insulating phase (RIP) at Landau fillings (ν) between 1/5 and 2/9. The magneto*conductivity* in the RIP has resonant behavior around 150 MHz, showing a *peak* at $\nu\sim0.21$. Our data support the interpretation of the RIP as due to some pinned electron solid. We have also investigated a narrowly confined 2DES recently found to have a RIP at $1/3<\nu<1/2$ and we have revealed features, not seen in DC transport, that suggest some intriguing interplay between the 1/3 FQHE and RIP.

Keywords: Reentrant insulating phase; 2DES; high-frequency transport.

The DC resistivity of high quality two dimensional electron systems (2DES) in GaAs/AlGaAs is well known to diverge at low temperature (T) for Landau filling $\nu=nh/eB$ (where n denotes 2DES density and B the perpendicular magnetic field) below[1] the 1/5 fractional quantum Hall effect (FQHE) and in a narrow ν range reentrant above[2] 1/5. Such a reentrant insulating phase (RIP) has been interpreted as a pinned electron solid with Wigner crystal (WC)[3] order, and the reentrance of the insulating transition is thought to be caused by competition between FQHE states and WC[4]. Recently it was shown that such a transition can shift to higher ν, and occur around the 1/3 FQHE, for a 2DES tightly confined in a narrow quantum well (QW).[5]

In this article, we report AC magnetotransport measurements on two GaAs/AlGaAs 2DES samples (sample 1 and 2) in the RIP around ν=1/5 and ν=1/3 respectively. Sample 1 is a 65-nm-wide QW with $n=5.9\times10^{10}\text{cm}^{-2}$ and mobility $\mu\approx8\times10^{6}\text{cm}^2/\text{Vs}$. Samples[2,6–8] with such high quality (μ over $10^{6}\text{cm}^2/\text{Vs}$) have been well known to display (in DC) a RIP at $\nu>1/5$. Sample 2 is an 8-nm-wide QW with $n=1.2\times10^{11}\text{cm}^{-2}$ and $\mu\approx2.6\times10^{5}\text{cm}^2/\text{Vs}$. It is from the same wafer as

used in the experiments of Ref. 5, which found a RIP at ν>1/3.

Figure 1(A) shows the scheme of our contactless, high frequency (f) (in RF/microwave range) magnetotransport measurements, employing similar techniques to those used previously.[9,10] A meandering metal film coplanar waveguide (CPW) is deposited on the sample surface. A network analyzer generates an AC signal which propagates through the CPW, setting up an AC electric field mainly confined to the slots between the center conductor and the broad side planes. The relative power absorption (P) by the 2DES is measured. Under conditions[9] of (1) high f, (2) low 2DES conductivity, (3) no reflections at ends of CPW, and (4) 2DES is in its long wavelength limit, one has $P = \exp(\frac{2lZ_0}{w}\mathrm{Re}(\sigma_{xx}))$ where $\mathrm{Re}(\sigma_{xx})$ is real part of the diagonal conductivity of the 2DES, l and w the total length (28mm) and slot width (30 μm) of the CPW and Z_0=50 Ω its characteristic impedance at $\sigma_{xx} = 0$. It turns out that conditions (1)-(4) are well satisfied for sample 2, allowing us to directly extract $\mathrm{Re}(\sigma_{xx})$ from P. The conditions are not fully satisfied[11] for sample 1, nonetheless we cast the measured P into a $\mathrm{Re}(\sigma^c_{xx})=(w/2lZ_0)\ln(P)$, and still refer to $\mathrm{Re}(\sigma^c_{xx})$ as "conductivity", which can actually differ from the true 2DES $\mathrm{Re}(\sigma_{xx})$ by a factor of order unity[12]. In this work we focus on magnetoconductivity measurements (sweeping B at different f's), which are complementary to spectroscopy measurements (sweeping f at different B's)[10,11], so as to facilitate the comparison with DC transport. Measurements are performed close to the low power limit, by reducing RF/microwave power till P no longer shows appreciable change.

Fig. 1(B) shows magnetotransport traces measured on sample 1, at $T \approx$40 mK and several f's ranging from 10 MHz to 250 MHz. The traces are vertically offset for clarity, and displayed from bottom to top in increasing order of f. Several representative filling factors are labeled, showing clearly resolved FQHE states at 1/3, 2/5, 2/7, 1/5 and 2/9, attesting to the high quality of the sample. For ν>2/9 the conductivity ($\mathrm{Re}(\sigma^c_{xx})$) shows only weak f-dependence. However, for ν between 2/9 and 1/5, in the RIP, large and nonmonotonic f-dependence is evident. Focusing on this region, we notice that at f=10 MHz, the conductivity is small, displaying a minimum near the center of the RIP. This resembles the behavior of low-T DC conductivity.[13] At higher f, such as 150 MHz, the conductivity is greatly enhanced, and displays a *peak* near the center of the RIP ($B\sim$11.6 T with $\nu\sim$0.21). At even higher f, for example 250 MHz, the conductivity falls back to smaller values and displays again a minimum in the RIP. The data thus reveal a clear resonance in $\mathrm{Re}(\sigma^c_{xx})$ (or absorption) near $f\sim$150 MHz. Similar resonant behavior is also noticed for ν below the 1/5 FQHE. The f dependence for ν much lower than 1/5 has also been recently investigated[11] and shows significantly different behavior, which is beyond the scope of this work.

Fig. 1(C) shows magnetotransport at several f's measured at elevated $T\approx$150 mK (T accurate within 15%). The strong resonant behavior of RIP conductivity (near 150 MHz) observed at 40 mK is no longer evident.

The observed resonant enhancement of low T magnetoconductivity in the RIP

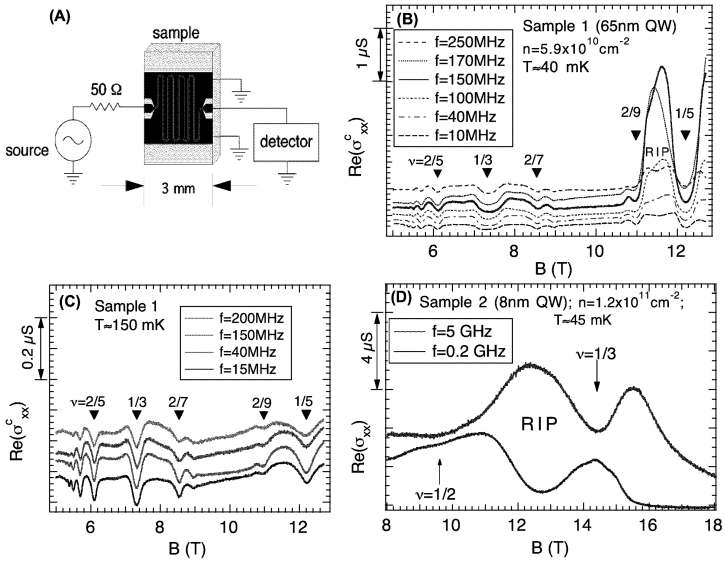

Fig. 1. **(A)**: Schematic of measurement circuit. Black regions represent the CPW metal films, consisting of the driven meander-shaped center line, separated from each of the two grounded side planes by a slot region (shown as the thin white meandering region) of width w. **(B)**: Sample 1 (65 nm QW), B-dependent Re(σ^c_{xx}) measured at $T \approx$40 mK. Offset traces from bottom to top were measured at f=10, 40, 100, 150, 170 and 250 MHz respectively. The f=150 MHz trace shows a resonant enhancement of conductivity in the RIP, peaked at $B\sim$11.6T, $\nu\sim$0.21. **(C)**: Sample 1 measured at $T\approx$150 mK. The resonance seen at 40 mK nearly disappears. Offset traces from bottom to top were measured at f=10, 40, 150 and 200 MHz respectively. Note the difference in vertical scale with panel (B). **(D)**:Sample 2 (8 nm QW, with a RIP for $1/3<\nu<1/2$). The lower trace shows magnetoconductivity at f=0.2 GHz, in comparison to the upper trace (offset) taken at 5 GHz. Measurements were done at $T \approx$45 mK.

near a well defined frequency supports the interpretation of such RIP as some disorder-pinned electron solid, with some order related to WC[14]. The resonance is interpreted as due to the pinning mode[15] of this solid. Probably because of lower disorder in sample 1, such a clear resonance in RIP was not observed in previous RF or microwave spectroscopy experiments[7,10] that were done on other wafers. The observed (at temperature $T_{\rm exp}\sim$ 40-50 mK) resonant frequency $f\sim$150 MHz satisfies $hf \ll k_{\rm B}T_{\rm exp}$, which reflects the highly collective nature of such state and rules out individual particle localization-delocalization transition[16] giving the resonance.

We have also investigated the high f magnetotransport of sample 2, the narrow QW with a RIP[5] above ν=1/3. We find that strong f-dependence of magnetoconductivity is observed at much higher f in sample 2 compared to sample 1. Fig. 1(D) shows two representative Re(σ_{xx}) traces taken at f=0.2 GHz and 5 GHz. At f=0.2 GHz, the magnetoconductivity displays a minimum in the RIP, at $\nu\sim$0.38 ($B\sim$12.6 T), the same ν at which experiments in Ref. 5 found a peak in DC resistivity. In-

terestingly, the magnetoconductivity displays a *maximum* at ν=1/3 instead of the expected FQHE minimum, which is recovered at elevated T. In contrast, at f=5 GHz, the magnetoconductivity in the RIP appears to be significantly enhanced and displays a peak, although we have not observed a clear resonant behavior up to 5 GHz. A minimum at ν=1/3 is evident in the f=5 GHz trace. Hence the abnormal behavior near ν=1/3 may indicate that there is some nontrivial f-dependence even at ν=1/3, where DC transport in Ref. 5 observed a FQHE[17] . It is also possible that due to different cooldown and illumination procedures, the sample behaves differently in our experiments than that in Ref. 5. More work is clearly needed, especially extending the measurements to higher f range and performing spectroscopy surveys, to better understand the RIP in the narrowly confined 2DES, and its likely intriguing relation with the ν=1/3 FQHE.

Acknowledgements

The high frequency measurements were performed at the National High Magnetic Field Lab, supported by NSF Cooperative Agreement No. DMR-0084173 and by State of Florida. We thank G. Jones, T. Murphy and E. Palm for assistance and W. Kang for helpful discussions. Financial support of this work was provided by AFOSR, DOE and NHMFL-IHRP.

References

1. R. L. Willet *et al.*, *Phys. Rev.* **B38**, 7881 (1988).
2. H. W. Jiang *et al.*, *Phys. Rev. Lett.* **65**, 633 (1990).
3. For reviews on WC, see H. Fertig and M. Shayegan, in *Perspectives in Quantum Hall Effects*, S. Das Sarma and A. Pinczuk eds. (Wiley, New York 1997), chap. 5 and 9.
4. P. K. Lam and S. M. Girvin, *Phys. Rev.* **B30**, 473 (1984); B. I. Halperin, *Helv. Phys. Acta*, **56**, 75 (1983).
5. I. Yang *et al.*, *Phys. Rev.* **B68**, 121302(R) (2003).
6. T. Sajoto *et al.*, *Phys. Rev. Lett.* **70**, 2321 (1993).
7. Y. P. Li *et al.*, *Solid State Commun.* **95**, 619 (1995);*ibid*, **96**, 379 (1995).
8. W. Pan *et al.*, *Phys. Rev. Lett.* **88**, 176802 (2002).
9. L. W. Engel *et al.*, *Phys. Rev. Lett.* **71**, 2638 (1993).
10. P. D. Ye *et al. Phys. Rev. Lett.* **89**, 176802 (2002).
11. Yong P. Chen *et al.*, unpublished.
12. This gives an uncertainty in the absolute magnitude of the conductivity data we present for sample 1, but has no significant influence on our findings regarding the B, f and T dependence of the conductivity.
13. V. J. Goldman, Bo Su and J. K. Wang, *Phys. Rev.* **B47**, 10548 (1993).
14. Theories (for example, R. Narevich, G. Murthy and H. A. Fertig, *Phys. Rev.* **B64**, 245326 (2001)) have suggested that the RIP may be a WC of composite fermions rather than electrons.
15. H. Fukuyama and P.A. Lee, *Phys. Rev.* **B18**, 6245 (1978); B. G. A. Normand, P. B. Littlewood and A. J. Millis, *Phys. Rev.* **B46**, 3920 (1992).
16. S. Kivelson, D-H. Lee and S-C. Zhang, *Phys. Rev.* **B46**, 2223 (1992).
17. We notice, however, that in Ref. 5 (its Fig. 1, 2 and 4), the DC resistivity of ν=1/3 did *not* fully tend to zero (within experimental limit).

Appendix G

Fukuyama-Lee Sum Rule

It turns out that in Fukuyama-Lee (Fukuyama and Lee, 1978), they made a (trivial) error of factor of 2 in the spectral weights (and thus the sum rule). In this appendix, we re-derive the pinning mode sum rule from Fukuyama and Lee (1978), for a 2D WC with density n in a perpendicular magnetic field B.

Start from the equation (4.3a) in their paper (hereafter referred to as FL), which gives the expression for $\sigma_{xx}(\omega)$ (neglecting any damping):

$$\sigma_{xx}(\omega) = -\frac{ne^2}{m}\frac{i\omega(\omega^2-\gamma^2)}{(\Omega_-^2-\omega^2)(\Omega_+^2-\omega^2)} \tag{G.1}$$

Here γ is the impurity pinning frequency (as we usually write as ω_0) and $\Omega_\pm$ are the frequencies of the two modes (pinning mode Ω_- and cyclotron mode Ω_+) given in (3.22) of FL:

$$\Omega_\pm^2 = \frac{1}{2}[\omega_c^2 + 2\gamma^2 \pm \omega_c(\omega_c^2+4\gamma^2)^{1/2}] \tag{G.2}$$

The $\sigma_{xx}(\omega)$ in above (1) is obviously purely imaginary at $\omega \neq \Omega_\pm$ and has singularities at $\Omega_\pm$—the corresponding real part of $\sigma_{xx}(\omega)$ will be delta function(s) at $\Omega_\pm$. For

example, when ω is near Ω_-, we rewrite $\sigma_{xx}(\omega)$ as

$$\sigma_{xx}(\omega) = -\frac{ne^2}{m}\frac{i}{(\Omega_- - \omega)}\frac{\omega(\omega^2-\gamma^2)}{(\Omega_- + \omega)(\Omega_+^2 - \omega^2)}$$

Since ω is near Ω_-, we perform the standard substitution for the singular term $\frac{i}{\Omega_- - \omega}$:

$$\frac{i}{\Omega_- - \omega} \longleftrightarrow \pi\delta(\Omega_- - \omega)$$

to extract its real part, and simply setting $\omega = \Omega_-$ in the rest of the expression (non-singular terms) and therefore obtain the real part of pinning mode conductivity:

$$\mathrm{Re}[\sigma_{xx}(\omega)] = -\frac{ne^2}{m}\pi\delta(\Omega_- - \omega)\frac{\Omega_-(\Omega_-^2-\gamma^2)}{(\Omega_- + \Omega_-)(\Omega_+^2 - \Omega_-^2)} = -\frac{ne^2\pi}{m}\frac{(\Omega_-^2-\gamma^2)}{2(\Omega_+^2 - \Omega_-^2)}\delta(\omega - \Omega_-)$$

from which we can read off directly (in Fukuyama-Lee's notation) that

$$\mathrm{Re}[\sigma_{xx}(\omega)] = \frac{ne^2\pi}{m}A_-\delta(\omega - \Omega_-) \tag{G.3}$$

with

$$A_- = -\frac{\Omega_-^2-\gamma^2}{2(\Omega_+^2 - \Omega_-^2)} \overset{\text{putting in (2)}}{==========} -\frac{\omega_c^2 - \omega_c(\omega_c^2+4\gamma^2)^{1/2}}{4\omega_c(\omega_c^2+4\gamma^2)^{1/2}} = \frac{1}{4}\{1-[1+4(\gamma/\omega_c)^2]^{-1/2}\}$$

This $A_-$is exactly half the value of (4.4b) in FL. (In similar procedure, for the cyclotron mode part (ω near Ω_+) one obtains $A_+ = -\frac{\Omega_+^2-\gamma^2}{2(\Omega_-^2-\Omega_+^2)} = \frac{1}{4}\{1 + [1 + 4(\gamma/\omega_c)^2]^{-1/2}\}$, also half the value given in (4.4b) of FL). The corresponding approximation formular in high magnetic field limit of $A_\pm$ (4.5ab) of FL should also be corrected to

$$A_- \sim \frac{1}{2}(\gamma/\omega_c)^2 \tag{G.4}$$

and $A_+ \sim \frac{1}{2}(1-(\gamma/\omega_c)^2)$. The right-hand axis scale in Fig. 4 of FL should also be

multiplied by 1/2 (with the two ticks now reading 0.5 and 0.25). Their results for peak frequencies $\Omega_\pm$ and (half) widths $\Gamma_\pm$ are not affected. Anyway, with (3) and (4) we obtain, *in strong magnetic field regime* ($\omega_c \gg \gamma$), the oscillator strength of pinning mode

$$S \equiv \int_0^\infty \mathrm{Re}[\sigma_{xx}(f)]\mathrm{d}f \equiv \frac{1}{2\pi}\int_0^\infty \mathrm{Re}[\sigma_{xx}(\omega)]\mathrm{d}\omega = \frac{ne^2}{2m}A_- \simeq (\frac{ne^2}{4m})(\frac{\gamma}{\omega_c})^2$$

Since $\Omega_- \simeq \gamma^2/\omega_c$ ((4.5a) of FL), we have

$$S/f_{\mathrm{pk}} \simeq \frac{(\frac{ne^2}{4m})(\frac{\gamma}{\omega_c})^2}{\Omega_-/(2\pi)} = \frac{ne^2\pi}{2m\omega_c} = \frac{ne\pi}{2B} \tag{G.5}$$

This is the same result that has been pointed out by M. M. Fogler earlier.

Appendix H

Supplementary Data on High-B WC Resonance in Sample P (Heterojunction)

H.1 Summary of Key Experimental Observations

- The high-B WC resonance of sample P was previously studied by Ye *et al.* (2002b) in B up to 18T (SCM1). It was found (see Fig. 3 in Ye *et al.* (2002b)) that as ν is decreased from 1/5, $f_{\rm pk}$ initially increases, then reaches a peak and decreases with increasing B. The drop in $f_{\rm pk}$ near ν=1/5 is probably an effect mainly related to the 1/5 FQHE (see also Sec. 5.3.3). The decreasing $f_{\rm pk}$ (with increasing B) at higher B was interpreted in Ye *et al.* (2002b) at that time as a precursor of the "classical" (Fukuyama and Lee, 1978) behavior ($f_{\rm pk} \propto 1/B$, see also Sec. 3.1). However...

- When we later measured sample P in a resistive magnet (up to 33T), we found (see Fig. H.1,H.2 and H.3) that at high n, the decreasing $f_{\rm pk}$ with increasing B found in Ye *et al.* (2002b) did not continue for B above $\sim$ 20T, instead, the

behavior changes to *increasing* with increasing B, up to 33T; at low n, however, the decreasing $f_{\rm pk}$ with increasing B found in Ye *et al.* (2002b) continues to 33T, but even here $f_{\rm pk}$ has not shown the "classical" ($1/B$, or being proportional to ν, at fixed n) behavior (see Fig. H.3 (f)). Then...

- When sample P was later measured (by G. Sambamdamurthy) in the hybrid magnet (up to 45T), it was found (Fig. H.4) that (above ∼30T) the low-n $f_{\rm pk}$ also starts to become increasing with increasing B !

Some other important aspects found on sample P include good agreement of $S/f_{\rm pk}$ at small ν (see Fig. 3.3 and discussions thereof) with the Fukuyama-Lee sum rule (such agreement indicates that all electrons are participating in the pinned WC), and a weakening n-dependence of $f_{\rm pk}$ seen at lower n (Fig. H.5)[1].

Problems posed by the data:

The complicated B-dependence (which also depends on n) of $f_{\rm pk}$ we observed appears to challenge the recent theories on disorder pinned WC and the pinning mode (Fertig, 1999; Fogler and Huse, 2000; Chitra *et al.*, 2002). These theories proposed two regimes (Sec. 3.1): the "classical", where $l_B<\xi_0$ (the disorder correlation length), and $f_{\rm pk}$ is expected to decrease ($\propto 1/B$) with increasing B; and the "quantum", where $l_B>\xi_0$ and $f_{\rm pk}$ is expected to increase (the details can depend on disorder statistics and vary among theories, however, our experimental data appear to support the existence of a dilute disorder as in Fertig (1999) which predict an almost linearly increasing $f_{\rm pk}$ with B in this regime, as discussed in Chap. 3.) with increasing B. Therefore as B is increased, one can imagine a quantum-to-classical crossover (l_B crossing over from above to below ξ_0) according to the theories, with $f_{\rm pk}$ changing from increasing with B to decreasing with B. However, we have observed (in all n) an opposite crossover with (as B is increased) $f_{\rm pk}$ changing from decreasing with B to increasing with B.

[1]Interestingly, the n below which the n-dependence of $f_{\rm pk}$ significantly weakens roughly corresponds also the apparent n below which the B-dependence (see Fig. H.3) of $f_{\rm pk}$ changes qualitatively for B between ∼20 to 33T.

Such a behavior is not expected by the theories and the B at which where the said $f_{\rm pk}$ changes its B-dependence is seen to strongly depend on n and thus does not correspond to a fixed l_B.

We will next demonstrate that, if one allows the simultaneous presence of two kinds of disorder with different correlation lengths, the complex behavior we observed may be understood qualitatively with a phenomenological model, which we present in Sec. H.2, in the framework of current pinning theories.

H.2 A Phenomenological "Two-Disorder" Model

In this section we briefly describe the "two-disorder" model. To compare with the experimental data, we will only be interested in the $f_{\rm pk}$ between, for example, $\sim$ 10 to 45T. We also neglect any FQHE effects.

We assume in this model that

1. There are two kinds of disorder in the sample, one with a long range correlation length (ξ_l) larger than, for example, $\sim$100 Å (note that $l_B\sim$80Å at B=10T); and the other with a short range correlation length (ξ_s) shorter than, for example, $\sim$30 Å (note that $l_B\sim$38Å at B=45T). The long range disorder alone would give (Chap. 3, see also Fukuyama and Lee (1978)) a ${f_{\rm pk}}^{(L)}= a/B$, where a is a phenomenological parameter (independent with B). We assume the short range disorder to be a dilute disorder similar to the one proposed by Fertig (1999). We discussed in Sec. 3.2.2 that existence of such dilute disorder is consistent with our experimental observations. We assume that with such short range disorder alone, it would results in a ${f_{\rm pk}}^{(S)}= bB$ (Sec. 3.2.2), where b is another (B-independent) phenomenological parameter.

2. When both disorder are present, their joint effect will give rise to a $f_{\rm pk}$ (larger than either ${f_{\rm pk}}^{(L)}$ or ${f_{\rm pk}}^{(S)}$), which, in this crude model, we simple take to be

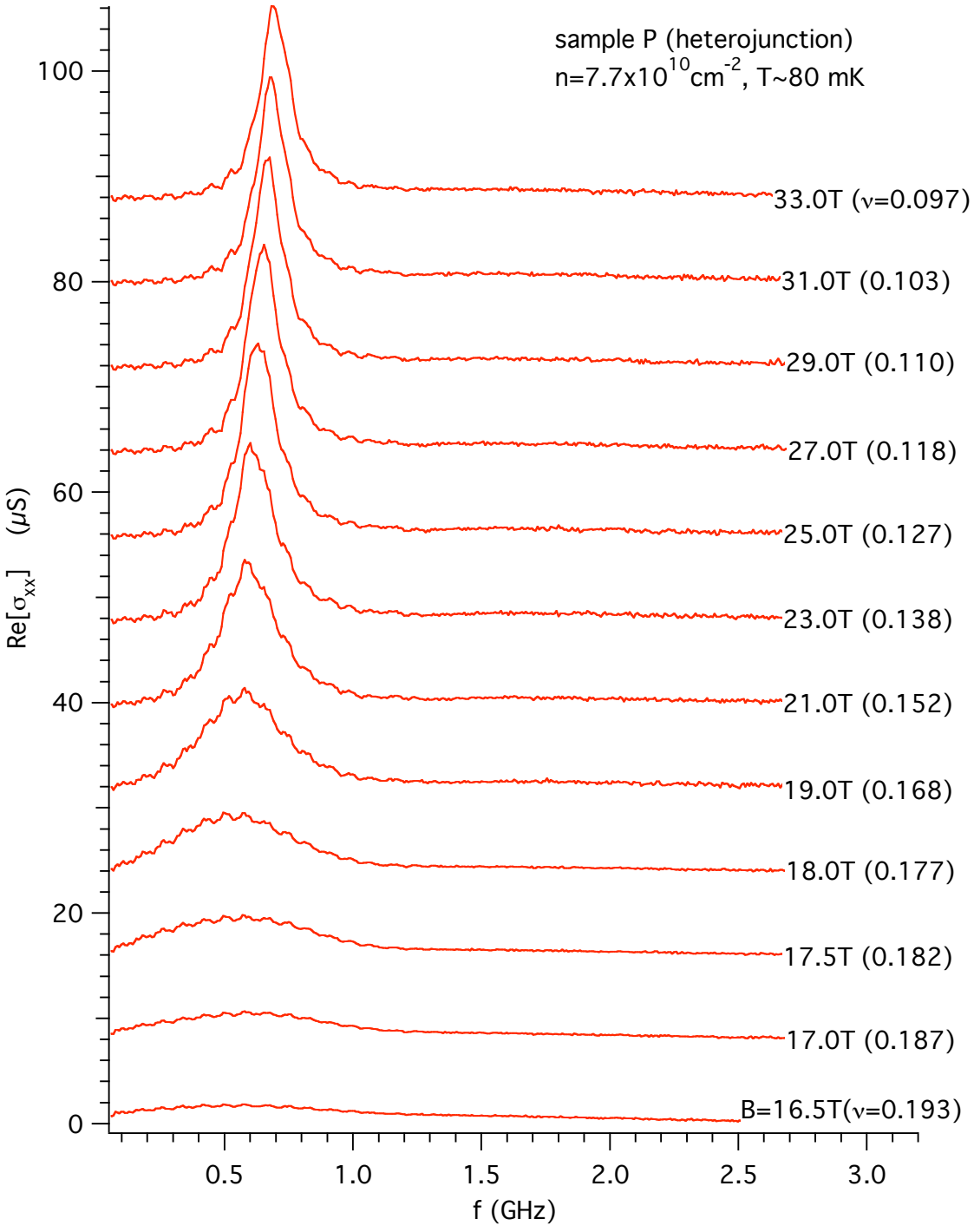

Figure H.1: Selected spectra measured from sample P (heterojunction) at n=7.7×10^{10}cm^{-2}. Traces are offset for clarity. Magnetic Field (B) of each trace is labeled at right.

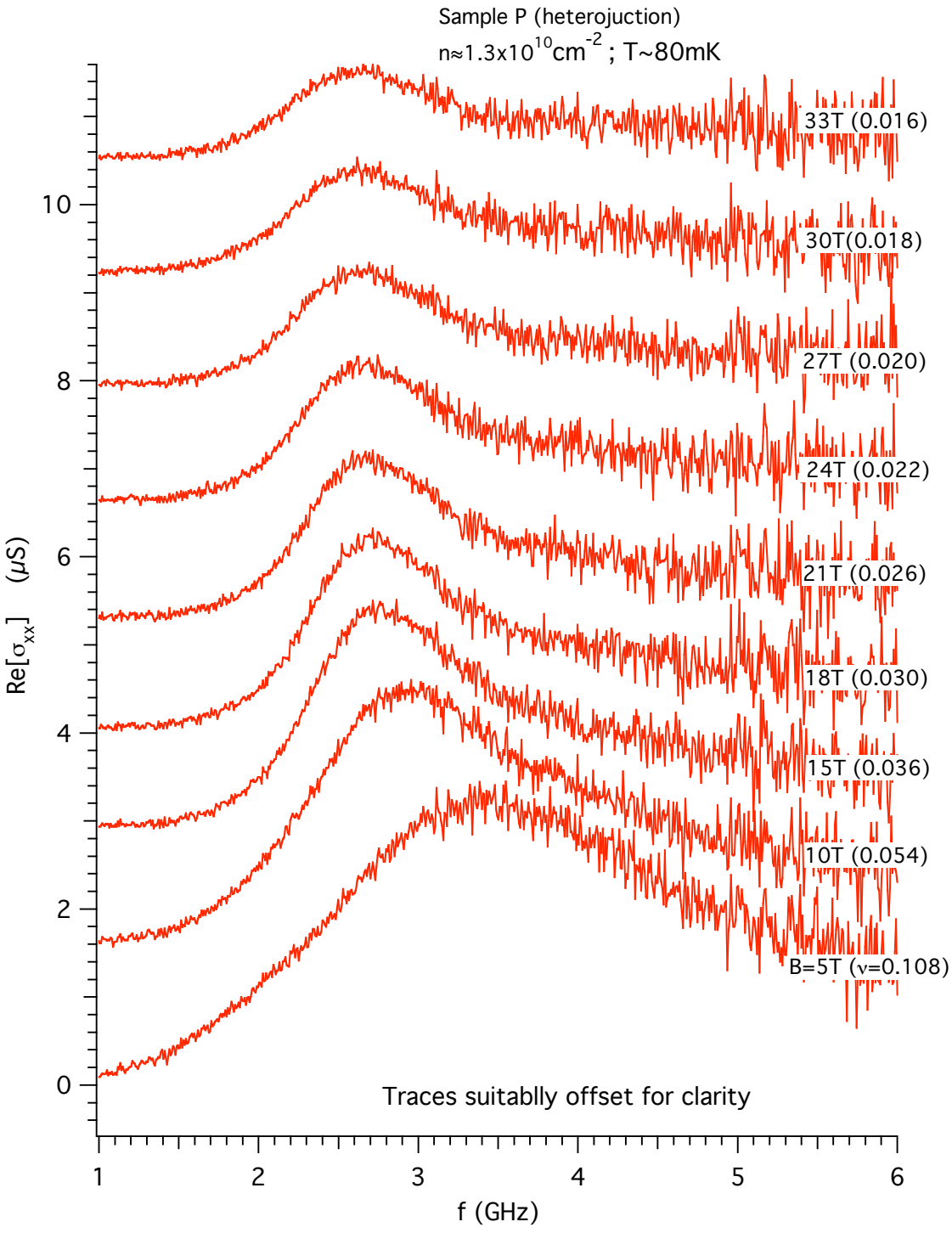

Figure H.2: Selected spectra measured from sample P (heterojunction) at n=1.3×10^{10}cm^{-2}. Traces are offset for clarity. Magnetic Field (B) of each trace is labeled at right.

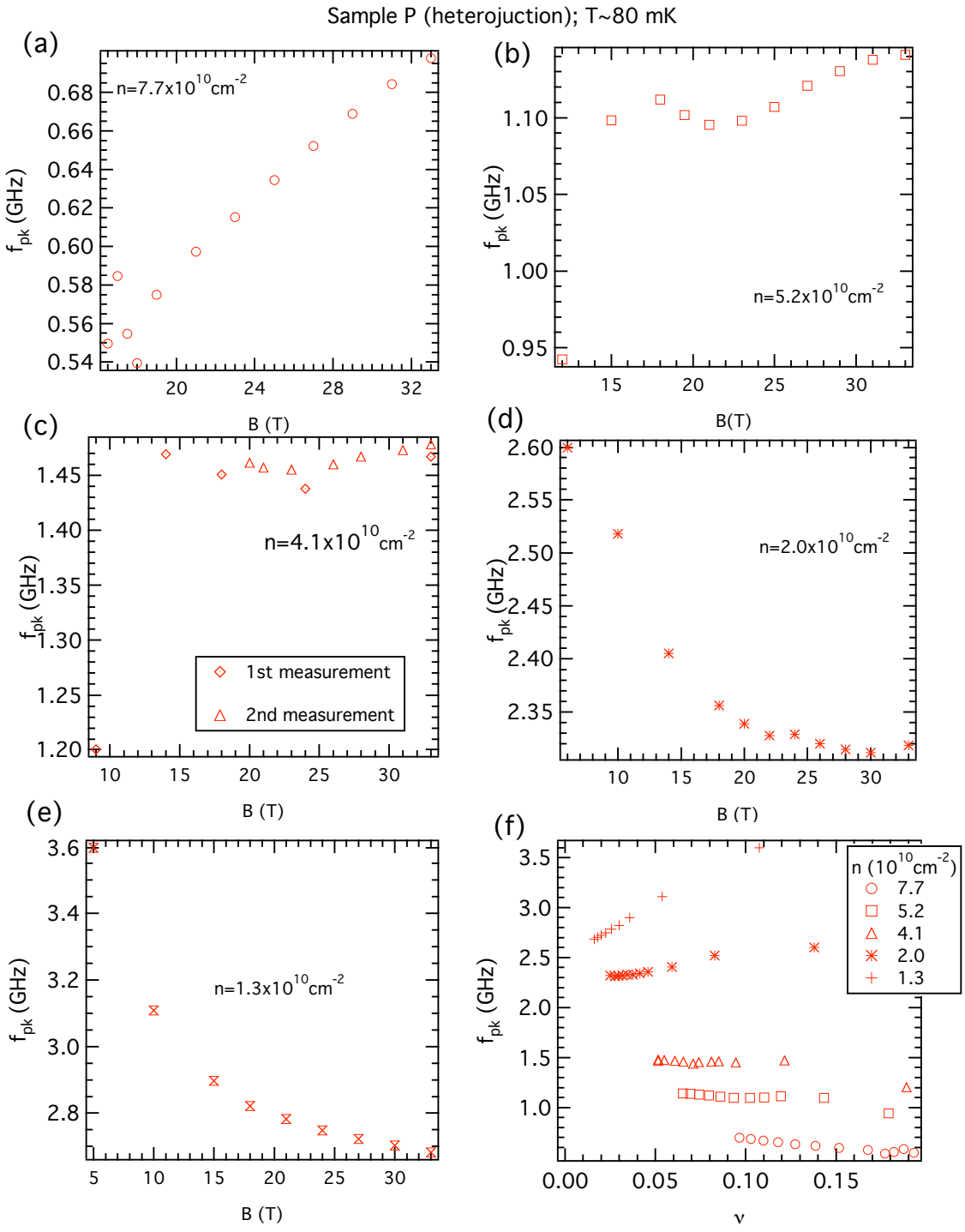

Figure H.3: (a)-(e) Sample P: $f_{\rm pk}$ vs B at five different n. (f) Summary of $f_{\rm pk}$vs ν.

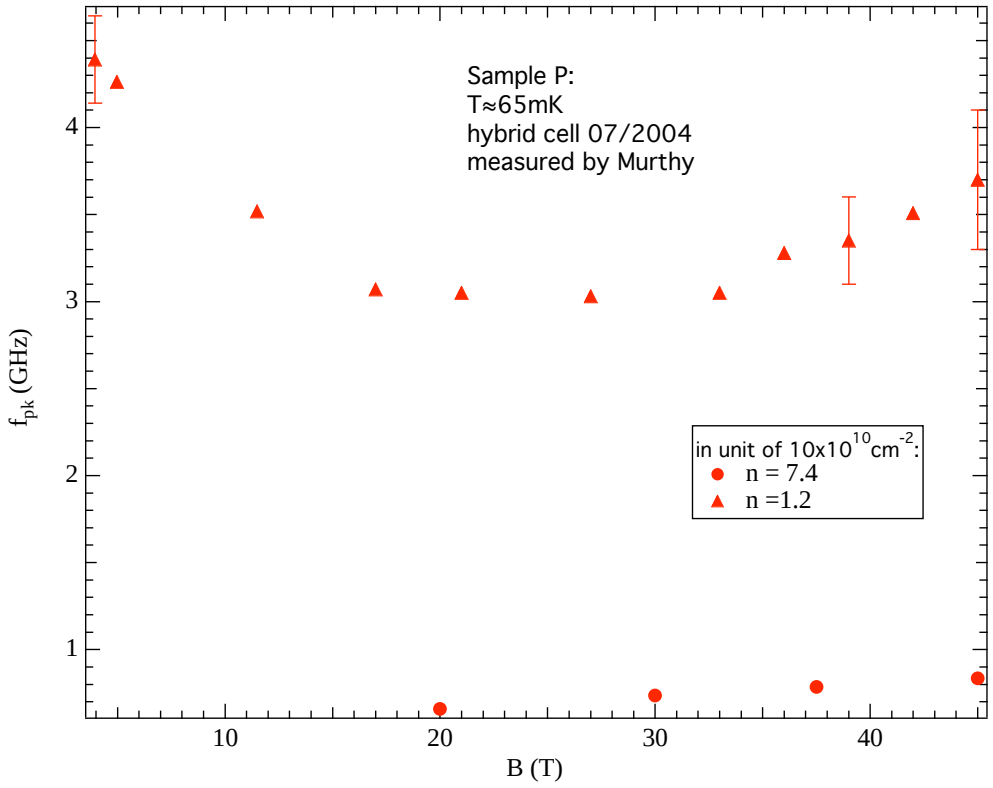

Figure H.4: Sample P: $f_{\rm pk}$vs B measured up to 45T at a few n.

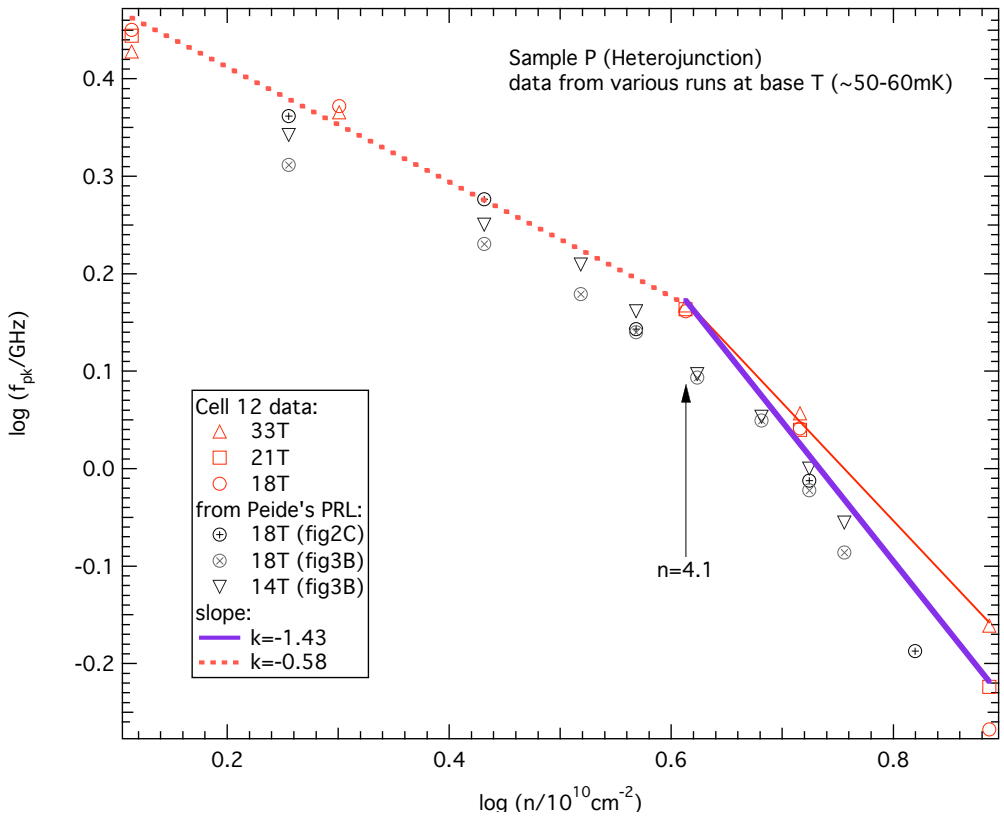

Figure H.5: Sample P: f_{pk}vs n on log-log plot.

$$f_{\rm pk}{}^{(L)}+f_{\rm pk}{}^{(S)}=a/B+bB.$$

We see that the "joint" $f_{\rm pk}=a/B+bB$ must have a minimum at $B_m=\sqrt{a/b}$, at which $f_{\rm pk}$ has the value $2\sqrt{ab}$. Thus the behavior that with increasing B, $f_{\rm pk}$ goes from decreasing with B to increasing with B is naturally produced in this model. We also notice that the minimum position $B_m=\sqrt{a/b}$ is controlled by the relative contributions of the two disorder to $f_{\rm pk}$. The experimental observation that B_m is higher at lower n can thus be explained if we assume a smaller relative contribution of the short range disorder part (b) at lower n (perhaps due to, for example, a lower "occupation" fraction of such *dilute*, short range, pit-like disorder sites at low electron density. This would also be consistent with the weakening n-depenence observed at low n, Fig. H.5).

Fig. H.6 demonstrates the "simulated" $f_{\rm pk}$ with this model, using appropriate chosen phenomenological parameters (a and b) to match the typically observed $f_{\rm pk}$ values and B_m values. (A) and (B) are for a high-n case and (C) and (D) for a low-n case.

At sufficiently high B ($l_B<\xi_s$), we expect $f_{\rm pk}$ to enter the "classical" ($1/B$) regime. Since our data did not show any indication of such a classical regimes even at 45T, we infer that ξ_s must be shorter than 38Å (l_B at 45T).

Although this model is motivated largely by the complicated data from sample P, the "two-disorder" picture can be quite general. This is consistent, for example, with the behavior of $f_{\rm pk}$ decreasing with increasing B, but slower than the $1/B$-dependence, that we often observed in other samples as well (Chap. 5, for example, Fig. 5.8). It will be very interesting to push the measurements at higher B and examine whether such a behavior will change to $f_{\rm pk}$ increasing with B, as would be expected within the "two-disorder" model.

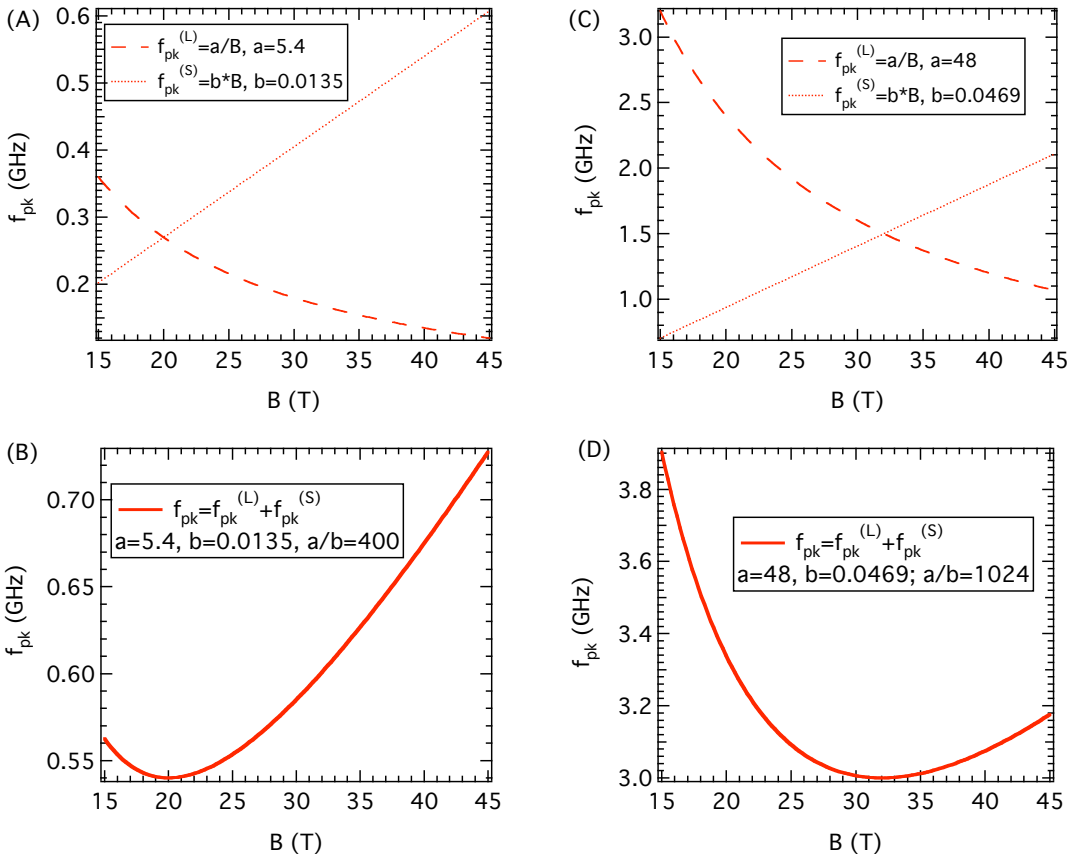

Figure H.6: "Two-disorder" model. (A): $f_{\rm pk}$ for a long range disorder with a=5.4 and for a short range disorder with b=0.0135 (the parameters are chosen to simulate a high-n situation). (B): The sum of the two $f_{\rm pk}$'s in (A). (C): $f_{\rm pk}$ for a long range disorder with a=48 and for a short range disorder with b=0.0469 (the parameters are chosen to simulate a low-n situation). (D): The sum of the two $f_{\rm pk}$'s in (C). $f_{\rm pk}$ plotted are in units of GHz, B in Tesla and the parameter a and b in GHz-T. It is assumed here that at 45T, l_B ($\sim$ 38Å) is still larger than the correlation length (ξ_s) of the short range disorder in the sample. See text for details.

Appendix I

Supplementary Data on IQHWC

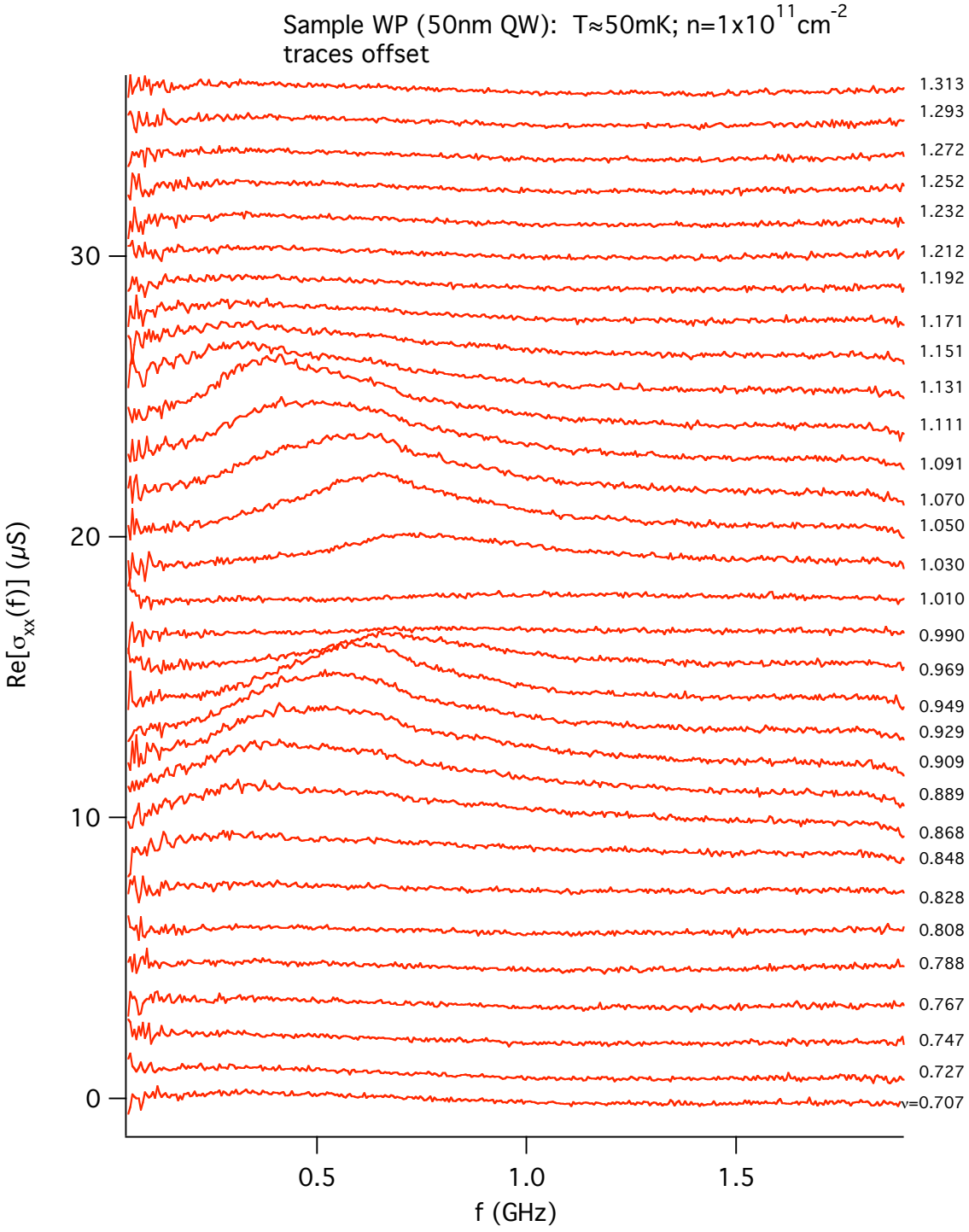

Figure I.1: Resonance around ν=1 in Sample WP.

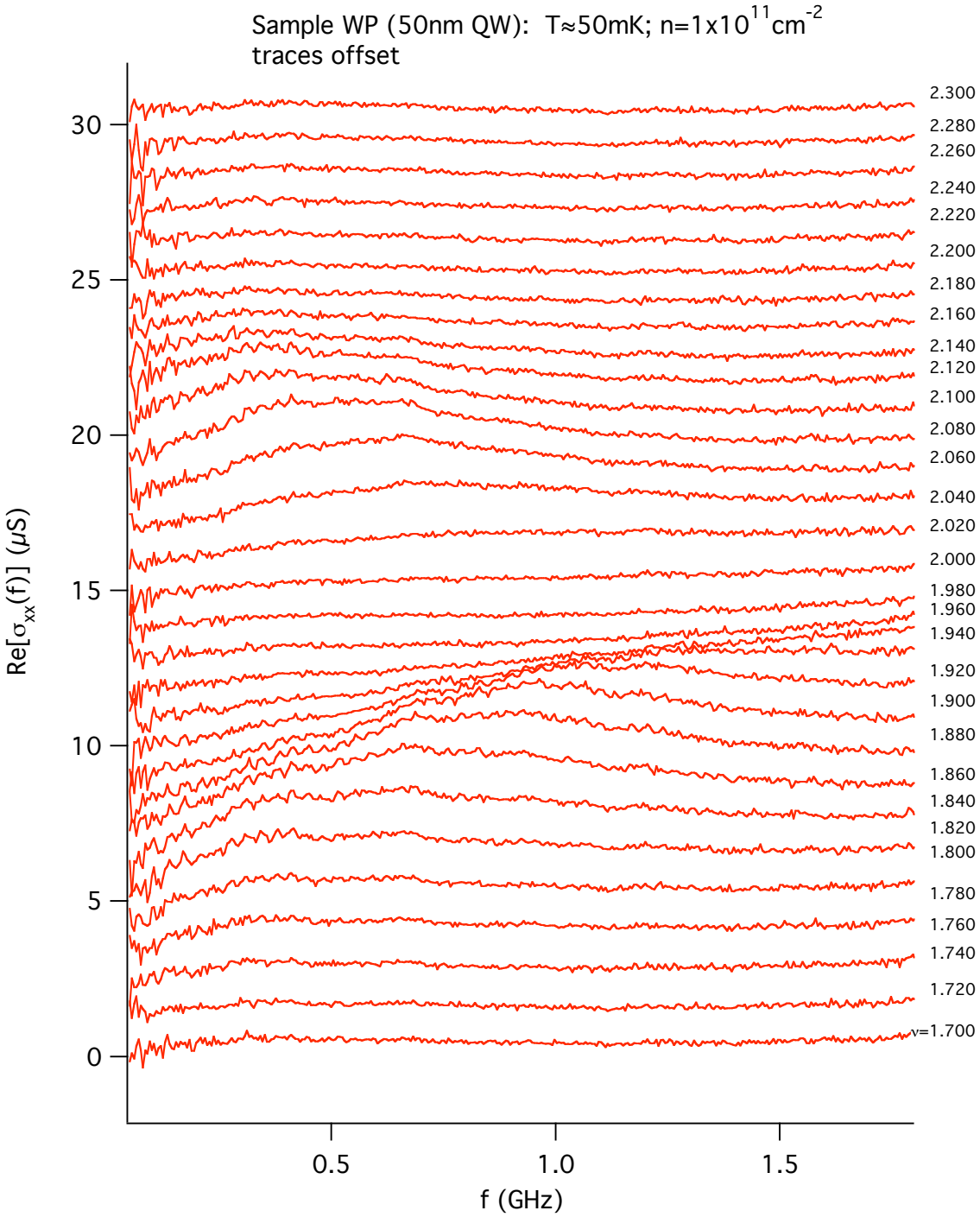

Figure I.2: Resonance around ν=2 in Sample WP.

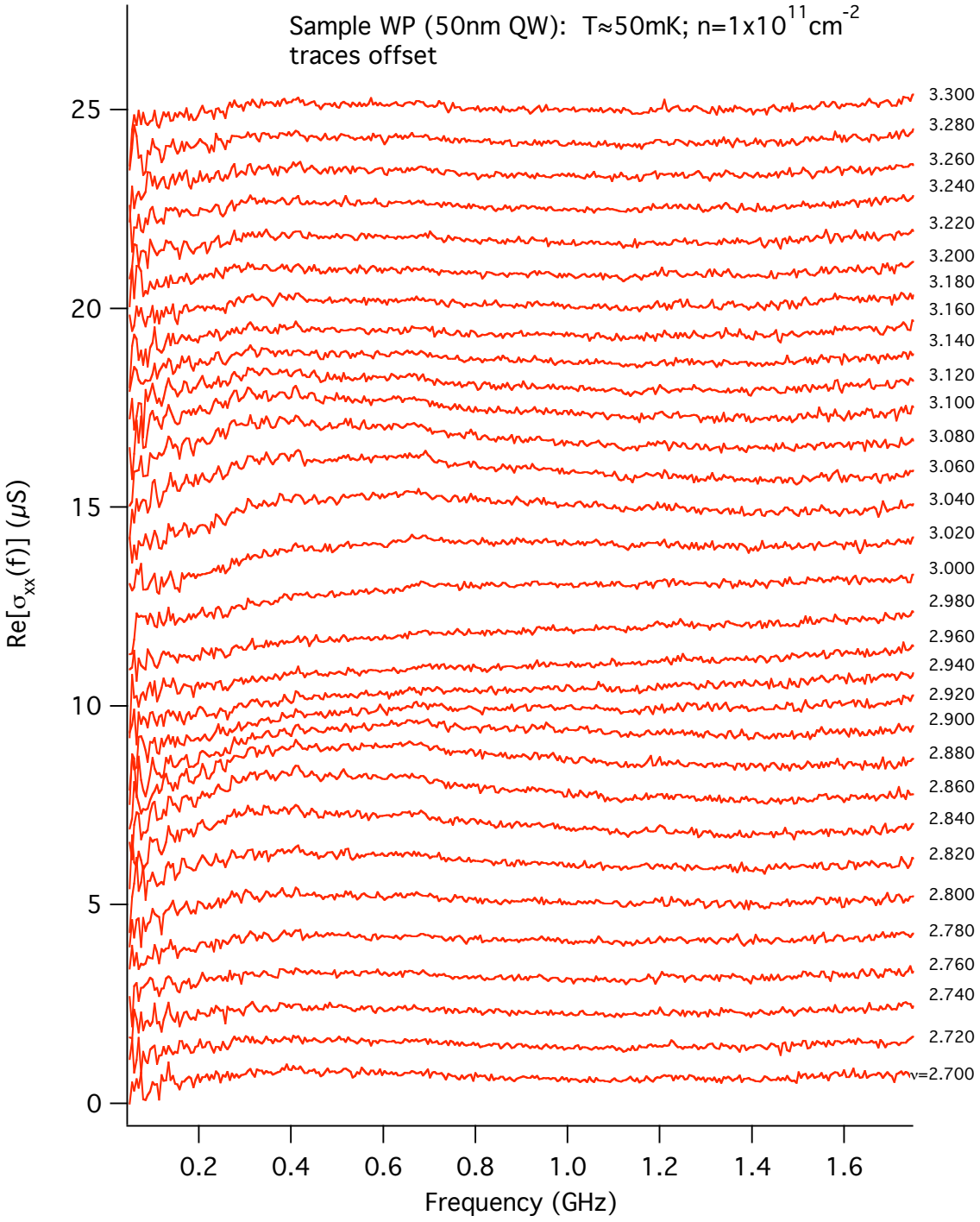

Figure I.3: Resonance around ν=3 in Sample WP.

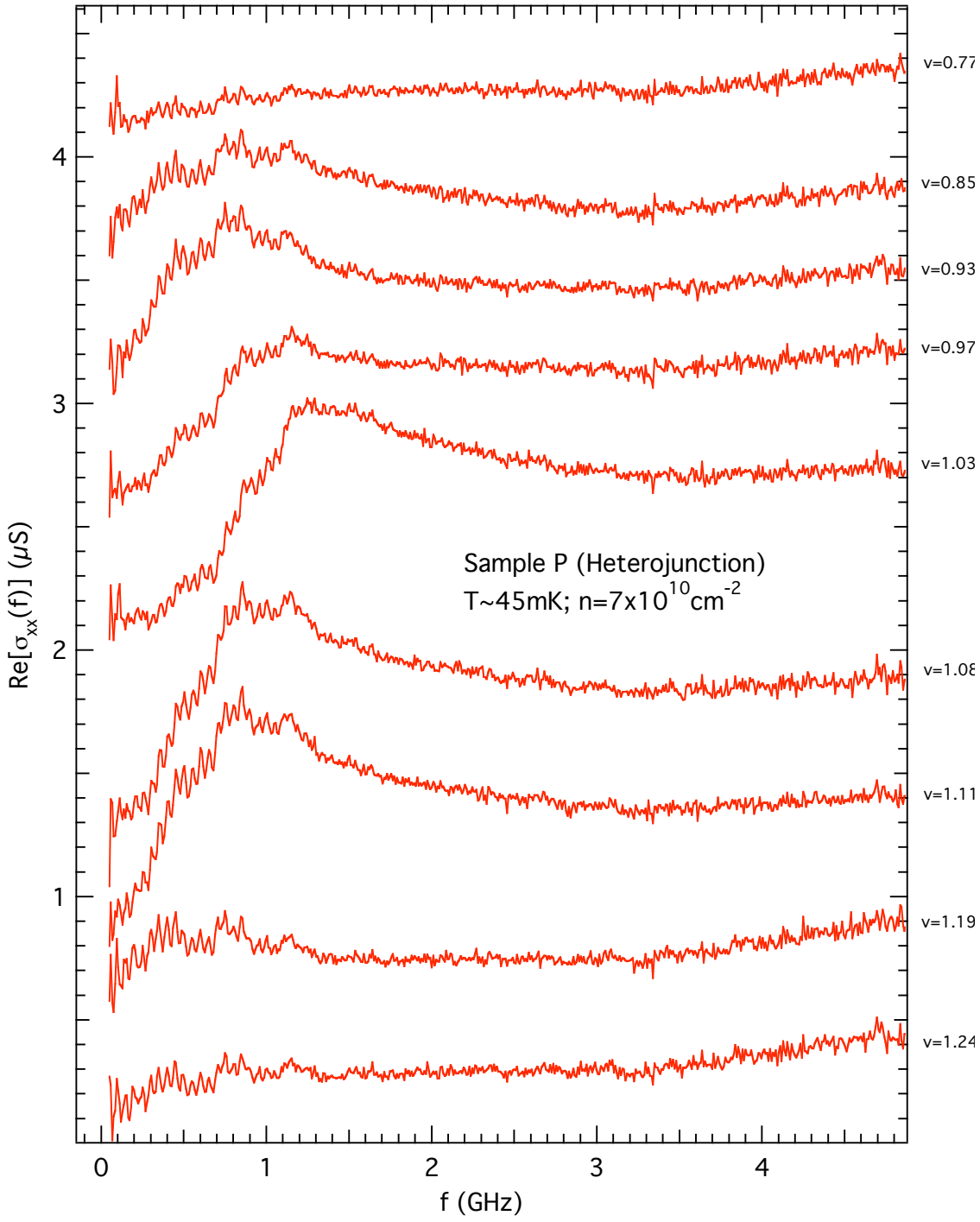

Figure I.4: Resonance around ν=1 in Sample P.

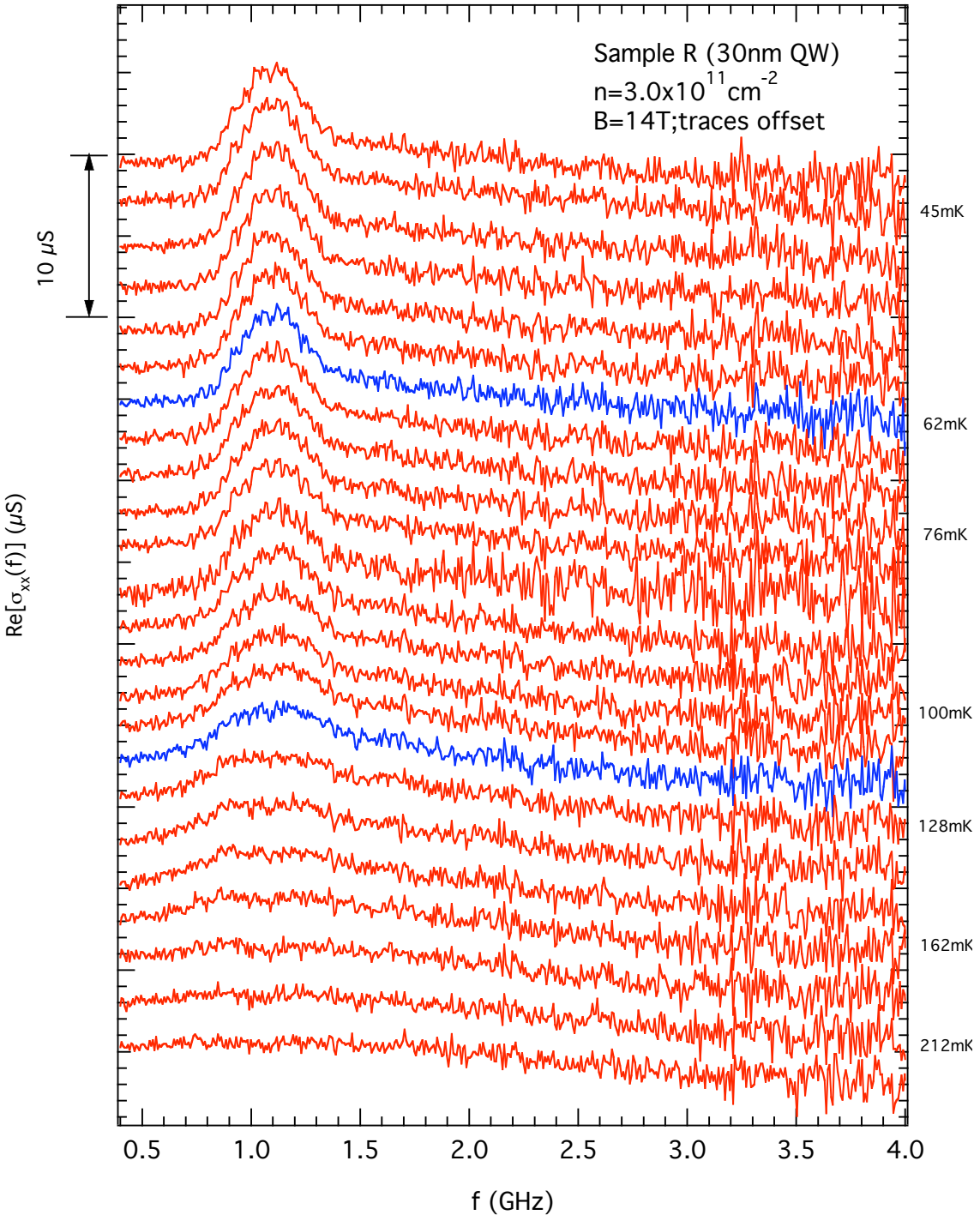

Figure I.5: An example of T-dependent IQHWC spectra, measured in Sample R.

Appendix J

Supplementary Data on "A" and "B" phases

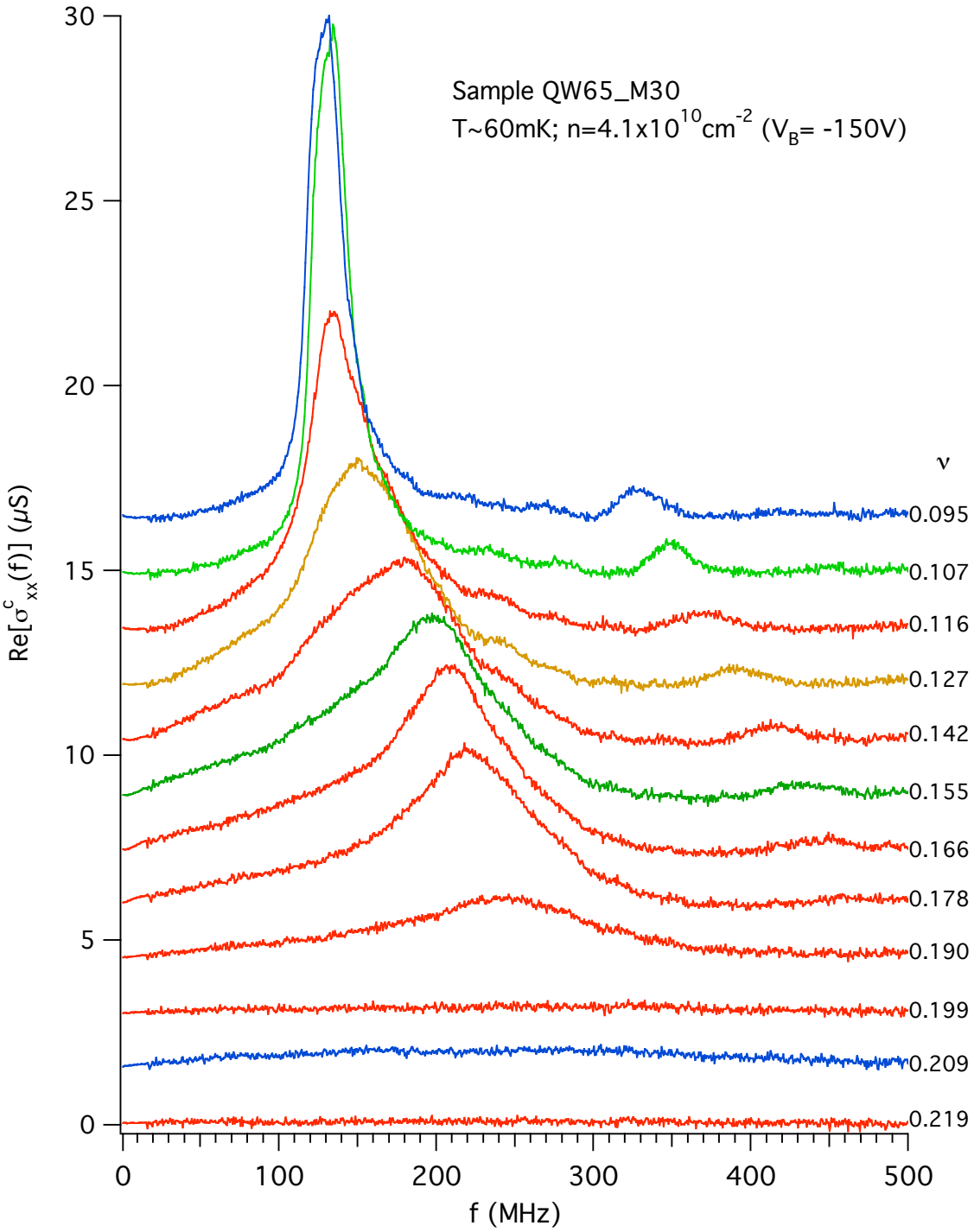

Figure J.1: Spectra measured from sample QW65_M30 at back gate V=-150V and n=4.1×10^{10}cm^{-2}. Traces are offset for clarity. Filling factor (ν) of each trace is labeled at right.

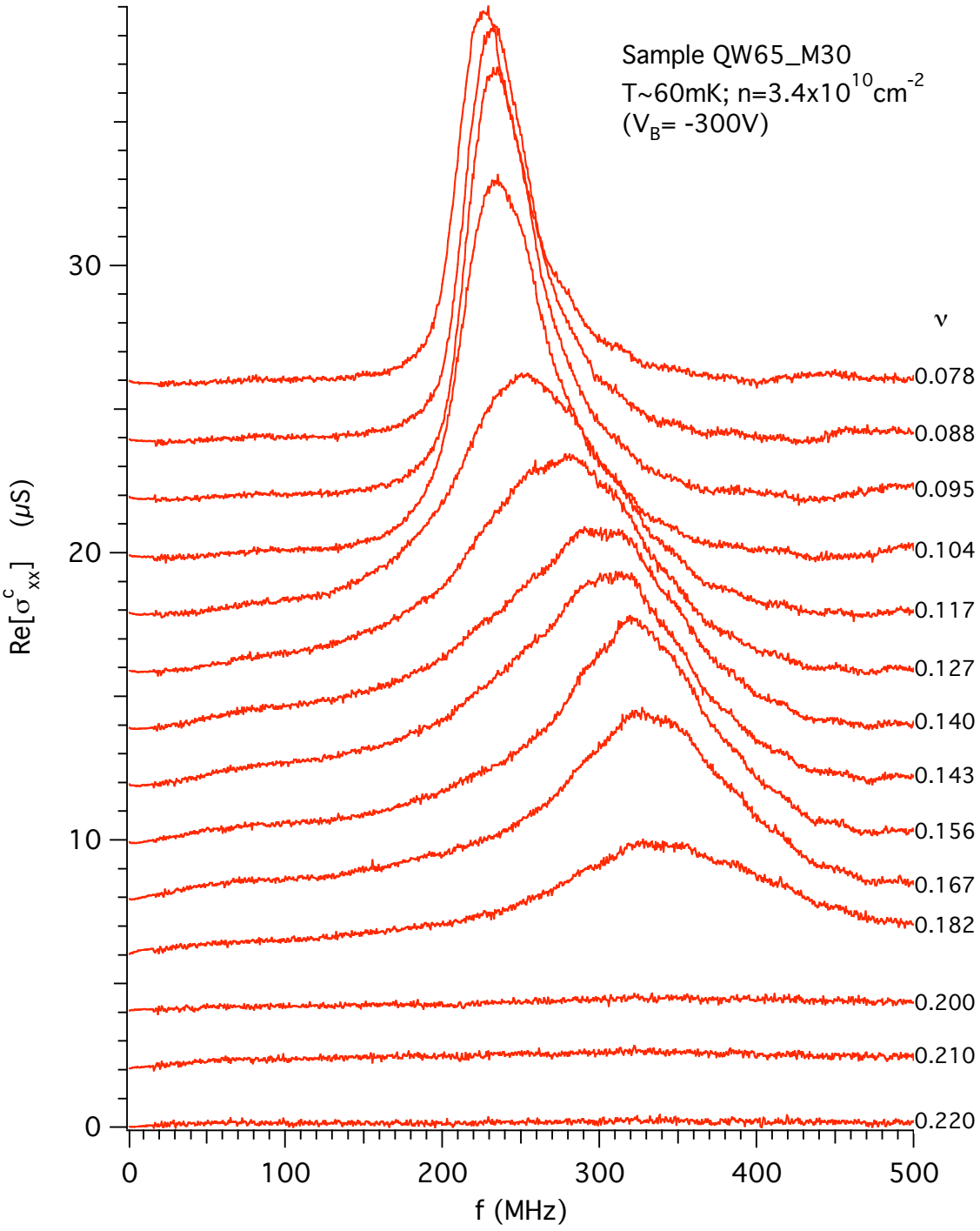

Figure J.2: Spectra measured from sample QW65_M30 at back gate V=-300V and n=3.4×10^{10}cm^{-2}. Traces are offset for clarity. Filling factor (ν) of each trace is labeled at right.

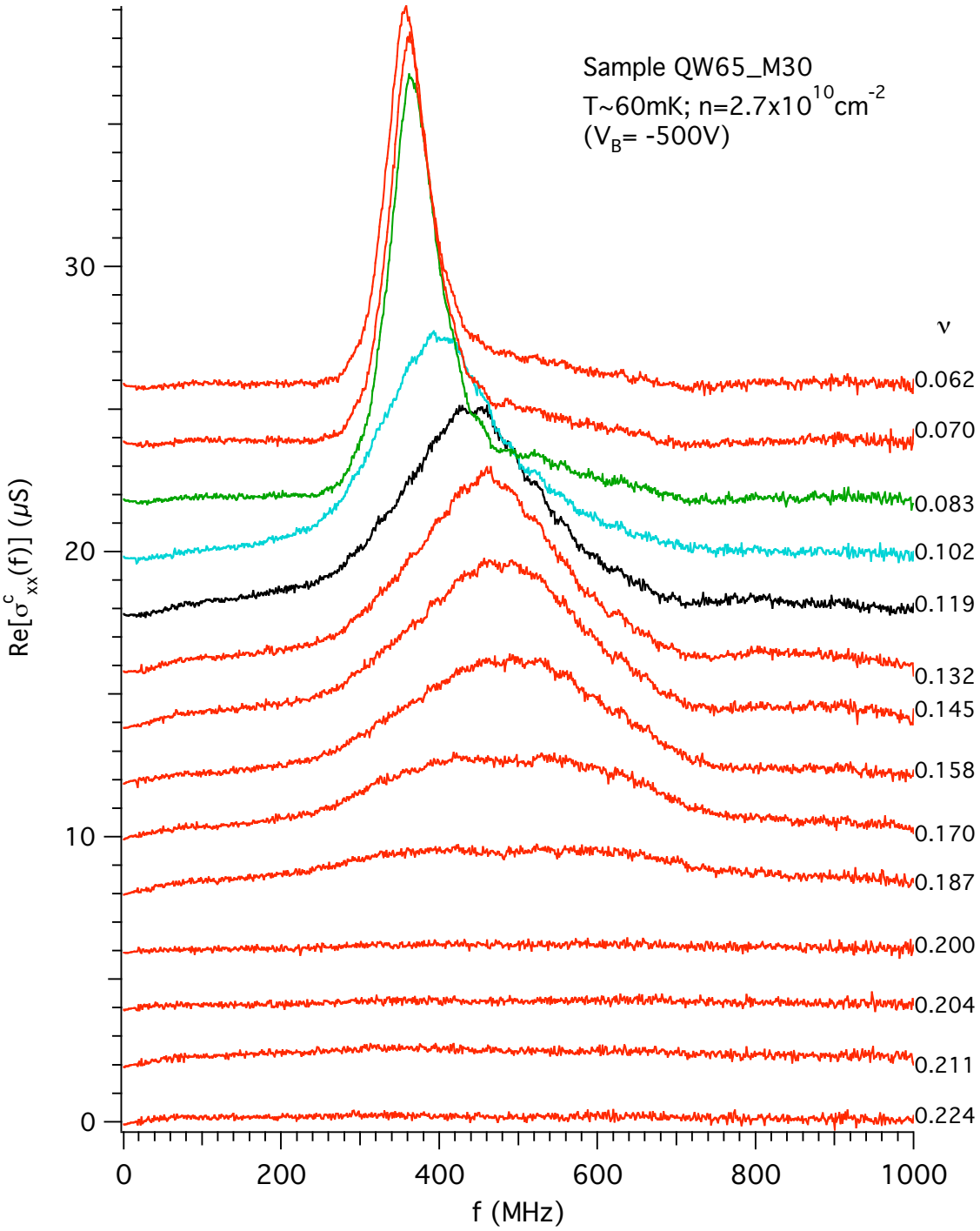

Figure J.3: Spectra measured from sample QW65_M30 at back gate V=-500V and n=2.7×10^{10}cm^{-2}. Traces are offset for clarity. Filling factor (ν) of each trace is labeled at right.

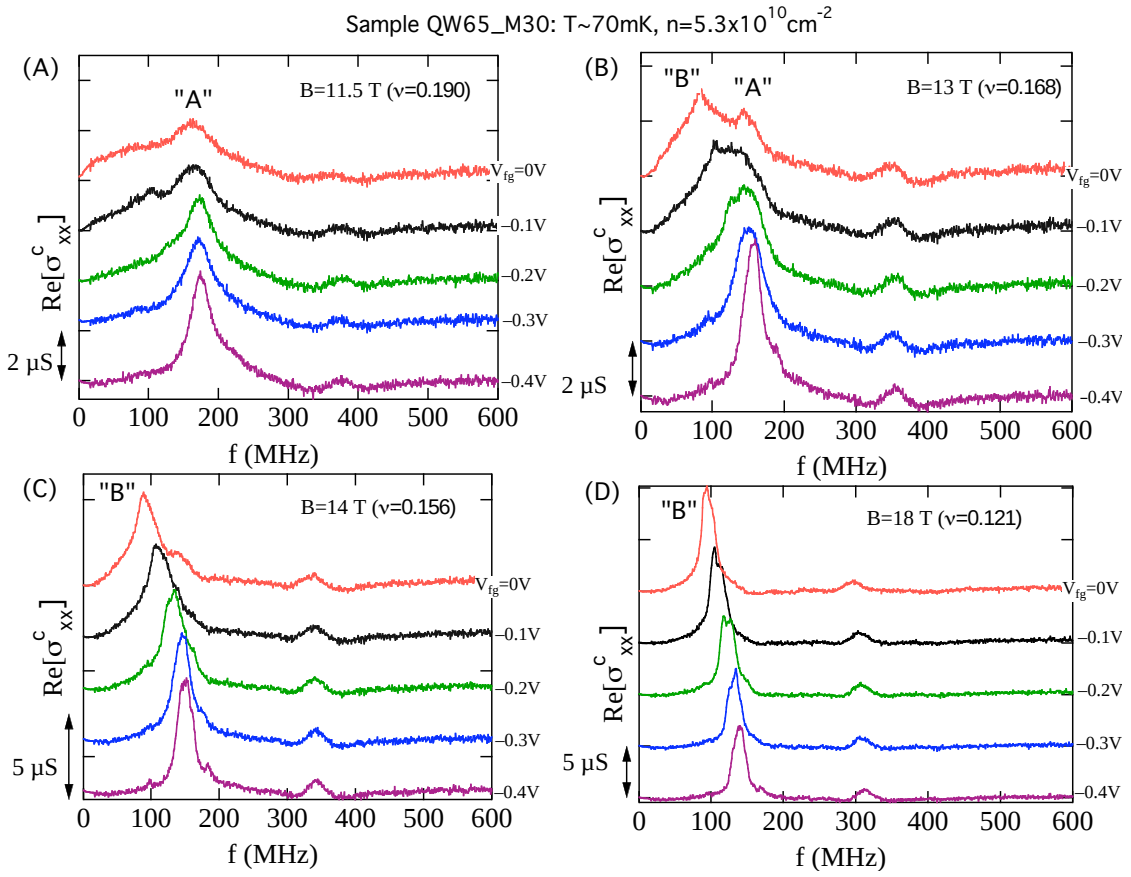

Figure J.4: Effect of CPW front gate voltage on the spectrum measured from sample QW65_M30 (n=5.3×10^{10}cm^{-2}, T 70mK) at 4 different magnetic fields (A): 11.5T; (B): 13T; (C): 14T; (D): 18T. Traces are offset for clarity. V_{fg} for each trace is labeled at right. f_{pk} of resonance "A" is seen to be insensitive to V_{fg} (although its line width does depend on V_{fg}). In contrast, f_{pk} of resonance "B" increases with increasing $|V_{fg}|$. Sambandamurthy *et al.* (2005a).

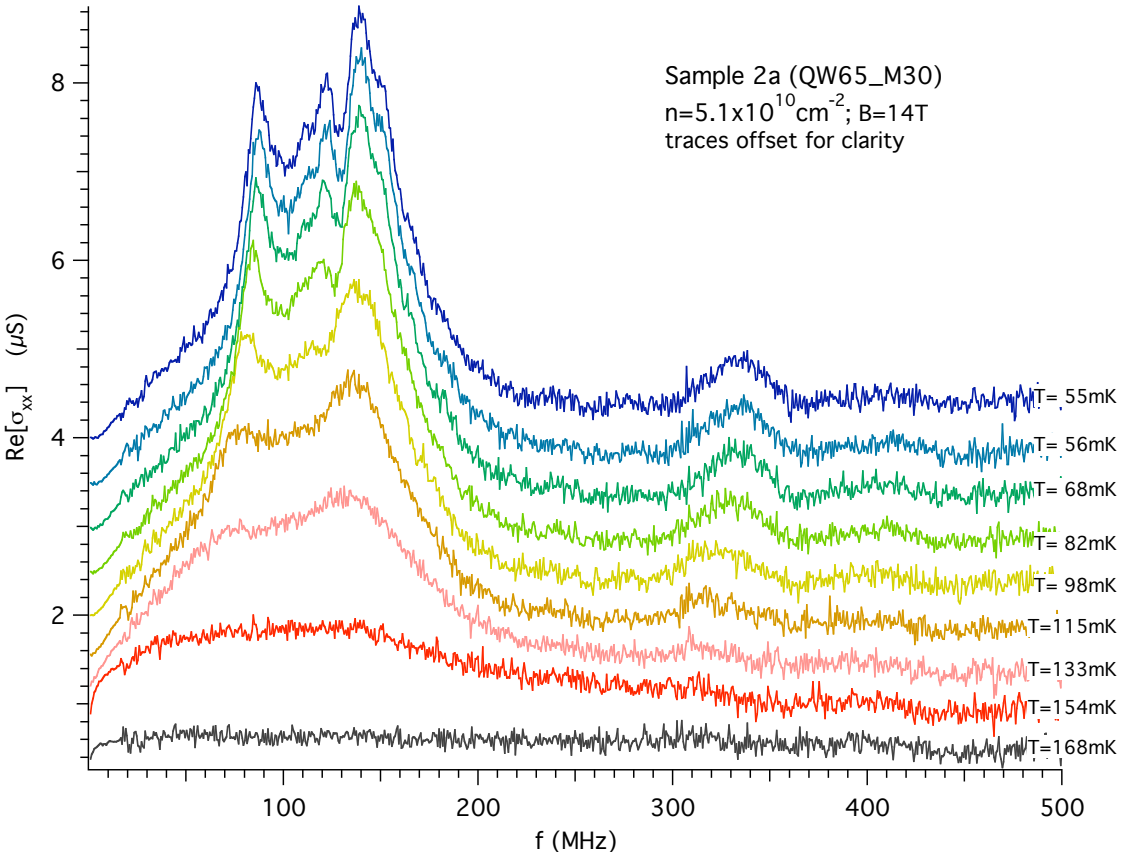

Figure J.5: Spectra measured at various T (labeled at right) from sample QW65_M30, at B=14T (ν=0.15, in the "A"-"B" transition regime) . Traces are offset for clarity.

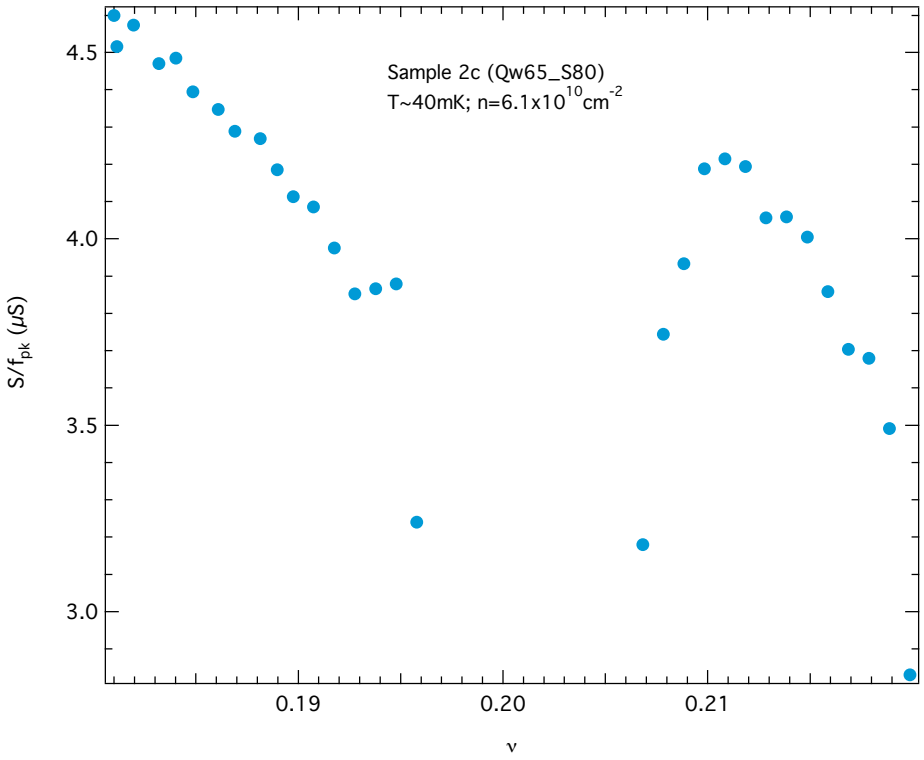

Figure J.6: $S/f_{\rm pk}$ extracted from the spectra shown in Fig. 5.6, measured in Sample 2c (QW65-S80). S here is extracted from the Lorentzian fit value, which does not include the background).

Appendix K

Pinned Bilayer Wigner Crystals with Pseudospin Magnetism

This appendix is a preprint of the article (Chen, 2005) (slightly updated version)

Abstract: We study a model of *pinned* bilayer Wigner crystals (WC) and focus on the effects of interlayer coherence (IC) on pinning. We consider both a pseudospin ferromagnetic WC (FMWC) with IC and a pseudospin antiferromagnetic WC (AFMWC) without IC. Our central finding is that a FMWC can be pinned more strongly due to the presence of IC. One specific mechanism is through the disorder induced interlayer tunneling, which effectively manifests as an extra pinning in a FMWC. We also construct a general "effective disorder" model and effective pinning Hamiltonian for the case of FMWC and AFMWC respectively. Under this framework, pinning in the presence of IC involves *interlayer* spatial correlation of disorder in addition to intralayer correlation, leading to *enhanced* pinning in the FMWC. The pinning mode frequency ($\omega_{\rm pk}$) of a FMWC is found to decease with the effective layer separation, whereas for an AFMWC the opposite behavior is expected. An abrupt drop of $\omega_{\rm pk}$ is predicted at a transition from a FMWC to AFMWC. Possible effects of in-plane magnetic fields and finite temperatures are addressed. Finally we discuss

some other possible ramifications of the FMWC as an electronic supersolid-like phase.

K.1 Introduction

Two dimensional systems (2DS) of electrons (or holes) subjected to a strong perpendicular magnetic field (B) have been among the most studied strongly-correlated systems in the past two decades, with such many-body phenomena as fractional quantum Hall effects and quantum Wigner crystals (WC) (both reviewed in Ref. (Das Sarma and Pinczuk, 1997)). Additional degrees of freedom introduced by bringing two parallel 2DS in close separation to form a bilayer system (BLS) can lead to new phenomena (see reviews in Refs. (Das Sarma and Pinczuk, 1997; Simon, 2005)) with no counterpart in the single layer case. The best known example is the bilayer excitonic condensate state (Fertig, 1989; Wen and Zee, 1992) (BECS) at total Landau filling $\nu_{\rm tot}$=1, which displays quantum Hall effect (Murphy *et al.*, 1994) and counterflow superfluidity (Kellogg *et al.*, 2004; Tutuc *et al.*, 2004). Carriers in such a state reside *simultaneously* in both layers and possess interlayer (phase) coherence (IC). The IC can even exist in the limit of vanishing interlayer tunneling (characterized by the symmetric-antisymmetric energy gap $\Delta_{\rm SAS}$ $\sim$0) and solely due to the interlayer Coulomb interaction (Simon, 2005). Alternatively, the IC can be described using a pseudospin (Yang *et al.*, 1994; Moon *et al.*, 1995) langauge, where pseudospins represent layer indices. The BECS is a pseudospin ferromagnet (Yang *et al.*, 1994; Moon *et al.*, 1995) and the associated Goldstone mode has indeed been observed (Spielman *et al.*, 2001).

At sufficiently small $\nu_{\rm tot}$, the ground state of the BLS is expected to be a bilayer Wigner crystal[1] (BWC) (Oji *et al.*, 1987). It is natural to ask whether IC can also exist in the crystal state. Such a possibility has been theoretically considered (Zheng

[1]WC-type phases have also been considered at $\nu_{\rm tot}$=1 as possible competing phases (Brey, 1990; Chen and J.Quinn, 1992; Côté *et al.*, 1992; Demler *et al.*, 2001; Veillette *et al.*, 2002; Yang, 2001)with BECS at intermediate layer separation.

and Fertig, 1995; Narasimhan and Ho, 1995), for finite as well as vanishing interlayer tunneling. It was found (Zheng and Fertig, 1995; Narasimhan and Ho, 1995) that when d/a (the effective layer separation, where d is the interlayer spacing and a is the mean intralayer spacing between carriers) is small, the BWC can be an one-component Wigner crystal with IC. This corresponds to a WC which is also a pseudospin easy-plane ferromagnet (Narasimhan and Ho, 1995). For larger d/a, on the other hand, the BWC is expected to be a two-component WC (TCWC) (Narasimhan and Ho, 1995). The two components (corresponding to the two layers) are "staggered" from each other in order to minimize interlayer Coulomb interaction. If interlayer tunneling is small, such a TCWC has negligible IC and is an easy-axis antiferromagnet[2] in pseudospin space. A rich array of crystal structures (Zheng and Fertig, 1995; Narasimhan and Ho, 1995; Esfarjani and Kawazoe, 1995; Goldoni and Peeters, 1996) was shown to be possible with a TCWC other than the standard hexagonal lattice (Bonsall and Maradudin, 1977). Dynamical properties of a BWC have been calculated (Goldoni and Peeters, 1996; Falko, 1994; Klironomos and Dorsey, 2005).

So far theories (Zheng and Fertig, 1995; Narasimhan and Ho, 1995; Esfarjani and Kawazoe, 1995; Goldoni and Peeters, 1996; Falko, 1994; Klironomos and Dorsey, 2005) on BWC have focused on the clean case. However, in real samples a BWC is always pinned by disorder and is therefore an insulating phase as observed in experiments (Manoharan *et al.*, 1996; Tutuc *et al.*, 2003). Disorder can also introduce a pinning gap in the magnetophonon excitation of a WC (Fukuyama and Lee, 1978; Normand *et al.*, 1992). Such a "pinning mode" (Fertig, 1999; Fogler and Huse, 2000; Chitra *et al.*, 2002) has been taken as a well-defined characteristic signature for a pinned WC measured in the single layer case (Li *et al.*, 1997; Hennigan *et al.*, 1998; Ye *et al.*, 2002b; Chen *et al.*, 2004c).

In this article we study *pinned* BWC and in particular, we focus on the effect

[2]With finite tunneling, it was shown (Narasimhan and Ho, 1995) that the TCWC can have a mixed ferromagnetic-antiferromagnetic order with a (small) net pseudospin magnetization.

of interlayer coherence (or pseudospin magnetism) on the pinning mode and experimentally detectable signatures that can *qualitatively* distinguish a pseudospin ferromagnetic (FM) WC from a pseudospin antiferromagnetic (AFM) WC in real bilayer systems.

After a brief review of the pinning mode in a single layer (SL) WC in Sec. K.2, we develop a simple model of pinned BWC in Sec. K.3 to calculate the pinning mode properties both with and without IC. First we demonstrate that local tunneling induced by disorder (such as barrier fluctuations) manifests as an effective pinning in the presence of IC and can lead to *enhanced* pinning in the FMWC. Then we present a more general model, where the concept of *effective disorder*, which depends on the electronic state, is emphasized. Under this framework, pinning in the presence of IC involves *interlayer* as well as intralayer spatial correlation of disorder, whereas only the latter is relevant for the pinning for a SL WC or a BWC without IC. The effect of d/a on the pinning mode frequency ($\omega_{\rm pk}$) is discussed in Sec. K.4. Qualitatively opposite behaviors are found for a FMWC and an AFMWC. We also predict an abrupt $\omega_{\rm pk}$ drop associated with a FM-to-AFM transition. In Sec. K.5 we discuss possible effects of in-plane magnetic fields ($B_{||}$) on a pinned FMWC. A proposal of performing "disorder tomography" using $B_{||}$ is presented. We also briefly discuss finite-temperature (T) effects. We discuss some other interesting properties (and their connection with pinning) of FMWC in Sec. K.6 before summarizing the paper in Sec. K.7.

K.2 Pinning of a Single Layer WC

In the presence of disorder[3], a WC cannot have true long range positional order (Chitra *et al.*, 2002). Its long wavelength and low energy excitation is the "pinning mode" (Fukuyama and Lee, 1978; Normand *et al.*, 1992; Fertig, 1999; Fogler and

[3]Provided it is sufficiently "weak", which perturbs (deforms) but does not destroy the WC.

Huse, 2000; Chitra *et al.*, 2002), which represents the collective oscillation of WC domains in the disorder potential. Such a pinning mode is manifested as a resonance in the frequency-dependent real diagonal conductivity ($\mathrm{Re}[\sigma_{xx}(\omega)]$), measurable from the power absorption spectrum of the WC subjected to an AC electric field (Li *et al.*, 1997; Ye *et al.*, 2002b). Major results from the current understanding of the pinning mode resonance are summarized below, where we consider a WC with density n subject to a (weak) disorder potential $V(\vec{r})$ (where $\vec{r}$ denotes the position vector in the 2D plane) and a strong perpendicular B:

(i) The frequency of the pinning mode resonance (ω_{pk}) is only determined by the *static* deformation (from the ideal lattice in the clean case) of the WC through its Larkin domain size (Fertig, 1999; Fogler and Huse, 2000; Chitra *et al.*, 2002). An explicit formula for ω_{pk}(in the high B limit) as given in Ref. (Chitra *et al.*, 2002) is[4]

$$\omega_{\mathrm{pk}} = C\frac{W}{\xi^6}\frac{1}{\mu}\frac{1}{B} \tag{K.1}$$

In this formula C is a constant involving only the carrier charge (e), μ is the shear modulus of the WC, W and ξ are the strength and correlation length of the (effective) disorder (see **(v)** below) potential ($V(\vec{r})$). They are defined from the two-point spatial correlator

$$\langle V(\vec{r})V(\vec{r}')\rangle = W D_\xi(|\vec{r}-\vec{r}'|) \tag{K.2}$$

where $D_\xi(r)$ is the correlation function with characteristic decay length ξ.

For an ideally 2D (infinitely thin) WC in high B, μ is expected to be close to

[4]Different theories (Fertig, 1999; Fogler and Huse, 2000; Chitra *et al.*, 2002) so far differ on the exponent of ξ appearing in Eq. (K.1) but this, as will be seen, is unimportant for our purposes.

its classical value (Bonsall and Maradudin, 1977)

$$\mu = \alpha \frac{n^{3/2} e^2}{\epsilon} \tag{K.3}$$

where ϵ is the effective dielectric constant of the medium and α a constant set by the crystal structure ($\sim$0.02 for the hexagonal lattice). Thus the expected n-dependence of $\omega_{\rm pk}$ is

$$\omega_{\rm pk} \propto n^{-\gamma} \tag{K.4}$$

with γ=3/2. Experimentally measured (Li *et al.*, 2000a) γ varies from 1/2 to 3/2. Its precise value is not qualitatively important for this work.

(ii) The determination of the line width ($\Delta\omega$) of the pinning mode resonance is less straightforward. It is now believed (Fertig, 1999; Fogler and Huse, 2000) to be a truly dynamical quantity and determined by the magnetophonon localization length. In general, (at a fixed B), $\Delta\omega$ increases with increasing disorder, but decreases with increasing Coulomb interaction strength.

(iii) The integrated intensity (S) of the pinning mode resonance directly reflects the participating density of the WC. It is shown (Fukuyama and Lee, 1978) that $S = (ne/4B)\omega_{\rm pk}$.

(iv) It has been suggested (Fertig, 1999) that the physical disorder responsible for the pinning comes mainly from the roughness associated with the interface that vertically confines the WC. Such disorder gives rise to a calculated (Fertig, 1999) $\omega_{\rm pk}$ comparable to that observed experimentally (Li *et al.*, 1997; Ye *et al.*, 2002b).

(v) Although the physical disorder is assumed to not to depend on the electronic state, the *effective* disorder ($V(\vec{r})$) which determines the Wigner crystal pinning, is electronic state dependent. More specifically, $V(\vec{r})$ is the physical disorder

appropriately *convoluted* with the electron form factor (wave function) (Fertig, 1999; Fogler and Huse, 2000; Chitra *et al.*, 2002) . As a consequence, the disorder correlation length ξ appearing in (K.1) above is that of the physical disorder (ξ_0) only when $\xi_0 > l_B$ (valid at sufficiently high B), where the magnetic length $l_B = \sqrt{\hbar/eB}$ is the size of one electron wave function. Otherwise (if $\xi_0 < l_B$), ξ should be set as l_B.

K.3 Pinned Bilayer Wigner Crystals with Pseudospin Magnetism

Now consider a BWC of equal densities (n) of electrons in each layer, with interlayer separation d and in a strong perpendicular B. We assume the disorder in the "top" layer ($V^t(\vec{r})$) and that in the "bottom" layer ($V^b(\vec{r})$) to be similar[5]:

$$V^t(\vec{r}) \sim V^b(\vec{r}) \sim V(\vec{r}) \tag{K.5}$$

where $V(\vec{r})$ obeys the disorder characteristics defined in Eq. (K.2) and already incorporates the appropriate *intralayer* electron form factor. Therefore, in the absence of the other layer, each would form a SL pinned WC with the same pinning mode as described in Sec. K.2. In the following we will use the superscripts "$n0$" to denote quantities associated with the pinning mode of such a SL WC, and "nn" for those associated with the BWC. We use N to denote the number of electrons in each layer (N=nA with A being the sample area) and pseudospin "↑" and "↓" for "top" and "bottom" layer indices respectively (we also assume both layers to be infinitely thin, located at z=$+d/2$ and z=$-d/2$ respectively, where (x, y, z)=$(\vec{r}, z)$ are 3D Cartesian coordinates for a 2D (intralayer) vector $\vec{r}$). We can ignore the real spin degree of

[5]Rigorously, we are assuming that $V^t(\vec{r})$ and $V^b(\vec{r})$ are two *realizations* of the same *random field* $V(\vec{r})$.

freedom for electrons in high B (the lowest Landau level).

Our model can be presented clearly in the first quantized language. We start with the *total* Hamiltonian for the pinned BWC

$$\hat{H} = \sum_{i=1}^{N} (\hat{H}_s(\vec{r}_i, \uparrow) + \hat{H}_s(\vec{r}_i, \downarrow)) + \hat{U}_{\rm int} + \hat{V}_{\rm dis} \tag{K.6}$$

In the above $\hat{H}_s$ is the single-particle part of the Hamiltonian, which also includes a neutralizing positive charge background (to keep the total Coulomb energy finite) but does *not* include disorder effects.

The Coulomb interaction among all electrons is

$$\begin{aligned} \hat{U}_{\rm int} &= \sum_{i<j}^{N} \frac{e^2}{|(\vec{r}_i, \uparrow) - (\vec{r}_j, \uparrow)|} + \sum_{i<j}^{N} \frac{e^2}{|(\vec{r}_i, \downarrow) - (\vec{r}_j, \downarrow)|} \\ &\quad + \sum_{i,j}^{N} \frac{e^2}{|(\vec{r}_i, \uparrow) - (\vec{r}_j, \downarrow)|} \end{aligned} \tag{K.7}$$

in which the first two terms represent intralayer interaction, the third term represents interlayer interaction, with $|(\vec{r}_i, \uparrow) - (\vec{r}_j, \uparrow)| = |(\vec{r}_i, \downarrow) - (\vec{r}_j, \downarrow)| = |\vec{r}_i - \vec{r}_j|$ and $|(\vec{r}_i, \uparrow) - (\vec{r}_j, \downarrow)| = \sqrt{|\vec{r}_i - \vec{r}_j|^2 + d^2}$.

The disorder part, $\hat{V}_{\rm dis}$, has two parts $\hat{V}_{\rm dis} = \hat{V}_{\rm pin} + \hat{T}_{\rm dis}$. One is the pinning within each layer

$$\hat{V}_{\rm pin} = \sum_{i=1}^{N} (V^t(\vec{r}_i, \uparrow) + V^b(\vec{r}_i, \downarrow)). \tag{K.8}$$

Note we have explicitly written out the configuration space coordinates above ((K.6)- (K.8)) to reflect its layer (pseudospin) dependent actions. For example,

$$V(\vec{r}, \uparrow)|\psi(\vec{r}) \otimes \downarrow\rangle = V(\vec{r}, \downarrow)|\psi(\vec{r}) \otimes \uparrow\rangle = 0 \tag{K.9}$$

for a single-particle state ψ.

The other part in $\hat{V}_{\rm dis}$ reflects effect of disorder induced (local) tunneling and is

given by

$$\hat{T}_{\rm dis} = T(\vec{r})\hat{F} \tag{K.10}$$

where $\hat{F}$ is simply the pseudospin flip operator

$$\hat{F}|\psi(\vec{r})\otimes\downarrow\rangle = |\psi(\vec{r})\otimes\uparrow\rangle, \hat{F}|\psi(\vec{r})\otimes\uparrow\rangle = |\psi(\vec{r})\otimes\downarrow\rangle \tag{K.11}$$

and the amplitude $T(\vec{r})$ is generally related to $V^t(\vec{r})$ and $V^b(\vec{r})$.

We first notice that if there were no interlayer coupling (for example $d \gg a \sim 1/\sqrt{n}$), both the interlayer interaction term in (K.7) and disorder induced tunneling (K.10) can be neglected and $\hat{H}$ decouples into two identical (only shifted in z) SL Hamiltonians. In this case the system reduces to two independent layers and its pinning mode resonance ($\mathrm{Re}[\sigma_{xx}(\omega)]$ spectrum) is simply the superposition of those of two identical SL WC, i.e, $\mathrm{Re}[\sigma_{xx}(\omega)]^{nn}$=2$\mathrm{Re}[\sigma_{xx}(\omega)]^{n0}$ with $\omega_{\rm pk}^{nn}$= $\omega_{\rm pk}^{n0}$, $\Delta\omega^{nn}$=$\Delta\omega^{n0}$ and S^{nn}=2S^{n0}.

In this article we are mainly interested in *interacting* bilayers and we focus on the effect of IC on the pinning mode of a BWC, in particular on $\omega_{\rm pk}$, which is the quantity that can be most accurately measured in experiments (Li *et al.*, 1997; Ye *et al.*, 2002b). To this end, we will consider and compare two idealized cases of a BWC with *no* IC (referred to as an "AFMWC") and a BWC with IC ("FMWC"), to be specified by the many-body Ansatz (K.13) and (K.19) in the following respectively. Our approach is to construct an *effective* Hamiltonian that maps the problem into a single layer one, with an *effective* disorder that captures the pinning physics in each case (AFMWC vs. FMWC), highlighting the difference made by IC, and calculate quantities such as $\omega_{\rm pk}$.

We also make the following additional assumptions, which greatly simplify the analysis but still keep the essential physics.

1. Assume small or vanishing interlayer tunneling ($\Delta_{\rm SAS}$) in absence of disorder.

We also assume the neutralizing positive charges are far away from the BWC. Together with the high B condition (which allows us to neglect the cyclotron kinetic energy of the electrons), the $\hat{H}_s$ part in $\hat{H}$ is nearly constant and can be neglected all together. Physically, this means that pinning is only determined by the electron-electron interaction ($\hat{U}_{\rm int}$) and electron-disorder interaction ($\hat{V}_{\rm dis}$): the static deformation is given by the configuration that minimizes the energy expectation of $\hat{U}_{\rm int} + \hat{V}_{\rm dis}$.

2. Assume $d \ll a$. This in particular allows us to effectively set $d{\sim}0$ in the Coulomb interaction term ($\hat{U}_{\rm int}$) in (K.7) and treat the inter and intralayer interactions on an equal footing. In this limit we can also assume the underlying lattice structure (in absence of disorder) to be the same (hexagonal) for the AFMWC and FMWC (Narasimhan and Ho, 1995).

3. Assume the following simple form for the disorder induced tunneling amplitude:

$$T(\vec{r}) = \tilde{g} V(\vec{r}) \tag{K.12}$$

where $\tilde{g} \geq 0$ is a small (we only consider the effect of disorder being weak perturbation) parameter. This is plausible because we expect the main source of relevant disorder in realistic, epitaxially-grown samples to come from the defects or fluctuations in the thin barrier separating the two layers. Such defects can constitute disorder in both layers, as well as facilitate local tunneling (Tutuc *et al.*, 2004; Shayegan, 2005), in proportional to the strength of such defects/fluctuations in the weak disorder limit. The positive sign of $\tilde{g}$ comes from the fact that such a tunneling-facilitating defect draws an electron closer into the barrier and farther away from the corresponding positive charged background/dopants, therefore constituting a positive disorder. We also expect $\tilde{g}$ to decrease with increasing effective layer separation d/a and go to zero at large

d/a (the decrease of $\tilde{g}$ with decreasing a reflects the Coulomb-blocking effect on the tunneling).

Later on we will briefly discuss the implication when the above assumptions are relaxed, which nonetheless will not change our qualitative conclusions.

Case 1. AFMWC (no IC).

A schematic picture (1D cross section) is shown in Fig. K.1(a). This corresponds to a "bipartite" (Narasimhan and Ho, 1995) lattice $\{\vec{R}_i\}_{i=1}^{2N}$ (deformed slightly from the ideal lattice $\{\vec{R}_i^0\}_{i=1}^{2N}$). We have relabeled the indices such that $i = 1, \ldots, N$ correspond to the "$\uparrow$" electrons and $i = N+1, \ldots, 2N$ correspond to "$\downarrow$" electrons. The many-body state of the AFMWC can be well approximated by the following ansatz (Narasimhan and Ho, 1995; Maki and Zotos, 1983) (after appropriate anti-symmetrization)

$$\Psi_{\text{AFMWC}} = \prod_{i=1}^{2N} |\psi_{\vec{R}_i}(\vec{r}_i) \otimes \rho_i\rangle \tag{K.13}$$

in which

$$\rho_i = \uparrow \text{ for } i = 1, \ldots, N \text{ and } \downarrow \text{ for } i = N+1, \ldots, 2N \tag{K.14}$$

and the single-particle Gaussian (up to a phase)
$\psi_{\vec{R}}(\vec{r}) = \frac{1}{\sqrt{2\pi} l_B} \exp[-\frac{|\vec{r}-\vec{R}|^2}{4l_B^2}] \exp[-\mathrm{i}\frac{\hat{z}\cdot(\vec{r}\times\vec{R})}{2l_B^2}]$ (where $l_B = \sqrt{\hbar/eB}$ is the magnetic length and $\hat{\mathrm{z}}$ the unit z-vector.)

With our index relabeling (and assumption $d \ll a$) we can rewrite

$$\hat{U}_{\text{int}} = \sum_{i<j}^{2N} \frac{e^2}{|\vec{r}_i - \vec{r}_j|} \tag{K.15}$$

Following Eq. (K.5,K.8,K.9,K.13,K.14) we easily see

$$\hat{V}_{\text{pin}} |\Psi_{\text{AFMWC}}\rangle \sim \sum_{i=1}^{2N} V(\vec{r}_i) |\Psi_{\text{AFMWC}}\rangle \tag{K.16}$$

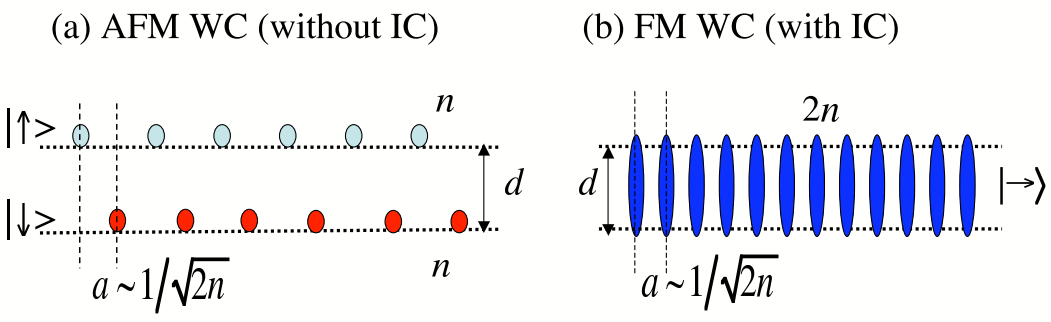

Figure K.1: Schematic (1D cross section, not to scale, d assumed to be $\ll a$) for an AFMWC (a) and a FMWC (b). Both have total densities $2n$ and the same underlying lattice structure (when not deformed by disorder). In (a) half the lattice electrons belong to the top layer (labeled as $\uparrow$) and the other half to the bottom layer (labeled as $\downarrow$). Electrons are only pinned by disorder from the individual layer. In (b) all electrons *simultaneously* belong to both layers (being in pseudospin state $|\rightarrow\rangle = \frac{1}{\sqrt{2}}|\uparrow\rangle + \frac{1}{\sqrt{2}}|\downarrow\rangle$), and are effectively pinned by the *joint* disorder (see the text for details) from both layers.

We also notice that, for the pseudospin flip operator $\hat{F}$, $\langle\psi(\vec{r})\otimes\rho|\hat{F}|\psi(\vec{r})\otimes\rho\rangle$=0 for a single particle state $\psi(\vec{r})$ and ρ=either $\uparrow$ or $\downarrow$. Therefore in the case of an AFMWC, the disorder induced tunneling $\hat{T}_{\rm dis}$ does *not* affect the pinning (static deformation) of the crystal[6].

The *effective* Hamiltonian for the *pinned* AFMWC is

$$\hat{H}^{pin}_{\rm AFMWC} = \sum_{i<j}^{2N} \frac{e^2}{|\vec{r}_i - \vec{r}_j|} + \sum_{i=1}^{2N} V(\vec{r}_i) \tag{K.17}$$

where the pseudospins have dropped out. Thus as far as pinning is concerned, the system maps to a SL of $2N$ electrons crystallizing in the effective disorder potential $V(\vec{r})$. The static deformation of such a crystal can be obtained in principle by minimizing the energy with respect to $\{\vec{R}_i\}_{i=1}^{2N}$, using the many-body Ansatz $\Psi_{\rm AFMWC}$ (K.13) with this Hamiltonian. For its pinning mode we simply have (from Sec. K.2)

$$\omega^{nn}_{\rm pk} = \omega^{n0}_{\rm pk}/2^{\gamma},\ \Delta\omega^{nn} < \Delta\omega^{n0},\ \text{and}\ S^{nn} = S^{n0}/2^{\gamma-1} \tag{K.18}$$

Case 2. FMWC (with IC). A schematic (1D cross section) is shown in Fig. K.1(b). In contrast to *Case. 1*, whose lattice is bipartite with the AFM order, here the lattice is one-component with all electrons in the pseudospin state $|\rightarrow\rangle$ ($=\frac{1}{\sqrt{2}}|\uparrow\rangle+\frac{1}{\sqrt{2}}|\downarrow\rangle$). Such FM order breaks the U(1) symmetry[7] of pseudospins (either *explicitly* by finite $\Delta_{\rm SAS}$ or *spontaneously* (only due to interlayer Coulomb interaction) for $\Delta_{\rm SAS}\sim$0)). The many-body ansatz for such a FMWC is

$$\Psi_{\rm FMWC} = \prod_{i=1}^{2N} |\psi_{\vec{R}_i}(\vec{r}_i)\otimes\rightarrow\rangle \tag{K.19}$$

(where $\psi_{\vec{R}}(\vec{r})$ is the same kind of Gaussian wavepacket used earlier).

[6] In a first order approximation (with small $\tilde{g}$), we can neglect the effect of $\hat{T}$ modifying the spin structure of the crystal.

[7] The full SU(2) symmetry of pseudospins is already broken *explicitly* by the bilayer capacitive charging energy.

Compared to *Case 1*, now $\hat{T}_{\rm dis}$ has a very different effect: it is easy to see that

$$\hat{T}_{\rm dis}(\vec{r})|\psi(\vec{r})\otimes\rightarrow\rangle = \tilde{g}V(\vec{r})|\psi(\vec{r})\otimes\rightarrow\rangle \tag{K.20}$$

for a single particle state $\psi(\vec{r})$. This means that, in contrast to the case of AFMWC (without IC), where $\hat{T}_{\rm dis}$ does not affect pinning as seen earlier, the disorder induced tunneling $\hat{T}_{\rm dis}$ in the presence of IC effectively acts as a pinning term (this in fact holds even for a general tunneling disorder (K.10)). In our case, this pinning is in addition to the original "intra-layer" pinning from $V(\vec{r})$, thus leads to enhanced pinning of a FMWC (K.19).

Now we construct a general *effective* disorder model in which the system is mapped into $2N$ electrons crystallizing in a single "$\rightarrow$" layer, and pinning effects such as that due to $\hat{T}_{\rm dis}$ above are absorbed in an effective disorder, given by the following "joint" disorder[8] ansatz (the reason for the choice will be soon apparent):

$$V^J(\vec{r}) = \frac{1}{\sqrt{2}}(V^t(\vec{r}) + V^b(\vec{r})) \tag{K.21}$$

with the *effective* pinning Hamiltonian being

$$\hat{H}^{pin}_{\rm FMWC} = \sum_{i<j}^{2N} \frac{e^2}{|\vec{r}_i - \vec{r}_j|} + \sum_{i=1}^{2N} V^J(\vec{r}_i). \tag{K.22}$$

The spatial correlator for such a "joint" disorder V^J now contains (in terms of

[8]One may explicit write V^J as $V^J(\vec{r},\rightarrow)$ to emphasize that it is an *effective disorder* acting on "$|\rightarrow\rangle$" electrons. V^J may also be formally thought as resulting from a kind of "convolution" in pseudospin space. However, a rigorous definition of such a convolution requires appropriately defining an invariant measure on a pseudospin algebra, and is beyond the scope of this paper.

the original bilayers) both intralayer (Eq. (K.2)) and *interlayer disorder-correlation*:

$$\begin{aligned}
&\langle V^J(\vec{r})V^J(\vec{r}')\rangle \\
&= \frac{1}{2}[\langle V^t(\vec{r})V^t(\vec{r}')\rangle + \langle V^b(\vec{r})V^b(\vec{r}')\rangle \\
&\quad +\langle V^t(\vec{r})V^b(\vec{r}')\rangle + \langle V^b(\vec{r})V^t(\vec{r}')\rangle] \\
&= W(1+g)D_\xi(|\vec{r}-\vec{r}'|)
\end{aligned} \tag{K.23}$$

in which we have introduced a phenomenological "coupling" parameter g between the disorder from the two layers:

$$\langle V^t(\vec{r})V^b(\vec{r}')\rangle = \langle V^b(\vec{r})V^t(\vec{r}')\rangle = gWD_\xi(|\vec{r}-\vec{r}'|). \tag{K.24}$$

Again we expect g to depend on the effective layer separation (d/a): g decreases for increasing d/a and drops to 0 at sufficiently large d/a. Now we see that V^J has disorder strength W^J=$(1+g)W$ and the same correlation length (ξ) as $V(\vec{r})$. Thus we obtain for the bilayer pinning mode properties (expressed in terms of corresponding SL "$n0$" quantities):

$$\omega_{\rm pk}^{nn} = \frac{1+g}{2^\gamma}\omega_{\rm pk}^{n0}, \quad S^{nn} = \frac{1+g}{2^{\gamma-1}}S^{n0}. \tag{K.25}$$

In contrast, the interlayer disorder-correlation (K.24) has no relevance for pinning of the AFMWC (K.17-K.18) or the SL ("$n0$") WC (Sec. K.2). Therefore the presence of IC has effectively *enhanced* the pinning disorder in the FMWC. This tends to increase both $\omega_{\rm pk}$ and $\Delta\omega$ from the respective SL values. On the other hand the doubled n (and strengthened Coulomb interaction) from the SL case will decrease $\omega_{\rm pk}$ and $\Delta\omega$. Due to the two competing effects, $\omega_{\rm pk}$ (K.25) and $\Delta\omega$ for the FMWC can be *either* higher or lower than the $\omega_{\rm pk}^{n0}$ and $\Delta\omega^{n0}$. In contrast, $\omega_{\rm pk}$ and $\Delta\omega$ for the AFMWC are *always* lower than the SL values. Detailed calculations (Chen *et al.*, 2005) (following

Ref. (Chitra *et al.*, 2002)) show that for the FMWC, if $\omega_{\rm pk}^{nn}=\omega_{\rm pk}^{n0}$, $\Delta\omega^{nn}<\Delta\omega^{n0}$.

The "effective disorder" model we give above does not directly specify the source of the inter-layer correlated disorder (such as barrier fluctuations) with the enhanced pinning mechanism. However it carries, through the choice of the "joint" disorder (K.21), the simple physical picture that, in the state of FMWC, since electrons have lost their original layer identity and move in both layers simultaneously and coherently, they are pinned by disorder from both layers. Such a general framework turns out to be convenient to analyze the BWC pinning properties in Sec. K.4 and K.5 below.

K.4 Effects of d/a and FMWC-AFMWC transitions

As seen from the above, for the FMWC, $\omega_{\rm pk}$ will *decrease* when the effective layer separation $\delta(=d/a)$ increases, due to the decrease of g (Eq. (K.25)). It has been shown (Zheng and Fertig, 1995; Narasimhan and Ho, 1995) that at some small critical δ_c, a transition from a FMWC (favored at $\delta<\delta_c$) to an AFMWC (favored at $\delta>\delta_c$) occurs. Since pinning in the AFMWC (without IC) does not involve g, such a transition would result in a sudden reduction of pinning and would give rise to an abrupt drop of $\omega_{\rm pk}$ (see Fig. K.2, in which we plot the schematic dependence of $\omega_{\rm pk}$ (normalized by the SL $\omega_{\rm pk}^{n0}$) on d/a).

If δ is further increased (in an AFMWC) such that d becomes comparable to or even larger than a, the interlayer Coulomb interaction will be reduced. This reduces the total Coulomb interaction (K.7) and effectively reduces the shear modulus (μ) of the BWC. From (K.1), this will give rise to an *increase* of $\omega_{\rm pk}$. In the limit of $d\gg a$, the system reduces to two independent SL WC and $\omega_{\rm pk}^{nn}/\omega_{\rm pk}^{n0}\to 1$.

Thus we have shown (Fig. K.2) that $\omega_{\rm pk}$ can have *opposite* behavior in the FMWC

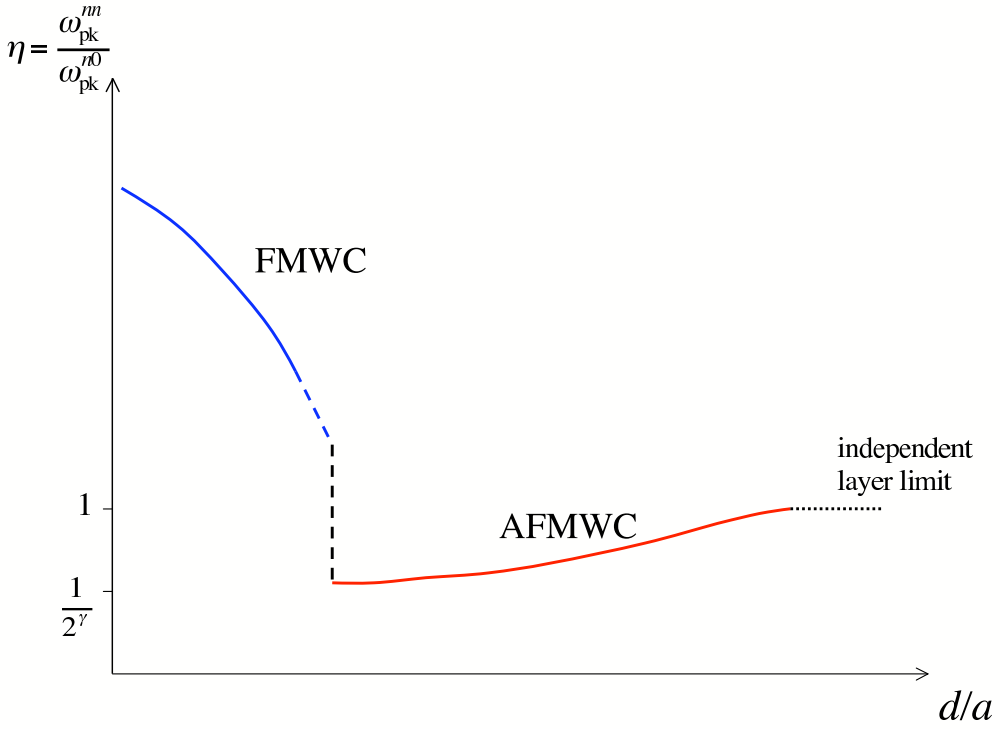

Figure K.2: Schematic (d/a)-dependence of η (BWC $\omega_{\rm pk}^{nn}$ normalized by SL $\omega_{\rm pk}^{n0}$), showing an *abrupt* FMWC to AFMWC transition (characterized by a sudden drop in $\omega_{\rm pk}^{nn}$) and a continuous AFMWC to independent-layer cross over. The asymptotic values of η for $d/a \to 0$ in AFMWC and $d/a \to \infty$ (independent layer limit) are $1/2^\gamma$ and 1 respectively (see Sec. K.3).

($\omega_{\rm pk}$ decreasing with increasing d/a) from that in the AFMWC ($\omega_{\rm pk}$ increasing with increasing d/a), and $\omega_{\rm pk}$ drops *abruptly* at a FMWC-AFMWC transition. Such behavior can qualitatively differentiate a FMWC from an AFMWC and signal the transition between the two.

In Ref. (Narasimhan and Ho, 1995) it is found that if tunneling ($\Delta_{\rm SAS}$) is finite, the BWC at $\delta>\delta_c$, although two-component, can have mixed AFM-FM order, corresponding to $|\rho_i\rangle=|\nearrow\rangle$ (i=1,...,N) and $|\rho_i\rangle=|\searrow\rangle$ (i=N+1,...,2N) in (K.13), where (pseudospin direction) "$\nearrow$"("$\searrow$") is "$\uparrow$"("$\downarrow$") tilted toward "$\rightarrow$" by angle θ. $\theta=\pi/2$ for the FMWC ($\delta<\delta_c$) and *drops* abruptly to a finite value ($0<\theta<\pi/2$) at the transition (at δ_c) (Narasimhan and Ho, 1995). Therefore we expect the abrupt drop of $\omega_{\rm pk}$ associated with the transition to survive even with a moderate $\Delta_{\rm SAS}$, although the *amplitude* of the drop will be smaller than the $\Delta_{\rm SAS}\sim 0$ case.

At finite $\delta>\delta_c$, Ref. (Narasimhan and Ho, 1995) also found several possible lattice structures (without disorder) and a continuous evolution among them as a function of δ. The evolution is gradual and is not expected to change the qualitative picture shown in Fig. K.2, in particular the presence of the abrupt drop of $\omega_{\rm pk}$ at the FM-AFM transition.

Since the enhancement of pinning in the FMWC is associated with the presence of IC, we expect the abrupt $\omega_{\rm pk}$ drop to be a generic feature whenever IC (or equivalently, ferromagnetism) is destroyed, even if it is driven by some other mechanisms (such as changing $\nu_{\rm tot}$ (Narasimhan and Ho, 1995), or possibly with sufficient layer imbalance (Tutuc *et al.*, 2003; Chen *et al.*, 2005)).

K.5 Effects of In-Plane Magnetic Fields and Finite Temperatures

In-plane magnetic fields ($B_{||}$). It is well known that $B_{||}$ can profoundly affect bilayer physics (Yang *et al.*, 1994), particularly in relation to interlayer phase coherence and pseudospin magnetism. In the case of a bilayer FMWC (with finite d), Zheng and Fertig (Zheng and Fertig, 1995) studied the effects of $B_{||}$ and found that applying a *small* $B_{||}$ can "twist" the IC, such that the charge distribution in one layer is shifted relative to the other layer, as shown in Fig. K.3. The relative shift is along the $B_{||}$ direction ($\hat{\mathrm{x}}$), and is given (Zheng and Fertig, 1995) by $\vec{b}_{||} = l_B^2(d/l_{B_{||}}^2)\hat{\mathrm{x}} = d(B_{||}/B)\hat{\mathrm{x}}$. In such a case, the interlayer disorder coupling induced by IC can also become "twisted" (Fertig, 2005), now involving interlayer disorder-correlation

$$\langle V^t(\vec{r})V^b(\vec{r}' + \vec{b}_{||})\rangle = gWD_\xi(|\vec{r} - \vec{r}' - \vec{b}_{||}|), \tag{K.26}$$

and this will duly affect the pinning. Therefore, measuring ω_{pk} while varying both the direction and magnitude of $B_{||}$ allows one to possibly probe a 2D "tomography" of the disorder!

At larger $B_{||}$, an incommensurability-driven transition to an "untwisted" state is expected to occur, when the energy cost of interlayer Coulomb interaction exceeds the energy gain from interlayer hopping (Zheng and Fertig, 1995). We expect such a transition to cause also an abrupt change of ω_{pk} in the pinning mode.

Finite temperatures (T). So far we have considered only T=0. Finite T is expected in particular to smear the abrupt drop in ω_{pk} associated with the FMWC-AFMWC transition as described in Sec. K.4. Above some characteristic T (T_*), such a drop would become unobservable. The typical energy difference between a FMWC and AFMWC has been shown (Zheng and Fertig, 1995; Narasimhan and Ho, 1995) to

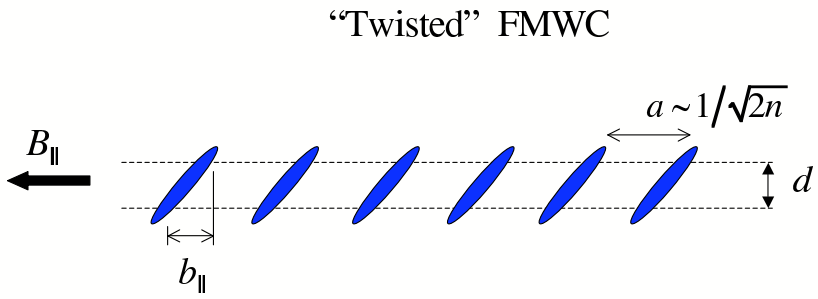

Figure K.3: A FMWC is "twisted" under a (small) in-plane magnetic field ($B_{||}$), which can also "twist" the IC-induced interlayer disorder coupling (now involving $\langle V^t(\vec{r})V^b(\vec{r}' + \vec{b}_{||})\rangle$, where $V^t(V^b)$ is the top(bottom) layer disorder. The "twist" $\vec{b}_{||}$=$d(B_{||}/B)\hat{\mathrm{x}}$, where $\hat{\mathrm{x}}$ is the direction of $B_{||}$.

be on the order of $\Delta E \sim 10^{-3}-10^{-2} e^2/\epsilon l_B$. From this, we can make a (very rough) estimate of T_* to be on the order of $\Delta E/k_B \sim 0.5$K (using a typical experimental $l_B \sim 100$Å and $\epsilon = 13$ for GaAs)[9].

K.6 More Remarks on FMWC

Finally we remark on two interesting aspects of the FMWC (K.19), particularly in the case of vanishing $\Delta_{\rm SAS}$, and speculate on effects in relation to pinning. We may rewrite the many-body state (K.19) in second-quantized form as

$$\Psi_{\rm FMWC} = \frac{1}{\sqrt{2}} \prod_i (c^\dagger_{\vec{R}_i,\uparrow} + e^{{\rm i}\phi} c^\dagger_{\vec{R}_i,\downarrow})|0\rangle, \tag{K.27}$$

with $\phi = 0$ for all i, where $c^\dagger_{\vec{r},\downarrow}$ ($c^\dagger_{\vec{r},\uparrow}$) is the second-quantized operator that creates an electron localized at $\vec{r}$ in down (up) layer. The ansatz (K.27) is formally analogous to that of the bilayer excitonic condensate state (BECS) (Simon, 2005; Fertig, 1989) ($\frac{1}{\sqrt{2}} \prod_i (c^\dagger_{\vec{k}_i,\uparrow} + c^\dagger_{\vec{k}_i,\downarrow})|0\rangle$) with single-particle states labeled with momenta ($\vec{k}_i$) replaced by those with lattice point positions ($\vec{R}_i$). The FMWC (K.27) possesses both long range positional order (broken translational symmetry) and phase (ϕ) coherence (broken U(1) symmetry), thus resembling a *supersolid* (Leggett, 1970; Yang, 2005) phase. If phase rigidity (Fertig, 2005) can exist in such a phase, superfluidity would occur. The superflow would be exhibited in the counterflow channel, similar to the case observed in the BECS (Kellogg *et al.*, 2004; Tutuc *et al.*, 2004). Although in practice such a superflow in the FMWC is likely to be suppressed by the pinning (at least in a linear response theory), it would be an interesting experiment to examine the counterflow with finite current above the *depinning* threshold, or under a sufficiently strong parallel magnetic field ($B_{||}$) which can reduce the effective pinning associated

[9] Also assuming the BWC has not melted at such T.

with IC or disorder induced interlayer tunneling[10] described in (K.10).

The Goldstone mode associated with the (spontaneously) broken U(1) symmetry represents an oscillatory wave in ϕ. Since ϕ is conjugate to the density difference between the two layers (Δn), such a U(1) mode inevitably involves interlayer charge transfer (oscillation in Δn) and will be coupled to the longitudinal and transverse phonons (which are hybridized in B) of the WC (Klironomos and Dorsey, 2005). We expect that such coupling to the U(1) mode (which disperses linearly in k) can not only *renormalize* the pinning gap (with enhanced pinning, as we have seen), but also the dispersion of the pinning mode (as the lowest lying hybridized mode)[11]. Such a dispersion change may be detectable in the k-resolved microwave spectroscopy experiments (Hennigan *et al.*, 1998; Chen *et al.*, 2004c) and also be used to identify the FMWC phase.

K.7 Conclusion

BWC can display a rich array of (pseudospin) quantum magnetism from FM to AFM order (Narasimhan and Ho, 1995). They are in many ways analogous to ^{3}He solid (Adams, 2004), which has many remarkable physical properties related to its quantum magnetism. For example, the AFMWC of triangular lattice structure may serve as a model system for frustrated spin system (Levitov and Novikov, 2005), and the FMWC may even be considered as an electronic supersolid-like phase as discussed above. In this article we have focused on the effects of pseudospin magnetism on the pinning by disorder, which always exists in a real BWC. Electrons in a FMWC have interlayer coherence (IC) and lose their individual layer identities, similar to the situation in the $\nu_{\rm tot} = 1$ quantum Hall state. We have shown that such IC can

[10] Disorder in tunneling is expected to be particularly detrimental to counterflow superfluidity (Wen, 2005). A parallel magnetic field can suppress interlayer tunneling (Zheng and Fertig, 1995).

[11] Analogous couplings have been studied for the helium supersolid, see for example (Cheng, 1981; Dorsey *et al.*, 2005).

take advantage of the interlayer correlation of disorder (such as through disorder in the barrier and the interlayer tunneling induced by such disorder) and *enhance* the effective pinning in the FMWC. The IC-enhanced pinning is a novel mechanism that has no counterpart in a single layer WC and is absent in a AFMWC without IC. For the pinning mode resonance, this has important consequences which may be used as experimental signatures of the different magnetic phases and phase transitions in BWC. For example, we predict $\omega_{\rm pk}$ to decrease with d/a in a FMWC but to increase with d/a in a AFMWC, with an *abrupt* drop of $\omega_{\rm pk}$ at a FMWC-AFMWC transition. We have also considered effects of $B_{||}$ and finite temperatures. Many predictions of our model are found to be consistent with a recent experimental work by Z. Wang *et al.* (Wang *et al.*, 2005).

Appendix L

Publications List During PhD

- Yong P. Chen, G. Sambamdamurthy, Z. H. Wang, R. M. Lewis, L. W. Engel, D. C. Tsui, P. D. Ye, L. N. Pfeiffer, and K. W. West, "Melting of a 2D Quantum Electron Solid", submitted.

- Yong P. Chen, "Pinned Bilayer Wigner Crystals with Pseudospin Magnetism", submitted to *Physical Review B*, available at http://arXiv.org/cond-mat/0507124.

- R. M. Lewis, Yong P. Chen, L. W. Engel, D. C. Tsui, L. N. Pfeiffer, and K. W. West, "Microwave resonance of the reentrant insulating quantum Hall phases in the 1st excited Landau Level", *Physical Review B, Rapid Communications* **71**, 081301 (2005).

- Yong P. Chen, R. M. Lewis, L. W. Engel, D. C. Tsui, P. D. Ye, Z. H. Wang, L. N. Pfeiffer, and K. W. West, "Evidence for Two Different Solid Phases of Two Dimensional Electrons in High Magnetic Fields", *Physical Review Letters* **93**, 206805 (2004).

- R. M. Lewis, Yong Chen, L. W. Engel, D. C. Tsui, P. D. Ye, L. N. Pfeiffer, and K. W. West, "Evidence of a First Order Phase Transition Between the Wigner Crystal and Bubble Phases of 2D Electrons in Higher Landau Levels", *Physical*

Review Letters **93**, 176808 (2004).

- E. Peled, D. Shahar, Y. Chen, E. Diez, D. L. Sivco, and A. Y. Cho,"Quantum Hall transitions in mesoscopic samples", Proceedings of the 16th International Conference on High Magnetic Fields in Semiconductor Physics, Tallahassee, Florida (2004), *International Journal of Modern Physics B*, **18**, 3575 (2004).

- Yong P. Chen, Zhihai Wang, R. M. Lewis, L. W. Engel, D. C. Tsui, P. D. Ye, L. N. Pfeiffer, and K. W. West, "Microwave Resonances in the Reentrant Insulating Phases around $\nu = 1/3$ and $\nu = 1/5$ in Two Dimensional Electron Systems", Proceedings of the 16th International Conference on High Magnetic Fields in Semiconductor Physics, Tallahassee, Florida (2004), *International Journal of Modern Physics B*, **18**, 3553 (2004).

- E. Peled, Y. Chen, E. Diez, D. C. Tsui, D. Shahar, D. L. Sivco, and A. Y. Cho, "Symmetries of the Resistance of Mesoscopic Samples in the Quantum Hall Regime", *Physical Review B* **69**, 241305(R) (2004).

- Yong Chen, R. M. Lewis, L. W. Engel, D. C. Tsui, P. D. Ye, L. N. Pfeiffer, and K. W. West, "Microwave Resonance of the 2D Wigner Crystal Around Integer Landau Fillings", *Physical Review Letters* **91**, 016801 (2003).

- E. Peled, D. Shahar, Y. Chen, E. Diez, D. L. Sivco, and A. Y. Cho, "Near Perfect Correlation of the Resistance Components of Mesoscopic Samples at the Quantum Hall Regime", *Physical Review Letters* **91**, 236802 (2003).

- E. Peled, D. Shahar, Y. Chen, D. L. Sivco, and A. Y. Cho, "The Quantized Hall Effect in the Presence of Resistance Fluctuations", *Physical Review Letters* **90**, 246802 (2003).

- R. M. Lewis, Yong Chen, L. W. Engel, D. C. Tsui, P. D. Ye, L. N. Pfeiffer, and K. W. West, "Wigner Crystallization about $\nu = 3$", Proceedings of the 15th

International Conference on Electronic Properties of Two Dimensional Systems, Nara, Japan (2003), *Physica E: Low Dimensional Systems and Nanostructures* **22**, 104 (2004)

- R. M. Lewis, Yong Chen, L. W. Engel, D. C. Tsui, P. D. Ye, L. N. Pfeiffer, and K. W. West, "Measurements of the Temperature Dependence of the Bubble Phase", Proceedings of the 15th International Conference on Electronic Properties of Two Dimensional Systems, Nara, Japan (2003), *Physica E: Low Dimensional Systems and Nanostructures* **22**, 119 (2004)

- P. D. Ye, Yong Chen, L. W. Engel, D. C. Tsui, R. M. Lewis, L. N. Pfeiffer, and K. W. West, "Domain Size vs Landau Filling for High Magnetic Field Wigner Crystal", Proceedings of the 15th International Conference on High Magnetic Fields in Semiconductor Physics, Oxford, England (2002).

Bibliography

Abrahams, E., S. V. Kravchenko, and M. P. Sarachik, 2004, Rev. Mod. Phys. **73**, 251.

Adams, E. D., 2004, J. Low. Temp. Phys. **135**, 695.

Anderson, P. W., 2004, A suggested 4 x 4 structure in underdoped cuprate superconductors: a Wigner supersolid, cond-mat/0406038.

Ando, T., A. B. Fowler, and F. Stern, 1982, Rev. Mod. Phys. **54**, 437.

Andrei, E., *et al.*, 1988, Phys. Rev. Lett. **60**, 2765.

Andrei, E., *et al.*, 1989, Phys. Rev. Lett. **62**, 1926.

Barrett, S. E., *et al.*, 1995, Phys. Rev. Lett. **74**, 5112.

Basov, D. N., and T. Timusk, 2005, Rev. Mod. Phys. **77**, 721.

Bayot, V., *et al.*, 1996, Phys. Rev. Lett. **76**, 4584.

Beamish, J. R., A. Hikata, L. Tell, and C. Elbaum, 1983, Phys. Rev. Lett. **50**, 425.

Biondi, M. A., *et al.*, 1958, Rev. Mod. Phys. **30**, 1109.

Blatter, G., *et al.*, 1994, Rev. Mod. Phys. **66**, 1125.

Bonsall, L., and A. A. Maradudin, 1977, Phys. Rev. B. **15**, 1959.

Brey, L., 1990, Phys. Rev. Lett. **65**, 903.

Brey, L., *et al.*, 1995, Phys. Rev. Lett. **75**, 2562.

Buhman, H., *et al.*, 1991, Phys. Rev. Lett. **66**, 926.

Ceperley, D., 1999, Nature (London) **397**, 386.

Chang, C. C., G. S. Jeon, and J. K. Jain, 2005, Phys. Rev. Lett. **94**, 016809.

Chen, H.-D., *et al.*, 2004a, Phys. Rev. Lett. **93**, 187002.

Chen, X. M., and J. J.Quinn, 1992, Phys. Rev. B. **45**, 11054.

Chen, Y., *et al.*, 2003, Phys. Rev. Lett. **91**, 016801.

Chen, Y. P., 2005, Pinned bilayer Wigner crystals with pseudospin magnetism, cond-mat/0507124.

Chen, Y. P., *et al.*, 2004b, Int. J. Mod. Phys. B **18**, 3553.

Chen, Y. P., *et al.*, 2004c, Phys. Rev. Lett. **93**, 206805.

Chen, Y. P., *et al.*, 2005, unpublished.

Cheng, Y., 1981, Phys. Rev. B. **23**, 157.

Chitra, R., and T. Giamarchi, 2004, Zero field Wigner crystal, cond-mat/0409187.

Chitra, R., T. Giamarchi, and P. Le Doussal, 2002, Phys. Rev. B. **65**, 035312.

Christensen, H. O., 2001, J. Phys. C **13**, R95.

Chui, S. T. (ed.), 1994, *Physics of the Electron Solid* (International Press, Boston).

Chui, S. T., and K. Esfarjani, 1991, Phys. Rev. B. **44**, 11498.

Cooper, K., *et al.*, 1999, Phys. Rev. B. **60**, R11285.

Côté, R., L. Brey, and A. H. MacDonald, 1992, Phys. Rev. B. **46**, 10239.

Côté, R., *et al.*, 1997, Phys. Rev. Lett. **78**, 4825.

Csathy, G., *et al.*, 2004, Phys. Rev. Lett. **92**, 256804.

Csathy, G., *et al.*, 2005a, Phys. Rev. Lett. **94**, 226802.

Csathy, G., *et al.*, 2005b, Phys. Rev. Lett. **94**, 146801.

Dagotto, E., 2005, Science **309**, 257.

Das Sarma, S., and A. Pinczuk (eds.), 1997, *Perspectives in Quantum Hall Effects* (Wiley and Sons).

Davies, J. H. (ed.), 1998, *The Physics of Low Dimensional Semiconductors: An Introduction* (Cambridge University Press).

Demel, T., D. Heitmann, P. Grambow, and K. Ploog, 1988, Appl. Phys. Lett. **53**, 2176.

Demler, E., A. Hanke, and S.-C. Zhang, 2004, Rev. Mod. Phys. **76**, 909.

Demler, E., C. Nayak, and S. Das Sarma, 2001, Phys. Rev. Lett. **86**, 1853.

Desrat, W., *et al.*, 2002, Phys. Rev. Lett. **88**, 256807.

Dobbs, E. R., 2001, *Helium Three* (Oxford University Press).

Dorsey, A. T., P. M. Goldbart, and J. Toner, 2005, Squeezing superfluid from a stone: Coupling superfluidity and elasticity in a supersolid, cond-mat/0508271.

Du, R. R., *et al.*, 1999, Solid State Commun. **109**, 389.

Efros, A. L., 1985, J. Exp. Theor. Phys. **62**, 1057.

Einspruch, N. P., and W. R. Frensley, 1994, *Heterostructures and Quantum Devices (Vol. 24 of VLSI Electronics)* (Academic Press).

Eisenstein, J. P., 2001, Solid State Commun. **117**, 123.

Eisenstein, J. P., *et al.*, 2002, Phys. Rev. Lett. **88**, 076801.

Engel, L. W., D. Shahar, Ç. Kurdak, and D. C. Tsui, 1993, Phys. Rev. Lett. **71**, 2638.

Engel, L. W., *et al.*, 1997a, Solid State Commun. **104**, 167.

Engel, L. W., *et al.*, 1997b, Physica E **1**, 111.

Esfarjani, K., and Y. Kawazoe, 1995, J. Phys. C **7**, 7217.

Ettouhami, A. M., 2005, private communication.

Ettouhami, A. M., F. D. Klironomos, and A. T. Dorsey, 2005, Anistropic states of two-dimensional electrons in high magnetic fields, cond-mat/0506459.

Evers, F., *et al.*, 2001, Physica B **298**, 187.

Falko, V. I., 1994, Phys. Rev. B. **49**, 7774.

Faniel, S., *et al.*, 2005, Phys. Rev. Lett. **94**, 046802.

Fertig, H. A., 1989, Phys. Rev. B. **40**, 1087.

Fertig, H. A., 1997, in *Perspectives in Quantum Hall Effects*, edited by S. Das Sarma and A. Pinczuk (Wiley and Sons, New York), chapter 3.

Fertig, H. A., 1999, Phys. Rev. B. **59**, 2120.

Fertig, H. A., 2005, private communication.

Fertig, H. A., *et al.*, 1994, Phys. Rev. B. **50**, 11018.

Fogler, M. M., 2001, Int. J. Mod. Phys. B **16**, 2924.

Fogler, M. M., 2002, Phys. Rev. Lett. **88**, 186402.

Fogler, M. M., 2003, Stripe and bubble phases in quantum Hall systems, cond-mat/0111001, pp. 98-138, in High Magnetic Fields: Applications in Condensed Matter Physics and Spectroscopy, ed. by C. Berthier, L.-P. Levy, G. Martinez (Springer-Verlag, Berlin, 2002).

Fogler, M. M., 2004, Physica E **22**, 98.

Fogler, M. M., and D. A. Huse, 2000, Phys. Rev. B. **62**, 7553.

Fogler, M. M., A. A. Koulakov, and B. I. Shklovskii, 1996, Phys. Rev. B. **54**, 1853.

Fradkin, E., and S. A. Kivelson, 1999, Phys. Rev. B. **59**, 8065.

Franz, M., 2004, Science **305**, 1410.

Fukui, T., S. Ando, and Y. K. Fukai, 1990, Appl. Phys. Lett. **57**, 1209.

Fukuyama, H., and P. A. Lee, 1978, Phys. Rev. B. **18**, 6245.

Fukuyama, H., P. M. Platzman, and P. W. Anderson, 1979, Phys. Rev. B. **19**, 5211.

Gaiffulin, M. B., *et al.*, 2000, Phys. Rev. Lett. **84**, 2945.

Gervais, G., *et al.*, 2005a, Phys. Rev. Lett. **93**, 266804.

Gervais, G., *et al.*, 2005b, Phys. Rev. Lett. **94**, 196803.

Girvin, S. M., 1999, The quantum hall effect: Noevel excitations and broken symmetries, cond-mat/9907002.

Girvin, S. M., and A. H. MacDonald, 1987, Phys. Rev. Lett. **58**, 1252.

Glattli, D. C., G. Deville, V. Duburcq, F. I. B. Williams, E. Paris, B. Etienne, and E. Y. Andrei, 1990, Surf. Sci. **229**, 344.

Goerbig, M. O., P. Lederer, and C. M. Smith, 2004a, Phys. Rev. B. **69**, 115327.

Goerbig, M. O., P. Lederer, and C. M. Smith, 2004b, Phys. Rev. Lett. **93**, 216802.

Goldman, V. J., M. Santos, M. Shayegan, and J. E. Cunningham, 1990, Phys. Rev. Lett. **65**, 2189.

Goldoni, G., and F. M. Peeters, 1996, Phys. Rev. B. **53**, 4591.

Goldys, E. M., S. A. Brown, R. B. Dunford, A. G. Davies, R. Newbury, R. G. Clark, P. E. Simmonds, J. J. Harris, and C. T. Foxon, 1992, Phys. Rev. B. **46**, 7957.

Green, A. G., 2000, Phys. Rev. B. **61**, 16299.

Green, A. G., I. I. Kogan, and A. M. Tsvelik, 1996, Phys. Rev. B. **54**, 16838.

Grimes, C. C., and G. Adams, 1979, Phys. Rev. Lett. **42**, 795.

Grüner, G., 1988, Rev. Mod. Phys. **60**, 1129.

Grüner, G., 1994, *Density Waves in Solids* (Addison Wesley).

Gunawan, O., *et al.*, 2004, Phys. Rev. Lett. **93**, 246603.

Haldane, F. D. M., E. H. Rezayi, and K. Yang, 2000, Phys. Rev. Lett. **85**, 5396.

Halperin, B. I., 1983, Helv. Phys. Acta **56**, 75.

Halperin, B. I., 1984, Phys. Rev. Lett. **52**, 1583.

Hanaguri, T., *et al.*, 2004, Nature (London) **430**, 1001.

Helgren, E., N. P. Armitage, and G. Grüner, 2004, Phys. Rev. B. **69**, 014201.

Hennigan, P. F., A. Beya, C. J. Mellor, R. Gaál, F. I. B. Williams, and M. Henini, 1998, Physica B **249**, 53.

Hoffman, J. E., *et al.*, 2002, Science **295**, 466.

Hohls, F., U. Zeitler, and R. J. Haug, 2001, Phys. Rev. Lett. **86**, 5124.

Imry, Y., and S. K. Ma, 1975, Phys. Rev. Lett. **35**, 1399.

Jain, J. K., 1989, Phys. Rev. Lett. **63**, 199.

Jain, J. K., 2000, Phys. Today **53**(4), 39.

Jiang, H. W., *et al.*, 1990, Phys. Rev. Lett. **65**, 633.

Kellogg, M., J. P. Eisenstein, L. N. Pfeiffer, and K. W. West, 2004, Phys. Rev. Lett. **93**, 036801.

Kim, E., and M. H. W. Chan, 2004a, Science **305**, 1941.

Kim, E., and M. H. W. Chan, 2004b, Nature (London) **427**, 225.

Kivelson, S., C. Kallin, D. P. Arovas, and J. R. Schrieffer, 1987, Phys. Rev. B. **36**, 1620.

Kivelson, S., D.-H. Lee, and S.-C. Zhang, 1992, Phys. Rev. B. **46**, 2223.

Klironomos, F. D., and A. T. Dorsey, 2005, Phys. Rev. B. **71**, 155331.

v. Klitzing, K., G. Dorda, and M. Pepper, 1980, Phys. Rev. Lett. **45**, 494.

Kosterlitz, J. M., and D. J. Thouless, 1973, J. Phys. C **6**, 1181.

Koulakov, A. A., M. M. Fogler, and B. Shklovskii, 1996, Phys. Rev. Lett. **76**, 499.

Kravchenko, S. V., and M. P. Sarachik, 2004, Rep. Prog. Phys. **67**, 1.

Kukushkin, I. V., N. J. Pulsford, K. von Klitzing, R. J. Haug, K. Ploog, and V. B. Timofeev, 1993, Europhys. Lett. **23**, 211.

Kukushkin, I. V., N. J. Pulsford, K. von Klitzing, K. Ploog, R. J. Haug, S. Koch, and V. B. Timofeev, 1992, Phys. Rev. B. **45**, 4532.

Lai, K., *et al.*, 2004, Phys. Rev. Lett. **93**, 156805.

Lam, P. K., and S. M. Girvin, 1984, Phys. Rev. B. **30**, 473.

Laughlin, R. B., 1983, Phys. Rev. Lett. **50**, 1395.

Lee, D., S. Kivelson, and S. Zhang, 1991, Phys. Rev. Lett. **67**, 3302.

Leggett, A. J., 1970, Phys. Rev. Lett. **25**, 1543.

Leggett, T., 2004, Science **305**, 1921.

Levesque, D., J. J. Weis, and A. H. MacDonald, 1984, Phys. Rev. B. **30**, 1056.

Levitov, L., and D. Novikov, 2005, private communication.

Lewis, R. M., and J. P. Carini, 2001, Phys. Rev. B. **64**, 073310.

Lewis, R. M., *et al.*, 2002, Phys. Rev. Lett. **89**, 136804.

Lewis, R. M., *et al.*, 2004a, Physica E **22**, 104.

Lewis, R. M., *et al.*, 2004b, Phys. Rev. Lett. **93**, 176808.

Lewis, R. M., *et al.*, 2005a, Phys. Rev. B. **71**, 081301(R).

Lewis, R. M., *et al.*, 2005b, unpublished.

Li, C. C., 1999, *Microwave conductivity of magnetic field induced insulating phase of the two-dimensional hole system in GaAs*, Ph.D. thesis, Princeton University.

Li, C. C., *et al.*, 1997, Phys. Rev. Lett. **79**, 1353.

Li, C. C., *et al.*, 2000a, Phys. Rev. B. **61**, 10905.

Li, C. C., *et al.*, 2000b, Phys. Rev. Lett. **92**, 186804.

Li, W. L., 2005, private communication.

Li, Y. P., 1993, *AC response of the reentrant insulating phase of two-dimensional electrons in the extreme quantum limit*, Ph.D. thesis, Princeton University.

Li, Y. P., *et al.*, 1991, Phys. Rev. Lett. **67**, 1630.

Li, Y. P., *et al.*, 1995a, Solid State Commun. **95**, 619.

Li, Y. P., *et al.*, 1995b, Solid State Commun. **96**, 379.

Li, Y. P., *et al.*, 1996, Solid State Commun. **99**, 255.

Liao, S. Y., 1990, *Microwave Devices and Circuits* (Prentice-Hall).

Lilly, M. P., *et al.*, 1999a, Phys. Rev. Lett. **82**, 394.

Lilly, M. P., *et al.*, 1999b, Phys. Rev. Lett. **83**, 824.

Lozovik, Y. E., and V. I. Yudson, 1975, JETP Lett. **22**, 11.

MacDonald, A. H., and M. P. A. Fisher, 2000, Phys. Rev. B. **61**, 5724.

MacDonald, A. H., and S. M. Girvin, 1986, Phys. Rev. B. **33**, 4009.

Maki, K., and X. Zotos, 1983, Phys. Rev. B. **28**, 4349.

Manoharan, H. C., Y. W. Suen, M. B. Santos, and M. Shayegan, 1996, Phys. Rev. Lett. **77**, 1813.

Millis, A. J., and P. B. Littlewood, 1994, Phys. Rev. B. **50**, 17632.

Moessner, R., and J. Chalker, 1996, Phys. Rev. B. **54**, 5006.

Moon, K., H. Mori, K. Yang, S. M. Girvin, A. H. MacDonald, L. Zheng, D. Yoshioka, and S.-C. Zhang, 1995, Phys. Rev. B. **51**, 5138.

Morf, R. H., 1979, Phys. Rev. Lett. **43**, 931.

Murphy, S. Q., J. P. Eisenstein, G. S. Boebinger, L. N. Pfeiffer, and K. W. West, 1994, Phys. Rev. Lett. **72**, 728.

Murray, C. A., W. O. Sprenger, and R. A. Wenk, 1990, Phys. Rev. B. **42**, 688.

Murthy, G., 2004, private communication.

Narasimhan, S., and T. Ho, 1995, Phys. Rev. B. **52**, 12291.

Narevich, R., G. Murthy, and H. A. Fertig, 2001, Phys. Rev. B. **64**, 245326.

Nelson, D. R., and B. I. Halperin, 1979, Phys. Rev. B. **19**, 2457.

Noda, T., M. Tanaka, and H. Sakaki, 1990, Appl. Phys. Lett. **57**, 1651.

Normand, B. G. A., P. B. Littlewood, and A. J. Millis, 1992, Phys. Rev. B. **46**, 3920.

Nunomura, S., S. Samsonov, and J. Goree, 2000, Phys. Rev. Lett. **84**, 5141.

Nunomura, S., *et al.*, 2002, Phys. Rev. E **65**, 066402.

Oji, H. C. A., A. H. MacDonald, and S. M. Girvin, 1987, Phys. Rev. Lett. **58**, 824.

Paalanen, M. A., R. L. Willett, P. B. Littlewood, R. R. Ruel, K. W. West, L. N. Pfeiffer, and D. J. Bishop, 1992a, Phys. Rev. B. **45**, 11342.

Paalanen, M. A., R. L. Willett, R. R. Ruel, P. B. Littlewood, K. W. West, and L. N. Pfeiffer, 1992b, Phys. Rev. B. **45**, 13784.

Pan, W., 2003, private communication.

Pan, W., R. R. Du, *et al.*, 1999, Phys. Rev. Lett. **83**, 820.

Pan, W., H. L. Stormer, D. C. Tsui, L. N. Pfeiffer, K. W. Baldwin, and K. W. West, 2002, Phys. Rev. Lett. **88**, 176802.

Pan, W., H. L. Stormer, D. C. Tsui, L. N. Pfeiffer, K. W. Baldwin, and K. W. West, 2003, Phys. Rev. Lett. **90**, 016801.

Park, T., *et al.*, 2005, Phys. Rev. Lett. **94**, 017002.

Paulius, L. M., W.-K. Kwok, R. J. Olsson, A. M. Petrean, V. Tobos, J. A. Fendrich, G. W. Crabtree, C. A. Burns, and S. Ferguson, 2000, Phys. Rev. B. **61**, 11910.

Pfeiffer, L., and K. W. West, 2003, Physica E **20**, 57.

Ploog, K. H., 1981, Ann. Rev. Mater. Sci. **11**, 171.

Polyakov, D. G., and B. I. Shklovskii, 1993, Phys. Rev. B. **48**, 11167.

Prange, R. E., and S. M. Girvin (eds.), 1990, *The Quantum Hall Effect* (Springer-Verlag).

Price, R., X. Zhu, P. M. Platzman, and S. G. Louie, 1993, Phys. Rev. B. **48**, 11473.

Quinlivan, D., *et al.*, 1990, Phys. Rev. Lett. **65**, 1816.

Read, N., 1989, Phys. Rev. Lett. **62**, 86.

Russer, R., and E. Bieble, 1994, in *Silicon-Based Millimeter-Wave Devices*, edited by J. F. Luy and P. Russer (Springer), chapter 1.

Ruzin, I. M., S. Marianer, and B. I. Shklovskii, 1992, Phys. Rev. B. **46**, 3999.

Sakaki, H., *et al.*, 1987, Appl. Phys. Lett. **51**, 1934.

Sambandamurthy, G., 2004, private communication.

Sambandamurthy, G., *et al.*, 2005a, unpublished.

Sambandamurthy, G., *et al.*, 2005b, Phys. Rev. Lett. **94**, 017003.

Santos, M. B., *et al.*, 1992, Phys. Rev. Lett. **68**, 1188.

Schmeller, A., J. P. Eisenstein, L. N. Pfeiffer, and K. W. West, 1995, Phys. Rev. Lett. **75**, 4290.

Schulz, H. J., 1993, Phys. Rev. Lett. **71**, 1864.

Shayegan, M., 1997, in *Perspectives in Quantum Hall Effects*, edited by S. Das Sarma and A. Pinczuk (Wiley and Sons, New York), chapter 9.

Shayegan, M., 2005, private communication.

Shibata, N., and D. Yoshioka, 2003, J. Phys. Spc. Japan **72**, 664.

Shkolnikov, Y. P., *et al.*, 2005, Phys. Rev. Lett. **95**, 066809.

Simon, S. H., 2005, Solid State Commun. **134**, 81.

Sondhi, S. L., *et al.*, 1993, Phys. Rev. B. **47**, 16419.

Spielman, I. B., J. P. Eisenstein, L. N. Pfeiffer, and K. W. West, 2001, Phys. Rev. Lett. **87**, 036803.

Spivak, B., 2002, Phys. Rev. B. **67**, 125205.

Spivak, B., and S. A. Kivelson, 2004, Phys. Rev. B. **70**, 155114.

Stormer, H. L., 1999, Rev. Mod. Phys. **71**, 875.

Stormer, H. L., and R. L. Willett, 1989, Phys. Rev. Lett. **62**, 972.

Stormer, H. L., and R. L. Willett, 1992, Phys. Rev. Lett. **68**, 2104.

Tan, J. N., J. J. Bollinger, B. Jelenkovic, and D. J. Wineland, 1995, Phys. Rev. Lett. **75**, 4198.

Tanatar, B., and D. M. Ceperley, 1989, Phys. Rev. B. **39**, 5005.

Taut, M., 2001, Phys. Rev. B. **64**, 165315.

Tešanović, Z., 2001, Phys. Rev. B. **93**, 217004.

Thomas, H., *et al.*, 1994, Phys. Rev. Lett. **73**, 652.

Tinkham, M., 1974, Rev. Mod. Phys. **46**, 587.

Tsui, D. C., 1999, Rev. Mod. Phys. **71**, 891.

Tsui, D. C., H. L. Stormer, and A. C. Gossard, 1982, Phys. Rev. Lett. **48**, 1559.

Tsukada, M., 1977, J. Phys. Soc. Jpn. **42**, 391.

Turner, P. J., *et al.*, 2003, Phys. Rev. Lett. **90**, 237005.

Tutuc, E., S. Melinte, E. P. De Poortere, R. Pillarisetty, and M. Shayegan, 2003, Phys. Rev. Lett. **91**, 076802.

Tutuc, E., M. Shayegan, and D. A. Huse, 2004, Phys. Rev. Lett. **93**, 036802.

Veillette, M. Y., L. Balents, and M. P. A. Fisher, 2002, Phys. Rev. B. **66**, 155401.

Vershinin, M., *et al.*, 2004, Science **303**, 1995.

Wang, Z., *et al.*, 2005, unpublished.

Wen, C. P., 1969, IEEE Trans. Microwave Theory and Tech. **17**, 1087.

Wen, X.-G., 2005, private communication.

Wen, X.-G., and A. Zee, 1992, Phys. Rev. Lett. **69**, 1811.

Wigner, E. P., 1934, Phys. Rev. **46**, 1002.

Wilks, J., 1967, *The Properties of Liquid and Solid Helium* (Oxford).

Willett, R. L., 1994, Surf. Sci. **305**, 76.

Willett, R. L., R. R. Ruel, K. W. West, and L. N. Pfeiffer, 1993, Phys. Rev. Lett. **71**, 3846.

Willett, R. L., *et al.*, 1988, Phys. Rev. B. **38**, 7881.

Williams, F. I. B., P. A. Wright, R. G. Clark, E. Y. Andrei, G. Deville, D. C. Glattli, O. Probst, B. Etienne, C. Dorin, C. T. Foxon, and J. J. Harris, 1991, Phys. Rev. Lett. **66**, 3285.

Williams, F. I. B., *et al.*, 1992, Phys. Rev. Lett. **68**, 2105.

Williams, R., 1990, *Modern GaAs Processing Methods* (Artech House Publishers).

Wu, X. G., and S. L. Sondhi, 1995, Surf. Sci. **51**, 14725.

Wulf, U., 1999, Phys. Rev. B. **59**, 6700s.

Xia, J. S., *et al.*, 2004, Phys. Rev. Lett. **93**, 176809.

Yang, I., *et al.*, 2003, Phys. Rev. B. **68**, 121302(R).

Yang, K., 2001, Phys. Rev. Lett. **87**, 056802.

Yang, K., 2005, private communication.

Yang, K., K. Moon, L. Zheng, A. H. MacDonald, S. M. Girvin, D. Yoshioka, and S. Zhang, 1994, Phys. Rev. Lett. **72**, 732.

Ye, P. D., Y. Chen, L. W. Engel, D. C. Tsui, R. M. Lewis, L. N. Pfeiffer, and K. W. West, 2002a, in *Proceedings of the 15th International Conference on High Magnetic Fields in Semiconductor Physics.*

Ye, P. D., L. W. Engel, D. C. Tsui, R. M. Lewis, L. N. Pfeiffer, and K. W. West, 2002b, Phys. Rev. Lett. **89**, 176802.

Yi, H., and H. A. Fertig, 1998, Phys. Rev. B. **58**, 4019.

Yi, H., and H. A. Fertig, 2000, Phys. Rev. B. **61**, 5311.

Yoon, J., C. C. Li, D. Shahar, D. C. Tsui, and M. Shayegan, 1999, Phys. Rev. Lett. **82**, 1744.

Young, A. P., 1979, Phys. Rev. B. **19**, 1855.

Young, D. P., *et al.*, 1999, Nature (London) **397**, 412.

Yu, Y., and S. Yang, 2002, Phys. Rev. B. **66**, 245318.

Zhang, S. C., T. H. Hansson, and S. Kivelson, 1989, Phys. Rev. Lett. **62**, 82.

Zheng, L., and H. A. Fertig, 1995, Phys. Rev. B. **52**, 12282.

Zhu, X., and S. G. Louie, 1995, Phys. Rev. B. **52**, 5863.